



# Synthesis of Sequence-Defined and Sequence-Controlled Polyphosphodiester and Their Self-Assembly

*by*

**Nadeema Appukutti**

A thesis submitted to the University of Kent in partial fulfilment of the  
requirements for the degree of Doctor of Philosophy



## **ABSTRACT**

Having control over the sequence is the ultimate key to achieve the high degree structural control over polymeric materials. The ability to control the sequence of building blocks in polymer leads to precise, well-managed synthetic macromolecules with unique and ordered chemical and physical properties. Synthetic macromolecules have entered almost every aspect of modern life, but the use of sequence (as is so potent in biology) has not yet been integrated. However, in the last few years, it has been demonstrated that sequenced-defined bio-oligomers such as oligonucleotides or oligopeptides can find applications in the fields of data storage, biomedicine, drug delivery and nanofabrication because of their versatile physical and chemical properties. Nature on planet earth is directed by poly(phosphoester)s (PPEs) in the form of deoxy & ribonucleic acid (DNA & RNA), and, as pyrophosphates, they store up chemical energy in organisms. Taking the organic polymer synthesis to the next level, we are synthesizing sequence-defined poly(phosphodiester)s using a library of non-nucleosidic monomers. We employ diols as monomers, each bearing a unique functionality such as long chain alkyls, aromatic or heteroaromatic rings. We have adapted the automated solid phase phosphoramidite synthesis commonly used for DNA to make our sequence-defined polymers, allowing us to programme and print specific sequences with ease. Like proteins, these polymers then self-assemble in a sequence-defined fashion to give uniform particles. These nanoparticles were studied using different analytical methods such as DLS, AFM and gel electrophoresis chromatography. Due to their biocompatibility and biodegradability, the PPEs are potentially capable of participating in molecular recognition or directing intracellular drug delivery.

## **DECLARATION**

I declare that the thesis entitled “Synthesis of Sequence-Defined and Sequence-Controlled Polyphosphodiester and Their Self-Assembly”, is my own original work and a requirement for the award of the degree of Doctor of Philosophy to University of Kent. This thesis has not been submitted by me for the award of any other degree of any other Institute.





## **ACKNOWLEDGEMENTS**

It is a pleasure to look back at the past journey and remember the people who have helped and supported me along this long but fulfilling road.

First, I'd like to express my deepest gratitude to my supervisor Dr Christopher Serpell. He has been a strong and supportive advisor to me throughout my PhD and, I am forever grateful for the research opportunity and dedicated support and guidance.

I am indebted to University of Kent for this opportunity and the funding which made this a reality. I also express my sincere thanks to the academics and staff of the School of Physical Sciences.

My utmost gratitude also goes to Dr Joseph Jones for his fundamental contributions on the project and for sharing his knowledge and, I must thank Kevin Howland and Ian Brown, who provided much needed help throughout the years.

Nothing more important than the working atmosphere and the people contributing to it daily. I must thank Serpell group for all the great time we spent together in the lab and, especially Saeed and Emerald for always keeping my spirits high. I would like to dedicate all my efforts to my loving husband Nuwan De Silva, and I would not have completed this road without his constant love, care.

Finally, I thank God almighty for giving me the opportunity and guidance to achieving my goal.

## LIST OF PUBLICATIONS

- I. Appukutti, N.; de Vries, A.; Gudeangadi, P.; Claringbold, B.; Garrett, M.; Reithofer, M.; Serpell, C. Sequence-Complementarity Dependent Co-Assembly of Phosphodiester-Linked Aromatic Donor-Acceptor Trimers. *ChemRxiv* **2021**. This content is a preprint and has not been peer-reviewed.
- II. Appukutti, N.; Jones, J.; Serpell, C. J. Sequence Isomerism in Uniform Polyphosphoesters Programmes Self-Assembly and Folding. *Chem. Commun.* 2020, 10–13.
- III. Appukutti, N.; Serpell, C. J. High Definition Polyphosphoesters: Between Nucleic Acids and Plastics. *Polym. Chem.* 2018, 9 (17), 2210–2226.

## List Of Tables

Table 1.1 Comparison of natural polymer with synthetic polymers.	18
Table 2.1 Sample concentration in TBE and TAMg with their fitted parameters.	98
Table 2.2 Summary of self-assembly by sequence, buffer, and concentration. [a] No observable self-assembly. Critical aggregation concentrations can be inferred from the degree of dilution required to achieve this.	98
Table 4.1 Sequence patterns of self-sequencing polymers with donor-acceptor monomers.	160

## List of Schemes

Scheme 1.1 General polycondensation of phosphorus dichloride with diols.	39
Scheme 1.2 Classical strategies for the synthesis of cyclic phosphoesters.	39
Scheme 1.3 Ring-opening polymerization of cyclic phosphoesters.	40
Scheme 2.1 Synthesis of phosphoramidite reagent compatible with phosphoramidite solid phase synthesis using a diol as the starting material: mono-protection of diol with DMT-Cl followed by the phosphoramidite activation.	57
Scheme 2.2 Mono protection of BPA with trityl chloride.	59
Scheme 2.3 Synthesis of BPA phosphoramidite reagent.	60
Scheme 3.1 Synthesis of NDI diol 3.1.	116
Scheme 3.2 Synthesis of DAN diol monomer 3.2.	118
Scheme 3.3 Synthesis of phosphoramidite reagent for solid phase synthesis with diols. (a) NDI phosphoramidite reagent 3.4. (b) DAN phosphoramidite reagent 3.6	121
Scheme 3.4 Synthesis of DAN and NDI trimers and DAN and NDI trimers sequences.	135
Scheme 4.1 Polymerisation reaction of diols with phosphorous oxychloride.	157
Scheme 4.2 Synthesis of DAN2 (4.2) derivative as an electron rich donor monomer.	159
Scheme 4.3 Synthesis of crosslinked polymer with 4,4',4''-methanetriyltriphenol	165

## List of Figures

Figure 1.1 Degrees of sequence regulation of polymers.	19
Figure 1.2 Structure of DNA a) monomer b) adenine pairs with thymine and cytosine pairs with guanine. (Image available at <a href="https://chem.libretexts.org/Bookshelves/Introductory_Chemistry">https://chem.libretexts.org/Bookshelves/Introductory_Chemistry</a> )	21
Figure 1.3 a) Amino acids with a variant group(R) (b) Amino acid in different PH	23
Figure 1.4 Levels of Structural complexity of proteins. Defined principal architecture of biopolymers leads to formation of secondary and tertiary structures. Adapted with permission from reference (CrystEngComm 2015) <sup>16</sup>	25
Figure 1.5 Structural DNA nanotechnology A) Conventional Watson–Crick hybridization B) Holliday junction enables a new approach to create a 2D DNA array or 3D DNA cube <sup>27</sup> C) DNA origami enables users to create large nanoscale objects with arbitrary shapes D) DNA bricks enable users to create	

any arbitrary nanoscale objects similar to Lego <sup>28</sup> . Adapted with permission from reference (Advanced Optical Materials 2019) <sup>20</sup>	27
Figure 1.6 Template polymerisation principle.	31
Figure 1.7 Sequence-controlled polymers. (a) Macrocyclic building blocks with five-base-long PNA anticodons assemble on a DNA template and can be coupled through the reactive groups A and B to generate sequence-controlled polymers that bear no structural resemblance to nucleic acids. (b) Examples of polymer building blocks that can be stitched together to form sequence-defined materials using this approach. Adapted with permission from reference (Nature Chemistry 2013) <sup>50</sup>	33
Figure 1.8 Subclasses of phosphorus (V)-containing polymers.	37
Figure 2.1 Solid-phase synthetic route to generate sequence-defined DNA-polymer conjugates described by Sleiman and co-workers. Adapted with permission from reference (Nat. Chem. 2013) <sup>4</sup>	54
Figure 2.2 Synthesis of sequence-controlled Cy3-HE <sub>12</sub> -DNA or Cy3Cy3-HE <sub>12</sub> -DNA conjugates and their self-assembly behaviour. Adapted with permission from reference (Am. Chem. Soc. 2018). <sup>17</sup>	55
Figure 2.3 <sup>1</sup> H NMR of trityl protected BPA recorded in DMSO.	60
Figure 2.4 <sup>1</sup> H NMR of BPA phosphoramidite reagent recorded in DMSO.	61
Figure 2.5 <sup>31</sup> P NMR of BPA phosphoramidite reagent recorded in DMSO.	62
Figure 2.6 (a) The phosphoramidite non-nucleosidic oligomer synthesis cycle (b) DNA synthesiser (c) Trityl histogram of BPA oligomer (failed at 11 <sup>th</sup> coupling).	63
Figure 2.7 Denaturing polyacrylamide gel electrophoresis (20%) showing the product BPA oligomer.	65
Figure 2.8 Designed sequence patterns for C12-HEG oligomers.	66
Figure 2.9 Chemical structures of C12 <sub>10</sub> -HEG <sub>10</sub> and (C12-HEG) <sub>10</sub>	67
Figure 2.10 (a) Synthesis of sequence-defined polyphosphodiester. (b) Trityl histograms showing successful synthesis. (c) Denaturing polyacrylamide gel electrophoresis (20%) showing single products (M <sub>w</sub> = 6021 g mol <sup>-1</sup> ). T <sub>20</sub> DNA (M <sub>w</sub> = 6019 g mol <sup>-1</sup> ) is provided as a molar mass comparison.	69
Figure 2.11 Mass spectrum of C12 <sub>10</sub> -HEG <sub>10</sub> , with expansions of the triply and quadruply charged peaks corresponding to a monoisotopic mass of 6020.93 Da (calculated exact mass is 6020.77 Da).	69
Figure 2.12 Mass spectrum of (C12-HEG) <sub>10</sub> , with expansions of the triply and quadruply charged peaks corresponding to a monoisotopic mass of 6021.00 Da (calculated exact mass is 6020.77 Da).	70
Figure 2.13 DLS (left) and NR emission measurements (right) on C12 <sub>10</sub> -HEG <sub>10</sub> (top) and (C12-HEG) <sub>10</sub> (bottom) in TBE buffer at 100 μM.	73
Figure 2.14 DLS (left) and NR emission measurements (right) on C12 <sub>10</sub> -HEG <sub>10</sub> (top) and (C12-HEG) <sub>10</sub> (bottom) in TBE buffer at 10 μM.	74
Figure 2.15 DLS (left) and NR emission measurements (right) on C12 <sub>10</sub> -HEG <sub>10</sub> (top) and (C12-HEG) <sub>10</sub> (bottom) in TBE buffer at 1 μM.	75
Figure 2.16 TEM images of C12 <sub>10</sub> -HEG <sub>10</sub> , 100 μM, TBE buffer.	77
Figure 2.17 TEM images of C12 <sub>10</sub> -HEG <sub>10</sub> , 10 μM, TBE buffer.	78
Figure 2.18 TEM images of C12 <sub>10</sub> -HEG <sub>10</sub> , 1 μM, TBE buffer.	79
Figure 2.19 AFM images of C12 <sub>10</sub> -HEG <sub>10</sub> , 100 μM, TBE buffer.	80
Figure 2.20 AFM images of C12 <sub>10</sub> -HEG <sub>10</sub> , 10 μM, TBE buffer.	80

Figure 2.21 TEM images of (C12-HEG) <sub>10</sub> , 100 μM, TBE buffer.	81
Figure 2.22 Self-assembly in TBE buffer of (a) C12 <sub>10</sub> -HEG <sub>10</sub> and (b) (C12-HEG) <sub>10</sub> as analysed by TEM.	82
Figure 2.23 DLS (left) and NR emission measurements (right) on C12 <sub>10</sub> -HEG <sub>10</sub> (top) and (C12-HEG) <sub>10</sub> (bottom) in TAMg buffer at 100 μM.	84
Figure 2.24 DLS (left) and NR emission measurements (right) on C12 <sub>10</sub> -HEG <sub>10</sub> (top) and (C12-HEG) <sub>10</sub> (bottom) in TAMg buffer at 10 μM.	85
Figure 2.25 DLS (left) and NR emission measurements (right) on C12 <sub>10</sub> -HEG <sub>10</sub> (top) and (C12-HEG) <sub>10</sub> (bottom) in TAMg buffer at 1 μM.	86
Figure 2.26 TEM images of C12 <sub>10</sub> -HEG <sub>10</sub> , 100 μM, TAMg buffer.	87
Figure 2.27 AFM images of C12 <sub>10</sub> -HEG <sub>10</sub> , 100 μM, TAMg buffer. AFM images of C12 <sub>10</sub> -HEG <sub>10</sub> , 10 μM, TAMg buffer.	88
Figure 2.28 TEM images of (C12-HEG) <sub>10</sub> , 100 μM, TAMg buffer.	89
Figure 3.1 The polar/π model of aromatic stacking with the (a) electron-rich benzene and the (b) electron-deficient hexafluorobenzene. Typical stacking modes are (c) offset face-to-face, (d) edge-to-face, and (e) face-centered stacking.	106
Figure 3.2 The polar/π model of aromatic stacking with the electron-rich 1,5-Dialkoxynaphthalene (DAN) and the electron-deficient 1,4,5,8-Naphthalene tetracarboxylic acid diimide (NDI) with typical stacking modes. <sup>15</sup>	109
Figure 3.3 Generation of donor-acceptor [2]catenane.	110
Figure 3.4 The chemical structure of the first aromatic electron D-A oligomer and its representative pleated stacking mode (right).	112
Figure 3.5 The folding patterns targeted by DAN and NDI compounds.	113
Figure 3.6 Structures of DAN and NDI oligomers and the 1:1 DAN-NDI heteroduplex for oligomers (right).	114
Figure 3.7 <sup>1</sup> H NMR spectra of the NDI diol 3.1 with CDCl <sub>3</sub> as solvent.	117
Figure 3.8 (a) Model crystal structure from literature <sup>39</sup> (b) Hyper Chem optimised phosphate linked DAN-NDI structure.	118
Figure 3.9 <sup>1</sup> H NMR spectra of the DAN diol derivative 3.2 with glycol side chains with CDCl <sub>3</sub> as solvent.	119
Figure 3.10 The lengths of the side chains with the aromatic rings calculated with Mercury crystal structure visualisation software.	120
Figure 3.11 Mass spectra of mono protected derivatives: (a) DAN-DMT (+ESI) (b) NDIDMT (-ESI).	122
Figure 3.12 <sup>31</sup> P NMR of phosphoramidite reagents (a) DAN (b) NDI.	123
Figure 3.13 Trityl Histogram for synthesis of (a) DAN <sub>20</sub> (b) NDI <sub>20</sub> .	125
Figure 3.14 UV/Vis spectra of a) NDI absorption is at high concentration is shown with solid line and low concentration with dashed line, b) DAN absorption is at high concentration is shown with solid line and low concentration with dashed line, and a CT region of a spectrum of donor-acceptor combination (right).	126
Figure 3.15 UV absorption of DAN and NDI 20mers	127
Figure 3.16 Sequences of DAN and NDI 12mers.	128
Figure 3.17 Trityl histogram for 12mers: DAN <sub>12</sub> , NDI <sub>12</sub> and DAN <sub>6</sub> NDI <sub>6</sub> .	129
Figure 3.18 UV absorption of DAN and NDI 12mers a) all four combinations in water b) 1:1 mixture of DAN <sub>12</sub> and NDI <sub>12</sub> .	130
Figure 3.19 Proposed self-stacking model for NDI <sub>12</sub> .	131

Figure 3.20 The DAN and NDI 12mers in water (left). The DAN polymer visualized on 20% polyacrylamide gel with Stains-all (right).	133
Figure 3.21 Mass spectrum of DAN <sub>3</sub> , corresponding to a monoisotopic mass of 1132.38 Da.	136
Figure 3.22 Mass spectrum of NDI <sub>3</sub> , corresponding to a monoisotopic mass of 1265.25 Da.	137
Figure 3.23 UV absorptions of homotrimers in different solutions taken using a Nanodrop spectrometer at 1mM (a) DAN <sub>3</sub> (b) NDI <sub>3</sub> .	138
Figure 3.24 (a) UV/Vis absorption of DAN <sub>3</sub> (1 mM), NDI <sub>3</sub> (1 mM) and the 1:1 mixture. (b) DAN <sub>3</sub> , NDI <sub>3</sub> and 1:1 solution in water.	139
Figure 3.25 UV absorption of DAN <sub>3</sub> NDI <sub>3</sub> 1:1 solution in different solutions at 10 mM concentration.	139
Figure 3.26 UV/Vis absorption of DAN <sub>3</sub> :NDI <sub>3</sub> (1:1) at 25 °C and 45 °C in different solutions at 10 mM concentration.	140
Figure 3.27 AFM (top) and TEM (bottom) images of DAN <sub>3</sub> deposited from water.	141
Figure 3.28 AFM (top) and TEM (bottom) images of NDI <sub>3</sub> deposited from water.	142
Figure 3.29 AFM (top) and TEM (bottom) images of DAN <sub>3</sub> :NDI <sub>3</sub> (1:1) deposited from water.	143
Figure 3.30 (a) UV/vis spectra observed for DAN-NDI-DAN in different solutions (25 °C and heated at 45 °C). (b) UV/Vis absorption spectra for NDI-DAN-NDI in different solutions (25 °C and heated at 45 °C). The concentrations of both trimers were kept at 10 mM and the spectrum shows the visible region.	145
Figure 3.31(a) UV/vis spectra observed for DAN-NDI-DAN (b) UV/Vis absorption spectral observed for NDI-DAN-NDI. The concentrations of trimers were increased from 500 μM to 20 mM. The side graphs show the enlarged spectra in the visible region. The spectra were measured in water at room temperature.	146
Figure 3.32 UV absorption of 1:1 mixture of the DAN-NDI-DAN and NDI-DAN-NDI in water.	147
Figure 3.33 The predicted secondary structures for DAN-NDI trimers. (a) The pleated, alternating DAN-DAN-DAN trimer. (b) The pleated, alternating NDI-DAN-NDI trimer. (c) The duplex structure (DAN <sub>3</sub> : NDI <sub>3</sub> ).	148
Figure 3.34 AFM of DAN-NDI-DAN trimers deposited from water.	149
Figure 3.35 TEM of DAN-NDI-DAN trimers deposited from water.	150
Figure 3.36 AFM (top) and TEM (bottom) of NDI-DAN-NDI trimers deposited from water.	151
Figure 3.37 Self-assembly of alternating trimers. (a) DAN-NDI-DAN (b) NDI-DAN-NDI.	152
Figure 4.1 Monomers for self-sequencing polymers.	158
Figure 4.2 Electron-poor (NDI) and electron-rich (DAN) aromatics form stacked charge transfer complexes in solution.	159
Figure 4.3 DAN-NDI polymers. 2% agarose gel stained with stains-all.	161
Figure 4.4 DLS data (size - intensity distribution) for uncontrolled DAN and NDI polymers (a) DAN (b) DAN <sub>2</sub> (c) NDI (d) DAN + NDI (e) DAN <sub>2</sub> + NDI (f) DAN + DAN <sub>2</sub> + NDI.	163
Figure 4.5 Estradiol (a) and BPA (b) monomers.	164
Figure 4.6 Reaction scheme for the self-condensation reaction of COF-1.	166
Figure 4.7 Summary of classical COFs and their structure. <sup>16</sup>	167

Figure 4.8 Synthesis of phosphate-based porous organic polymers P-POP-1 and P-POP-2. 168

Figure 4.9 Solid phase  $^{31}\text{P}$  NMR spectrum for cross linked-network polymer. 170

Figure 4.10 Triphenyl crosslinked polymer against 1 Kb DNA ladder in 2% agarose gel stained with Stains-All. 171



## Table of Contents

Chapter 1	17
1 Introduction	17
1.1 Polymers .....	17
1.2 Biopolymers .....	19
1.2.1 Sequence regulation in biopolymers	20
1.2.2 Engineered Self-Assembly of Biopolymers	24
1.3 Biological Inspiration .....	27
1.3.1 Bioconjugates	29
1.3.2 Peptide/Protein polymer conjugates	29
1.3.3 DNA polymer conjugates	30
1.3.4 Strategies for sequence regulation	31
1.4 Phosphorous containing polymers.....	36
1.4.1 Phosphorous in nature	36
1.4.2 Approach for phosphorous-containing non-natural polymers	37
1.4.3 Polyphosphoesters (PPEs)	37
1.4.4 Polyphosphoesters via Ring Opening Polymerization and Polycondensation	39
1.4.5 Chemical synthesis of sequence-defined poly(phosphodiester)s	40
1.5 Thesis Aims .....	45
1.6 References .....	47
Chapter 2	52
2 Self-assembly and folding of sequence defined polyphosphoesters.	52
2.1 Introduction .....	52
2.2 Result and discussion. ....	57
2.2.1 Non nucleosidic monomer synthesis	57
2.2.2 Synthesis of BPA-phosphate oligomers	62
2.2.3 <b>C12-HEG</b> sequence isomers system	65
2.3 Conclusion.....	101
2.4 References .....	103
Chapter 3	105
3. Oligophosphodiester DAN-NDI charge transfer complexes in aqueous media.	105

3.1	Introduction .....	105
3.1.1	Interaction between DAN and NDI aromatic units .....	108
3.2	Aim of the Chapter. ....	115
3.3	Sequence defined DAN and NDI via solid phase synthesis.....	116
3.3.1	Synthesis of DAN and NDI monomers .....	116
3.3.2	Synthesis of DAN and NDI polymers .....	120
3.3.3	Synthesis and charge transfer association of DAN and NDI polymers in aqueous media .....	124
3.4	Sequence controlled DAN and NDI trimer complexes in aqueous media.....	133
3.4.1	Synthesis of DAN and NDI trimers .....	134
3.4.2	Homo trimers characterisation .....	136
3.4.3	Characterisation of heterotrimers .....	144
3.5	Conclusion.....	153
3.6	Reference .....	154
<b>Chapter 4</b> .....		<b>156</b>
4	Poly phosphates via a simple synthesis method .....	156
4.1	Introduction .....	156
4.2	General polymer synthesis .....	157
4.3	Self-sequencing of donor-acceptor monomers.....	158
4.4	Phosphate based polymers with different types of monomers .....	163
4.5	Crosslinked polymer.....	165
4.5.1	Result and discussion .....	168
4.6	Conclusion.....	172
4.7	Reference .....	173
<b>Chapter 5</b> .....		<b>174</b>
5	Experiment .....	174
5.1	Solvents and reagents .....	174
5.2	Instrumentation.....	174
5.3	Chemical synthesis .....	178
5.3.1	Synthesis of monomers .....	178
5.3.2	Synthesis of Trimers .....	187
5.3.3	Reactions with phosphorous oxychloride .....	188

## **Abbreviations**

%, Percentage

≈, Approximately

°C, Degrees celsius

μL, Microlitre

μM, Micromolar

AFM, Atomic force microscopy

BPA, Bisphenol A

DLS, Dynamic light scattering

DMAP, 4-dimethylamino pyridine

DNA, Deoxyribose nucleic acid

EtOH, Ethanol

M, Molarity

mM, millimolar

MS, Mass spectrometry

PAGE, Mercury polyacrylamide gel electrophoresis

RNA, Ribo nucleic acid

TBE, Tris borate EDTA

TEM, Transmission electron microscopy

TLC, Thin layer chromatography

UV-Vis, Ultraviolet visible spectroscopy








## Chapter 1

### 1 Introduction

#### 1.1 Polymers

Polymers are large, chain-like molecules made from small repeating units called monomers. Natural as well as synthetic polymers play a crucial role in everyday life. The physical and chemical properties and functions of a polymer are determined by the monomeric units and the length and distribution of lengths of the polymer. Polymers can be divided into two main categories, homopolymers which include many copies of a single repeating units, and copolymers which includes two or more different units. Polymer properties are strongly dependent on their architecture, and primary structure (the order of the monomers) is vital in determining the eventual properties of the resulting polymer. The simplest type of polymer architecture is a linear chain; however, the introduction of branch points leads to a wide variety of potential, more complex, architectures. The possibility of controlling monomer sequences in polymers provides the ability to control the information at the sub molecular level in the polymer chains, opening up interesting prospects for advanced polymer synthesis. Two subsets of copolymers exist: while *sequence-controlled* polymers have approximate control over the polymer length, choice of monomers, their ratio, and order, *sequence-defined* polymers have uniform, perfectly defined sequence polymers with precise length. With respect to sequence, when compared to their biological counterparts, synthetic polymers appear very primitive. It is expected that more complex and advanced materials would be made possible with higher level sequence regulation.

**Table 1.1** Comparison of natural polymer with synthetic polymers.

	Primary structure	Folding	Self-assembly	Functions
<b>Natural Polymers</b>	Define the sequence at monomer level 	Can have programmed Uniform structures such as $\alpha$ helix $\beta$ sheets 	Controlled by molecular recognition and monodisperse aggregates will form	Structure Catalysis Communication Data storage
<b>Synthetic Polymers</b>	The sequence control is limited to block-copolymer level 	Disordered and Non-uniform structures will form	Hydrophobic self-assembly structures will form to give micelles, etc. 	Bulk materials Rheological control Nanopatterning Drug delivery
<b>Artificial sequence polymers</b> have potential for high stability and scalable synthesis 				

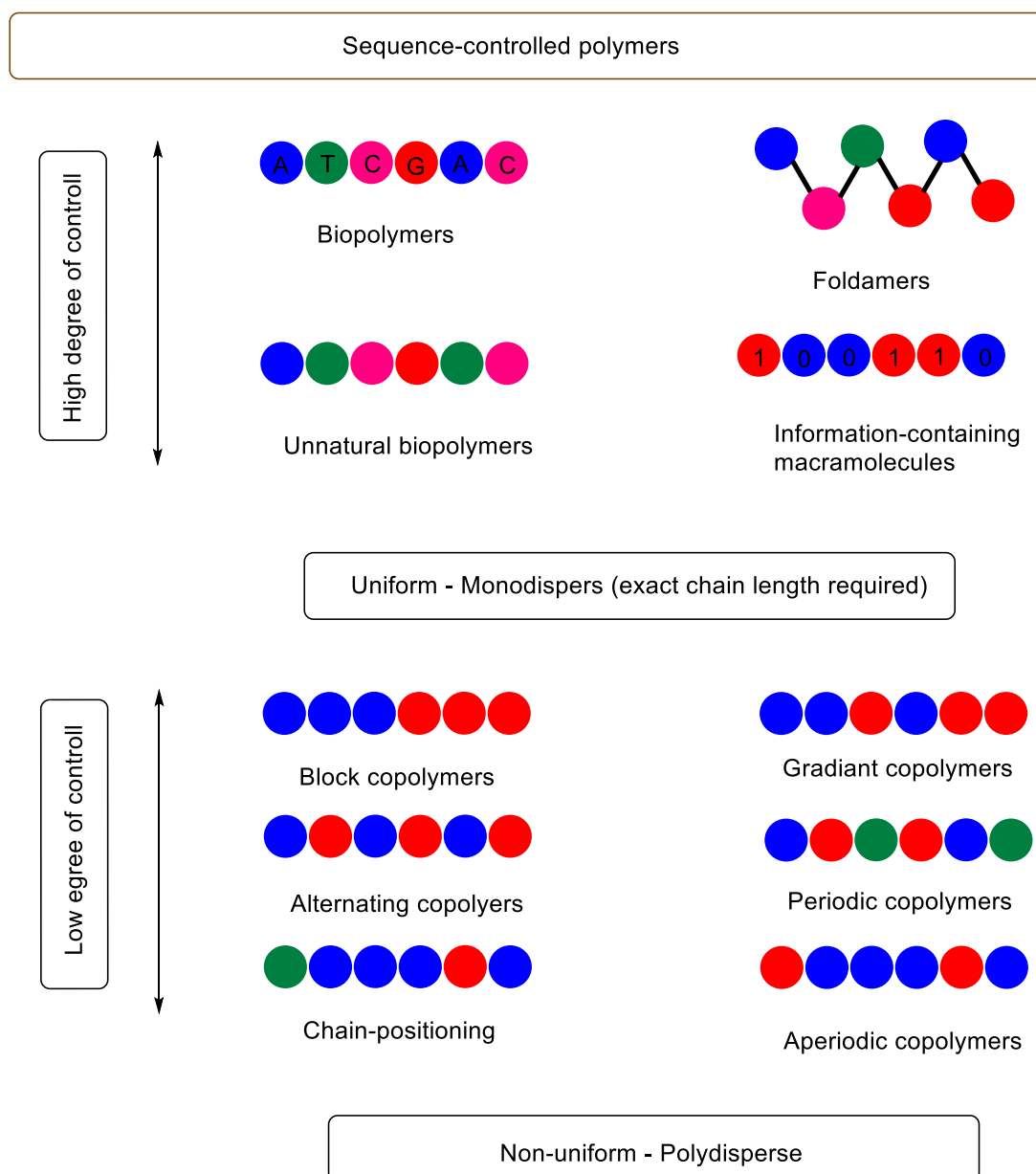


**Figure 1.1** Degrees of sequence regulation of polymers.

## 1.2 Biopolymers

Biopolymers are polymers which occur in nature, or in modified biological systems. Nature contains many examples of biological polymers: nucleic acids (deoxyribonucleic acid and ribonucleic acid), proteins, polysaccharides (starch, chitin), and other materials such as lignin.

Nucleic acids and proteins are the two of the most significant biopolymers. In contrast to starch, lignin, etc. proteins and nucleic acids can have variable side chains with different chemistries which are important in their structure and function. Proteins and nucleic acids have perfectly defined chain length, monomer sequence and chirality. The precise control of the primary sequence provides structural and functional diversity which drives the molecular complexity required by all living organisms. Sequence defined biopolymers involve in protein engineering and DNA-templated polymerizations and they also serve as molecular information storage and participate in molecular recognition.<sup>1,2</sup>

### 1.2.1 Sequence regulation in biopolymers

The specific monomeric sequences underlining the primary structures of these macromolecules determine their highly specialized functions. This remarkable control at the molecular scale is extremely important, as this specific sequence determine the 3D structures and the folding properties of the natural polymers. Examples include protein folding and storage of genetic data.

#### 1.2.1.1 Nucleic acids as sequence-defined biopolymer

Nucleic acids are built from nucleotide units. These are comprising of one of two sugars (ribose and 2'-deoxyribose which respectively generate RNA and DNA) on to which nucleobase is appended to give a nucleoside. A phosphate group is added to the 5' OH to give a nucleotide. In a nucleic acid strand, the nucleoside units are joined through the phosphate group of one nucleotide to OH group on the carbon 3 of the sugar unit of a second nucleotide to yield a phosphodiester linkage. The resulting strand is a polymer (a polynucleotide) whose backbone is a repeating sugar-phosphate chain with a variable heterocyclic nucleobase attached to the side. DNA exists in the cell nucleus and stores the genetic information of living organisms, the



blueprint of its life. The base sequence of DNA encodes all the information that is needed for reproduction. DNA replication is a critical event in the cells. However, errors can occur at this stage, and random changes might take place in sequence of bases and it could result in damaged unrepaired DNA which may give rise to mutations. DNA carries the genetic information for making protein and the sequence of DNA determine the order of amino acids in a protein molecule.

The DNA double helix structure contains a specific sequence of four types of nucleotides that are specified by the bases adenine, guanine, cytosine and thymine. Complimentary base-pairing occurs between A:T and C:G, and is mediated by hydrogen bonding between the nucleobases. Double-stranded DNA has very well-defined dimensions, which make it a useful monomer for nanomaterials.<sup>3,4</sup> The right-handed double-helical B-form DNA is the most common DNA structure, with 0.34 nm between each base, a helical pitch of 10.5 base pairs, and a diameter of 2 nm.<sup>5</sup>

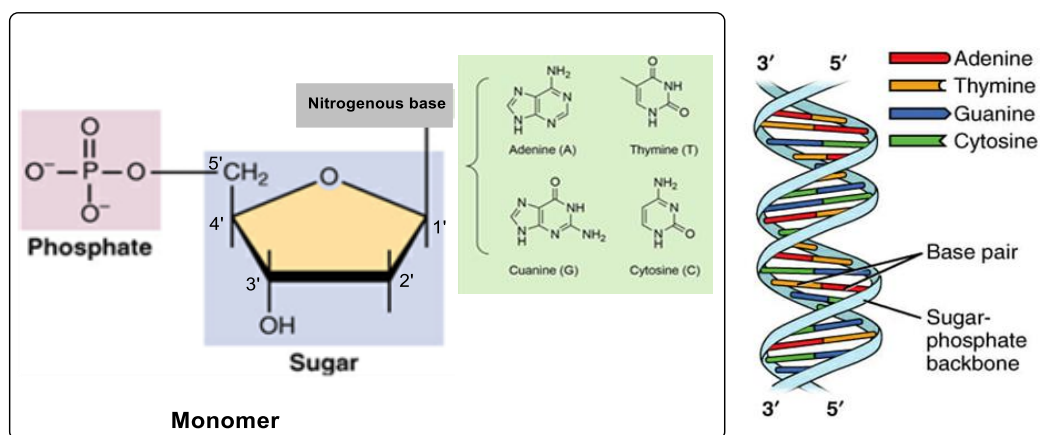


**Figure 1.2** Structure of DNA a) monomer b) adenine pairs with thymine and cytosine pairs with guanine.

(Image available at [https://chem.libretexts.org/Bookshelves/Introductory\\_Chemistry](https://chem.libretexts.org/Bookshelves/Introductory_Chemistry))

Unlike DNA, RNA is present mostly as single-strands and has adenine, guanine, cytosine, and uracil as bases. There are three major types of RNA which play a role during the journey from DNA to protein (messenger RNA (mRNA), ribosomal RNA (rRNA), and transfer RNA (tRNA)), which are distinguished first by function and structures at monomer and 3D levels.<sup>6</sup>

Since sequence is central to the biological purposes of nucleic acids, they must be synthesised in a *sequence-defined* manner. Sequence-defined nucleic acids are synthesized in two main polymerization processes: replication, and transcription. In replication processes, double-stranded DNA with a specific sequence structure is separated into its two strands, and each will act as templates for the new strands of DNA. DNA polymerase adds bases complementary to the newly generated DNA strands to create complementary strands. In the transcription mechanism of DNA to mRNA, the information in DNA is transferred to a messenger RNA (mRNA) molecule with the help of RNA polymerase. During transcription, the DNA of a gene serves as a template for complementary base-pairing. The resulting mRNA is a single-stranded copy of the gene, which next must be translated into a protein molecule.<sup>6,7</sup>

#### 1.2.1.2 Protein as sequence defined biopolymer

Proteins are biopolymers with specific sequence structure constructed by different  $\alpha$ -amino acid monomers, and they are one of the most abundant organic molecules in living systems and have the most diverse range of functions of all macromolecules. Each amino acid consists of a carboxylic acid, with an amino group on the (alpha) carbon. The alpha carbon also displays a variable side chain.<sup>6</sup>

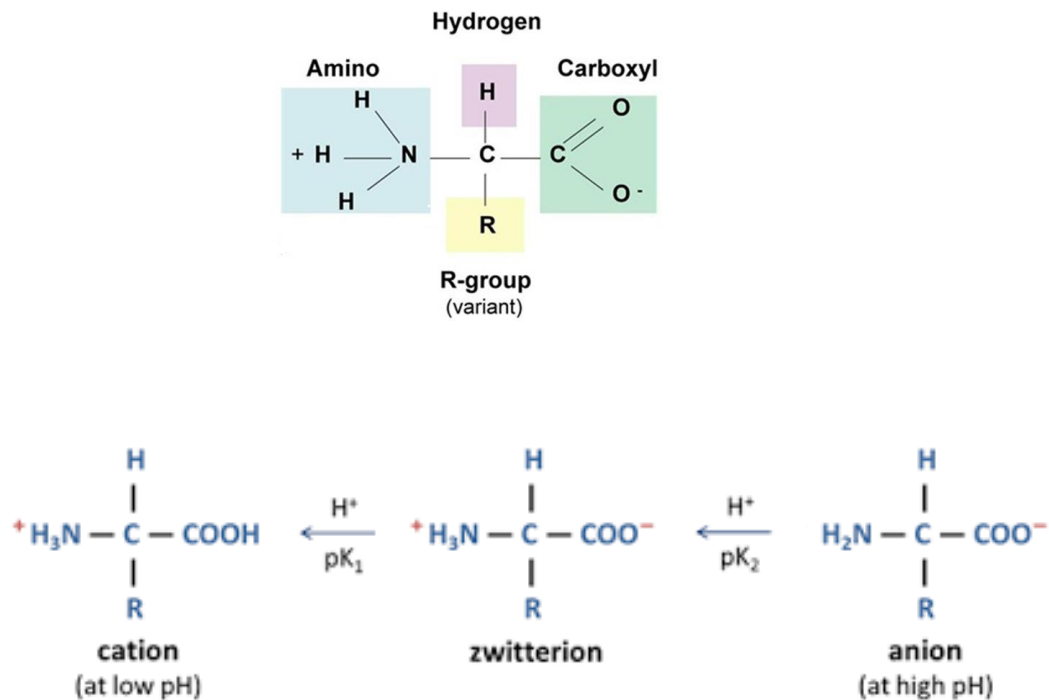


**Figure 1.3** a) Amino acids with a variant group(R) (b) Amino acid in different PH

Amino acids can act as both an acid and base due to the presence of the amino and carboxyl functional groups. Amino acids are zwitterions: molecule with at least one has positive and one negative electrical charge on functional groups. The (neutral) zwitterion is the usual form amino acids exist in solution and depending on the pH, there are two other forms, an anion at high pH and a cation at low pH.<sup>8</sup>

There are 20 proteogenic amino acid side chains and based on their chemical properties, the amino acids can be divided into four groups: hydrophobic, polar uncharged, charged, and “special cases”. These side chains can interact with one another to cause the polymer chain to adopt certain shapes or conformations. Side chain modification can be used to improve functional as well as conformational properties of polypeptides.

The primary (i.e., sequence) structure of proteins determines the secondary, tertiary, and quaternary structure, thereby influencing the biological properties and functions of proteins. Proteins may be structural (e.g., keratin, collagen, elastin), regulatory (e.g., the Lac repressor protein) contractile (e.g., myofilaments, myosin), or protective (antibodies). Protein may also serve in chemical processes (i.e., enzymes), in transport, storage, or as membrane components and they can behave as toxins or medicine. Proteins are synthesized by a translation process where mRNA serves as a template. During the process, the nucleotide sequence of the mRNA is transcribed into an amino acid sequence, ensuring sequence-definition.

### 1.2.2 Engineered Self-Assembly of Biopolymers

Self-assembly is a process in which a disordered system forms an organized structure without external direction. In the context of sequence-*defined* polymers, self-assembly, refers to, process which organized structure spontaneously forms from individual components.

Depending on the conformation and stereochemical configuration of the constituent amino acids, for proteins, the two most abundant secondary structural elements are known as  $\alpha$ -helices and  $\beta$ -sheets. These motifs have been taken out of their biological setting and used to create synthetic materials. In 1974, It was proposed that polypeptide chains taking cyclic ring structure could self-assemble by stacking to form peptide nanotubes.<sup>9</sup> Later engineered structures of cyclic peptide nanotubes were developed by Ghadiri and co-workers.<sup>10-12</sup> The authors have formed a planar ring that could be self-assembled, one on top of the other, to form tubular structures of the desired diameter using the concept of alternating D- and L-amino acids in the context of a cyclic peptide. Lanreotide is another cyclic peptide that was shown to self-assemble into tubular structures. Regular  $\beta$ -sheet which form gels have also

been reported.<sup>13</sup> Self-assembly has provided a powerful way of making materials and organizing them into functional constructs designed for a specific purpose and, the ability of peptides and proteins to adopt specific secondary, tertiary and quaternary structures provides unique opportunities for the design of nanoscale materials.<sup>14,15</sup>

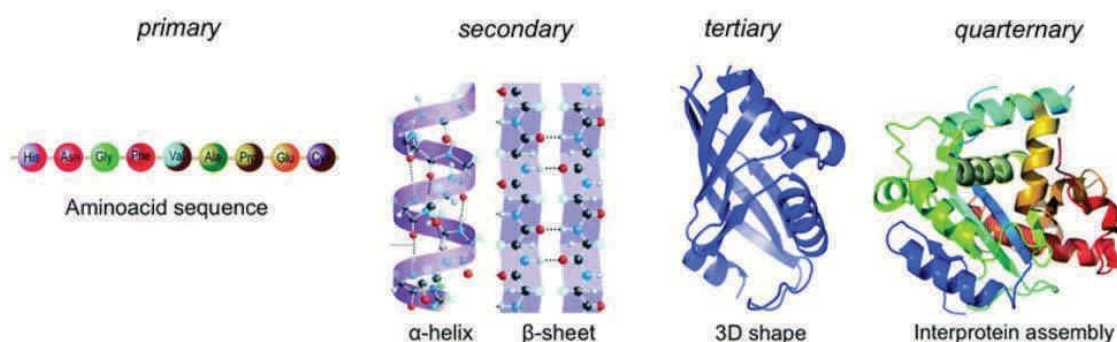


**Figure 1.4** Levels of Structural complexity of proteins. Defined principal architecture of biopolymers leads to formation of secondary and tertiary structures. Adapted with permission from reference (CrystEngComm 2015)<sup>16</sup>

DNA generally forms helical structures out of base complementary (Watson-Crick base pairing) in duplex, and it is one of the most promising candidates for bottom-up self-assembly. Single-stranded DNA can self-assemble into nanostructures which are able to act both as a structural and functional element. DNA nanostructures are relatively easy to design and fairly predictable in their geometric structures which leads to a growing interest in the field.<sup>17</sup>

Programmed self-assembly is highly effective for generating a wide range of structures with desired structural shapes. DNA can easily be paired with a complementary sequence and that allows two pieces of DNA to stick together. Seeman and his group proposed that DNA could be used as a regular physical

material for the self-assembly of various 3D nanoscale structures.<sup>18–20</sup> Branched DNA junctions are known to be a crucial part of biological processes, but it was the visionary idea of Seeman to repurpose these for structural applications. His original idea was that DNA junctions, assembled into a crystalline array, could be used as a scaffold for the organization of macromolecules, such as proteins.<sup>21</sup> To create desired nanostructures with DNA, it is needed to construct rigid building blocks for use as assembly units. Double-crossover (DX) junctions can act as building blocks for the formation of long-range DNA lattices.<sup>22,23</sup> Their design is based on a pair of Holliday junctions fused through a pair of double-helices, and they have high stability.

In 2006, Rothemund introduced the concept of scaffolded DNA origami<sup>2</sup>. The origami method design utilizes short stranded, (staple DNA strands that direct the folding of a long single-stranded DNA, (scaffold strand) into desired shapes and patterns such as squares, five-pointed stars, disks, and smiley faces. In 2009, three different strategies to take the origami method into three dimensions were reported. With the reported strategies, six different scaffold strands were used to form the six sides of a large cube and one side acted as a lid which could be opened in response to a specific DNA input.<sup>24</sup>

Apart from that, many other strategies are also possible such as concept of single-stranded DNA tiles introduced by the Yin's group. They created objects with similar complexity to DNA origami without the need for a scaffold.<sup>25</sup> Later they extended the method to create 3D Lego-like bricks.<sup>26</sup>

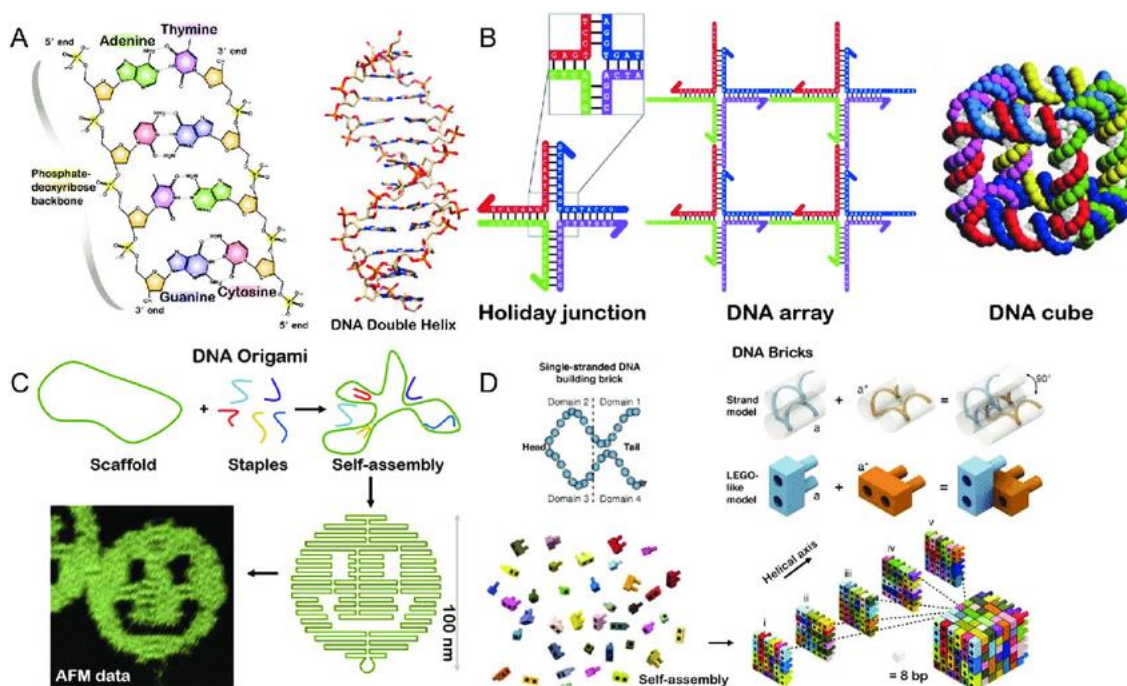


**Figure 1.5** Structural DNA nanotechnology A) Conventional Watson–Crick hybridization B) Holliday junction enables a new approach to create a 2D DNA array or 3D DNA cube<sup>27</sup> C) DNA origami enables users to create large nanoscale objects with arbitrary shapes D) DNA bricks enable users to create any arbitrary nanoscale objects similar to Lego<sup>28</sup>. Adapted with permission from reference (Advanced Optical Materials 2019)<sup>20</sup>

### 1.3 Biological Inspiration

Supramolecular chemistry enables the development of large multicomponent chemical systems. These complexes are held together by noncovalent interactions between molecules such as van der Waals forces,  $\pi$ - $\pi$ interactions (interactions between molecules carrying  $\pi$  systems), hydrogen bonds, electrostatic interactions, metal-ligand coordination, and mechanical bonds. Supramolecular chemistry is inspired by natural systems which also large and complex molecular assemblies held together by the same types of interaction.

In biological systems, function is determined by structure, and the structural control covers molecular to the macroscopic levels. In such a system, having well-defined

building blocks is essential to avoid functional failures. Biological systems create ordered supramolecular polymers which present ordered internal structures and determined shapes. As much as we would like to be able to produce self-assembling systems mimicking nature and/or create systems with same complexity as nature, the process of creating such a system is limited by our current understanding in terms of predictable structural and functional assembly when many components and interactions are involved. Furthermore, biological polymerization strategies offer almost perfectly well defined and large (in terms of molecular weight) polymer products, which is another challenge when it comes to emulating nature. However, systems with non-natural building blocks have their own advantages such as unlimited backbone and side chain possibilities, as well as tuneable solvent compatibility.

Although it is a great challenge, scientists take advantage of supramolecular chemistry and to design complex nanoscale architectures displaying different architecture and functionality. For example, DNA nanotechnology is a branch of nanotechnology, (understanding, control, and application of synthetic structures to create new and improved materials) in which the predictable hybridisation of DNA is used to fabricate finely detailed nanostructures. Researchers have combined these two concepts, supramolecular chemistry, and DNA self-assembly to create supramolecular DNA nanotechnology in which DNA is put together with non-nucleosidic molecules. For example, organic aliphatic molecules can be used to construct branched DNA building blocks with an organic core and Sleiman's group produced a supramolecular DNA hexagon which was used as an organizational scaffold for gold nanoparticles.<sup>3</sup> Because of their broad capability, biomolecule self-



assembly has emerged over as a hybrid methodology that combines nature's molecular tools with synthetic nanoscale constructs.

### 1.3.1 Bioconjugates

Bioconjugation is a powerful and simple way to integrate the properties of two individual components: biopolymers and synthetic polymers, covalently linked to give polymer bioconjugates. These hybrids have proved utility in a number of fields including drug delivery (enhancing solubility and therapeutic activity of bonded biological molecules)<sup>29</sup>, biomimetic sensors<sup>30</sup> or gene therapy.<sup>31</sup>

### 1.3.2 Peptide/Protein polymer conjugates

The modification of biomacromolecules through the attachment of synthetic polymers has led to a new family of highly advanced biomaterials with enhanced properties.<sup>32</sup> Chemical modification of proteins can enhance protein stability in biological systems and construct protein-drug conjugates. These advancements are critically important in biological applications. Polypeptides can be covalently bound with simple synthetic polymers and the resultant bioconjugates have the potential to combine the advantages of both biological and synthetic molecules. For example, proteins are often combined with poly(ethylene glycol) (PEG) and properties of PEG such as biocompatibility, lack of immunogenicity, antigenicity and toxicity, and solubility make this a perfect candidate for bioconjugation.<sup>33</sup>

Molecules that have an affinity for water are called hydrophilic molecules and those that naturally repel water is called hydrophobic. Attachment of hydrophilic methoxy PEG to bovine serum albumin was reported around 1970, and this bioconjugate was introduced to extend blood life and control immunogenicity of proteins.<sup>34</sup> The field of polymer bioconjugates is very broad due to the diversity of biological polymers

and synthetic polymers that are available for conjugation. This leads to a wide array of physical, chemical, and biological properties, and hence distinct potential applications.<sup>31,32</sup>

### 1.3.3 DNA polymer conjugates

Block copolymers are comprised with two or more chemically different molecular chains to create macromolecules and self-assembly of block copolymers can be used to design and control the shape and dimension of resulting nanostructures. Amphiphilic block copolymers, can self-assemble into spherical micelles (spheres), cylindrical micelles (cylinders), lamellae and vesicles vesicles.<sup>35–38</sup>

The capacity to organize functional groups into well-defined, arbitrary pattern is a unique feature of DNA nanostructures. DNA sequence, the properties, and functions of DNA block copolymer (DBC) materials can be fine-tuned for designated applications. For instance, conjugating hydrophilic polymers results in water-soluble DBCs, which can be used for hydrogel formation.<sup>39</sup>

DNA can also be conjugated with a synthetic hydrophobic polymer to obtain amphiphilic DNA block copolymers which can self-assemble into micellar structures with hydrophobic core inside and hydrophilic DNA corona at the surface. Several researchers have worked on investigating the assembly of the different kinds of polymers covalently attached with single-strand DNA (ssDNA). For example, Mirkin reported on poly(styrene) (PS) attached to a short segment of single-stranded DNA (ssDNA), and assembly behaviour of the amphiphilic DNA block copolymers successively.<sup>40</sup> The same group have also developed a strategy to prepare DNA-brush block copolymer micelles with a biodegradable core of polycaprolactone (PCL) and a dense layer of oligonucleotides as the corona.<sup>41</sup>

As a novel hybrid material, DBCs behave with a higher level of controllability because of the very well-defined primary structure of DNA which also makes it ideal as a material of construction. In 2016, the Sleiman group reported the self-assembly of sequence-defined hydrophobic polymers on DNA cages based on the synergistic action of hydrophobic interactions and precise base pairing interactions.<sup>42</sup> Block copolymer self-assembly is a useful fabrication method used to create materials for wide-ranging practical applications such as nanolithography, drug-delivery, and catalysis.<sup>43</sup>

#### 1.3.4 Strategies for sequence regulation

Creating well-ordered synthetic polymer sequence and manipulating the resulting 3D architectures has so far been restricted to simple structures in comparison with their biological counterparts. Polymerizations based on biological approaches are highly efficient. However, synthetic chemistry offers many more possibilities in terms of chemical diversity.

##### 1.3.4.1 Templatation methods

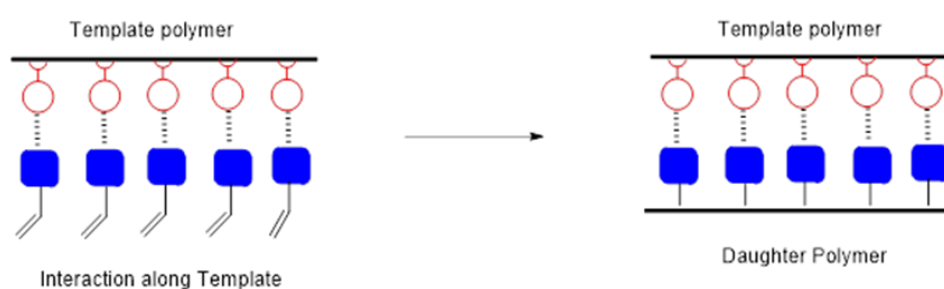


**Figure 1.6** Template polymerisation principle.

Development of sequence regulated materials has been inspired by template-assisted procedures as seen in the natural synthesis of biomacromolecules.<sup>44,45</sup> In such approaches, the monomer units are linked to a performed macromolecule and polymerized. The use of information-rich biopolymers as templates for the generation of synthetic sequence-specific polymers seems a promising approach towards the ultimate goal of precise monomer positioning, and DNA has been identified as a potential template for polymerisation.

Gilham and co-workers reported the first non-enzymatic template directed reaction in 1966<sup>35</sup>. In the presence of water-soluble carbodiimide, the synthesis involved ligation short thymidine oligonucleotide 5'-phosphates on oligoadenylate templates. In 2002, DNA nano scaffolds has been a synthesised using template method by Lars<sup>46</sup> and Lynn.<sup>47</sup> Then in 2003 Lynn's concept of reductive amination reaction of peptide nucleic acids (PNAs) was further developed by Liu's group replacing it with amine acylation<sup>48</sup> and later they developed a strategy to translate DNA templates into *sequence-defined* synthetic polymers unrelated to nucleic acids<sup>49</sup>. A variety of synthetic polymers were obtained using macrocyclic PNA adapter, which contain reactive groups (A or B) that can be used to hold the PNA anticodon along the template to form long sequence-specific polymers <sup>50</sup>(Error! Reference source not found.).

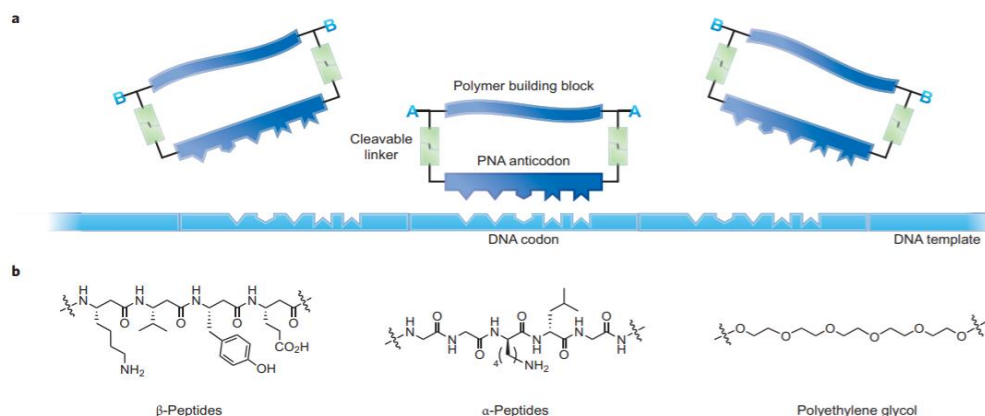


**Figure 1.7** Sequence-controlled polymers. (a) Macrocyclic building blocks with five-base-long PNA anticodons assemble on a DNA template and can be coupled through the reactive groups A and B to generate sequence-controlled polymers that bear no structural resemblance to nucleic acids. (b) Examples of polymer building blocks that can be stitched together to form sequence-defined materials using this approach. Adapted with permission from reference (Nature Chemistry 2013)<sup>50</sup>

#### 1.3.4.2 Step-Growth Polymerizations

Step-growth polymerization is a stepwise reaction where bi-functional or multifunctional monomers add up to form a polymer step by step. In a step growth process, reaction proceeds rapidly at the beginning, but the molecular weight increases slowly so high molecular weights can only be achieved at the end of the process.

In terms of monomer sequence regulation, step growth polymerisation leads to poor controlled chain length and molecular weight distribution. Even though the method has some limitation, step-growth polymerisation can be used to create complex sequence-controlled copolymer structures by introducing different monomers sequentially.

Lutz and co-workers employed azide alkyne cycloaddition to prepare functional periodic copolymers<sup>51</sup>. Another route involving step-growth radical polymerization: which a polymer forms by the successive addition of free-radical building blocks, developed by Kamigaito and coworkers.<sup>52</sup> In the process both radical and cationic polymerization processes are active in a single reaction, and this allowed two different monomers that react via different mechanism to integrated in to same polymer chain. Kamigaito's group synthesized periodic ABCC-periodic vinyl copolymers using metal-catalyzed step-growth radical polymerization. A one-pot sequence-specific polymerization strategy was developed for the sequential addition of monomers by You and coworkers.<sup>53,54</sup>

In each step, different monomers were added to the chain. Recently, Meyer and co-workers have investigated a step-growth strategy to prepare sequence-*controlled* PLGA<sup>55-57</sup> Ring opening polymerisation is a polymerisation process where the terminal end of the cyclic molecule is reacts with another cyclic monomer, hence opening its ring system to form a longer polymer chain. Usually poly(lactic-co-glycolic acid) (PLGA) copolymers are synthesized by ring opening polymerization of lactide and glycolide that leads to random sequences. They are important biodegradable polymers for biomedical applications, but sequence control of these polymers may lead to more precise control of size, degradability, and thermal properties.

#### 1.3.4.3 Chain growth polymerisation

Chain-growth polymerization involves the addition of monomers to an active centre of the growing chain, and it can proceed via radical, anionic, cationic, or ring-opening mechanisms. Chain growth polymerization is usually performed in one pot, and therefore chain-growth copolymerization was not classically sequence-regulated.

This irregularity is derived from the poor regulation in polymerization reactions such as some side reactions and cross-propagation with comonomers.

Radical polymerisation is a chain-growth process, in which polymer grows by successive insertion of monomer units through their double bonds. In the 1990s there has been a new method introduced for synthesis of sequence-*controlled* polymers, combining living polymerisation with conventional radical polymerisation. The new method is called controlled/living radical polymerisation (CRP).<sup>58-60</sup> In a living or controlled/living chain-growth mechanism, all chains are initiated and grow simultaneously. This technique allows the synthesis of macromolecules with complex topologies such as block copolymers, graft copolymers or multifunctional stars.

Reversible addition-fragmentation chain transfer (RAFT) polymerization is highly favoured for wide range of functional monomers and promotes homogeneous chain growth leading to low polydispersity.<sup>61,62</sup> Single monomer addition strategy with selective monomers was first reported in 1990s by Higashimuras' group. They have applied this strategy for their living cationic polymerization of vinyl ethers and styrene derivatives

#### 1.3.4.4 Multistep growth synthesis

Multistep growth synthesis is the best available strategy granting the initial access to sequence defined polymers. In this method monomers are added stepwise during the process with freely selectable number of monomers. Solid-phase synthesis is a multistep growth synthesis method where one of the reactants attached to insoluble solid support (cross-linked polymer beads, controlled-pore glass, solid nanoparticles, soluble polymer supports, or fluorescent tags) and the transform to give the resulting

product. The rest of the components are in solution. This approach was first introduced by Merrifield at the beginning of the 1960's<sup>63</sup>, and has been widely applied for preparation of peptides<sup>64</sup> and oligonucleotides.<sup>65</sup> The insoluble solid supports allow reaction of support-bound, end-functionalized monomers in a step-by-step manner. The other reactive groups in the monomer are protected to avoid the side-reactions. Therefore, at the completion of each step, the excess of reagents is washed away, and products can be conveniently isolated. This method has been usually studied for peptides and oligonucleotides but also utilized for non-natural bio-oligomers and foldamers.<sup>66</sup> More recently, solid phase strategies have also been investigated for synthetic polymers.<sup>67</sup>

## 1.4 Phosphorous containing polymers

### 1.4.1 Phosphorous in nature

Many cellular compounds contain phosphorus as an essential element. It occurs as a building block in genetic materials (DNA and RNA), in the energy currency adenosine triphosphate (ATP), and in phospholipids which form cell membranes. Free elemental phosphorus is highly reactive as an element and more stable as a compound with bonds to other elements such as oxygen. Therefore, in biology, phosphorus occurs mainly in the form of phosphate esters. DNA and RNA are the carriers of genetic information and carry the instructions for growth, development, functioning, and reproduction of cells. ATP, which is responsible for a large part of energy transfer in living cells consists of adenine linked to a ribose sugar which is connected to a phosphoester anhydride (pyrophosphate) of three phosphate units. Overall, the phosphate group is perfectly suitable for many applications in nature and serves as one of the most versatile elements.<sup>68</sup>



### 1.4.2 Approach for phosphorous-containing non-natural polymers

Synthetic chemistry gives the opportunity to the formation of many more phosphorus-derivatives to build up polymers with various properties. Phosphorus-containing high-performance polymers have been extensively studied during the last few decades. Phosphorus forms mostly trivalent or pentavalent compounds and forms various polymeric compounds having P-P, P-C, P-N and P-O linkages. Phosphorous can be introduced into the polymer backbones and/or to the side chains in a variety of chemical structures. There are many reports and patents, on the synthesis of polyphosphate polymer derivatives including polyphosphates phosphites<sup>69,70</sup> phosphoramidates<sup>71</sup> and polyphosphonates.<sup>71,72</sup>

### 1.4.3 Polyphosphoesters (PPEs)

Polyphosphoesters (PPEs) are phosphorous-containing polymers with robust phosphodiester bonds in the main chain and they have structural similarity to nucleic and teichoic acids. PPEs are noted for their fire resistance, plasticity, lubricity, and thermal stability.

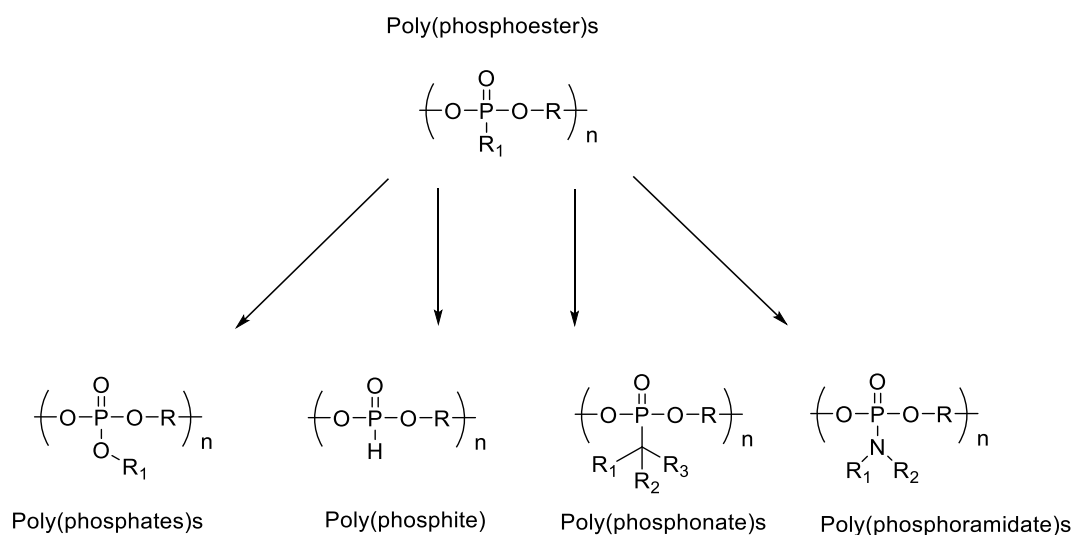


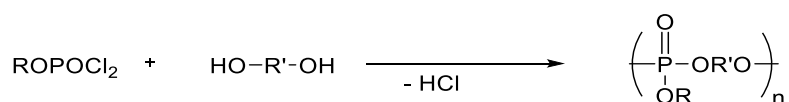
**Figure 1.8** Subclasses of phosphorus (V)-containing polymers.

In PPEs, the phosphorus atoms in the polymer backbone are pentavalent and it can be functionalised both on the main chain and on the side chain. PPEs are categorized into different structural modifications; poly(phosphate)s, poly(phosphonate)s, poly(phosphate)s and poly(phosphoamidate)s (Figure 1.8).

Due to their ability to adjust the properties into unique situations, biocompatibility, biodegradability, and structural similarity to nucleic and teichoic acids PPEs are attractive for biomedical applications, such as tissue engineering, drug and gene delivery. These applications require materials with advanced properties, especially customizable or tuneable materials with bioactivity. These highly organized PPEs are biodegradable through enzymatic digestion of phosphate bonds under physiologic conditions.<sup>73-76</sup> In 1970s Penczek and co-workers focused on the development of efficient methods of polymerization, and their efforts were driven by the remarkable structural similarities between PPEs and teichoic and nucleic acids.<sup>7</sup> The group developed the first strategies towards the PPE synthesis (mainly water soluble) and the potential biological applications. Phosphorus-based flame retardants are an important category in flame-retardant systems and are widely used as an additive in engineering plastics because of its smoke-free, non-toxic, and non-corrosive products. Polyphosphonates and polyphosphates are of commercial interest because of their flame-retarding characteristics and their potential as high-performance plastics<sup>77,78</sup> In between two extremes of nucleic acids and plastics there is an emerging area of chemical space, that of non-natural precision phosphoesters and high definition polyphosphoesters: between nucleic acids and plastics was discussed in our review in 2018<sup>79</sup>.

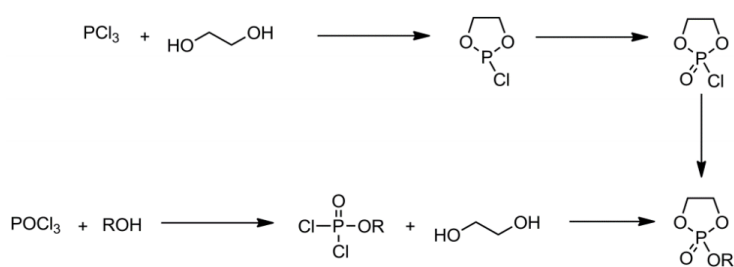
#### 1.4.4 Polyphosphoesters via Ring Opening Polymerization and Polycondensation

PPEs can be prepared by various synthetic routes. James Arvin reported the synthesis of aromatic polyphosphates by the polycondensation of phosphorus oxychloride with bisphenol A<sup>80</sup> for the first time in 1936. Polycondensation is a step-growth synthesis approach for phosphorus containing polymers and one of the most widely used methods for the preparation of PPEs due to readily available monomers.<sup>81</sup> PPEs can be synthesised with reacting diols with an equimolar amount of dichlorophosphates.<sup>82,83</sup>



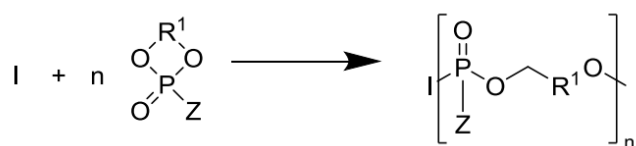
**Scheme 1.1** General polycondensation of phosphorus dichloride with diols.

Direct polycondensation requires a relatively high temperature (~200 °C) in order to complete the reaction. Usually, the reaction is carried out in the inert atmosphere and evolved HCl can be removed by passing gas through the reaction mixture. The drawback of this process is that, at a higher temperature the ester group in starting dichloride may participate in transesterification and may lead to insoluble polymers with side reactions being difficult to eliminate, although they can be limited when using aromatic diols with aromatic dichlorophosphates.<sup>82</sup>



**Scheme 1.2** Classical strategies for the synthesis of cyclic phosphoesters.

In addition to polycondensation, typical ring-opening polymerization (chain growth strategy) of five- or six-membered cyclic phosphoesters is applied for PPE synthesis. The polymers prepared by such methods may carry functional (pendant) groups, which allow further postpolymerization modification by different techniques. This technique is capable of a wide range of resulting polymers, water-soluble<sup>84-86</sup> to hydrophobic<sup>87,88</sup> depending on the character of the pendant group on the cyclic phosphorus-containing monomer.



Z = alkyl, aryl, Oalkyl, Oaryl

R<sup>1</sup> = (-CH<sub>2</sub>-)<sub>2,3</sub>

**Scheme 1.3** Ring-opening polymerization of cyclic phosphoesters.

#### 1.4.5 Chemical synthesis of sequence-defined poly(phosphodiester)s

DNA is naturally the most important phosphate based functional polymer. The formation of phosphodiester bonds between the 3'hydroxyl group of one monomer and the 5' hydroxyl of the other monomer is a promising reaction for poly nucleotide formation. The first successful dinucleotide formation was reported by Michelson and Tod in 1955. The product was conformed to have the structure of the 3'- 5'- internucleotide phosphodiester linkage in DNA.<sup>89</sup>

It was a major challenge in DNA synthesis to achieve all the right identity and order of the desired nucleobases in the sequence and, Khorana and co-workers developed a method to overcome this early challenge with phosphodiester chemistry.<sup>89,90</sup> Using

the protocol, oligonucleotides of a few bases could be synthesized conveniently. The method had advantages, as the efficiency of each coupling step can be calculated by measuring the absorbance of released DMT cation. However, the utility of protocol was limited because of branching at the internucleotidic phosphate linkage and the time-consuming purification after each coupling step.

Later in the 1975, Letsinger introduced the chlorophosphite method or phosphite-triester approach.<sup>91,92</sup> The introduction of trivalent phosphite compounds instead of pentavalent phosphate compounds was based upon the fact that P(III) derivatives are more reactive than corresponding P(V) compounds because P(III) derivatives are easily oxidised into P(V). The method opens a window for the investigation of backbone modification. Later, Letsinger's work in solution was further developed by Caruthers.<sup>93,94</sup>

Marvin Caruthers developed phosphoramidite chemistry in the 1980s for oligonucleotide synthesis.<sup>94</sup> This method was later enhanced by combination with solid-phase synthesis techniques and, today it is the first choice for oligonucleotide synthesis. The phosphoramidite reagents permitted full and easy automation of oligonucleotide synthesis. The method consists of a four-step cycle that adds one base at a time to a growing chain attached to a solid support. First, the synthesis begins with deprotecting the hydroxyl group of the unit that is attached to a solid support using trichloroacetic acid (to obtain free hydroxyl groups at 5'-end of the nucleoside, if already present). Second a new DMT-protected phosphoramidite is coupled to the 5' hydroxyl group in the presence of an activator (typically, tetrazole) to form a phosphite triester. Third, a capping step, acetylates any unbound 5' hydroxyl groups stopping further nucleoside additions so there are no deletion mutations, only truncated products. Acetic anhydride activated by DMAP or *N*-

methylimidazole is usually used in this step as capping solution. Fourth, iodine oxidation converts the phosphite to a phosphate which makes it more stable in acidic conditions, producing a cyanoethyl protected phosphate backbone. To allow the cycle to continue, the DMT protecting group of the newly attached monomer is removed and this detritylation step is usually monitored using its UV absorbance to track coupling efficiencies as individual bases are added. It is proven that a DMT-based protection strategy is the most beneficial when combined with phosphoramidite chemistry on solid support system because of the strong absorption of DMT cation which can be used to spectroscopically evaluate the yield after each coupling.<sup>65</sup> DNA biosynthesis proceeds in the 5'- to 3'-direction, adding monomers only to the 3' end of the growing strand, which makes it impossible for DNA polymerases to synthesize both strands simultaneously, whereas phosphoramidite oligonucleotide synthesis proceeds 3' to 5' direction opposite to the DNA biosynthesis because the growing oligonucleotide is connected to the solid support via the 3' carbon, and thus synthesis proceeds in the 3'-5' direction.

#### 1.4.5.1 Oligonucleotide modification towards non-natural poly(phosphodiester)s

The modified oligonucleotides, with improved properties, can be used in the sequence specific control of gene expression and have immense potential as therapeutic agents<sup>87</sup>. Both the solid phase synthesis of oligonucleotides and the enzymatic incorporation of nucleotides into a template move forward in last several decades allowing researchers to synthesize non-biogenic bases and backbone modification.

Non-nucleosidic phosphoramidites derived from substituted diols and, 1,2-Diol system has been used to construct the non-nucleosidic backbone to create a wide

range of non-nucleosidic ‘modifiers’.<sup>95</sup> Most commercially available non-nucleosidic ‘modifiers’ are florescent probes or act to introduce functionality which will enable conjugation of the oligonucleotide to another species.<sup>96</sup> There is also another type, commonly called ‘spacers’. Spacers are, as their name suggests, designed to add space either within an oligonucleotide sequence or between the oligo and they are able to break the usual helicity of DNA.<sup>97</sup> This provides greater conformational flexibility to DNA strands. Hairpin loops are a common form of nucleic acid secondary structure that plays an essential and common role in gene expression and DNA recombination and transposition<sup>98</sup>, and these structures can be achieved easily using spacers. Precise length of the spacer arm can be controlled with multiple additions of different length spacers which is important in hairpin DNA structure formation. There have been various studies using oligo ethylene glycols from tetraethylene glycol (TetEG) to octaethylene glycol (OEG),<sup>99</sup> or hydrocarbon chains (C8 to C16)<sup>100</sup> to investigate what the ‘best’ spacer for hairpin structures. Spacers also play an important part in DNA nanotechnology. Sleiman has used phosphoramidite chemistry to create a series of dendrons with two to eight branching and spacer units to create highly unusual structures. By attaching an organic-soluble dendron comprised of splitters and four HEG chains to a DNA strand, a macroamphiphile was created.<sup>101</sup> When assembled in a mixture of acetonitrile and aqueous buffer, these short block copolymers create distinct, long-range fibers. By replacing the HEG chains with C12 chains (with or without C6 spacers), the group was able to produce DNA-amphiphiles which self-assembled in water, to give micelles<sup>101</sup>. Most recently, DNA amphiphiles have been decorated for constructing more complex architectures, such as hollowed vesicles.<sup>102</sup> DNA amphiphiles have shown great promise as drug delivery vehicles, because the hydrophobic domains can modify to

carry small molecule therapeutics and many groups have focused on amphiphilic DNA structures to enhance their potential biomedical applications.

With modifications, existing protocols for sequence- controlled or sequence defined polymer synthesis can be used to create non-natural sequence-*defined* polymers. Such a method should be tolerant to broad range of monomers due to the wide range of monomer availability. The connection between sequence and properties of polymers for non-biological macromolecules is not a well-defined area but scientists have shown greater interest of the area in last decade and, synthesis of long polymer sequences is one of the big challenges in the field.

Sequence defined polymers can be designed for storage of information, as shown by Lutz<sup>103,104</sup>. His group reported that selection of the appropriate monomers linked with each other through chemoselective repeating cycles of amidification and CuAAC reactions led to creation of a (0,1) binary code. The encoded oligomers were prepared using AB and CD building blocks (A = acid, B = alkyne, C = amine, D = azide). The code was composed with one coding and one non-coding AB unit complemented by a noncoding spacer monomer CD. Even with limited technology, these sequence-*controlled* polymer storage systems offer great perspectives.

Final properties of polymers such as folding and self-assembly influenced by the polymers structure. In contrast to biological polymers, folding of non-natural polymers opens new prospects in synthetic chemistry. Controlled single-chain polymers could fold into structures that mimic important natural processes such as protein folding, and DNA packing. Non-natural oligomeric sequences that have the unique ability to fold into well-defined confirmations in solutions are known as foldamers. Foldamers organize themselves by supramolecular interactions such as



metal-ligand coordination,  $\pi$ -stacking or hydrogen bonding and their structural complexity can only truly extend to simple secondary structures such as helices, sheets or turns. Helical foldamers offer a great variety of molecular architectures. Those structures are far surpassing than biopolymer building blocks because of the variety of backbone structures and side chains. Peptidomimetic foldamers are developed to possess common features of natural polypeptides, with some advantages over the parent molecule, such as greater stability of the helix, lower susceptibility to metabolism and the greater flexibility in design. Numerous types of foldamer backbones such as peptoids, *N,N'*-linked ureas, hydroxyamides, aromatic oligoamides, and aromatic tertiary amides have been investigated in great depth.<sup>105,106</sup> Most of these foldamers rely on H-bonding or  $\pi$ -stacking interactions.

## 1.5 Thesis Aims

Researchers have been extensively exploring the synthesis of completely non nucleocidic sequence defined nanostructures to develop functional systems for a wide range of applications. However, achieving superior levels control over the primary structure of a polymer is challenging and require a great deal of endurance.

The research covered in this thesis is focused on sequence-*defined* non-natural polyphosphodiester, particularly on the possibility of obtaining new and useful features by exploiting sequence variation. Even if this class of molecules has not yet found applications, the unique possibility to tune the primary structure offered by these polymers, enables the synthesis of macromolecules with finely defined new properties. For all of these reasons, these new molecules are promising candidates for the implementation of next-generation polymers.

Chapter 2 discusses the application of solid phase synthesis to create non-natural polymers with hydrophobic and hydrophilic moieties. Over the past few decades various strategies have been investigated for monomer sequence control. Our strategy allows to create polyphosphodiester with well-defined sequence. The created polymers display unique and engrossing folding and self-assembly in aqueous media.

Chapter 3 discusses sequence-programmed folding of DAN-NDI polyphosphodiester. The electrostatic complementarity of DAN and NDI units have proven to be interact with each other to form pleated secondary structure to higher order architectures. Here we describe the insertion of DAN and NDI in various sequences within a 12-mer to trimers.

Chapter 4 reports an approach to simpler, less wasteful, solution-phase method to synthesises well defined and/or potentially functional polymers.

## 1.6 References

- (1) Brudno, Y.; Liu, D. R. *Chem. Biol.* **2009**, *16* (3), 265–276.
- (2) Hill, D. J.; Mio, M. J.; Prince, R. B.; Hughes, T. S.; Moore, J. S. *Chemical Reviews*. December 12, 2001, pp 3893–4011.
- (3) Aldaye, F. A.; Sleiman, H. F. *Angew. Chemie Int. Ed.* **2006**, *45* (14), 2204–2209.
- (4) Rothmund, P. W. K. *Nature* **2006**, *440* (7082), 297–302.
- (5) T. Ming Chu. B-Form, A-Form, and Z-Form of DNA - Biology LibreTexts [https://bio.libretexts.org/Bookshelves/Genetics/Book%3A\\_Working\\_with\\_Molecular\\_Genetics\\_\(Hardison\)/Unit\\_I%3A\\_Genes\\_Nucleic\\_Acids\\_Genomes\\_and\\_Chromosomes/2%3A\\_Structures\\_of\\_Nucleic\\_Acids/2.5%3A\\_B-Form\\_A-Form\\_and\\_Z-Form\\_of\\_DNA](https://bio.libretexts.org/Bookshelves/Genetics/Book%3A_Working_with_Molecular_Genetics_(Hardison)/Unit_I%3A_Genes_Nucleic_Acids_Genomes_and_Chromosomes/2%3A_Structures_of_Nucleic_Acids/2.5%3A_B-Form_A-Form_and_Z-Form_of_DNA) (accessed Mar 24, 2021).
- (6) Penczek, S.; Klosinski, P. *Models of Biopolymers Polymerization by*; Penczek, S., Ed.; CRC Press, 1990.
- (7) Fazel-rezai, R. *BIOMEDICAL ENGINEERING – FRONTIERS AND CHALLENGES Edited by Reza Fazel-Rezai*; 2011.
- (8) Hadjesfandiari, N.; Parambath, A. In *Engineering of Biomaterials for Drug Delivery Systems: Beyond Polyethylene Glycol*; Elsevier, 2018; pp 345–361.
- (9) Mracec, M.; Gruia, A.; Borota, A.; Curpan, R.; Halip, L.; Mracec, M. *Rev. Chim.* **2009**, *60* (5), 488–490.
- (10) Ghadiri, M. R.; Granja, J. R.; Milligan, R. A.; McRee, D. E.; Khazanovich, N. *Nature* **1994**, *372* (6507), 709.
- (11) Buriak, J. M.; Ghadiri, M. R. *Mater. Sci. Eng. C* **1997**, *4* (4), 207–212.
- (12) Valéry, C.; Paternostre, M.; Robert, B.; Gulik-Krzywicki, T.; Narayanan, T.; Dedieu, J.-C.; Keller, G.; Torres, M.-L.; Cherif-Cheikh, R.; Calvo, P.; Artzner, F. *Proc. Natl. Acad. Sci. U. S. A.* **2003**, *100* (18), 10258–10262.
- (13) Biles, J. E.; McNeal, T. P.; Begley, T. H.; Hollifield, H. C. *J. Agric. Food Chem.* **1997**, *45* (9), 3541–3544.
- (14) Hamley, I. W. *Angew. Chemie Int. Ed.* **2007**, *46* (43), 8128–8147.
- (15) Klug, A. *Angew. Chemie Int. Ed. English* **1983**, *22* (8), 565–582.
- (16) Allendorf, M. D.; Stavila, V. *CrystEngComm* **2015**, *17* (2), 229–246.
- (17) Douglas, S. M.; Dietz, H.; Liedl, T.; Högberg, B.; Graf, F.; Shih, W. M. *Nature* **2009**, *459* (7245), 414–418.
- (18) Seeman, N. C. *Structural DNA Nanotechnology*; Cambridge University Press: Cambridge, 2015; Vol. 22.
- (19) Seeman, N. C. *Mol. Biotechnol.* **2007**, *37* (3), 246–257.
- (20) Bui, H.; Díaz, S. A.; Fontana, J.; Chiriboga, M.; Veneziano, R.; Medintz, I. L.

- Adv. Opt. Mater.* **2019**, 7 (18), 1900562.
- (21) Seeman, N. C. *J. Theor. Biol.* **1982**, 99 (2), 237–247.
  - (22) Fu, T. J.; Seeman, N. C. *Biochemistry* **1993**, 32 (13), 3211–3220.
  - (23) Li, X.; Yang, X.; Qi, J.; Seeman, N. C. *J. Am. Chem. Soc.* **1996**, 118 (26), 6131–6140.
  - (24) Andersen, E. S.; Dong, M.; Nielsen, M. M.; Jahn, K.; Subramani, R.; Mamdouh, W.; Golas, M. M.; Sander, B.; Stark, H.; Oliveira, C. L. P.; Pedersen, J. S.; Birkedal, V.; Besenbacher, F.; Gothelf, K. V.; Kjems, J. *Nature* **2009**, 459 (7243), 73–76.
  - (25) Wei, B.; Dai, M.; Yin, P. *Nature* **2012**, 485 (7400), 623–626.
  - (26) Ke, Y.; Ong, L. L.; Shih, W. M.; Yin, P. *Science (80-. )*. **2012**, 338 (6111), 1177–1183.
  - (27) Seeman, N. C. *Nature* **2003**, 421 (6921), 427–431.
  - (28) Ke, Y.; Ong, L. L.; Shih, W. M.; Yin, P. *Science (80-. )*. **2012**, 338 (6111), 1177–1183.
  - (29) Edwardson, T. G. W.; Carneiro, K. M. M.; McLaughlin, C. K.; Serpell, C. J.; Sleiman, H. F. *Nat. Chem.* **2013**, 5 (10), 868–875.
  - (30) Niemeyer, C. M. *ChemInform* **2010**, 33 (13), no-no.
  - (31) Thordarson, P.; Le Droumaguet, B.; Velonia, K. *Appl. Microbiol. Biotechnol.* **2006**, 73 (2), 243–254.
  - (32) Lutz, J. F.; Börner, H. G. *Prog. Polym. Sci.* **2008**, 33 (1), 1–39.
  - (33) Veronese, F. M.; Pasut, G. *Drug Discov. Today* **2005**, 10 (21), 1451–1458.
  - (34) Abuchowski, A.; Van Es, T.; Palczuk, N. C.; Davis, F. F. *J. Biol. Chem.* **1977**, 252 (11), 3578–3581.
  - (35) Cabral, H.; Miyata, K.; Osada, K.; Kataoka, K. *Chem. Rev.* **2018**, 118 (14), 6844–6892.
  - (36) Wang, X.; Guerin, G.; Wang, H.; Wang, Y.; Manners, I.; Winnik, M. a. *Science (80-. )*. **2007**, 317 (5838), 644–647.
  - (37) Sakurai, S.; Momii, T.; Taie, K.; Shibayama, M.; Nomura, S.; Hashimoto, T. *Macromolecules* **1993**, 26 (3), 485–491.
  - (38) Discher, D. E.; Eisenberg, A. *Science (80-. )*. **2002**, 297 (5583), 967–973.
  - (39) Kwak, M.; Herrmann, A. *Angew. Chemie - Int. Ed.* **2010**, 49 (46), 8574–8587.
  - (40) Li, Z.; Zhang, Y.; Fullhart, P.; Mirkin, C. A. *Nano Lett.* **2004**, 4 (6), 1055–1058.
  - (41) Zhang, C.; Hao, L.; Calabrese, C. M.; Zhou, Y.; Choi, C. H. J.; Xing, H.; Mirkin, C. A. *Small* **2015**, 11 (40), 5360–5368.
  - (42) Chidchob, P.; Edwardson, T. G. W.; Serpell, C. J.; Sleiman, H. F. *J. Am.*

- Chem. Soc.* **2016**, *138* (13), 4416–4425.
- (43) *Amphiphilic Block Copolymers*; Alexandridis, P. ., Lindman, B., Eds.; Springer Berlin Heidelberg: Berlin, Heidelberg, 2016.
  - (44) Ida, S.; Ouchi, M.; Sawamoto, M. *J. Am. Chem. Soc.* **2010**, *132* (42), 14748–14750.
  - (45) Hibi, Y.; Ouchi, M.; Sawamoto, M. *Nat. Commun.* **2016**, *7*, 1–9.
  - (46) Eckardt, L. H.; Naumann, K.; Matthias Pankau, W.; Rein, M.; Schweitzer, M.; Windhab, N.; Von Kiedrowski, G. *Nature* **2002**, *420* (6913), 286.
  - (47) Li, X.; Zhan, Z. Y. J.; Knipe, R.; Lynn, D. G. *J. Am. Chem. Soc.* **2002**, *124* (5), 746–747.
  - (48) Rosenbaum, D. M.; Liu, D. R. *J. Am. Chem. Soc.* **2003**, *125* (46), 13924–13925.
  - (49) Niu, J.; Hili, R.; Liu, D. R. *Nat. Chem.* **2013**, *5* (4), 282–292.
  - (50) O'Reilly, R. K. *Nat. Chem.* **2013**, *5* (4), 252–253.
  - (51) Berthet, M. A.; Zarafshani, Z.; Pfeifer, S.; Lutz, J. F. *Macromolecules* **2010**, *43* (1), 44–50.
  - (52) Satoh, K.; Ozawa, S.; Mizutani, M.; Nagai, K.; Kamigaito, M. *Nat. Commun.* **2010**, *1* (1), 6.
  - (53) Yan, J. J.; Wang, D.; Wu, D. C.; You, Y. Z. *Chem. Commun.* **2013**, *49* (54), 6057–6059.
  - (54) Yu, L.; Wang, L.-H.; Hu, Z.-T.; You, Y.-Z.; Wu, D.-C.; Hong, C.-Y. *Polym. Chem.* **2015**, *6* (9), 1527–1532.
  - (55) Stayshich, R. M.; Meyer, T. Y. *J. Am. Chem. Soc.* **2010**, *132* (31), 10920–10934.
  - (56) Gosse, C.; Boutorine, A.; Aujard, I.; Chami, M.; Kononov, A.; Cogné-Laage, E.; Allemand, J.-F.; Li, J.; Jullien, L. *J. Phys. Chem. B* **2004**, *108* (20), 6485–6497.
  - (57) Li, J.; Rothstein, S. N.; Little, S. R.; Edenborn, H. M.; Meyer, T. Y. *J. Am. Chem. Soc.* **2012**, *134* (39), 16352–16359.
  - (58) Matyjaszewski, K.; Shigemoto, T.; Fréchet, J. M. J.; Leduc, M. *Macromolecules* **1996**, *29* (12), 2–6.
  - (59) Matyjaszewski, K.; Spanswick, J. *Mater. Today* **2005**, *8* (3), 26–33.
  - (60) Grishin, D. F.; Grishin, I. D. *Russ. J. Appl. Chem.* **2011**, *84* (12), 2021–2028.
  - (61) Richardson, R. A. E.; Guimaraes, T. R.; Khan, M.; Moad, G.; Zetterlund, P. B.; Perrier, S. *Macromolecules* **2020**, *53* (18), 7672–7683.
  - (62) Grishin, D. F.; Grishin, I. D. *Russ. J. Appl. Chem.* **2011**, *84* (12), 2021–2028.
  - (63) Merrifield, R. B. *J. Am. Chem. Soc.* **1963**, *85* (14), 2149–2154.

- (64) Jung, G.; Beck-Sickinger, A. G. *Angew. Chemie Int. Ed. English* **1992**, 31 (4), 367–383.
- (65) Beaucage, S. L.; Iyer, R. P. *Tetrahedron* **1992**, 48 (12), 2223–2311.
- (66) Badi, N.; Lutz, J. F. *Chem. Soc. Rev.* **2009**, 38 (12), 3383–3390.
- (67) Solleder, S. C.; Schneider, R. V.; Wetzels, K. S.; Boukis, A. C.; Meier, M. A. R. *Macromol. Rapid Commun.* **2017**, 38 (9), 2017.
- (68) Paquin, F.; Rivnay, J.; Salleo, A.; Stingelin, N.; Silva, C. J. *Mater. Chem. C* **2015**, 3 (June 2014), 10715–10722.
- (69) Chaubal, M. V.; Wang, B.; Su, G.; Zhao, Z. *J. Appl. Polym. Sci.* **2003**, 90 (14), 4021–4031.
- (70) Maiboroda, V. D.; Datskevich, L. A. *Polym. Sci. U.S.S.R.* **1964**, 6 (10), 2113–2117.
- (71) Liu, Y.; Yan, N.; Li, F.; Chen, P. *Polym. Int.* **2013**, 62 (3), 390–396.
- (72) Imai, Y.; Sato, N.; Ueda, M. *Die Makromol. Chemie, Rapid Commun.* **1980**, 1 (7), 419–422.
- (73) Westheimer, F. H. *Science* **1987**, 235 (1), 1173–1178.
- (74) Zhang, S.; Zou, J.; Zhang, F.; Elsabahy, M.; Felder, S. E.; Zhu, J.; Pochan, D. J.; Wooley, K. L. *J. Am. Chem. Soc.* **2012**, 134 (44), 18467–18474.
- (75) Gustafson, T. P.; Lonneck, A. T.; Heo, G. S.; Zhang, S.; Dove, A. P.; Wooley, K. L. *Biomacromolecules* **2013**, 14 (9), 3346–3353.
- (76) Wang, Y. C.; Yuan, Y. Y.; Du, J. Z.; Yang, X. Z.; Wang, J. *Macromolecular Bioscience*. 2009, pp 1154–1164.
- (77) Zhang, K.; Wu, K.; Zhang, Y.-K.; Liu, H.-F.; Shen, M.-M.; Hu, W. *Polym. Plast. Technol. Eng.* **2013**, 52 (5), 525–532.
- (78) Minegishi, S.; Komatsu, S.; Kameyama, A.; Nishikubo, T. *J. Polym. Sci. Part A Polym. Chem.* **1999**, 37 (7), 959–965.
- (79) Appukutti, N.; Serpell, C. J. *Polym. Chem.* **2018**, 9 (17), 2210–2226.
- (80) Katz, R. S. *Eur. J. Polit. Res. Polit. Data Yearb.* **2015**, 54 (1), 309–315.
- (81) Lapienis, G.; Penczek, S. *Macromolecules* **1974**, 7 (2), 166–174.
- (82) Tang, Ben Zhong, A. S. A.-E.-A. *Phosphorus-Based Polymers*; Monge, S., David, G., Eds.; Polymer Chemistry Series; Royal Society of Chemistry: Cambridge, 2014; Vol. 1.
- (83) Busch, H.; Majumder, S.; Reiter, G.; Mecking, S. *Macromolecules* **2017**, 50 (7), 2706–2713.
- (84) Kazanskii, K.; Kuznetsova, V.; Pretula, J.; Penczek, S. *Polym. Gels Networks* **1996**, 4 (4), 335–349.
- (85) Steinbach, T.; Ritz, S.; Wurm, F. R. *ACS Macro Lett.* **2014**, 3 (3), 244–248.

- (86) Huang, S.-W.; Wang, J.; Zhang, P.-C.; Mao, H.-Q.; Zhuo, R.-X.; Leong, K. W. *Biomacromolecules* **2004**, 5 (2), 306–311.
- (87) Libiszowski, J.; Kałużynski, K.; Penczek, S. *J. Polym. Sci. Polym. Chem. Ed.* **1978**, 16 (6), 1275–1283.
- (88) Zhai, X.; Huang, W.; Liu, J.; Pang, Y.; Zhu, X.; Zhou, Y.; Yan, D. *Macromol. Biosci.* **2011**, 11 (11), n/a-n/a.
- (89) Khorana, H. G.; Razzell, W. E.; Gilham, P. T.; Tener, G. M.; Pol, E. H. *J. Am. Chem. Soc.* **1957**, 79 (4), 1002–1003.
- (90) KHORANA, H. G. In *Reflections on Biochemistry*; Elsevier, 1976; Vol. 109, pp 273–281.
- (91) Letsinger, R. L.; Finnan, J. L.; Heavner, G. A.; Lunsford, W. B. *J. Am. Chem. Soc.* **1975**, 97 (11), 3278–3279.
- (92) Letsinger, R. L.; Lunsford, W. B. *J. Am. Chem. Soc.* **1976**, 98 (12), 3655–3661.
- (93) Tsou, K. C.; Yip, K. F. *J. Macromol. Sci. Part A - Chem.* **1973**, 7 (5), 1097–1116.
- (94) Beaucage, S. L.; Caruthers, M. H. *Tetrahedron Lett.* **1981**, 22 (20), 1859–1862.
- (95) Berndl, S.; Herzig, N.; Kele, P.; Lachmann, D.; Li, X.; Wolfbeis, O. S.; Wagenknecht, H.-A. *Bioconjug. Chem.* **2009**, 20 (3), 558–564.
- (96) Defrancq, E.; Singh, Y.; Spinelli, N. *Curr. Org. Chem.* **2008**, 12 (4), 263–290.
- (97) Kayushin, A.; Demekhina, A.; Korosteleva, M.; Miroshnikov, A.; Azhayev, A. *Nucleosides, Nucleotides and Nucleic Acids* **2011**, 30 (7–8), 490–502.
- (98) Bikard, D.; Loot, C.; Baharoglu, Z.; Mazel, D. *Microbiol. Mol. Biol. Rev.* **2010**, 74 (4), 570–588.
- (99) Pils, W.; Micura, R. *Nucleic Acids Res.* **2000**, 28 (9), 1859–1863.
- (100) Hariharan, M.; Siegmund, K.; Saurel, C.; McCullagh, M.; Schatz, G. C.; Lewis, F. D. *Photochem. Photobiol. Sci.* **2014**, 13 (2), 266–271.
- (101) Carneiro, K. M. M.; Avakyan, N.; Sleiman, H. F. *Wiley Interdiscip. Rev. Nanomedicine Nanobiotechnology* **2013**, 5 (3), 266–285.
- (102) Kamps, A. C.; Cativo, M. H. M.; Chen, X. J.; Park, S. J. *Macromolecules* **2014**, 47 (11), 3720–3726.
- (103) Al Ouahabi, A.; Kotera, M.; Charles, L.; Lutz, J.-F. *ACS Macro Lett.* **2015**, 4 (10), 1077–1080.
- (104) Al Ouahabi, A.; Charles, L.; Lutz, J.-F. *J. Am. Chem. Soc.* **2015**, 137 (16), 5629–5635.
- (105) Guichard, G.; Huc, I. *Chem. Commun.* **2011**, 47 (21), 5933.
- (106) Li, X.; Yang, D. *Chem. Commun.* **2006**, 32, 3367–3379.

## Chapter 2

### 2 Self-assembly and folding of sequence defined polyphosphoesters.

Portions of the work in this Chapter have been published as “Sequence isomerism in uniform polyphosphoesters programmes self-assembly and folding” by Nadeema Appukutti, Joseph R. Jones and Christopher J. Serpell in April 2020 Chemical Communications (5307-5310)

#### 2.1 Introduction

The research covered in this chapter concerns design and synthesis of sequence-defined completely non-nucleosidic copolymers, and their self-assembly in aqueous media.

DNA is a fascinating sequence-defined polymer found in biology. Among many available approaches, routine DNA synthesis is currently based on phosphoramidite chemistry. The methods used in solid-phase DNA synthesis have quickly been extended to other building blocks, besides DNA, and researchers can now incorporate a wide variety of molecules as ‘insertions’ into any given DNA sequence using phosphoramidite derivatives.<sup>1-4</sup> This progress in DNA synthesis has laid the foundation for the synthesis of DNA-amphiphile hybrids and has significant influence in synthetic DNA assembly. Amphiphilic self-assembly can create well-defined nanostructures using a completely different set of interactions to structural DNA nanotechnology. These two types of interactions can introduce the capability of block copolymers for long-range self-assembly into DNA system. For this reason,



the combination of the two orthogonal approaches provides a powerful platform with great opportunities for novel, useful and dynamic nanotechnology.

Solution-phase conjugations of DNA to hydrophobic polymers requires end-to-end coupling of a highly hydrophilic and charged DNA strand with a hydrophobic polymer chain, resulting in sub-optimal yields. Additionally, in such methods, the polymer block is usually synthesised first through traditional polymerisation methods, with resultant dispersity, prior to its transformation into a phosphoramidite and conjugation to the DNA. This results in DNA amphiphiles that display molecular weight variation and structural dispersity which often translate to the overall assembly. In contrast, the solid phase approach to DNA amphiphile synthesis has allowed access to a wide variety of linear and branched DNA amphiphiles.

Sleiman and co-workers reported a solid-phase approach for synthesising monodisperse dendritic alkyl-DNA conjugates in high yields using commercially available starting materials.<sup>5</sup> Later they used stepwise solid-phase synthesis to prepare monodisperse, sequence-defined DNA-polymer conjugates<sup>4</sup> (**Error! Reference source not found.**). They used classic phosphoramidite chemistry which has also been applied in the synthesis of other DNA conjugates such as oligopyrenotide<sup>6</sup>, oligonucleotide oligospermine<sup>7</sup> and glycol-conjugates<sup>8</sup> appended to DNA. The researchers employed hydrophilic hexa(ethylene glycol) blocks and hydrophobic hexa(ethylene), or C12, blocks are commercially available as the corresponding dimethoxytrityl (DMT) protected phosphoramidites. Varying the number or sequence of the obtained oligomers up to twelve attached blocks they have finely tuned the hydrophobicity<sup>4</sup>. Additionally, the self-assembly and the influence of the attached oligomers on the formation of higher order three-dimensional structures was studied. In another approach, the use of perfluorocarbon

containing phosphoramidites for DNA strand synthesis, which was referred to as “DNA-teflon” also demonstrated by the Sleiman group.<sup>9</sup> Two phosphoramidite building blocks bearing either hexa(ethylene glycol) or perfluorinated side chains were used to synthesis non-natural polymers. The desired copolymers were formed with two building blocks coupled by automated phosphoramidite chemistry on a DNA synthesiser. The self-assembly of the “DNA-teflon” was investigated by dynamic light scattering (DLS) and atomic force microscopy, whereby spherical micelles with a perfluorocarbon core and DNA corona and narrow size distribution were observed.

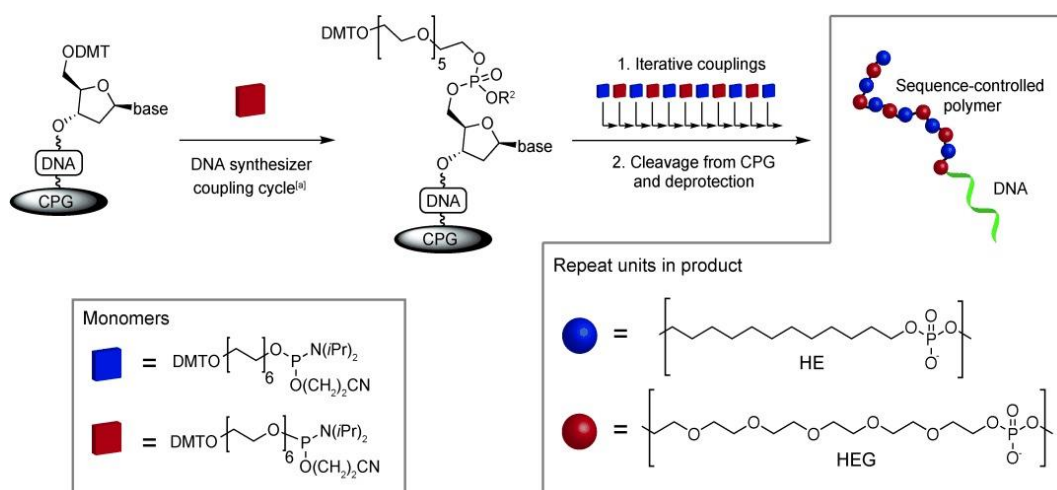


**Figure 2.1** Solid-phase synthetic route to generate sequence-defined DNA-polymer conjugates described by Sleiman and co-workers. Adapted with permission from reference (Nat. Chem. 2013)<sup>4</sup>

DNA amphiphiles self-assemble into several morphologies due to phase separation of their hydrophilic and hydrophobic components. The range of accessible morphologies can also be tailored by varying the ratio of hydrophilic to hydrophobic blocks. Spherical particles are the most common geometry obtained for self-assembled DNA amphiphiles. Many DNA amphiphiles have been observed to form

spherical micelles with diameters ranging from 5-50 nm.<sup>4,10–12</sup> In addition to spherical geometries, hollowed vesicles, and one-dimensional rod-shaped assemblies (3D structures extended in one dimension) have also been obtained from DNA amphiphiles.<sup>13–16</sup> DNA amphiphiles have shown great promise as drug delivery vehicles, either by incorporating small molecule drug agents or using the oligonucleotide portion as the therapeutic itself.

In 2018 Sleiman's group reported the discovery of site-specific introduction of a single cyanine dye (Cy3) molecule into sequence-controlled DNA amphiphiles results in a complete morphological switch from spheres to 1D fibres.<sup>17</sup> The Cy3-modified DNA-polymer conjugate was synthesised, which consisted of a 19mer DNA segment at one end, attached to 12 hexaethylene (HE) units, to which one or two units of Cy3 dye were appended at the opposite end (Cy3-HE<sub>12</sub>-DNA and Cy3Cy3-HE<sub>12</sub>-DNA). The strands were synthesised by solid-phase synthesis using phosphoramidite chemistry (Figure 2.2).

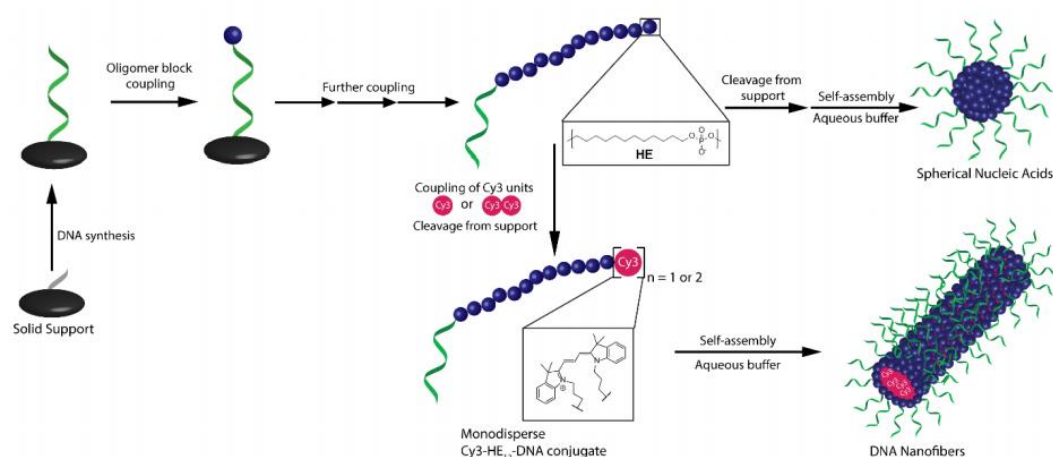


**Figure 2.2** Synthesis of sequence-controlled Cy3-HE<sub>12</sub>-DNA or Cy3Cy3-HE<sub>12</sub>-DNA conjugates and their self-assembly behaviour. Adapted with permission from reference (Am. Chem. Soc. 2018).<sup>17</sup>

Lutz and co-workers have developed several systems that result in sequence-defined oligomers for aiming at encoded macromolecular sequences for data storage. In a first approach, the synthesis of phosphoramidite oligomers was conducted using a cross-linked polystyrene solid support, that provided the highly efficient and well established and optimised phosphoramidite coupling.<sup>18</sup> Non-natural phosphoramidite monomers were defined as 0, 1, and 1' to encode the oligomers.

By performing the coupling reactions manually, sequence defined oligomers with lengths between pentamers up to 24mers were achieved. The polymers allowed for post-synthetic modification by copper-catalysed azide-alkyne cycloaddition (CuAAC) as terminal alkyne functions were incorporated. As a proof of principle, PEGylation of the polyphosphates was performed. The protocol was later extended by automating the coupling using a DNA synthesiser to obtain polymers with more than 100 monomers.<sup>19</sup> Three to twelve hours of relatively short times was taken for the process with high coupling efficiencies depending on the length of the sequences.

Even though many achievements towards DNA-polymer conjugates had been made in the literature, it is a great challenge to create completely non-natural DNA amphiphile inspired macromolecules with a well-defined sequence.

In comparison to DNA-polymer conjugates, sequence-defined, completely non-natural polymers can have an even broader range of sequence and backbone diversity as well as unlimited functional sidechains. Following the protein blueprint, sequence-defined polymers are perfect platform for generating extensive structural complexity, such as self-assembly into nanostructures, folding, the formation of stimuli-responsive sites, catalytic sites, and so on. This kind of synthesis approach

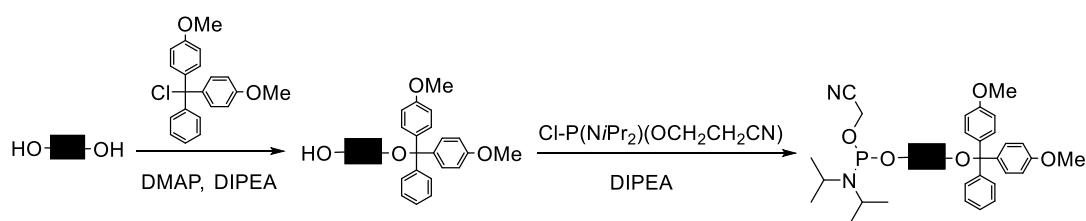
has been the subject of polymer, and materials science for several years. However, achieving absolute control over the primary structure in non-natural polymers is still challenging.

In this chapter, application of solid-phase phosphoramidite synthesis, commonly used to make DNA, in the creation of completely non-natural polymer with hydrophobic and hydrophilic units, i.e. designed for self-assembly, will be briefly discussed. This chapter then covers the behaviour of the sequenced systems in aqueous media.

## 2.2 Result and discussion.

### 2.2.1 Non nucleosidic monomer synthesis

The general approach of creation of reagents for solid phase phosphoramidite chemistry is to produce them from diols in two steps (Scheme 2.1). The reagents were chosen to give simple hydrophilic and hydrophobic unfunctionalized systems. Bisphenol A (BPA) and 1,12-dodecanediol chosen to give hydrophobic motifs and tetra ethylene glycol (TEG) was used as hydrophilic unit.

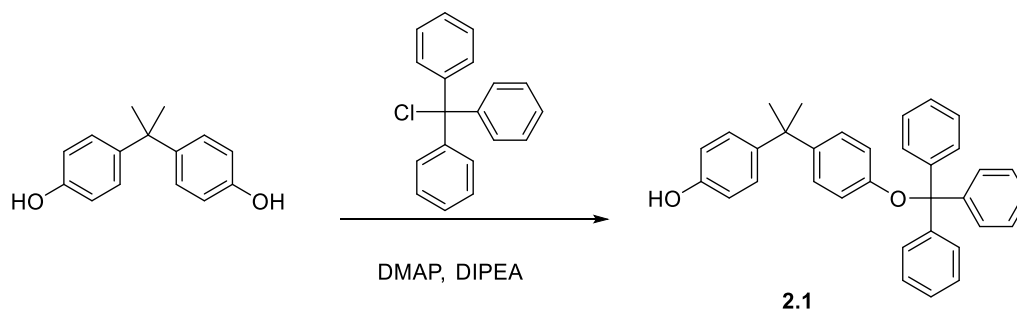


**Scheme 2.1** Synthesis of phosphoramidite reagent compatible with phosphoramidite solid phase synthesis using a diol as the starting material: mono-protection of diol with DMT-Cl followed by the phosphoramidite activation.

One of the hydroxyl groups of the diols was protected by reacting with 4,4'-dimethoxytrityl chloride (DMT-Cl). Several advantages can be envisioned for the

use of the 4,4'-dimethoxytrityl group as a hydroxyl protecting moiety: low cost and readily available as pure 4,4'-dimethoxytrityl chloride (DMT-Cl), and selective deprotection (which is vital in oligonucleotide synthesis because of the trityl monitor). The remaining alcohol was reacted with 2-cyanoethyl *N,N*-diisopropylchlorophosphoramidite under dry, O<sub>2</sub>-free, conditions to give the activated reagent.

Commercially purchased BPA was reacted with DMT following Scheme 2.2. The BPA dissolved in dry DCM was combined with 4-dimethyl aminopyridine (DMAP). DMT-Cl was then added, followed by the dropwise addition of *N,N*-diisopropylethylamine (DIPEA) over a period of 30 minutes. The reaction was stirred for 20 hours and then solvent was removed to obtain a brownish solid product with 43% yield. The completion of the reaction was confirmed with the TLC comparison with reactant and the final reaction mixture. The product was then purified using silica column chromatography (DCM: MeOH - 400:1). The obtained white coloured product changed into orange during the chromatography process. The collected fractions from the column chromatography were compared with the starting materials and unfortunately there was no new product isolated from the process. When bound to a molecule, DMT doesn't have much of a colour, but when it's removed with acid, the resulting solution of dimethoxy trityl cation has a brilliant orange colour. The observed colour suggest that the protecting group is falling off. The procedure was repeated several times, with the same result. Trityl ethers are acid labile and as silica is slightly acidic, and the phenolic alcohol is a better leaving group than an aliphatic alcohol, this might be resulting in premature DMT deprotection during the purification process. The synthesis was repeated with trityl chloride instead of DMT-Cl as protecting group which is a less labile to weak acids.



**Scheme 2.2** Mono protection of BPA with trityl chloride.

The mono-protection was successfully achieved with trityl chloride following the same procedure (Scheme 2.2) and the purification was carried out *via* column chromatography using basic alumina to avoid the acidic environment. The product **2.1** was purified via column chromatography (DCM: MeOH: Hexane-500:1:1) yielding the desired product as a white powder with 43% yield and product was confirmed by  $^1\text{H}$  NMR (Figure 2.3) which is good considering the statistical nature of the reaction places a theoretical maximum yield of 50% for the monoprotected form.

To create a BPA phosphoramidite, mono-protected BPA **2.1** was then reacted with chlorophosphoramidite reagent in a 1:1 ratio (Scheme 2.3). The chlorophosphoramidite reagent is highly sensitive to oxygen, hence the synthesis was carried out in under inert condition to avoid the oxidising the reagent or the product.

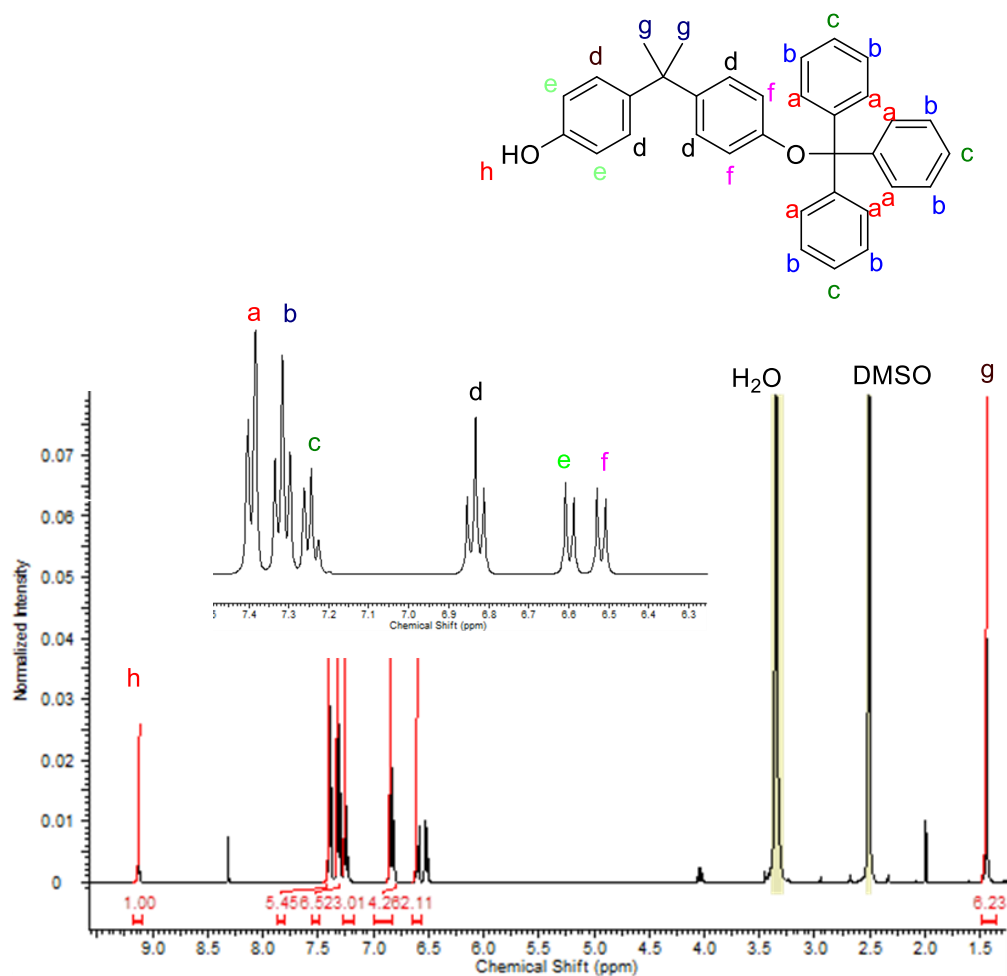
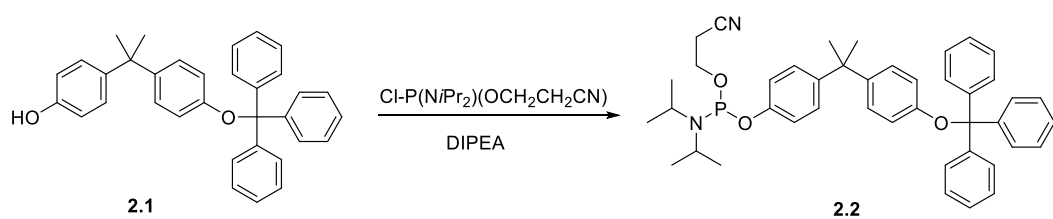


**Figure 2.3**  $^1\text{H}$  NMR of trityl protected BPA recorded in DMSO.



**Scheme 2.3** Synthesis of BPA phosphoramidite reagent.



The reaction of monoprotected BPA with the chlorophosphoramidite reagent was successfully complete and the product **2.2** was purified with an alumina plug. The product was vacuumed dried and stored connected to nitrogen gas to avoid oxidation. Obtained white product gave 32% yield and,  $^1\text{H}$  NMR was recorded in DMSO (Figure 2.4).  $^{31}\text{P}$  NMR is an excellent technique for studying phosphorus containing compounds and  $^{31}\text{P}$  NMR are typically report phosphoric acid (P(V)) around 0 ppm and trivalent (P(III)) phosphorous compound shift around 140 ppm. The observed peak at 140 ppm on the  $^{31}\text{P}$  NMR spectrum (Figure 2.5) confirmed the product as a phosphite-triester which was not oxidised during the purification process.

The synthesis of mono protected C12 and TEG diols derivatives were then attempted following the same procedure. Unfortunately, both C12 and TEG mono-protections failed to proceed regardless of multiple attempts.

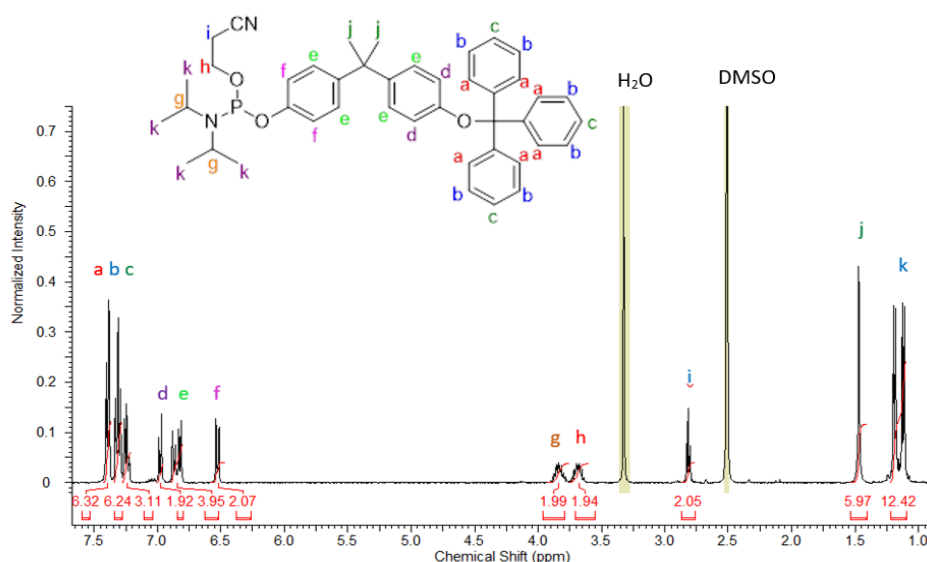


**Figure 2.4**  $^1\text{H}$  NMR of BPA phosphoramidite reagent recorded in DMSO.

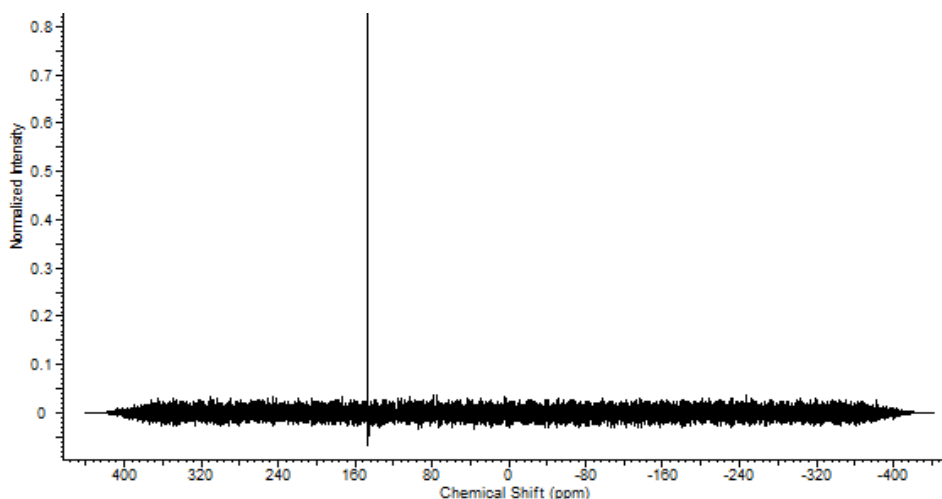


**Figure 2.5**  $^{31}\text{P}$  NMR of BPA phosphoramidite reagent recorded in DMSO.

### 2.2.2 Synthesis of BPA-phosphate oligomers

The synthesised BPA phosphoramidite reagent **2.2** was kept in oxygen free environment to avoid the oxidation until used in solid phase synthesis using an automated DNA synthesiser. The synthesis was adapted from the typical DNA synthesis protocol. The synthesis cycle is illustrated in Figure 2.6 (a) and contains four steps: (i) deprotection of the dimethoxytrityl group; (ii) coupling with a phosphoramidite unit; (iii) capping the strands that failed to undergo coupling and; (iv) oxidation of phosphorus (III) to more stable phosphorus (V). Perfect strands can be obtained after base-mediated deprotection and cleavage from solid support followed by purifications. The coupling step time was extended (600s) relative to standard DNA synthesis (30s) to improve the coupling efficiency and maximise product yield. Synthesis was performed on a 1  $\mu\text{mole}$  scale, starting from the required 1000Å CPG solid support. The efficiency was monitored by UV absorption of outgoing DMT cation. The trityl monitor detects the DMT (dimethoxytrityl) group as it is removed during the deblocking step. During synthesis, the trityl

information is displayed as a histogram on the instrument. In the event of a failure in the coupling chemistry, the trityl monitor shows it on histogram as a missing bar.

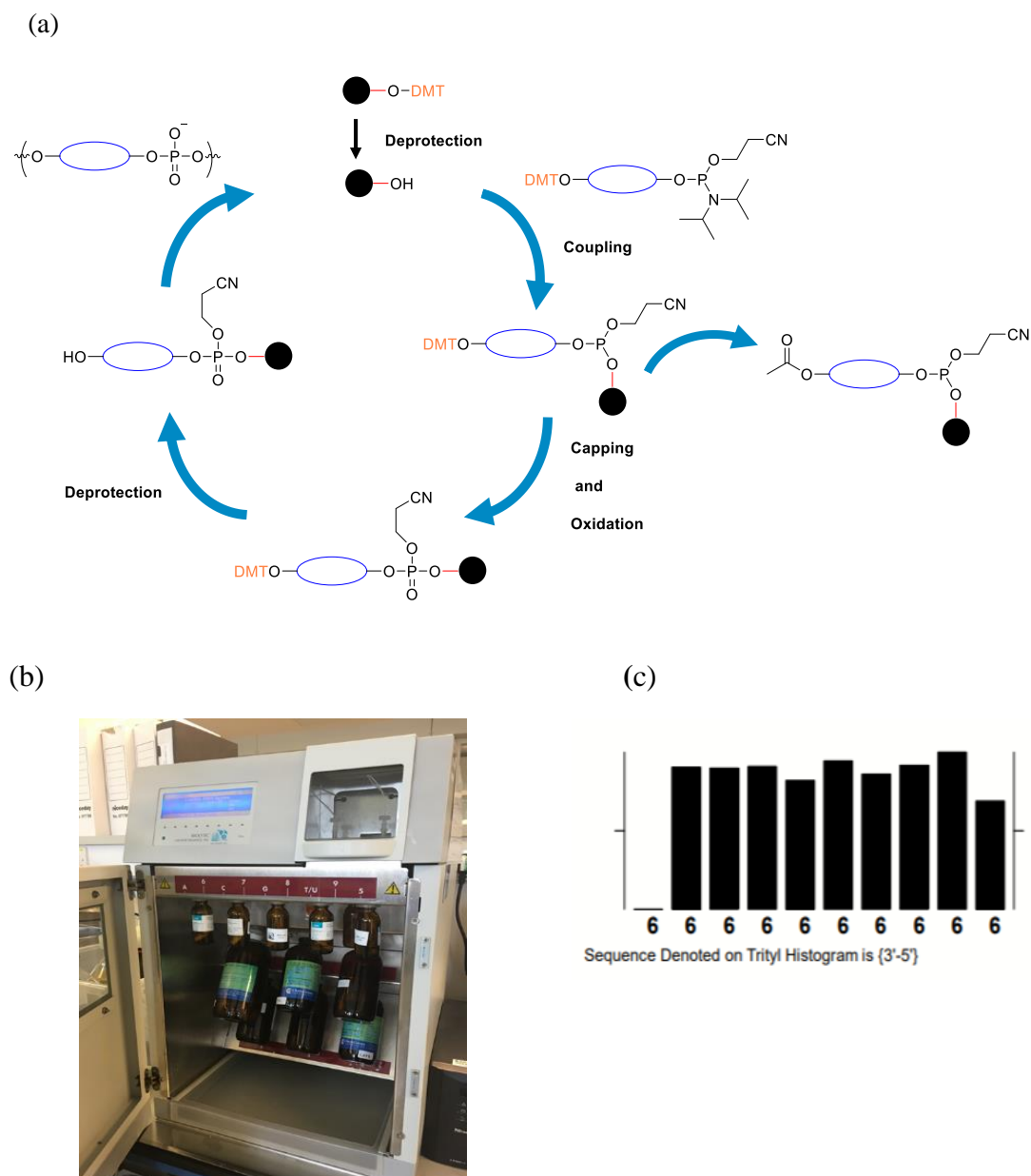


**Figure 2.6** (a) The phosphoramidite non-nucleosidic oligomer synthesis cycle (b) DNA synthesiser (c) Trityl histogram of BPA oligomer (failed at 11<sup>th</sup> coupling).

A 20-unit long BPA polymer synthesis was attempted using automated solid phase synthesiser but failed at the eleventh coupling (Figure 2.6 (c)). The BPA11 polymer was then cleaved and deprotected with ammonium hydroxide at 60 °C. The

purification was conducted by the ethanol precipitation method by adding 100  $\mu$ L of 3M sodium acetate, 500  $\mu$ L of 5M ammonium acetate and 2 mL of 100% ethanol to the polymer product. The mixture was then frozen overnight at -20 °C. This process is commonly used technique for concentrating and de-salting nucleic acids preparations in aqueous solution. With the backbone similarity the synthesised BPA11 was expected to behave similarly, however the pellet did not form as expected after centrifuging the mixture at full speed

#### 2.2.2.1 Electrophoretic mobility assays

Electrophoresis through agarose or polyacrylamide gels is commonly used to separate, identify, and purify nucleic acid fragments and proteins. The technique is simple, rapid to perform and capable of resolving fragments of DNA and/or RNA. Polyacrylamide gel electrophoresis (PAGE) is used as electrically neutral matrix to separate double-stranded DNA fragments according to size and single-stranded DNA according to size and conformation. Polyacrylamide gels are more effective than agarose gels in separating small fragments.

Denaturing Polyacrylamide Gel Electrophoresis (PAGE) was carried out for the sample at room temperature for 30 minutes at 250 V. Standard A<sub>20</sub> DNA sample was used as the reference. The DNA bands were visualised by incubation with Stains-All®.

The cationic dye Stains-All® visualizes the bands differently depending on its contact to other molecules: RNA stained blueish-purple, whereas DNA is stained blue and proteins staining red. This is an ideal dye for the visualization and identification of proteins on polyacrylamide gels because it differentiates between highly acidic proteins which stain blue and less acidic proteins which stain pink.

Stains-All® was selected as the first choice because of its ability to stain a variety of biopolymers, with the added benefit of multicolour readout.

The **BPA<sub>11</sub>** sample was observed as two bands on the poly acrylamide gel (Figure 2.7). A<sub>20</sub> nucleic acid was used as reference and both A<sub>20</sub> and the **BPA<sub>11</sub>** bands were bluish-purple in colour. The two bands may have appeared due to the coupling failure in the middle of the cycle, causing oligomers with two different lengths. The synthesis process was repeated a couple of times, and with the repetition the monomer synthesis yield got better. However, when the new batch of purified phosphoramidite reagent was employed in the automated solid phase synthesis process the coupling failed at the very start.

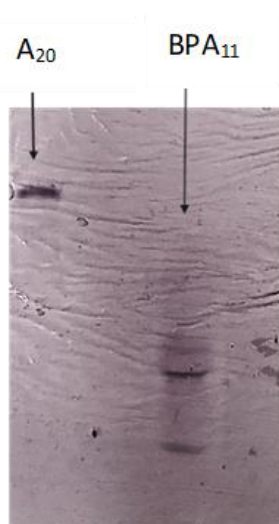


**Figure 2.7** Denaturing polyacrylamide gel electrophoresis (20%) showing the product BPA oligomer.

### 2.2.3 C12-HEG sequence isomers system

To more rapidly construct a scalable and highly monodisperse hydrophobic-hydrophilic systems, two monomers, commercially available as DMT protected phosphoramidite reagents, were purchased. To provide the hydrophobic motifs to

polymers chain, dodecane diol (**C12**) was selected and hexaethylene glycol (**HEG**) was picked as the hydrophilic unit.

**C12** and **HEG** monomers were transformed into polymers using automated solid-phase phosphoramidite chemistry. This approach offered monodisperse polymers in high yields and provided control over the length and sequence of the monomer units in the final structure. Success of the synthesis was observed with the trityl graphs (Figure 2.10 (b)). The final DMT was left on the strand due to the lack of UV-active groups in the final polymer which would enable UV quantification. The strands were then cleaved from the CPG support, cyanoethyl-deprotected using ammonium hydroxide, and purified *via* size exclusion chromatography. The DMT groups were then cleaved using 4 : 1 acetic acid : water. The optical absorption of the removed DMT at 500 nm was used to quantify the product, through comparison against a standard curve (using DMT-Cl) to obtain yields. The **C12-HEG** polymers expected to have near-perfect sequence control and minimal dispersity as the solid-phase synthesis provides a stepwise yield of up to 99.5%. The first approach was taken by creating 20mers of **C12** and **HEG** in a 1:1 ratio. Four different sequence patterns were initially planned to create with **C12** and **HEG** units illustrated in Figure 2.8.

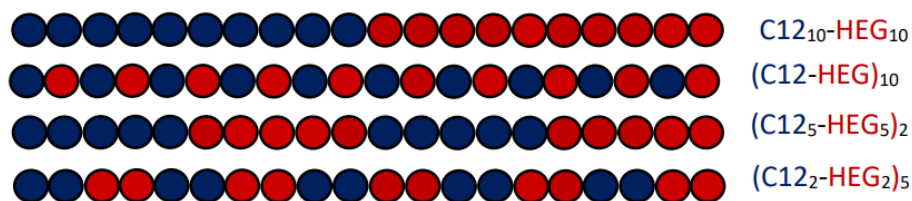


**Figure 2.8** Designed sequence patterns for **C12-HEG** oligomers.

The synthesis was conducted on a 1  $\mu\text{mol}$  scale, and the diblock arrangement **C12<sub>10</sub>-HEG<sub>10</sub>** and alternating **(C12-HEG)<sub>10</sub>** sequences were successfully synthesised using the same method reported in previous section (Figure 2.9). However, the **(C12<sub>5</sub>-HEG<sub>5</sub>)<sub>2</sub>** and **(C12<sub>2</sub>-HEG<sub>2</sub>)<sub>5</sub>** sequences proved more difficult to generate. **C12<sub>10</sub>-HEG<sub>10</sub>** diblock sequence showed an apparent yield of 116% and **(C12-HEG)<sub>10</sub>** showed a yield 59%, relative to the expected 1  $\mu\text{mol}$  maximum yield based upon the quoted loading of the solid support. The yield for **C12<sub>10</sub>-HEG<sub>10</sub>** showed more than 100%: this might be due to weighing, pipetting, and calibration-related errors. It has previously been found that the stepwise coupling tends to decrease when the incoming monomer was different from the preceding one.<sup>4</sup> This pattern can be observed here too, with the alternating polymer giving lower yield than the diblock sequence.

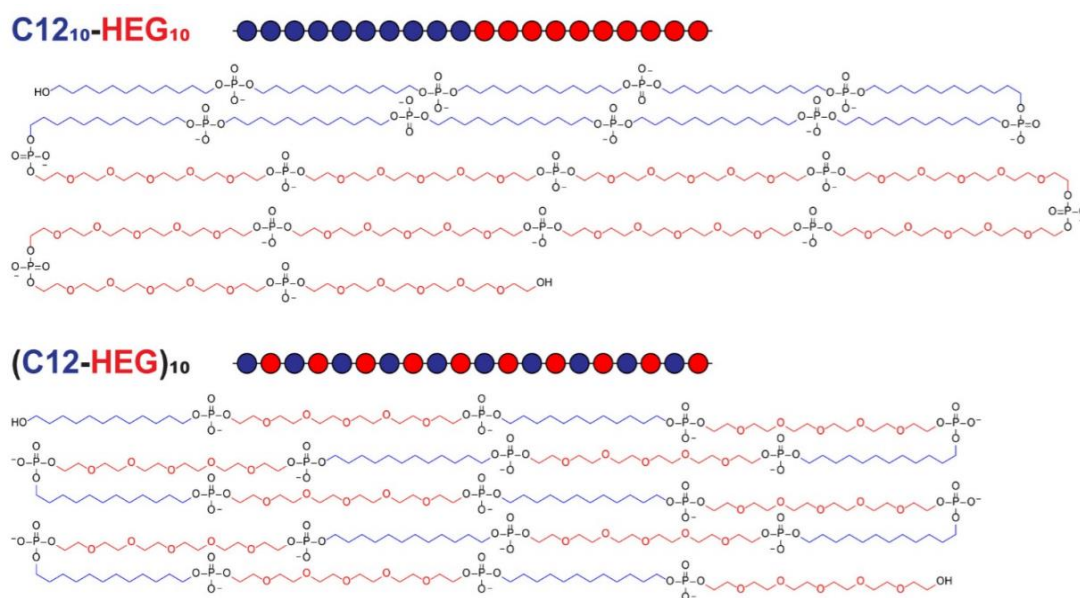


**Figure 2.9** Chemical structures of **C12<sub>10</sub>-HEG<sub>10</sub>** and **(C12-HEG)<sub>10</sub>**

As the synthesis progresses displayed histogram on the instrument shows consistence synthesis with the similar height bars. The successful synthesis was confirmed with gel electrophoresis. Initially, Stains-All® was used for visualising the band on the gel, as had proved successful for the BPA oligomer. However, no bands were observed for the **C12/HEG** samples after incubating with the stain for one hour. Despite allowing the gel to incubate in the stain overnight, the bands were still not seen on the gel. Next, SYBR safe, which is more sensitive towards DNA, was used as the stain, and also failed. Both Stains-All and SYBR safe are cyanine dyes and are able to interact with DNA by intercalation.<sup>20</sup> Taking into account that the **C12/HEG** primary structures have no aromatic units with which stacking interactions akin to intercalation could occur, cyanine dyes might not be the best choice of staining for gel staining. Methylene blue is commonly used as a nucleic acid stain and it does not intercalate in nucleic acid chains, instead operating primarily electrostatically.<sup>21</sup> Thus, use of methylene blue was found to be preferable to intercalating dyes for staining. The bands were visualised after incubating with methylene blue in water for approximately 15 min (Figure 2.10 (c)). DNA (20mer) was used as the reference and small differences observed for non-nucleosidic sequences in gel mobility related to the sequence of DNA strands are due to their small molecular weight difference. With the several attempts taken for the 20% polyacrylamide gel and staining, it is found that to visualise the bands on the gel, it was necessary to load a much greater quantity of the polymer (1 nmol) onto polyacrylamide gels than would be needed for DNA (10 pmol). The mono-isotopic mass of 6021 m/z was confirmed for the sequences with mass spectrometry (Figure 2.11 and Figure 2.12).



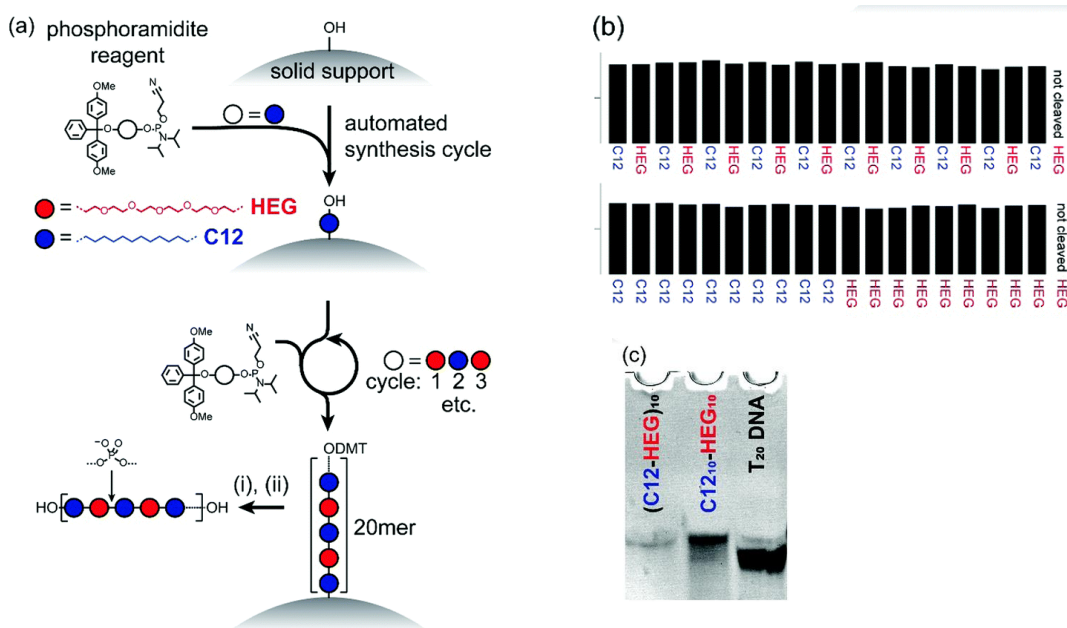


**Figure 2.10** (a) Synthesis of sequence-defined polyphosphodiester. (b) Trityl histograms showing successful synthesis. (c) Denaturing polyacrylamide gel electrophoresis (20%) showing single products ( $M_w = 6021 \text{ g mol}^{-1}$ ). T<sub>20</sub> DNA ( $M_w = 6019 \text{ g mol}^{-1}$ ) is provided as a molar mass comparison.

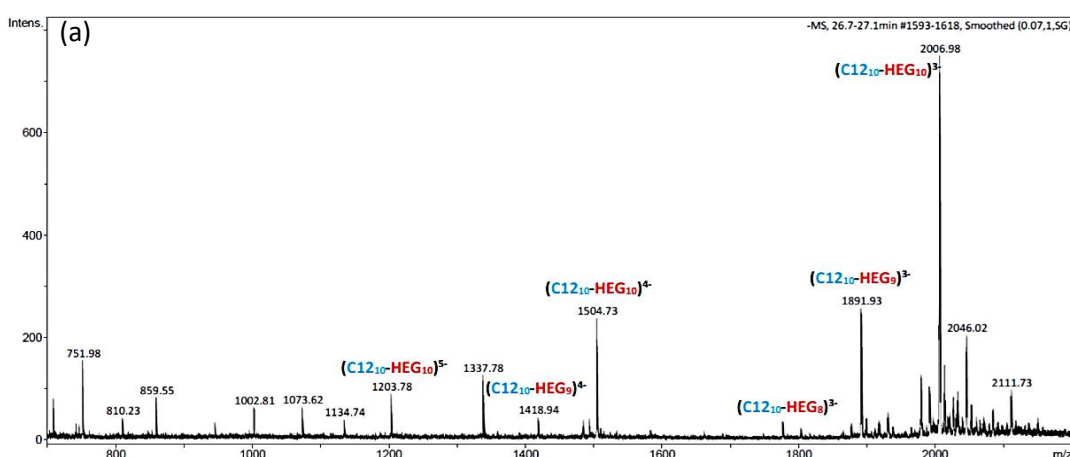


**Figure 2.11** Mass spectrum of C12<sub>10</sub>-HEG<sub>10</sub>, with expansions of the triply and quadruply charged peaks corresponding to a monoisotopic mass of 6020.93 Da (calculated exact mass is 6020.77 Da).

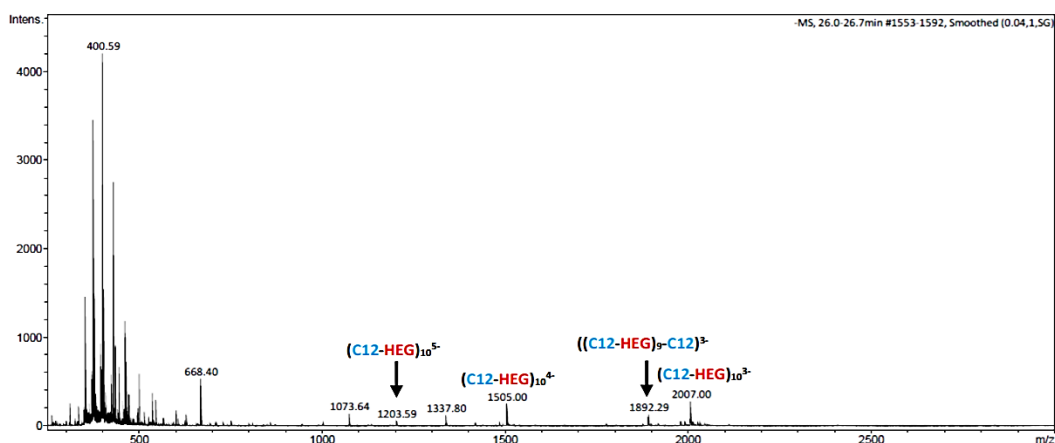


**Figure 2.12** Mass spectrum of (C12-HEG)<sub>10</sub>, with expansions of the triply and quadruply charged peaks corresponding to a monoisotopic mass of 6021.00 Da (calculated exact mass is 6020.77 Da).

The sequence of the hydrophobic hexaethylene (**C12**) blocks and hydrophilic hexaethylene glycol (**HEG**) blocks were expected to influence the self-assembly and folding motifs of polymer strands. The polymers were self-assembled in tris-acetate magnesium acetate buffer (TAMg, containing 12.5 mM Mg<sup>2+</sup>). Cations, and particular divalent cations such Mg<sup>2+</sup> greatly affect the structure and stability of DNA structures. The Mg<sup>2+</sup> ions interact with non-bridging oxygen of the phosphate groups and stabilize the self-assembly of duplexes and other structures by blocking the electrostatic repulsion between phosphate groups. Therefore, TAMg buffer was used for the investigation of the effect of block pattern on the amphiphilic self-assembly in solution. The polymers were also screened in (TBE, tris-borate EDTA) buffer. Since EDTA is a chelating agent, TBE buffer was used as the second buffer to study the self-assembly because it provides an Mg<sup>2+</sup> free environment which can use as a control for TAMg buffer self-assembly. The self-assembly behaviour of block copolymer **C12<sub>10</sub>-HEG<sub>10</sub>** was expected to show similar self-

assembly to DNA amphiphiles and investigations were carried out to confirm whether the phosphate-punctuated **C12** and **HEG** would behave as an amphiphile.

#### 2.2.3.1 Self-assembly of sequence isomers in TBE buffer

Dynamic light scattering (DLS) studies were performed for both polymers. DLS spectroscopy is used to determine the size distribution of particles. In the DLS experiment particle size is determined with the Brownian motion. This method can give results with high confidence for monodisperse suspensions of unaggregated nanoparticles and solutions containing large aggregates can be a challenge to analyse with this method.

Assuming the sphere formation self-assembly, the samples were first screened in TBE buffer. For the dilution studies, samples with different concentrations were prepared by diluting 100  $\mu\text{M}$  sample. The samples were screened in timed intervals (0 hr, 1 hr, 2 hr, 3 hr, 24 hr) to give apparent (since the calculation assumes a sphere, but we have no prior knowledge of shape) hydrodynamic diameters.

For the block copolymer **C12<sub>10</sub>-HEG<sub>10</sub>** at 100  $\mu\text{M}$  (Figure 2.13), DLS gave hydrodynamic diameters, starting from 72 nm and increasing up to 615 nm over a period of 4 hours. The hydrodynamic diameter appeared as initial peak at 274 nm at lower concentration of 10  $\mu\text{M}$  (Figure 2.14), gradually increased up to 714 nm, but after 24 hours the peak had returned to 255 nm. The sequence was also studied at 1  $\mu\text{M}$  (Figure 2.15) concentration but the observed data quality was poor. At this concentration, the apparent particle size fluctuated between 122 and 413 nm but the data quality was too poor to analyse further. At different concentrations, **C12<sub>10</sub>-HE<sub>10</sub>** hydrodynamic diameters observed to be wide range of values. This suggest that different superstructures are generated at different concentrations. However, the DLS

data for isomer **(C12-HEG)<sub>10</sub>** suggested comparably more stable structures over the 24 h timeframe (Figure 2.13). At 100  $\mu\text{M}$  concentration, the assembled structures exhibited a diameter of 615 nm as detected by DLS. At 10  $\mu\text{M}$  (Figure 2.14), the peak was again stable, while at 1  $\mu\text{M}$  (Figure 2.15), the concentration was too low, the scattering from the particles was weak and the measurement results were noisy.

The self-assembly of both sequences was examined with fluorescent membrane probe Nile Red (NR) in parallel to the DLS studies. Nile Red is highly efficient in its capability to identify different aggregate morphologies formed by amphiphile mixtures since NR fluorescence depends on the polarity of the environment. Compared with the hydrophobic environments, Nile Red's fluorescence intensity is very weak in water.<sup>22,23</sup> Therefore, NR can be used to monitor the hydrophobic environments formed as a result of self-assembly. For **C12<sub>10</sub>-HEG<sub>10</sub>** at 100  $\mu\text{M}$ , the integrated fluorescence intensity gradually increased with time. After the first four hours the fluorescence intensity remained stable. At 10  $\mu\text{M}$  and 1  $\mu\text{M}$ , the initial intensity was at its highest and it then decreased to a stable level. The **(C12-HEG)<sub>10</sub>** sequence also showed increasing intensity at 100  $\mu\text{M}$  over time and stabilized at high intensity, but at 10  $\mu\text{M}$  it was observed as gradually decreasing intensity. At 1  $\mu\text{M}$ , fluorescence intensities were not significantly different, and the signal was weak from the start (**Error! Reference source not found.**). The integrated fluorescence intensity for the block sequence was significantly higher than the alternating polymer. This intensity rise indicates that placements of C12 units together provided greater hydrophobic volume.

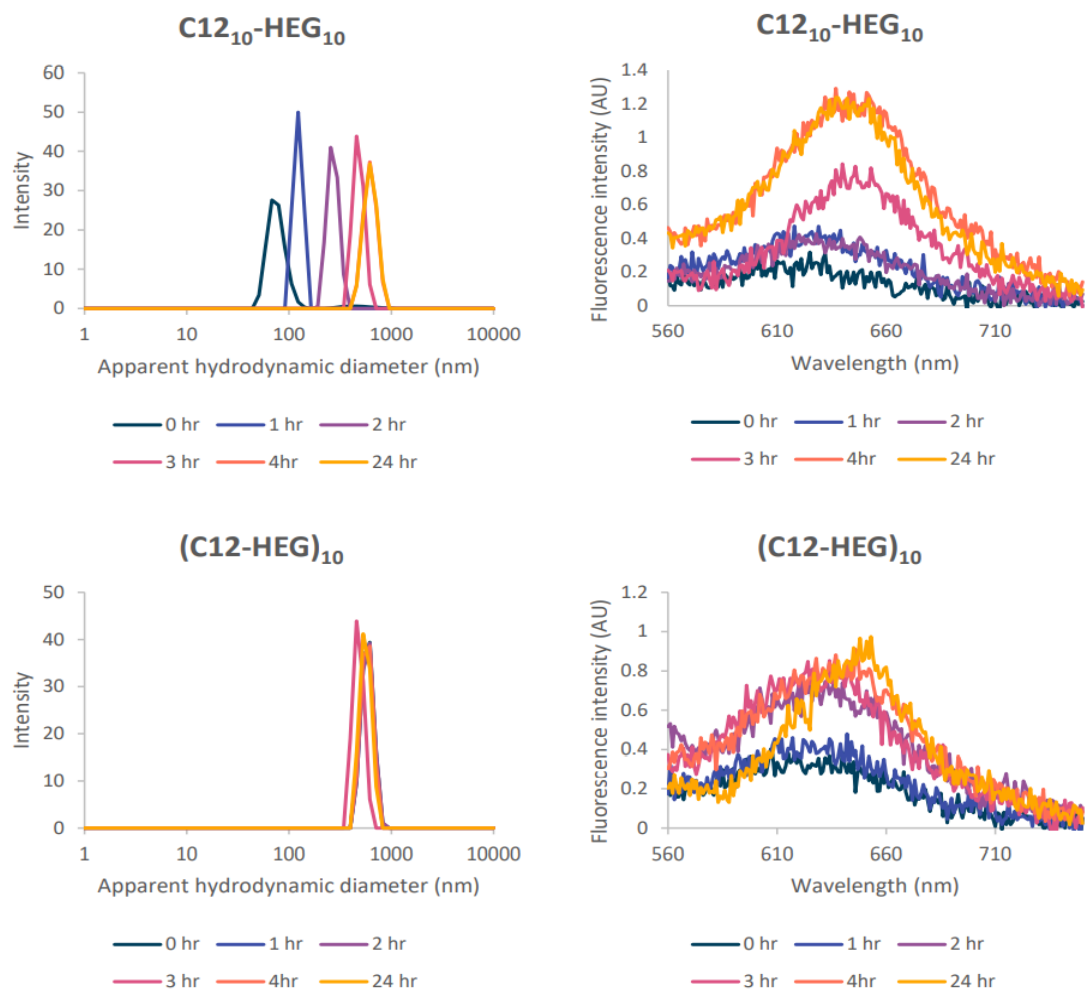


**Figure 2.13** DLS (left) and NR emission measurements (right) on **C12<sub>10</sub>-HEG<sub>10</sub>** (top) and **(C12-HEG)<sub>10</sub>** (bottom) in TBE buffer at 100  $\mu$ M.

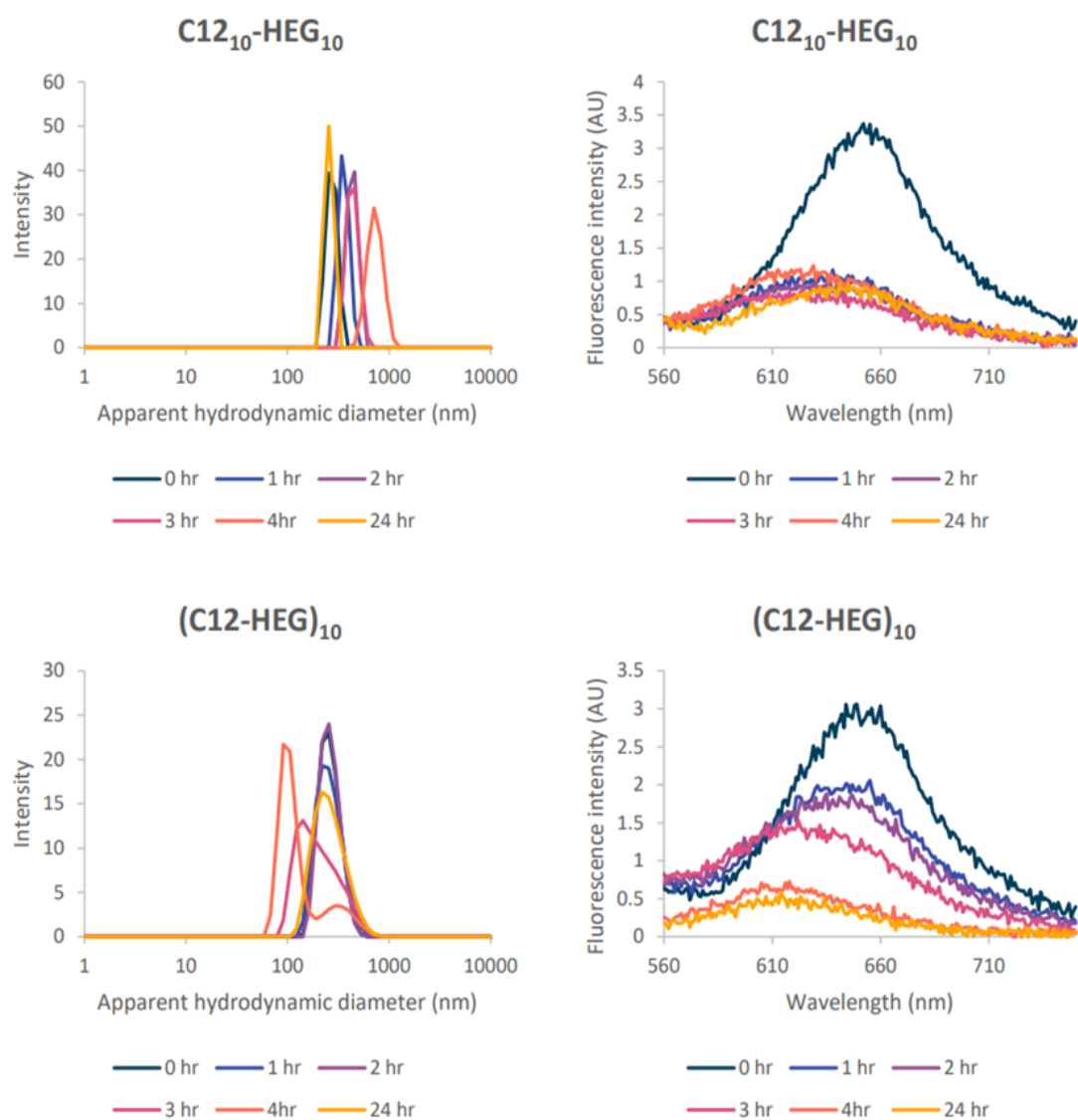


**Figure 2.14** DLS (left) and NR emission measurements (right) on  $C12_{10}\text{-HEG}_{10}$  (top) and  $(C12\text{-HEG})_{10}$  (bottom) in TBE buffer at 10  $\mu\text{M}$ .

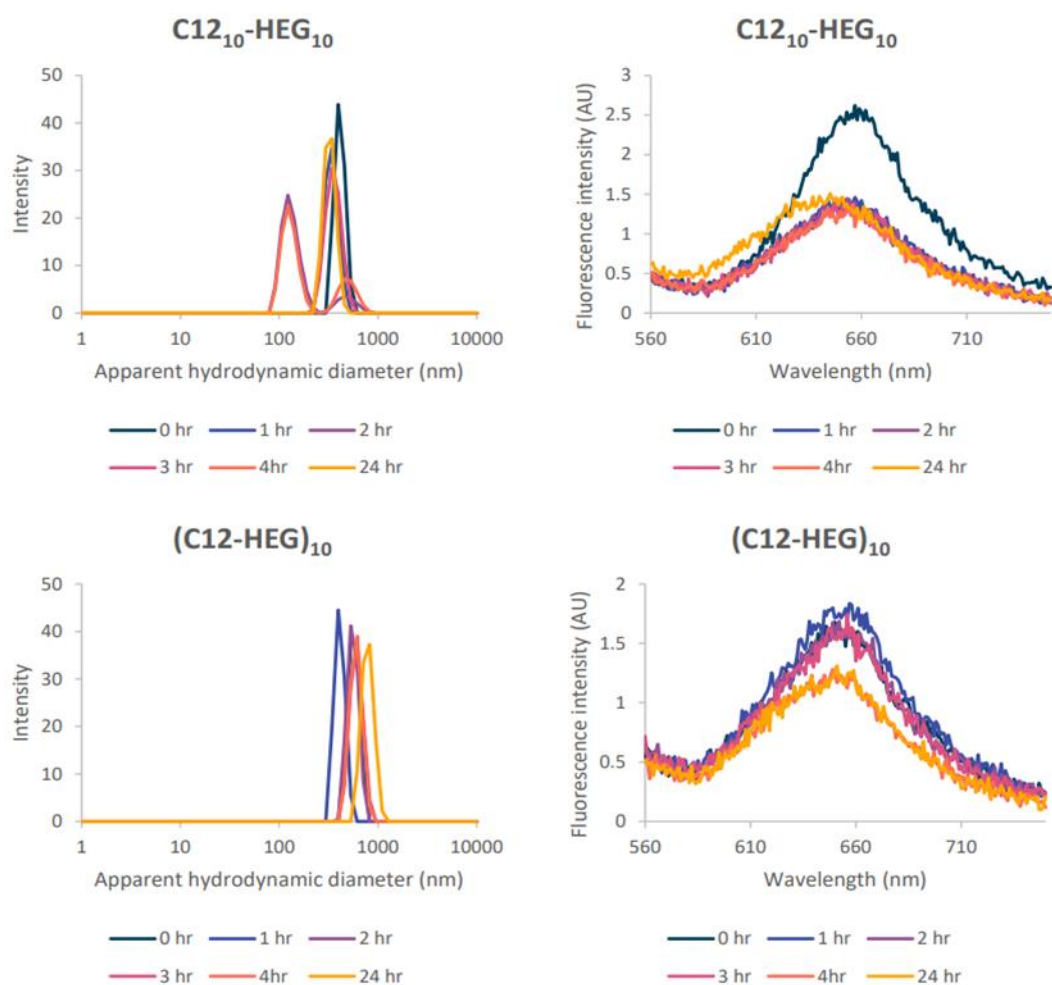


**Figure 2.15** DLS (left) and NR emission measurements (right) on  $C12_{10}\text{-HEG}_{10}$  (top) and  $(C12\text{-HEG})_{10}$  (bottom) in TBE buffer at 1  $\mu\text{M}$ .

The structures of the self-assembled nanomaterials were studied by transmission electron microscopy (TEM) and atomic force microscopy (AFM). The images were taken after 24h incubation. (Sample intensities for some samples shows no difference in peaks within two consecutive readings and those peaks overlaps in the graphs)

The **C12<sub>10</sub>–HEG<sub>10</sub>** sample in TBE at 100  $\mu\text{M}$  concentration the TEM images showed large twisting rope shapes with multiple micrometres in length and 10 – 40 nm in width. Some structures represented the unrolled nanoribbons (Figure 2.16). The structures were confirmed by the AFM (Figure 2.19). The diluted samples at 10  $\mu\text{M}$  and 1  $\mu\text{M}$  were also so examined with TEM and AFM. At 10  $\mu\text{M}$ , **C12<sub>10</sub>–HEG<sub>10</sub>** primarily lamellare structures appeared on TEM and small spherical shapes and long fibre shapes were also found randomly (Figure 2.17), which was also confirmed with AFM (**Error! Reference source not found.**). However, at 1  $\mu\text{M}$ , mainly 41 nm long and  $19 \pm 3$  nm prolate particles were found on TEM (Figure 2.18). It appears that small prolate particles are the first stage of self-assembly structures and these small particle merge to form lamellae which would then roll off to produce fibres with morphologies as seen at 100  $\mu\text{M}$  (Figure 2.22 (a)).

The structural conversion studied with TEM in different concentrations are consistent with DLS and NR data. The sample for preparation were done by dilution so the studied assemblies must be dynamic, allowing the fibres to break down into lamellae and seeds.



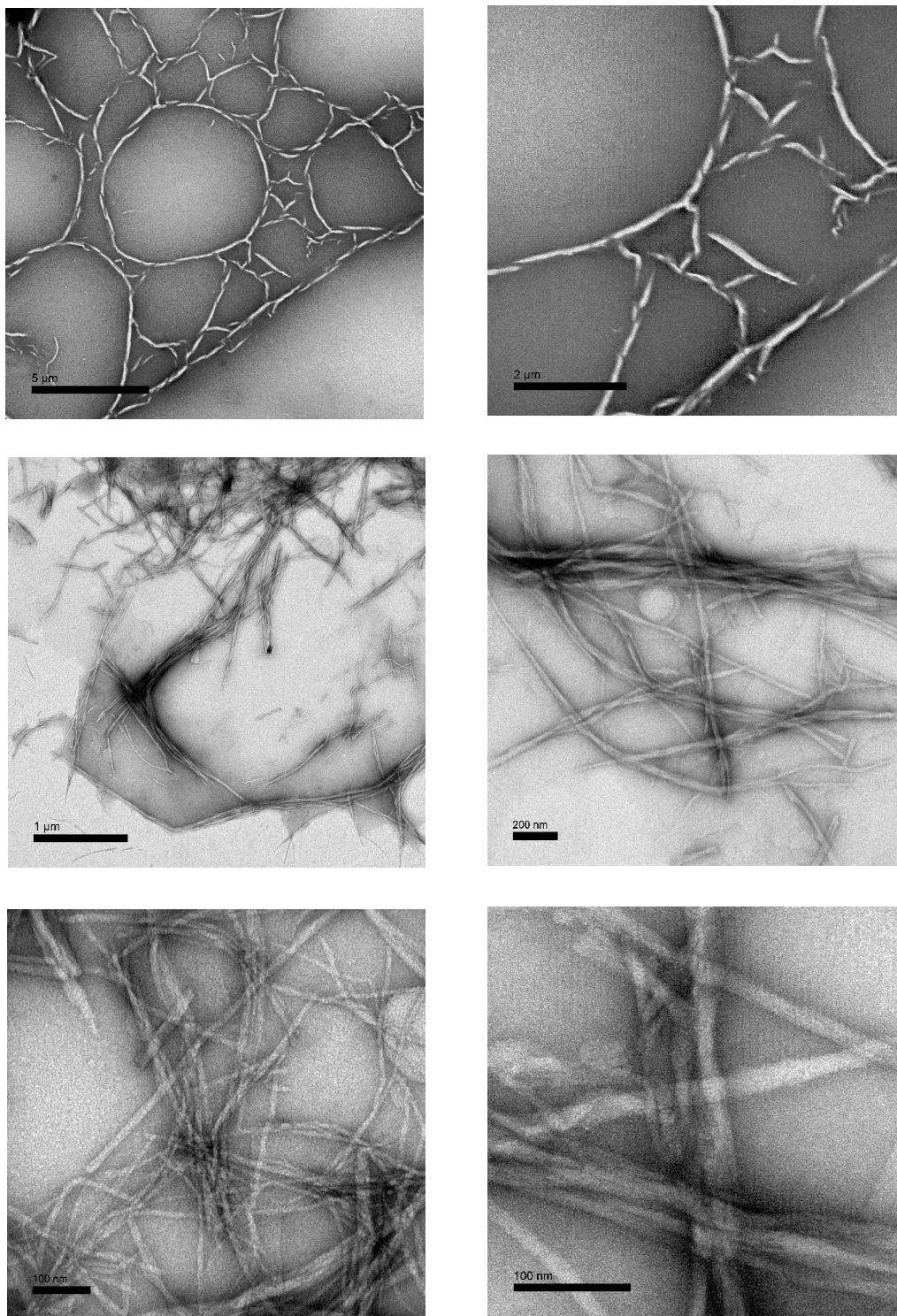


**Figure 2.16** TEM images of **C12<sub>10</sub>-HEG<sub>10</sub>**, 100 μM, TBE buffer.



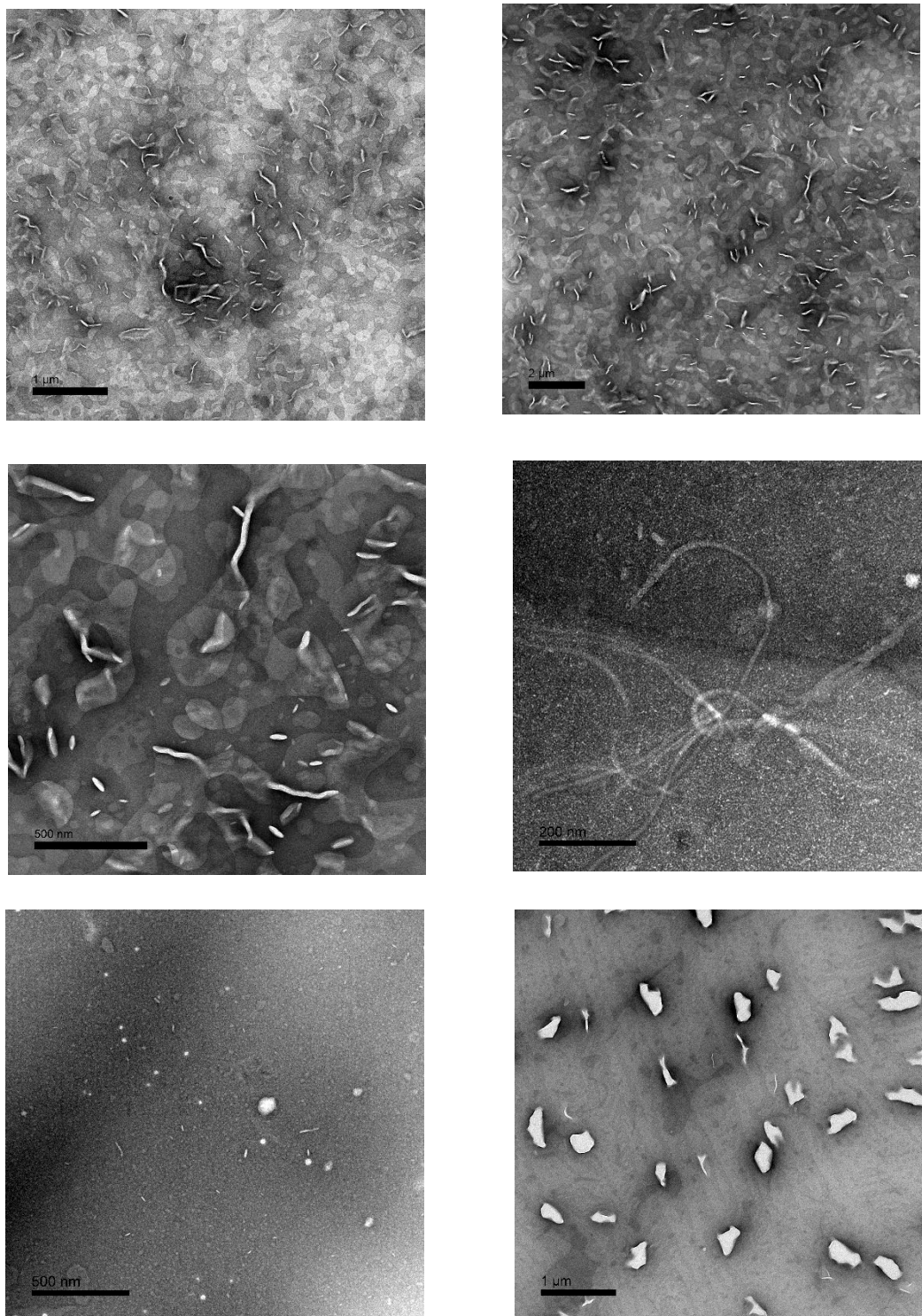


**Figure 2.17** TEM images of **C12<sub>10</sub>-HEG<sub>10</sub>**, 10 μM, TBE buffer.



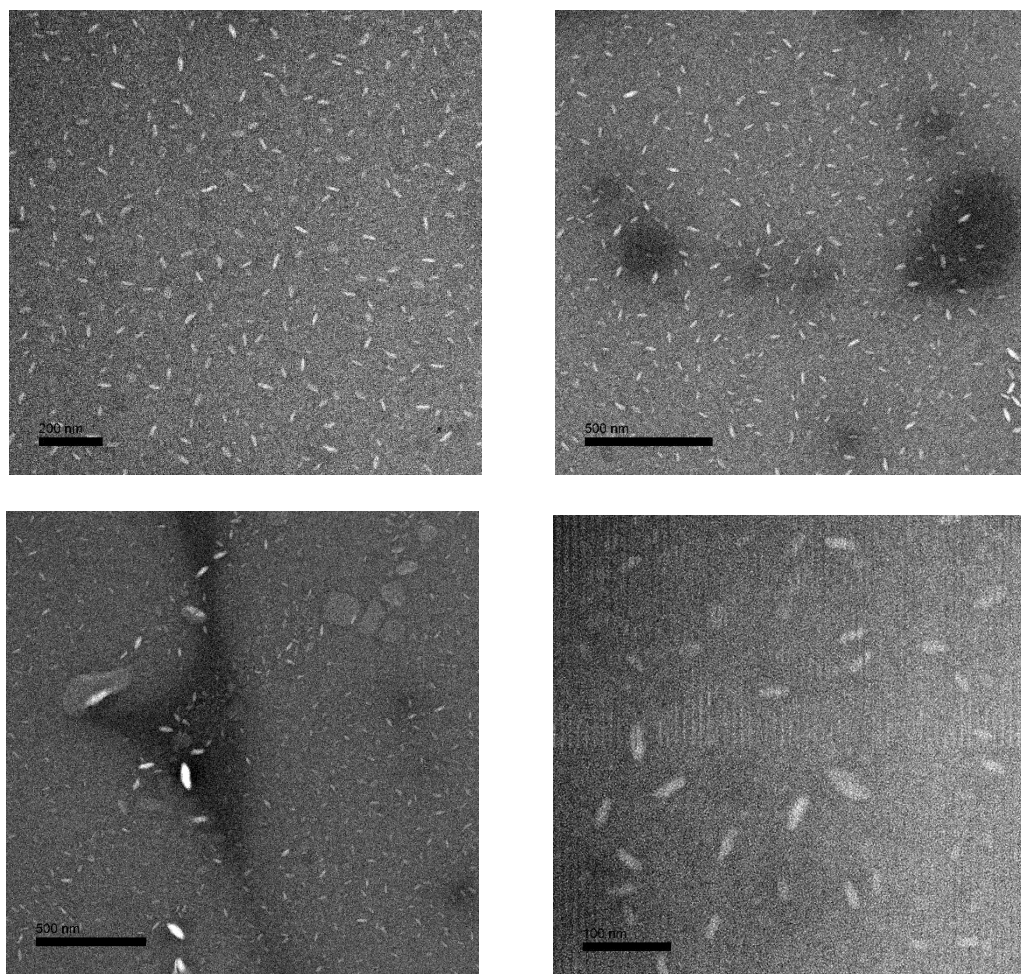


**Figure 2.18** TEM images of **C12<sub>10</sub>-HEG<sub>10</sub>**, 1 μM, TBE buffer.

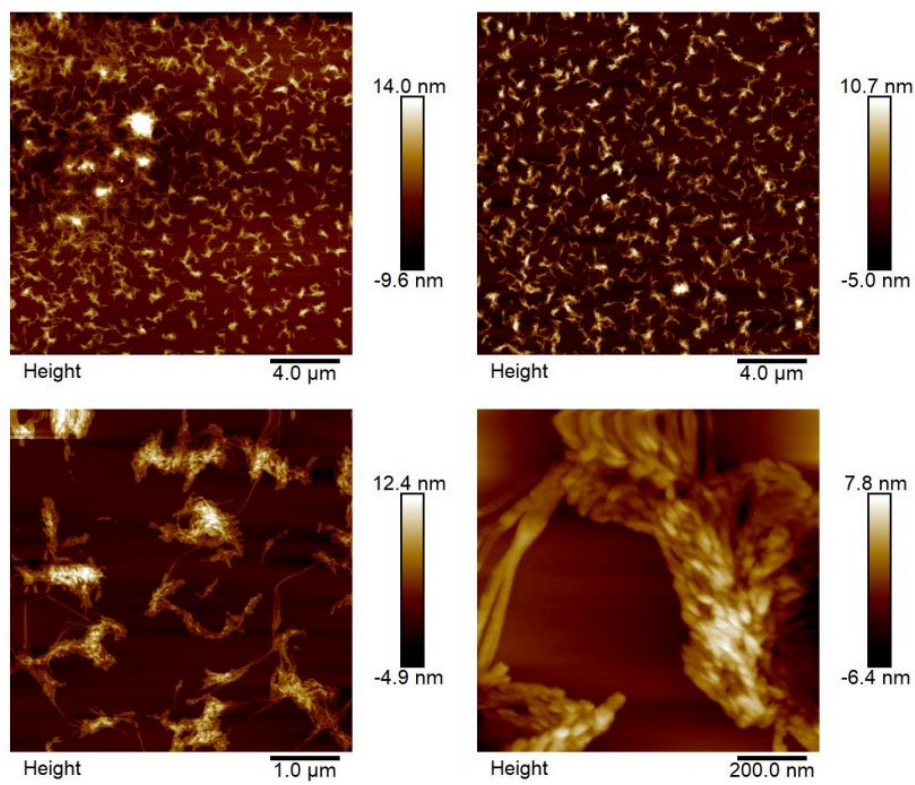


**Figure 2.19** AFM images of C12<sub>10</sub>-HEG<sub>10</sub>, 100 μM, TBE buffer.

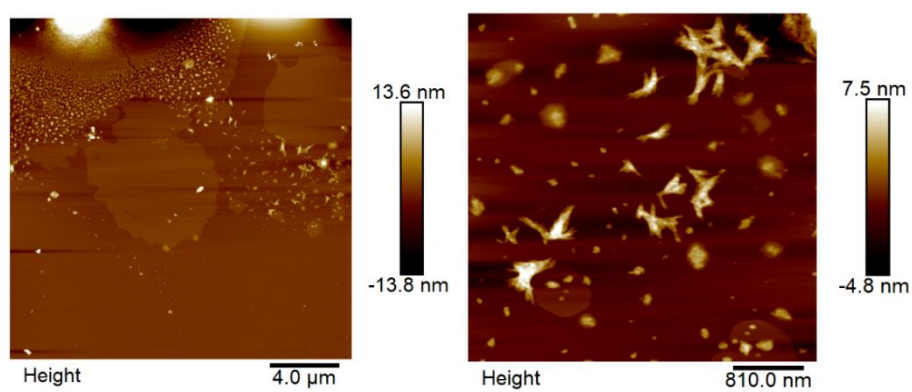


**Figure 2.20** AFM images of C12<sub>10</sub>-HEG<sub>10</sub>, 10 μM, TBE buffer.

The **(C12-HEG)<sub>10</sub>** assemblies were also studied by TEM and AFM. With TBE buffer at 100  $\mu\text{M}$ , few irregular aggregates were appeared as shown in figure (Error! Reference source not found.). These aggregates might be a result of random coils gathering together to form occasional patches due to increased hydrophobicity (

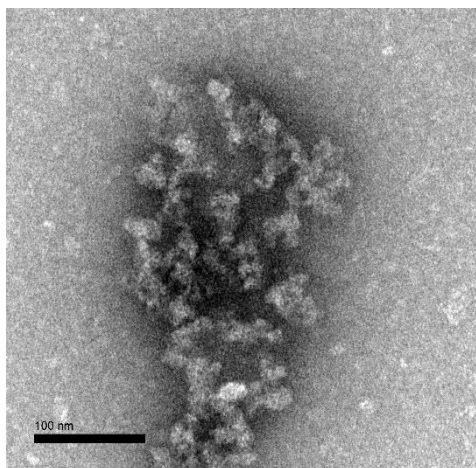


**Figure 2.30 (b).**

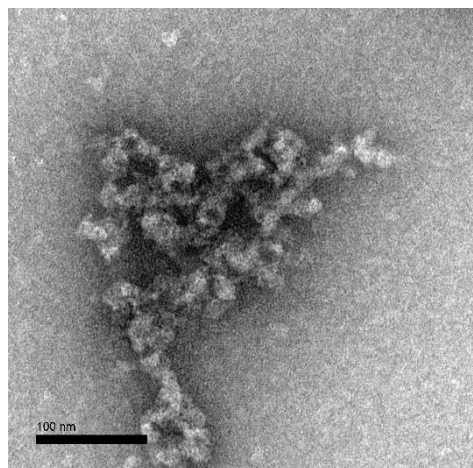


**Figure 2.21** TEM images of **(C12-HEG)<sub>10</sub>**, 100  $\mu\text{M}$ , TBE buffer.



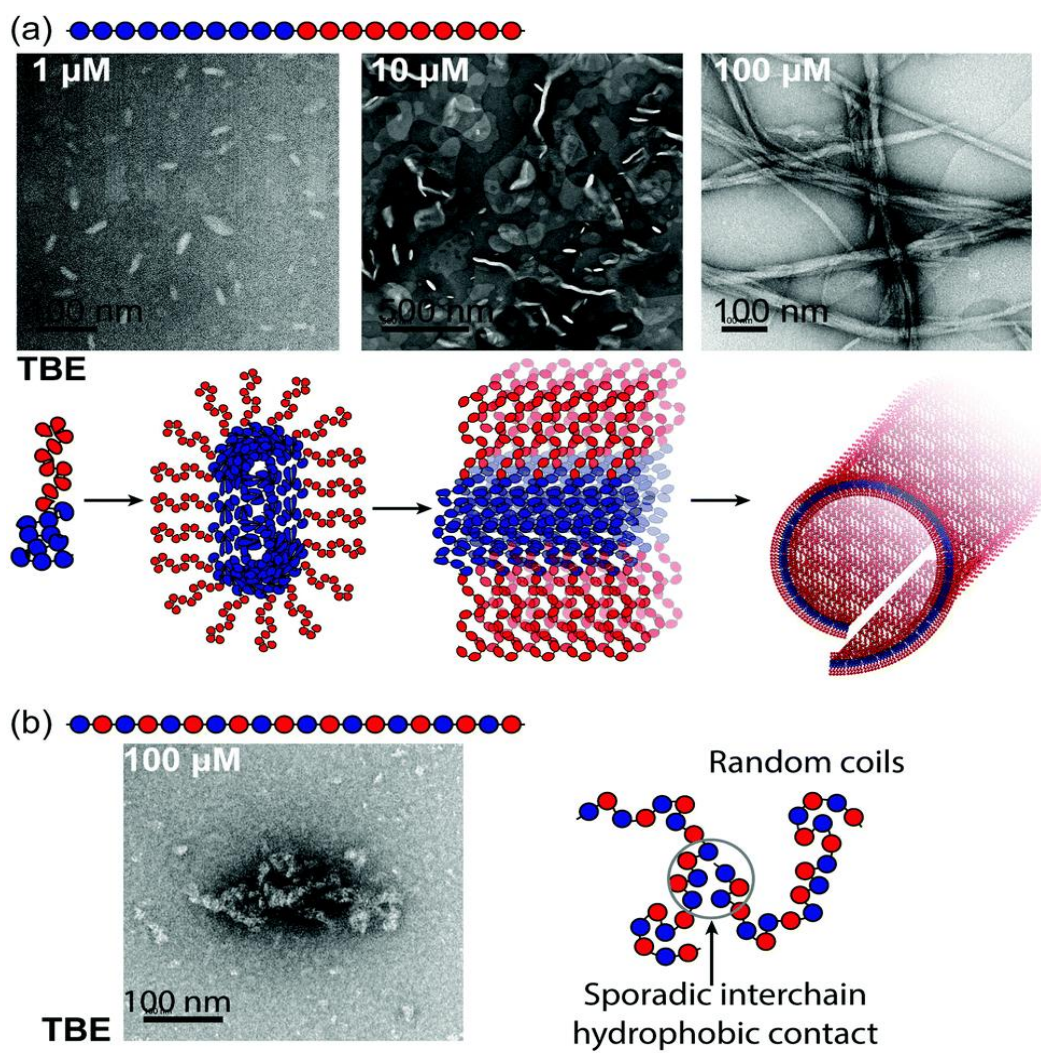


**Figure 2.22** Self-assembly in TBE buffer of (a) **C12<sub>10</sub>-HEG<sub>10</sub>** and (b) **(C12-HEG)<sub>10</sub>** as analysed by TEM.

#### 2.2.3.2 Self-assembly of sequence isomers in TAMg buffer

The sequence isomer self-assemblies were then studied in TAMg buffer. Again, the samples were first studied with DLS to have a rough idea on size distribution. Immediate formation of assemblies with an apparent diameter of 712 nm was measured for the block copolymer **C12<sub>10</sub>-HEG<sub>10</sub>** at 100  $\mu$ M. Over 24 h, the overall size distribution decrease non-linearly to 295 nm (Figure 2.23). The diluted sample at 10  $\mu$ M appeared as a stable population around 600 nm (Figure 2.24). At 1  $\mu$ M, particle size switched from around 115 nm to 16 nm over 24 hours which is consistent with single chain nanoparticles (SCNPs) (Figure 2.25). The data quality was too poor at this dilution to be confident with the analysis. NR emission was recorded in parallel to the DLS measurements. The strongest NR emission was found to be at 100  $\mu$ M but at all the concentrations the emissions were decreased with time.

A stable population with 615 nm particle diameter was observed in DLS for alternating polymer (**C12-HEG**)<sub>10</sub> at 100  $\mu$ M (Figure 2.23). The NR fluorescence intensity at this concentration decreased with the time. The data collected at lower concentrations 10  $\mu$ M (Figure 2.24) and 1  $\mu$ M (Figure 2.25) were not of sufficient quality to be used. The NR emission at 10  $\mu$ M initially started at high intensity and decreased to be stable and at 1  $\mu$ M intensity did not change significantly within 24 h.

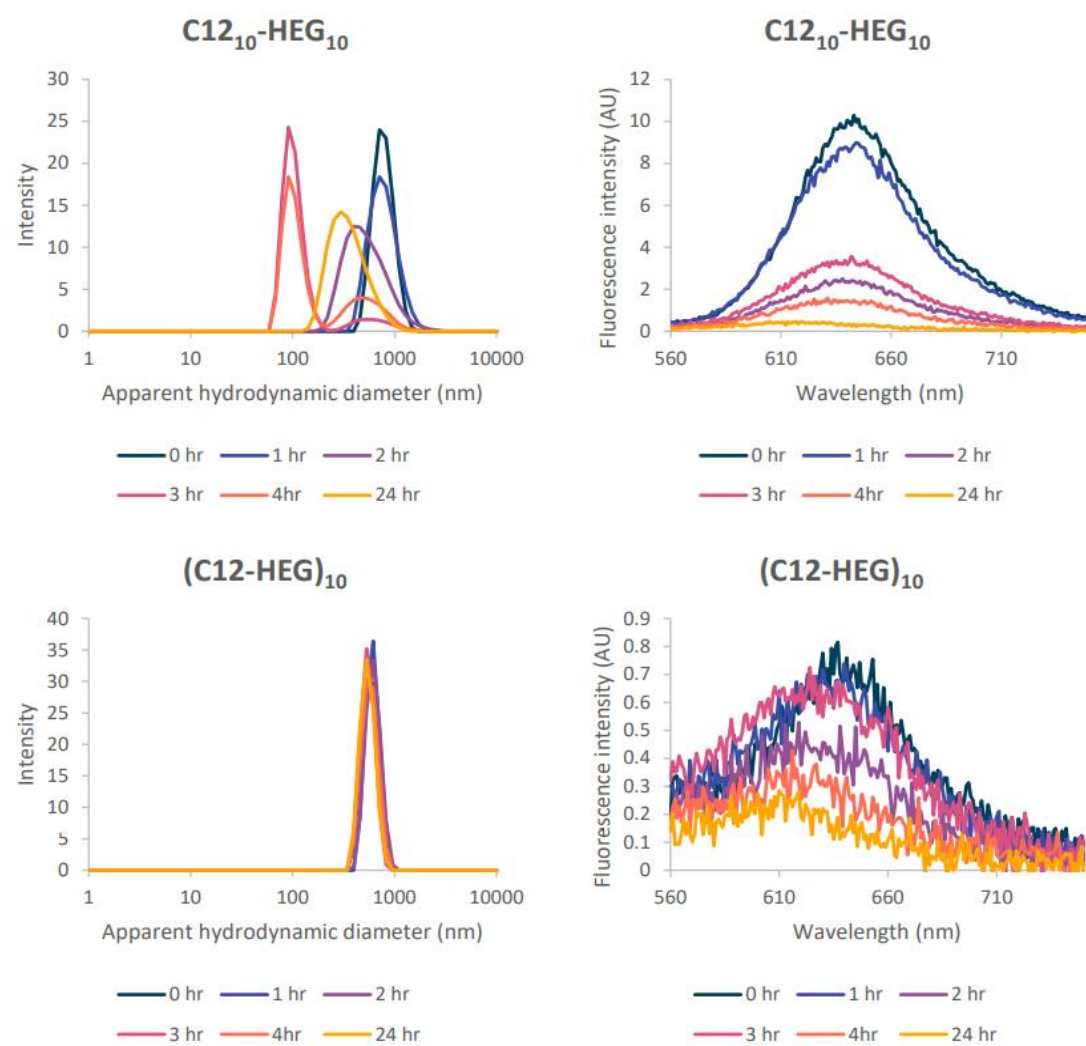


**Figure 2.23** DLS (left) and NR emission measurements (right) on  $C12_{10}$ -HEG $_{10}$  (top) and  $(C12\text{-}HEG)_{10}$  (bottom) in TAMg buffer at 100  $\mu$ M.



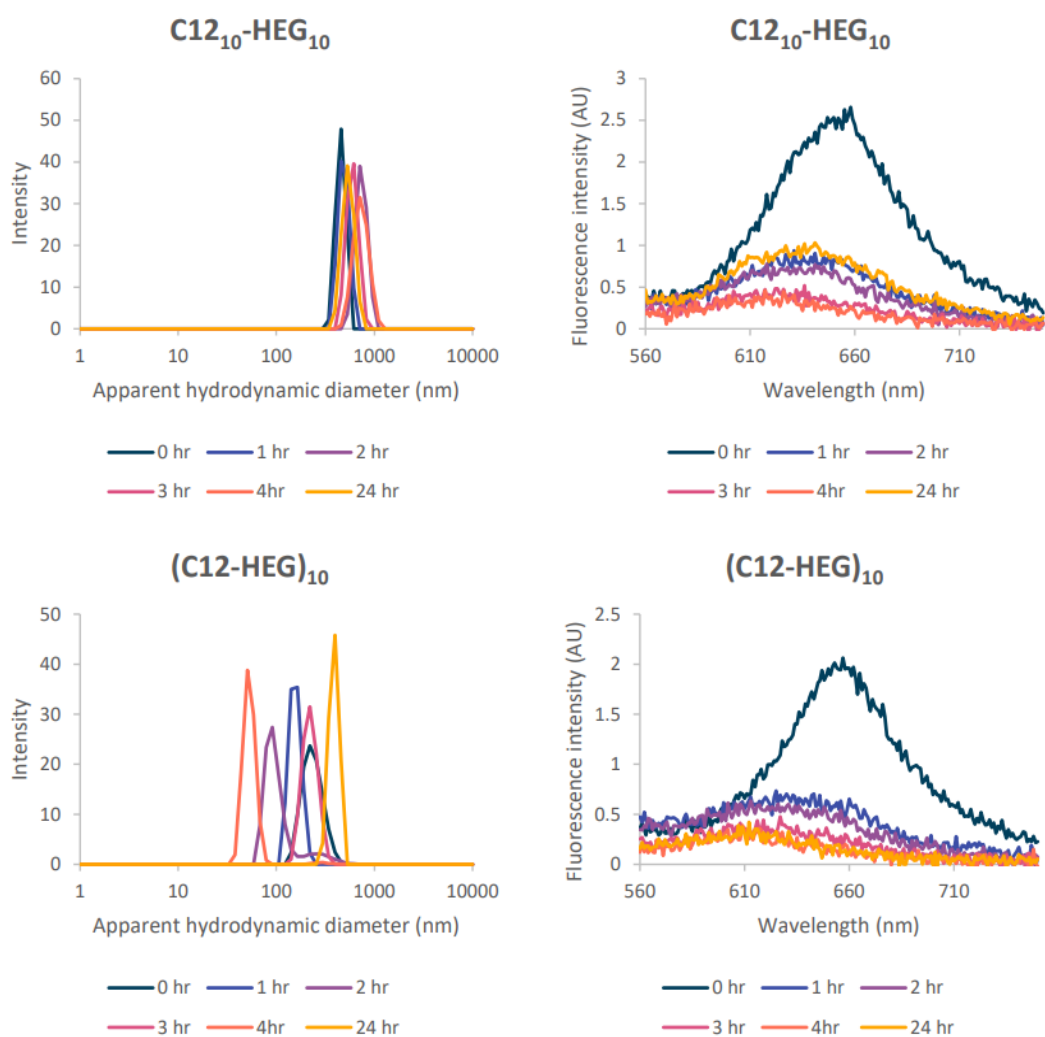


**Figure 2.24** DLS (left) and NR emission measurements (right) on **C12<sub>10</sub>-HEG<sub>10</sub>** (top) and **(C12-HEG)<sub>10</sub>** (bottom) in TAMg buffer at 10  $\mu$ M.

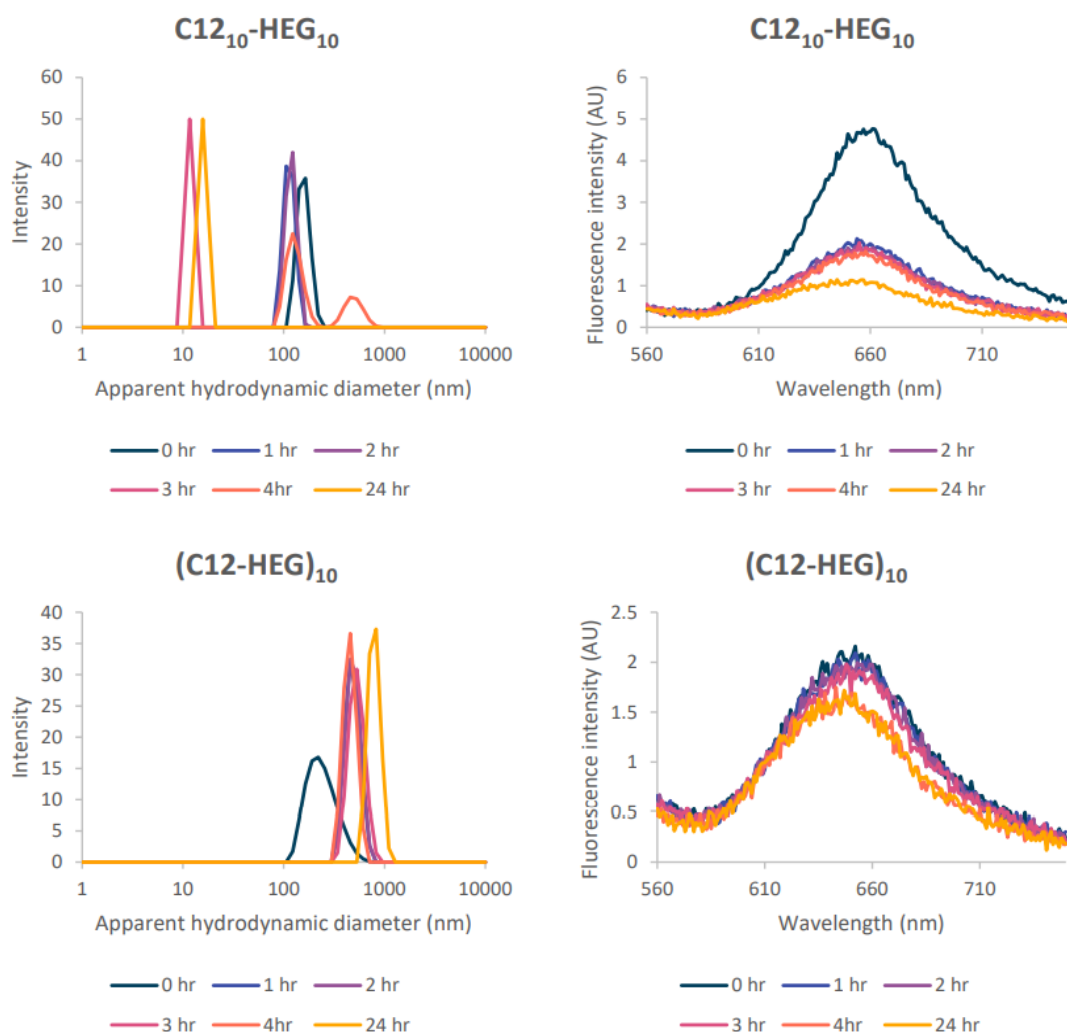


**Figure 2.25** DLS (left) and NR emission measurements (right) on  $\text{C12}_{10}\text{-HEG}_{10}$  (top) and  $(\text{C12-HEG})_{10}$  (bottom) in TAMg buffer at  $1\ \mu\text{M}$ .

Then the self-assembly of  $\text{C12}_{10}\text{-HEG}_{10}$  was investigated using TEM. It was observed that the block copolymer assembled into small prolate particles with  $18 \pm 4\ \text{nm}$  in length by  $7 \pm 1\ \text{nm}$  in diameter at  $100\ \mu\text{M}$  (Figure 2.26). These particles were more uniform than the small ‘seed’ structures observed for  $\text{C12}_{10}\text{-HEG}_{10}$  at  $1\ \mu\text{M}$  in TBE buffer. Because of the presence of  $\text{Mg}^{2+}$  ions in the solution, even at the

higher concentrations, TAMg buffer promotes collapse polymers to form more consistent particles. AFM showed ‘lumpy’ structures for higher concentrations but with dilution samples the structures were revealed to be spherical particles with  $1.3 \pm 0.6$  nm high,  $22.5 \pm 8.5$  nm diameter (Figure 2.27). These structures suggest SCNP formation. The lumpiness of the structures formed at 100  $\mu$ M could then be the aggregates of SCNPs in solution

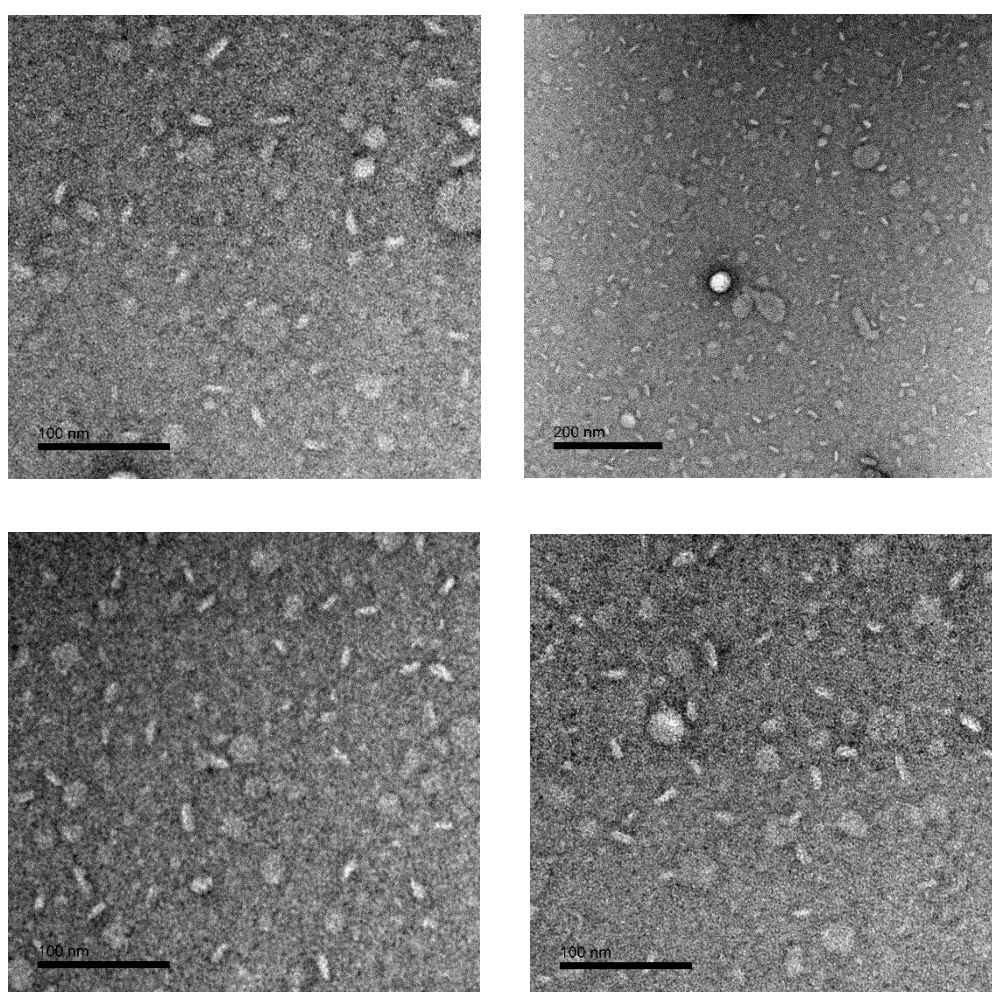


**Figure 2.26** TEM images of **C12<sub>10</sub>-HEG<sub>10</sub>**, 100  $\mu$ M, TAMg buffer.



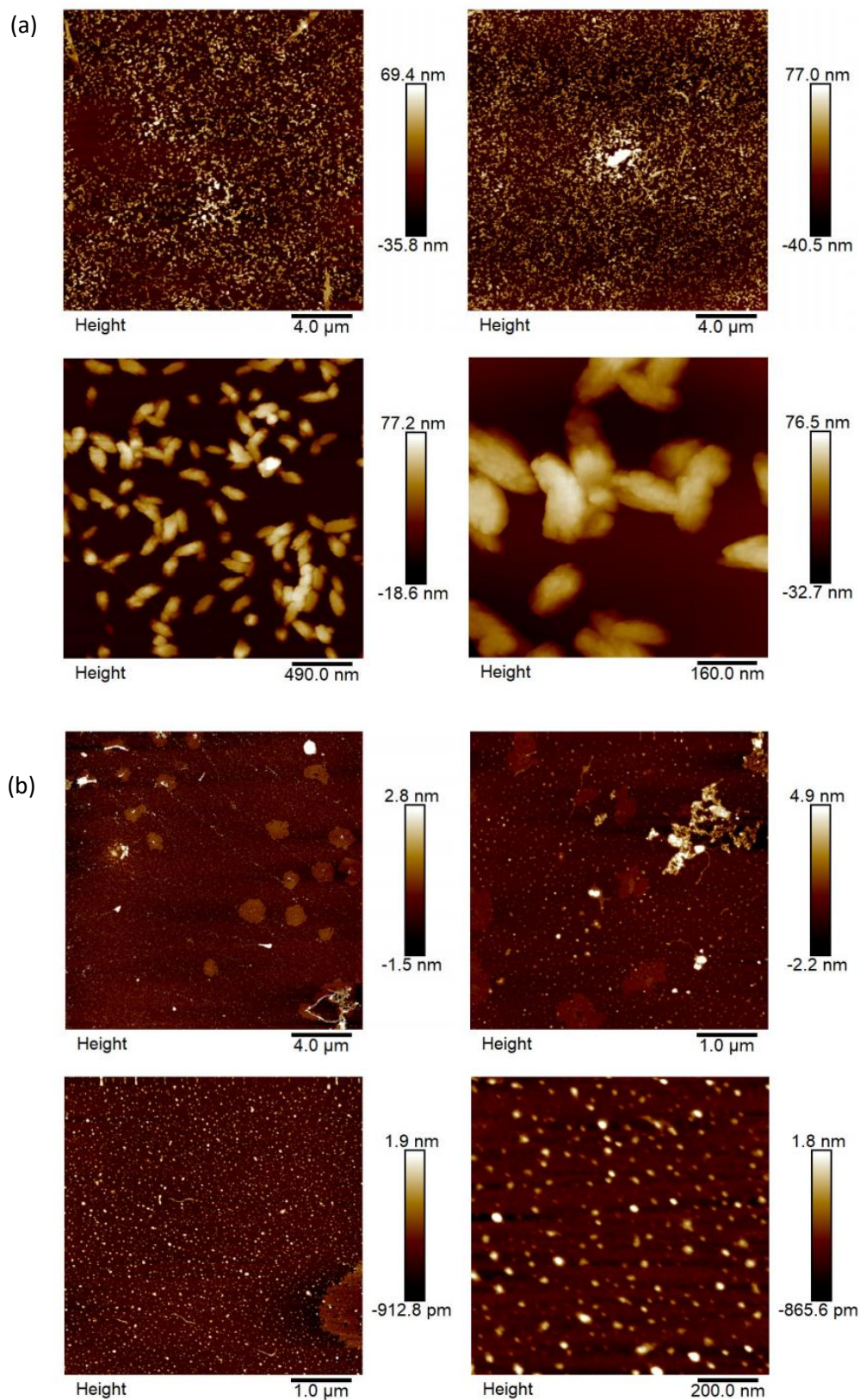


**Figure 2.27** AFM images of **C12<sub>10</sub>-HEG<sub>10</sub>**, 100  $\mu\text{M}$ , TAMg buffer. AFM images of **C12<sub>10</sub>-HEG<sub>10</sub>**, 10  $\mu\text{M}$ , TAMg buffer.

The alternating polymer **(C12-HEG)<sub>10</sub>** was simultaneously studied with TEM and AFM. At 100  $\mu$ M discoid structures were observed  $6.1 \pm 1.0$  nm by  $14.6 \pm 3.2$  nm (Figure 2.28) and confirmed by AFM (Figure 2.29). The smallest dimension of observed particle is much larger than the previously studied maximum distance of a concertina conformation of the alternating polymers (3.8 nm). <sup>24</sup>This is the first time that self-assembly of discs has been experimentally observed in alternating polymers and it is hard to come to a conclusion at this stage what kind of substructure could be given by **(C12 HEG)<sub>10</sub>**.

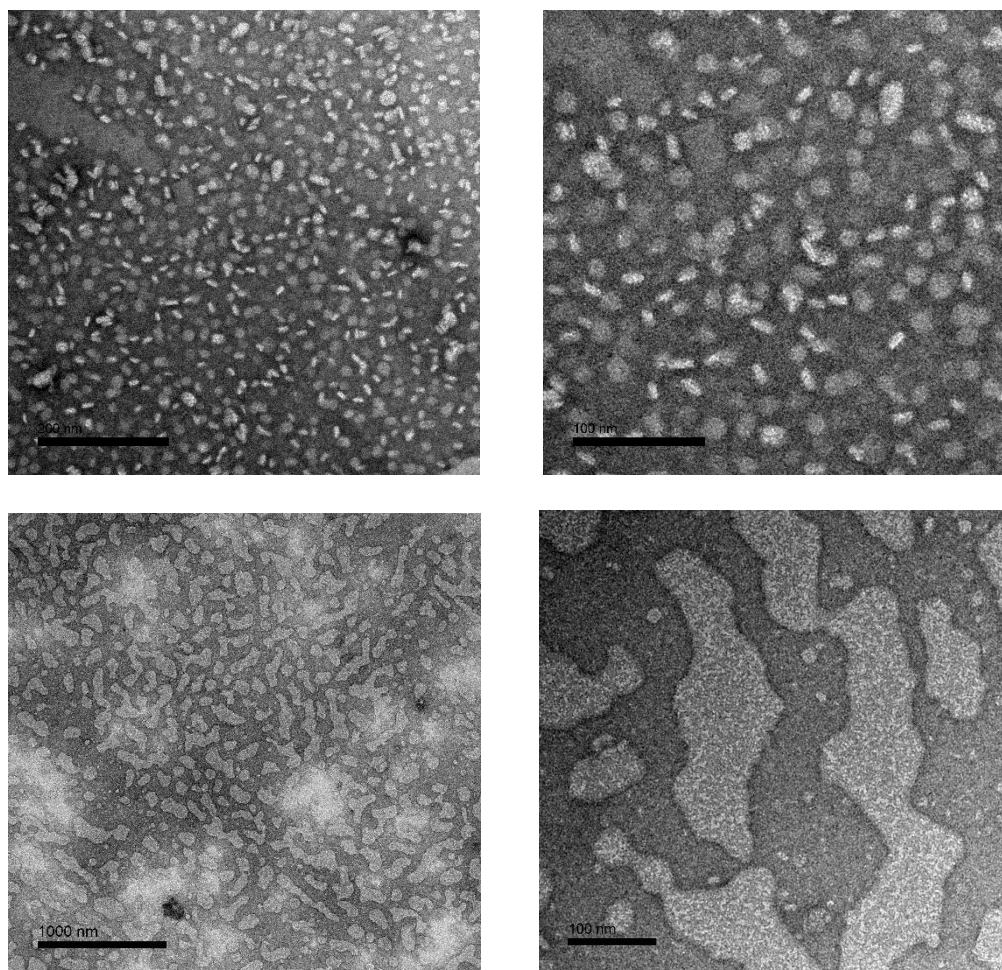


**Figure 2.28** TEM images of **(C12-HEG)<sub>10</sub>**, 100  $\mu$ M, TAMg buffer.



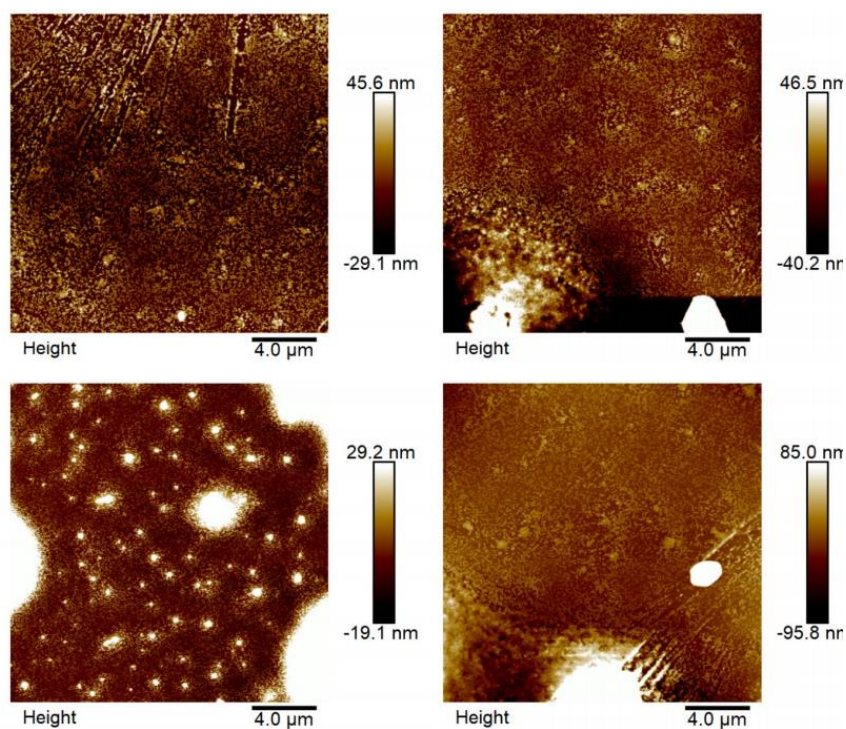


**Figure 2.29** AFM images of (C12-HEG)<sub>10</sub>, 100 μM, TAMg buffer.

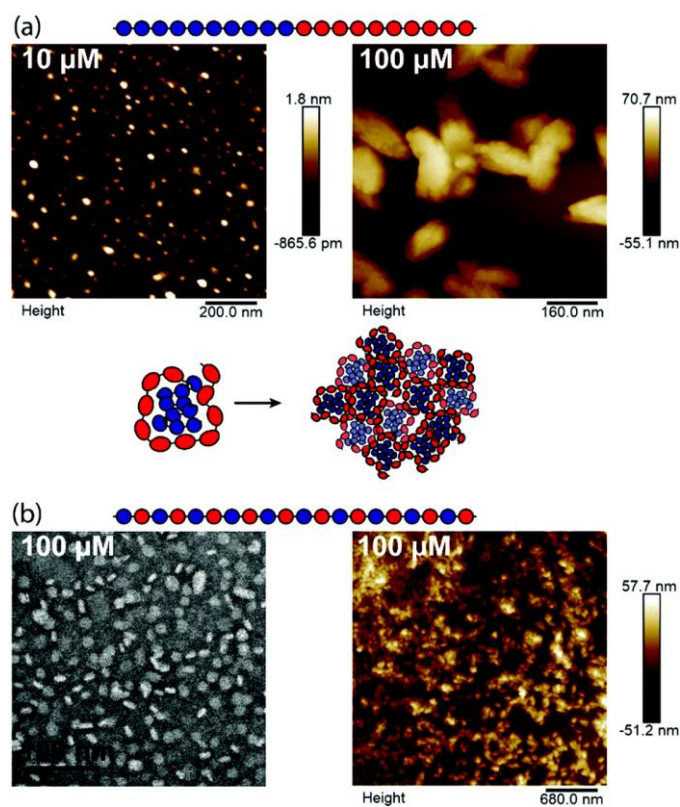


**Figure 2.30** Self-assembly in TAMg buffer of (a) C12<sub>10</sub>-HEG<sub>10</sub> and (b) (C12-HEG)<sub>10</sub>, analysed by TEM and AFM.

### 2.2.3.3 Static light scattering (SLS) and small angle X-ray scattering (SAXS)

Light scattering data on macromolecules (e.g. proteins, nucleic acids, as well as assemblies and larger entities composed of them) can combine with size exclusion chromatography, gel electrophoresis and mass spectrometry to understand the dynamic and structural features.<sup>25</sup> Static light scattering involves recording the amount of light scattered by a sample at a range of angles relative to the direction of the incident light source and/or for different sample concentrations. Recording the intensity of light scattered at different angles allows theoretical models to be used to determine the size, shape, or structure of the scattering material.

The scattering experiments were conducted using an ALV-CGS3 goniometer-based system supplied by ALV GmbH, operating a laser at wavelength  $\lambda = 633$  nm. Time averaged scattering intensity data were recorded over the angular range  $12 < \theta < 150^\circ$  at  $1^\circ$  intervals. The aim of this study was to investigate whether light scattering techniques can contribute to a meaningful characterisation of the higher order structures that was recorded by TEM and AFM. Ideally, a successful application would allow for the estimation of characteristic dimensions and provide structural information for the **C12-HEG** systems.

Typically, scattering techniques use either standard linear plots (e.g. Zimm or Guinier plots) or employ least squares fitting to an appropriate model for estimating an intensity-weighted average particle size,  $\langle R_G \rangle_z$ .<sup>26,27</sup> The limitations of the method are that it should be applied to dilute, monodisperse and isotropic solutions of particles. The Zimm or Guinier plot usually applied when it can be assumed that the sample consists of dilute, monodisperse and isotropic particles in solution. Both methods allow the determination of an average Radius of Gyration  $R_g$  according to an analysis of angular variation in the measured scattered intensity  $I(q)$ .

Previous characterisation by microscopy for the **C12-HEG** isomers identified as a concentration dependence. Higher order structures were observed at higher concentrations, and, at low concentrations, the particles appeared to form ‘seed’-like particles with both TBE and TAMg buffer. At low concentrations, the samples were adjudged to be more uniform and standard linear plots might be applicable to those samples. But it would be necessary to adopt a somewhat different approach for the samples at higher concentrations, where higher order structures were observed.

As an alternative to the general Zimm and Guinier methods, a generalised Guinier-Porod model (Hammouda, 2010) may be applied for non-spherical objects that exhibit complex phase behaviour.<sup>28</sup> The Guinier Plot allows the determination of the Radius of Gyration  $R_g$  from the measured scattered intensity  $I(q)$ . Hammouda explained the application of a generalised Guinier-Porod model to empirical data and interpretation of the fitted parameters detail.<sup>28</sup> Briefly, a minimal complexity empirical model may be formulated in terms of two dimensionality parameters,  $s$  and  $d$ , and a characteristic size,  $R$ . The scattering variable is defined as  $q = (4\pi/\lambda) \sin(\theta/2)$  where  $\lambda$  is the wavelength of the light source and  $\theta$  is the scattering angle. However, this takes away some flexibility needed for systems with, for example, high polydispersity.

The model takes from:

$$I(q) = \left(\frac{G}{q^s}\right) \cdot \exp\left(-\frac{q^2 R^2}{3-s}\right) \quad , q \leq q^*$$

$$I(q) = \frac{D}{q^d} \quad , q \geq q^*$$

Where  $q^* \sim 1/R$  and  $D$  and  $G$  are scaling factors calculated to make the function  $I(q)$  and its derivative continuous at  $q^*$ .



The **C12<sub>10</sub>-HEG<sub>10</sub>** prepared in TBE buffer at 10  $\mu\text{M}$ , Guinier plot of the SLS data suggests a population of particles of average size of  $\langle RG \rangle_z = 103 \pm 22$  nm. However, the low- $q$  SLS data suggested a second, less numerous, population of fairly larger particles  $\langle RG \rangle_z \approx 500$  nm. At this concentration, divergence of the data at low- $q$  compared to the fitted GP model is typically encountered for samples containing a broad distribution of particle masses. However, for the sample the high- $q$  data appears to indicate a consistent, most numerous particle population.

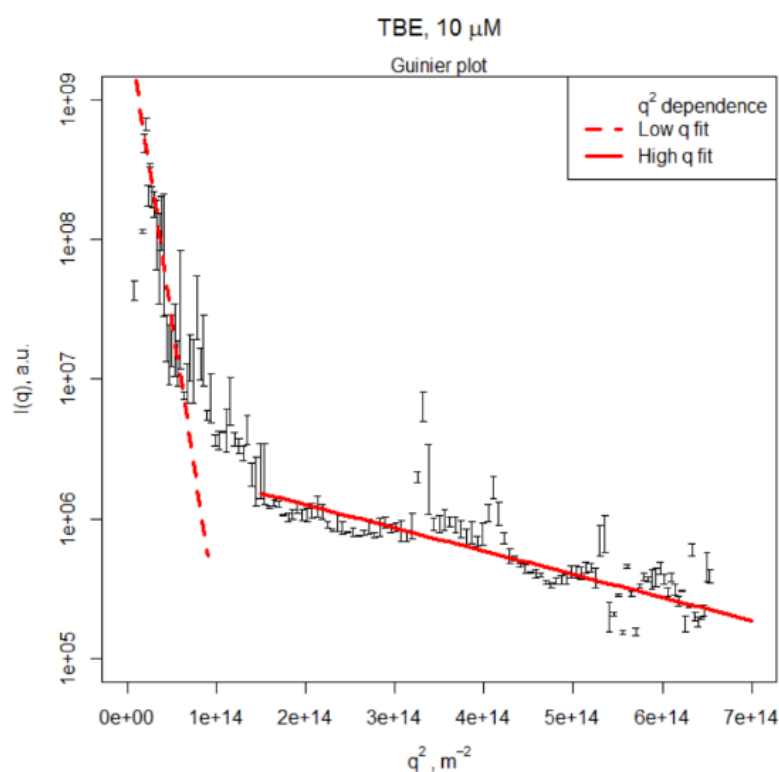


**Figure 2.31** Guinier plot to estimate the mean particle size,  $\langle RG \rangle_z$ , for **C12<sub>10</sub>-HEG<sub>10</sub>** in TBE buffer at 10  $\mu\text{M}$ . The high- $q$  fit identifies the most numerous particle population. The low- $q$  fit indicates the presence of some larger structures.

Samples then prepared at concentrations  $20 \leq C \leq 100 \mu\text{M}$  showed an incremental change in the scattering profile. This conforms the gradual transition to large, higher order structures or else a network. The analysis of these data was found to be consistent with structures observed with the TEM and AFM where we studied the change of self-assembly with the concentration.

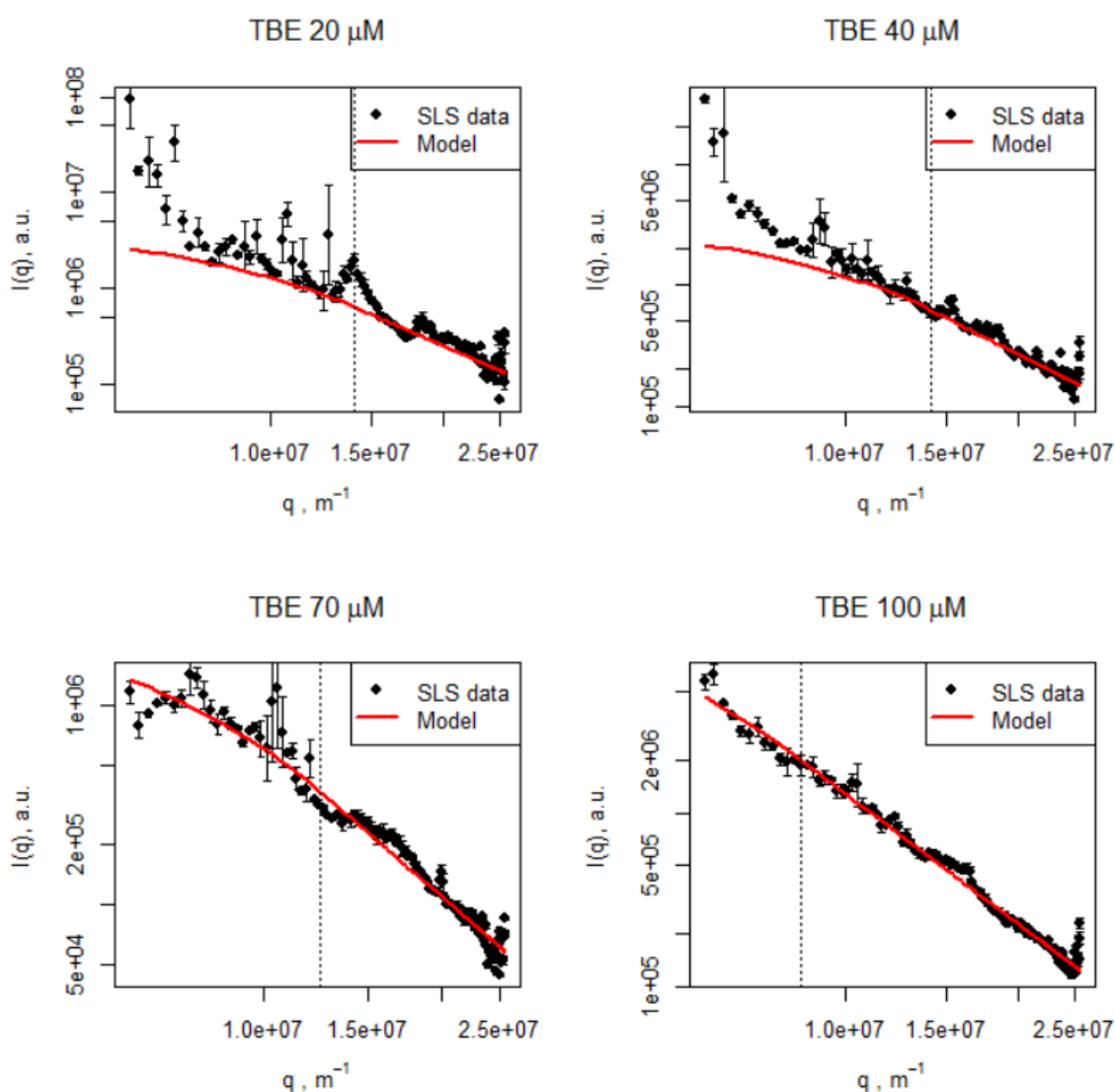


**Figure 2.32** Fits of the generalised Guinier-Porod model to data recorded for C12<sub>10</sub>-HEG<sub>10</sub> in TBE buffer, showing change in the scattering profile according to sample concentration.

**C12<sub>10</sub>-HEG<sub>10</sub>** samples prepared in TAMg buffer at 4  $\mu\text{M}$  were observed to have non-isotropic particles of size  $\langle RG \rangle_z = 107 \pm 5$  nm. Samples prepared at greater concentrations, in the range  $7 \leq c \leq 100$   $\mu\text{M}$  showed incremental change in the scattering profile consistent with initial cluster formation and then formation of large, highly anisotropic, higher order structures.

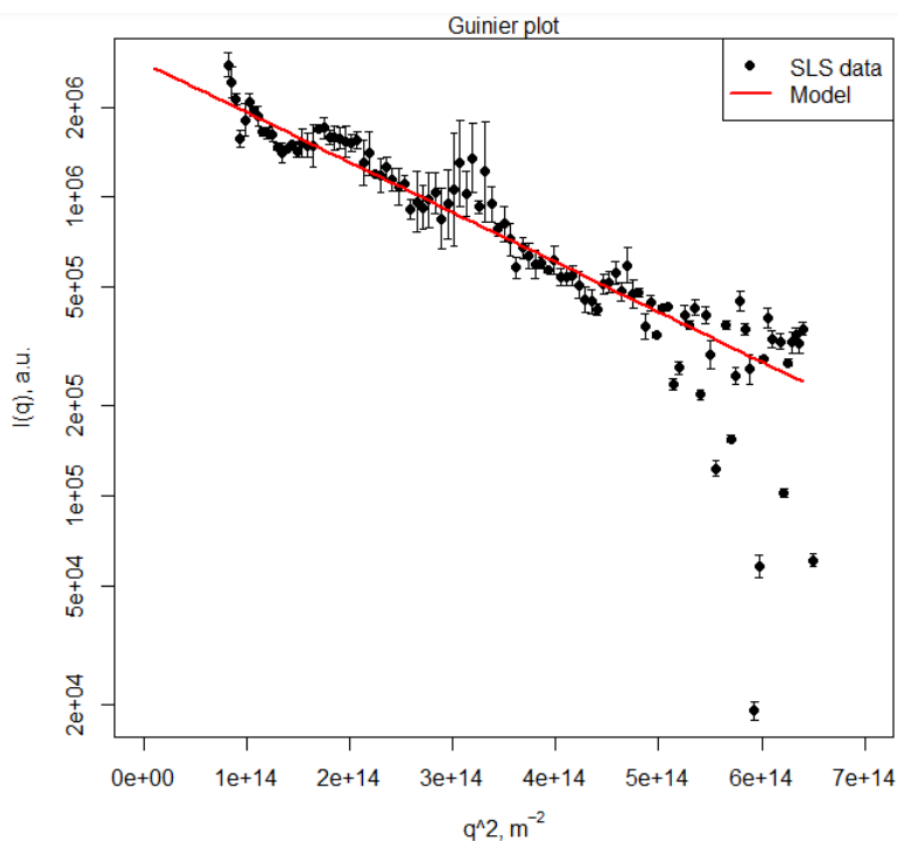


**Figure 2.33** Guinier plot to estimate the mean particle size,  $\langle RG \rangle_z$ , for **C12<sub>10</sub>-HEG<sub>10</sub>** in TAMg buffer at 4  $\mu\text{M}$ .

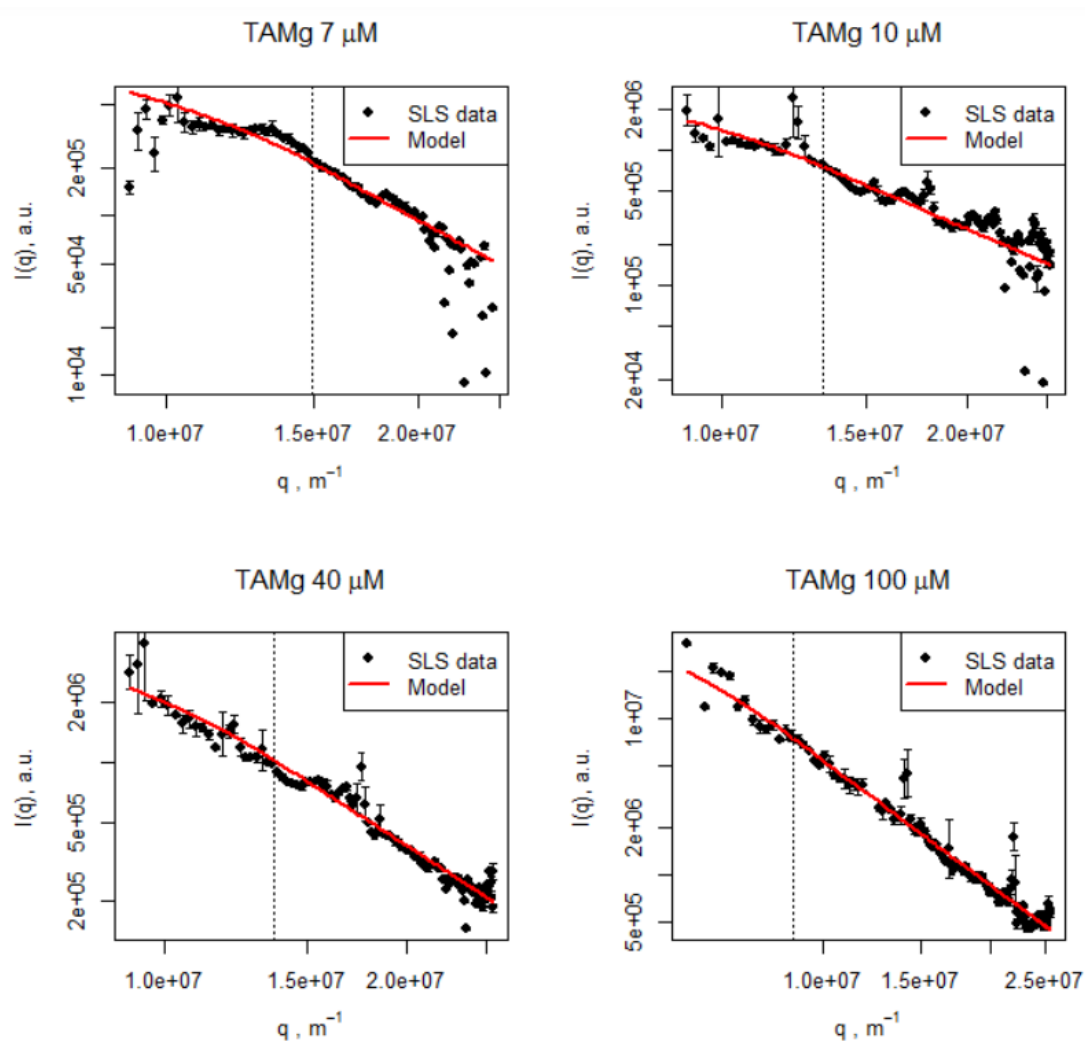


**Figure 2.34** Fits of the generalised Guinier-Porod model to data recorded for **C12<sub>10</sub>-HEG<sub>10</sub>** in TAMg buffer, showing change in the scattering profile according to sample concentration.

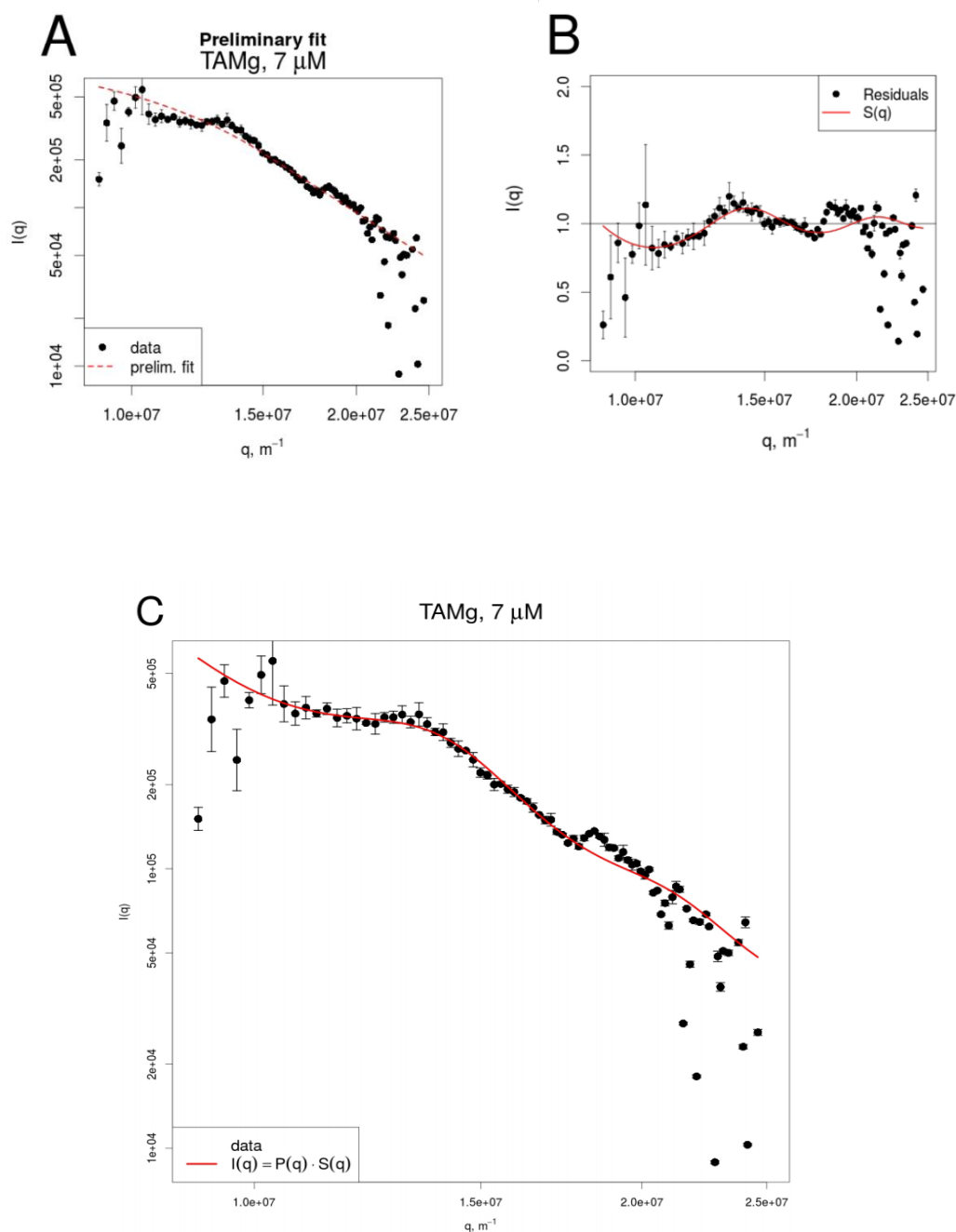


**Figure 2.35** Fit to scattering data for **C12<sub>10</sub>-HEG<sub>10</sub>** in TAMg buffer at 7  $\mu\text{M}$ . [A] Upon fitting the generalised Guinier-Porod model,  $P(q)$ , an oscillatory pattern to the residuals may be more or less apparent, according to concentration. [B] We suggest this pattern might be explained by a structure factor,  $S(q)$ , thereby incorporating the effect of an excluded volume due to particle size over the measured  $q$ -range. [C] shows the resulting composite model for the empirical scattering profile,  $I(q)=P(q)S(q)$ .

**Table 2.1** Sample concentration in TBE and TAMg with their fitted parameters.

Buffer	Sample concentration, $\mu\text{M}$	Fitted parameters	
		s	d
TAMg	4	0.14	3.2
	7	0.65	2.86
	10	0.78	2.62
	40	0.73	2.64
	100	1.47	2.67
TBE	10	0	2.65
	20	0	2.65
	40	0.5	2.42
	70	0.85	2.58
	100	1.42	2.51

(C12-HEG)<sub>10</sub> in different concentrations did not scatter light with sufficient intensity for analysis.

**Table 2.2** Summary of self-assembly by sequence, buffer, and concentration. [a] No observable self-assembly. Critical aggregation concentrations can be inferred from the degree of dilution required to achieve this.

Buffer	C12 <sub>10</sub> -HEG <sub>10</sub>		(C12-HEG) <sub>10</sub>	
	TBE	TAMg	TBE	TAMg
100 $\mu\text{M}$	Scrolls	Lumpy particles/ clusters	Random aggregates	Discs, film
10 $\mu\text{M}$	Lamellae	SCNPs	Random coil	Film
1 $\mu\text{M}$	Prolate seeds	[a]	[a]	[a]
0.1 $\mu\text{M}$	[a]	[a]	[a]	[a]

A conventional approach to measuring the size of self-assembled higher ordered structures was not successful. However, it has proven that self-assembly formation is concentration dependent and how gradually the higher order structures that form according to solution conditions. Analysing of obtained data was challenging since the available range of length scales via the light scattering experiment can provide only partial information with respect to this system and these results would be greatly enhanced by the complementary information available via an X-ray or neutron scattering experiments. With a view to confirming the results obtained by the light scattering and gaining more accurate dimensional estimates, a SAXS experiment was conducted for both sequence isomers. However, this did not yield useful data due to poor scattering contrast.

#### 2.2.3.4 Computer Modelling and Simulation

Computational modelling supports experimental observations and helps to draw conclusions from them by revealing molecular level interactions and mechanisms. Dr Tomasz Piskorz, under supervision of Prof Fernanda Duarte at the University of Oxford contributed the self-assembly models of **(C12)<sub>2</sub>-(HEG)<sub>2</sub>** and **(C12-HEG)<sub>2</sub>** 4mers. This system consisted with similar structural pattern as diblock **C12<sub>10</sub>-HEG<sub>10</sub>** and alternating **(C12-HEG)<sub>10</sub>** polymers but made the problem computationally tractable. The computational modelling and simulation done by Dr Piskorz was used with permission to get a better understanding of the self-assembly behaviour of synthesised **C12-HEG** isomers.

Short oligomers with 4 units were simulated using the coarse-grained (CG) Martini force-field, within the GROMACS simulation package (version 2019.2).<sup>29</sup> The parameterization approach employed in Martini emphasizes the transferability and compatibility of the force field in addition to reproduction of thermodynamic data.

Martini uses a chemical building block mapping methodology where the same chemical groups are represented by the same CG bead in all different molecules. The Martini force field has parameters available for an increasing number of molecules. Standard parameters were used for the alkane chain and the phosphate group. For the PEG chain and end alcohol groups, the parameters developed by Rossi et al. were employed.<sup>30</sup>

As shown in the figure (Figure 2.36 (b)) after 1.5  $\mu$ s simulations for the **C12<sub>2</sub>-HEG<sub>2</sub>** and **C12-HEG<sub>2</sub>** reached equilibrium, and this is shown as flattening of solvent accessible surface area (SASA). The block 4mer **C12<sub>2</sub>-HEG<sub>2</sub>** shows a lower value for SASA compared to alternating oligomer **C12-HEG<sub>2</sub>**. These difference in SASA suggest that **C12<sub>2</sub>-HEG<sub>2</sub>** forms a more packed structure than alternating **C12-HEG<sub>2</sub>** oligomer. Largest cluster structure indicated for **C12<sub>2</sub>-HEG<sub>2</sub>** cluster analysis observed to be long-ordered compact structure with a compact and ordered hydrophobic core, surrounded by glycol chains (Figure 2.36 (c)). The largest cluster of the alternating oligomer **C12-HEG<sub>2</sub>** creates a dense and disordered network. These structure spans over the whole system and crosses periodic boundaries (Figure 2.36 (d)).

Simulations of 4mers are consistent with the results of experimental work of 20mers. The elongated ordered structures predicted for diblock **C12<sub>2</sub>-HEG<sub>2</sub>** oligomer agrees with TEM imaging of structures obtained by self-assembly of **C12<sub>10</sub>-HEG<sub>10</sub>** oligomers. Simulations of the alternating **C12-HEG<sub>2</sub>** oligomer leads to a disorganised aggregation. This agrees with the **C12-HEG<sub>10</sub>** self-assembly, where irregular aggregates were observed by TEM.



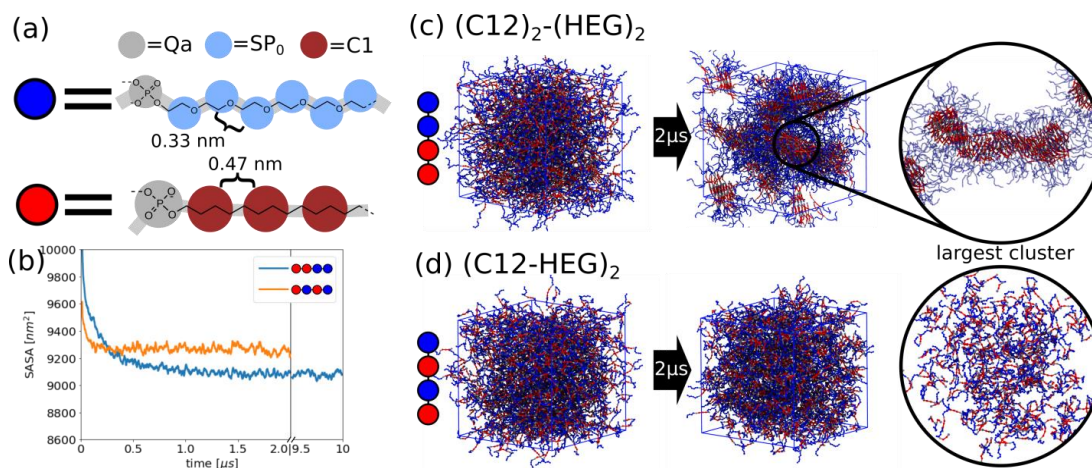


**Figure 2.36** (a) CG representation of oligomers consisting of glycol chain (blue) and hexadecane chain (red). The colour of the circles indicates bead type in Martini force-field. (b) Evolution of solvent accessible surface area (SASA); both systems reach equilibrium after 1.5 μs. (c-d) Initial and final snapshots from 2 μs simulations of randomly displacement (c) diblock **C12<sub>2</sub>-HEG<sub>2</sub>** oligomers and (d) alternate **(C12-HEG)<sub>2</sub>** oligomers. The structures in the circles present the largest cluster present in the final snapshot.

## 2.3 Conclusion

This chapter describes a new strategy for the synthesis of sequence defined, completely non-natural polyphosphodiester. A key concept is that control of length and sequence at the monomer level translates to highly uniform phosphate-based oligomers. Overall, it is found that the introduction of solid phase phosphoramidite method to create non-nucleosidic oligomers is efficient and straight forward. We have demonstrated the strategies to tackle many of the limitations hindering the success of creating sequence defined single chain nanoparticle and characterisation. The sequence regulation of the polyphosphodiester has been accomplished using **C12** and **HEG** building blocks.

The synthesised macromolecules were viewed as amphiphilic block copolymers **C12<sub>10</sub>-HEG<sub>10</sub>**, and alternating polymers **(C12-HEG)<sub>10</sub>** where the hydrophilic block

consists of 10 **HEG** units and Hydrophobic block consists of 10 **C12** units. The displayed self-assembly polymers were directly influenced by sequence. The resulting structures showed interesting nanostructures that are not usually found in self-assemble polymer systems. The resulting nanostructures have been far more interesting than our initial hypotheses: classical star micelle/worm/vesicle schema. Observed structures were produced with direct dissolution, rather than a solvent switch and system is also show structural switch with the influence of the salt. These findings raise interesting prospects for interface with biology, opening up the ability to alter nanostructures based on the specific environment that could be used to develop new diagnostics, drug carriers, or therapeutic systems themselves. Additionally, the method could be utilized to create polymer sequences with different composition and leads to the exciting prospect of creation a wide variety of sequence-defined polymers.

## 2.4 References

- (1) Niels ten Brummelhuis; Sebastian Wieczorek; Patrick Wilke; Thorsten Schwemmer; Hans G. Börner. *Sequence-Controlled Polymers: Synthesis, Self-Assembly, and Properties*; 2014; Vol. 1170.
- (2) Usman, N.; Ogilvie, K. K.; Jiang, M. Y.; Cedergren, R. J. *J. Am. Chem. Soc.* **1987**, *109* (25), 7845–7854.
- (3) Kwak, M.; Herrmann, A. *Chem. Soc. Rev.* **2011**, *40* (12), 5745–5755.
- (4) Edwardson, T. G. W.; Carneiro, K. M. M.; Serpell, C. J.; Sleiman, H. F. *Angew. Chemie - Int. Ed.* **2014**, *53* (18), 4567–4571.
- (5) Edwardson, T. G. W.; Carneiro, K. M. M.; McLaughlin, C. K.; Serpell, C. J.; Sleiman, H. F. *Nat. Chem.* **2013**, *5* (10), 868–875.
- (6) Häner, R.; Garo, F.; Wenger, D.; Malinovskii, V. L. *J. Am. Chem. Soc.* **2010**, *132* (21), 7466–7471.
- (7) Nothisen, M.; Kotera, M.; Voirin, E.; Remy, J.-S.; Behr, J.-P. *J. Am. Chem. Soc.* **2009**, *131* (49), 17730–17731.
- (8) Dubber, M.; Fréchet, J. M. J. *Bioconjug. Chem.* **2003**, *14* (1), 239–246.
- (9) de Rochambeau, D.; Barlóg, M.; Edwardson, T. G. W.; Fakhoury, J. J.; Stein, R. S.; Bazzi, H. S.; Sleiman, H. F. *Polym. Chem.* **2016**, *7* (31), 4998–5003.
- (10) Schnitzler, T.; Herrmann, A. *Acc. Chem. Res.* **2012**, *45* (9), 1419–1430.
- (11) Li, Z.; Zhang, Y.; Fullhart, P.; Mirkin, C. A. *Nano Lett.* **2004**, *4* (6), 1055–1058.
- (12) Wu, Y.; Sefah, K.; Liu, H.; Wang, R.; Tan, W. *Proc. Natl. Acad. Sci.* **2010**, *107* (1), 5–10.
- (13) Jia, F.; Lu, X.; Tan, X.; Zhang, K. *Chem. Commun.* **2015**, *51* (37), 7843–7846.
- (14) Alemdaroglu, F. E.; Herrmann, A. *Org. Biomol. Chem.* **2007**, *5* (9), 1311–1320.
- (15) Chien, M. P.; Rush, A. M.; Thompson, M. P.; Gianneschi, N. C. *Angew. Chemie - Int. Ed.* **2010**, *49* (30), 5076–5080.
- (16) Kamps, A. C.; Cativo, M. H. M.; Chen, X. J.; Park, S. J. *Macromolecules* **2014**, *47* (11), 3720–3726.
- (17) Bousmail, D.; Chidchob, P.; Sleiman, H. F. *J. Am. Chem. Soc.* **2018**, *140* (30), 9518–9530.
- (18) Al Ouahabi, A.; Charles, L.; Lutz, J.-F. *J. Am. Chem. Soc.* **2015**, *137* (16), 5629–5635.
- (19) Al Ouahabi, A.; Kotera, M.; Charles, L.; Lutz, J.-F. *ACS Macro Lett.* **2015**, *4* (10), 1077–1080.

- (20) Grandgirard, J.; Poinso, D.; Krespi, L.; Nénon, J. P.; Cortesero, A. M. *CrossRef List. Deleted DOIs* **2011**, 103 (3), 239–248.
- (21) Johnson, K. M.; Hanekamp, T.; Stayton, M. M. *Biopolym. Cell* **1997**, 13 (3), 250–253.
- (22) Greenspan, P.; Fowler, S. D. *J. Lipid Res.* **1985**, 26 (7), 781–789.
- (23) Greenspan, P.; Mayer, E. P.; Fowler, S. D. *J. Cell Biol.* **1985**, 100 (3), 965–973.
- (24) Xu, Q.; Li, S.; Yu, C.; Zhou, Y. *Chem. – A Eur. J.* **2019**, 25 (17), 4255–4264.
- (25) Lorber, B. (2018). arXiv preprint arXiv:1810.00611.
- (26) Andersson, M.; Wittgren, B.; Wahlund, K.-G. *Anal. Chem.* **2003**, 75 (16), 4279–4291.
- (27) Pedersen, J. S. In *Neutrons, X-rays and Light: Scattering Methods Applied to Soft Condensed Matter*; Elsevier, 2002; pp 391–420.
- (28) Hammouda, B. *J. Appl. Crystallogr.* **2010**, 43 (4), 716–719.
- (29) Periole, X.; Marrink, S.-J. *Methods Mol. Biol.* **2013**, 924, 533–565.
- (30) Rossi, G.; Fuchs, P. F. J.; Barnoud, J.; Monticelli, L. *J. Phys. Chem. B* **2012**, 116 (49), 14353–14362.

## Chapter 3

### 3. Oligophosphodiester DAN-NDI charge transfer complexes in aqueous media.

Portions of the work in this Chapter have been pre-printed as “Sequence-complementarity dependent co-assembly of phosphodiester-linked aromatic donor-acceptor trimers” by N. Appukutti, A. de Vries, P. Gudeangadi, B. Claringbold, M. Garrett, M. Reithofer and C. Serpell in October 2021 in ChemRxiv.

#### 3.1 Introduction

Non-covalent interactions are of great interest to chemists and biologists who study the molecular structure and function of biological systems. Noncovalent bonds such as electrostatic, van der Waals, hydrogen bonding, metal coordination, and aromatic-aromatic interactions are critical in maintaining the three-dimensional structures of large molecules. When introduce new building blocks to create novel systems. It is required to understand all the individual building blocks and their fording nature.

Molecular self-assembly through non-covalent interactions is a fundamental part of countless natural and synthetic materials. The importance of  $\pi$ - $\pi$  interactions in biology, for example in determining and maintaining the three-dimensional structure of proteins and DNA, have led to various applications in different fields. In DNA, interactions between the stacked nucleotide bases (base stacking) within the individual strands add to the overall stability of the DNA double-helix, while desolvation of the aromatic faces of the bases upon stacking is thought to provide a significant driving force for the formation of the double-helix structure.<sup>1</sup>

There have been significant efforts to understand the relationship between folding of natural biomolecules and their primary structure, along with its function and malfunction, and scientists have borrowed the organizational motifs from nature and employed that knowledge for the development and application of novel and synthetic materials. An assembly driven by non-covalent interactions allows for many different chain conformations and could lead to distinct folding motifs, which may not necessarily evolve in nature.

In material science, self-assembly has been found to be a powerful tool for the design and construction of supramolecular systems. In supramolecular chemistry, superstructure is highly studied, and most research focuses on the predictable structural control of synthetic materials. Interactions between aromatic units have been used in a variety of folding and self-assembling systems and here we focus on donor-acceptor type aromatic-aromatic interactions.

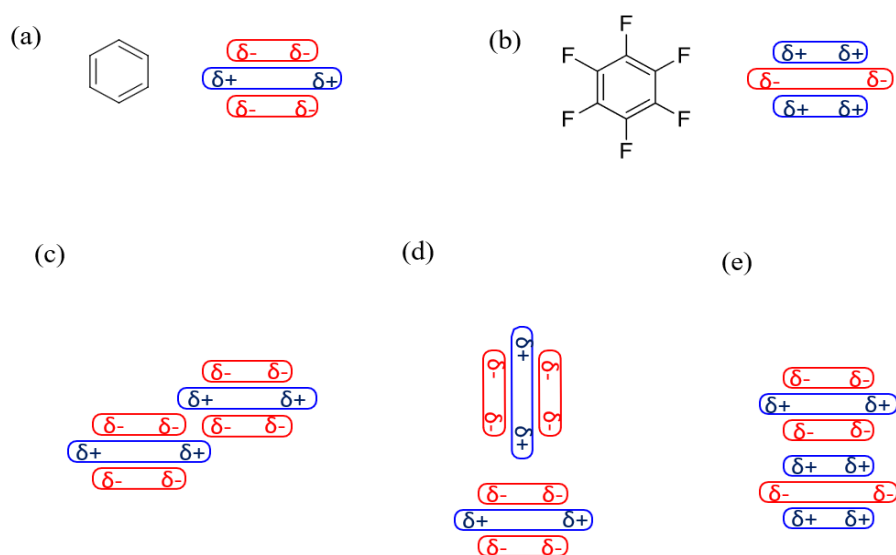


**Figure 3.1** The polar/pi model of aromatic stacking with the (a) electron-rich benzene and the (b) electron-deficient hexafluorobenzene. Typical stacking modes are (c) offset face-to-face, (d) edge-to-face, and (e) face-centered stacking.

In 1990, the classical model for interactions between aromatic units, known as the polar/ $\pi$  model was established by Hunter and Sanders.<sup>2</sup> The model predicts aromatic stacking geometry using the quadrupole moment that arises from  $\pi$ -electron density on polarized aromatic rings. Simple aromatic rings, like benzene, are electron-rich (i.e. with a partial negative charge) on their top and bottom faces, and electron-deficient (partial positive charge) along their peripheries (Figure 3.1). On the other hand, functionalised rings such as hexafluorobenzene, have a relatively electron-deficient aromatic core and an electron-rich periphery associated with the electronegative fluorine atoms. Aromatics can therefore be classified according to the nature of their core. For example, benzene would generally be referred to as an electron-rich aromatic, while hexafluorobenzene would be described as electron-deficient. The “polar/ $\pi$ ” model predicts that when two relatively electron-rich benzene molecules interact, they will maximize complementary electrostatics. This results in stacking in an off-set parallel or an edge-to-face geometry since a face-centered interaction will produce electrostatic repulsion. On the other hand, the interaction of benzene with the electron deficient hexafluorobenzene is predicted to occur in an alternating face-centered stacked geometry and both structures have been confirmed in the solid state.<sup>3,4</sup> The face-centered interaction between benzene and hexafluorobenzene is known as an aromatic donor–acceptor interaction where benzene is the donor (electron-rich) and hexafluorobenzene is the acceptor (electron-deficient).

Direct complementary interaction between aromatic substituents was examined closely by Wheeler and Houk looking at the interaction energies between substituted face-centered stacked benzene dimers.<sup>5</sup> They found that the substituent effects in the sandwich configuration of the benzene dimer do not involve the  $\pi$  system. Instead,

the origin of such attraction should be viewed as a direct interaction between the substituent groups (X) and the aromatic ring. Their work has helped refine this model and painted an alternative picture for predicting the preferred interaction geometries between two or more aromatic units. The model is referred to as the “local, direct interaction” model.<sup>6</sup> Both models discussed above describe the mechanisms behind aromatic–aromatic interactions and one should consider both models while predicting or assessing stacked aromatic molecules.

### 3.1.1 Interaction between DAN and NDI aromatic units

1,5-Dialkoxy-naphthalene (DAN) derivatives and 1,4,5,8-naphthalenetetracarboxylicacid diimide (NDI) derivatives are the central focus of this chapter. DAN is a prototypical electron-rich aromatic due to electron-donating alkoxy group and NDI is a prototypical electron deficient aromatic due to electron-withdrawing imide carbonyl groups. The electrostatic potential of these two molecules reveals a polarization of the aromatic core derived from the electron-donating alkoxy groups and electron-withdrawing imide carbonyl groups, respectively. An important aspect of the DAN and NDI structures is that they are roughly the same size which is important in the stacking. DAN and NDI as individual components usually adopt either an edge-to-face or an offset face-to-face (parallel displaced) stacking mode to best alleviate repulsive forces (Figure 3.2). DAN usually self-stacks in a herringbone arrangement, while NDI is observed to stack in an off-set fashion. When mixed, DAN and NDI stack in an alternating, face-centered fashion to maximize complementary electrostatic interactions, and corresponding  $\pi$  orbital mixing results in a charge-transfer absorbance band and the complex has a characteristic red-purple colour.<sup>7–13</sup> Face-centered stacking geometry of DAN and NDI mixture has been observed in the solid state and in solution.<sup>1,12</sup>



However, solvation/desolvation have considerable impact on the aromatic-aromatic association, especially in aqueous environments.<sup>14</sup>

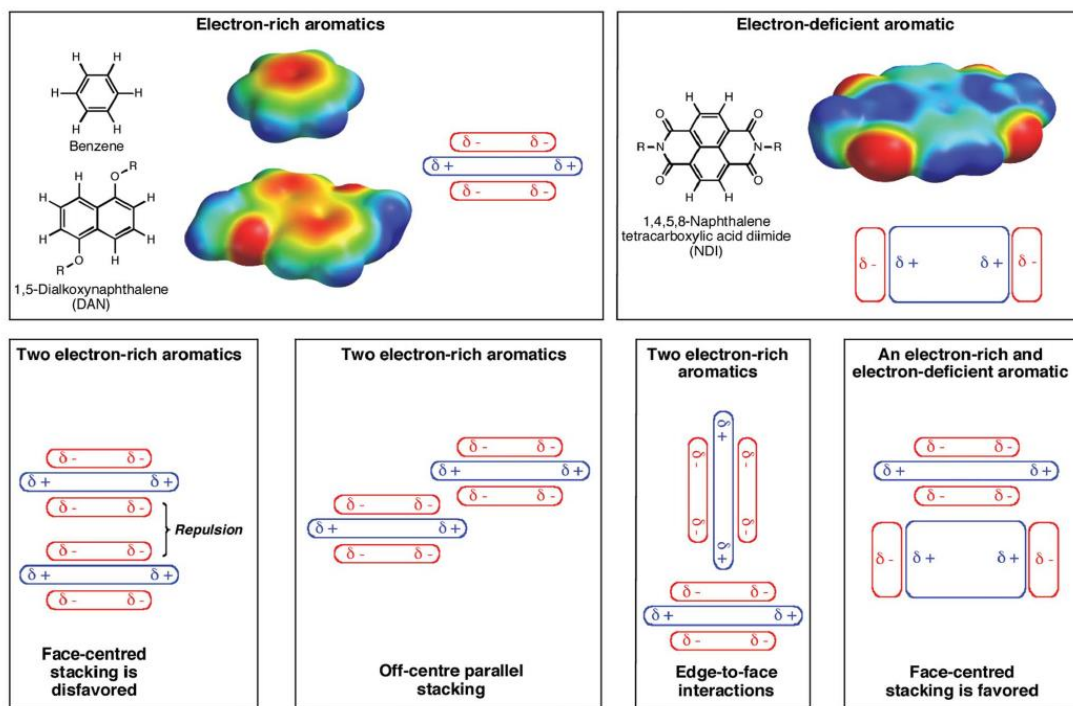


**Figure 3.2** The polar/pi model of aromatic stacking with the electron-rich 1,5 Dialkoxynaphthalene (DAN) and the electron-deficient 1,4,5,8-Naphthalene tetracarboxylic acid diimide (NDI) with typical stacking modes. Adapted with permission from reference (ChemCom, 2012)<sup>15</sup>

The donor-acceptor (D-A) interaction is better described as the sum of van der Waals forces, the solvophobic effect, local electrostatic effects and charge transfer.<sup>16–18</sup> D-A interactions have been used to direct the kinetically controlled synthesis of advanced architectures such as mechanically interlocked structures for several years. In 1980s, Stoddart and co-workers were the first to use D-A interactions as template to obtain interlocked molecules with complex topologies.<sup>19,20</sup> Liu and co-workers showed the formation of a highly organised D-A complex simply by solid state grinding. Upon

grinding, a purple colour started to appear, which was an indication of charge-transfer complex between the electron-rich crown ether and electron deficient pyridine-NDI.<sup>21</sup>

Use of D-A stacks in a compact face to-face geometry has widely been used as template for complex structures such as foldamers<sup>22–24</sup> rotaxanes,<sup>25–27</sup> and catenanes.<sup>18,28,29</sup> Sanders et al. have extensively studied the versatile nature of D-A interactions of NDI and DAN building blocks. Using 1,4,5,8-naphthalenediimide thiol and the  $\pi$ -donor dialkoxynaphthalene thiol as the main building blocks, the Sanders and Pantoş groups have reported the synthesis of a range of [2]catenanes.<sup>18,28</sup> By exploiting  $\pi$ - $\pi$  stacking and hydrophobic interactions, Sanders' group have constructed a diverse array of disulfide-linked catenanes from complementary electron-deficient naphthalene diimide and electron-rich dialkoxynaphthalene motifs. One striking example is the generation of donor-acceptor [2]catenane from an equimolar solution of  $\pi$ -deficient naphthalene diimide and  $\pi$ -rich 1,5-dialkoxynaphthalene dithiol building blocks ( Figure 3.3).<sup>30</sup>

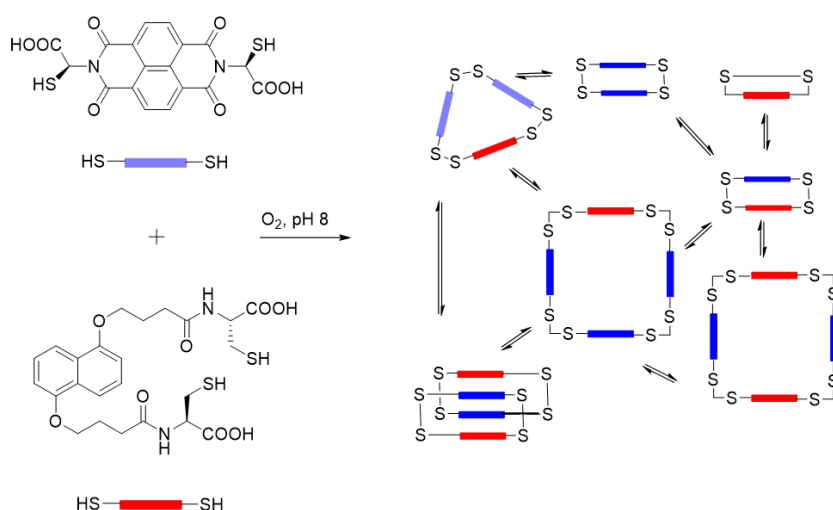


**Figure 3.3** Generation of donor-acceptor [2]catenane.

The Matile group utilized DAN–NDI association to template a synthetic ion channel.<sup>31</sup> A rigid-rod scaffold was synthesized with eight phenyl groups and eight NDI units. Twisted helix structure which lacked space for ions to pass through its internal cavity was adopted to create this scaffold. The DAN monomer addition enabled a conformational change into an open barrel structure that allowed ions to pass through a passage. A red solution was observed due to face-centered DAN–NDI association. Experimental evidence and modelling supported the model in which the DAN–NDI interaction forced the rigid-rod scaffold to untwist into the barrel structure. The barrel structure provided enough space within its internal cavity to transport ions with some selectivity.

A series of bis-amide functionalized DAN and NDI monomers which formed gels in non-polar solvents through hydrogen bonds and/or aromatic donor-acceptor interactions were investigated by Ghosh et al.<sup>32</sup> The DAN–NDI assembly was strongly influenced by solvent polarity, distance between the aromatic core and the amide functionality along the side chain. The DAN–NDI mixtures assembled into an alternating D–A arrangement only when the side chain length on both monomers were approximately equal. Using similar self-assembling NDI monomeric scaffolds, they also reported the assembly of 1D fibers<sup>33,34</sup> and 2D vesicles<sup>35</sup> derived from NDI-NDI interactions.

The Iverson group has been developing a class of foldamers, called aedamers (aromatic electron donor-acceptor oligomers). Those aedamers employ the aromatic-aromatic complexation between electron rich 1,8-dialkoxy-naphthalene (DAN) and electron-deficient 1,4,5,8-naphthalenetetracarboxylic diimide (NDI) “building blocks”.<sup>7</sup> The most important feature of these aedmaers is the modular design. The specific design allows facile solid-phase synthesis. Not only that the design also

allows to incorporate a wide variety of linkers that might possibly be used to modify folding and binding properties. There are also useful spectroscopic handles that are consistent with aedamers adopting a folded conformation in solution. Since the original publication of aedamers appeared in 1995, there have been several reported foldamers based on aromatic interactions.

The aedamer developed by Lokey et al. is the first folding molecule to use donor-acceptor aromatic-aromatic interactions to determine the secondary structure of a complex synthetic molecule in aqueous solution.<sup>7</sup> The molecule was designed connecting the two donor-acceptor moieties with properly flexible linkers, and, in an alternating fashion. The resulting oligomer was folded into a pleated structure in water by alternating electron-rich and electron-deficient aromatic units driven by the hydrophobic effect (Figure 3.4). The close face-centered stacking (3.4 Å) of complementary aromatic components leads to close pi orbital interaction which allows CT interaction between the aromatic units.

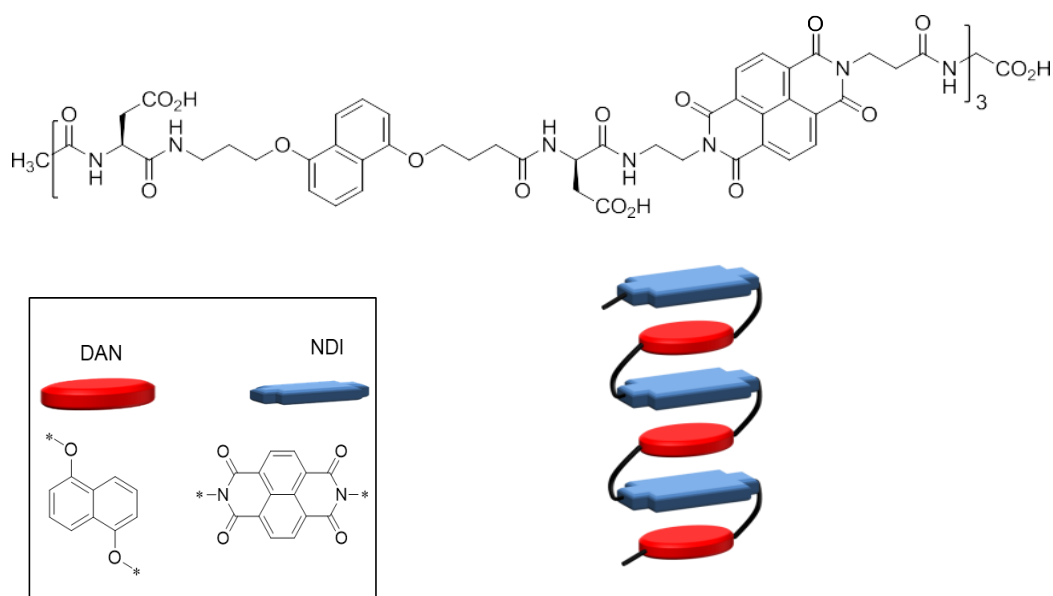


**Figure 3.4** The chemical structure of the first aromatic electron D–A oligomer and its representative pleated stacking mode (right).

Reczek synthesised DAN and NDI monomers series with different alkyl groups attached and he discovered that 1:1 mixtures of DAN and NDI monomers can form liquid crystals.<sup>36</sup> The liquid crystalline state of these mixtures exhibited a strong CT band and characteristic red colour of DAN–NDI association. The DAN–NDI interaction was employed to drive the self-assembly of some truly novel supramolecular systems. Zych synthesized a series of ten dimers comprised of DAN and NDI units tethered together by different amino acid linker residues.<sup>8</sup> The amino acid linkers give different lengths and degrees of rigidity to the created dimer structures. The CT absorption, molar absorptivity, and percent hypochromism were studied for the DAN and NDI dimer and trimers. Studies suggested a dynamic interaction between DAN and NDI with different possible conformations have a face-centered geometry.

Gabriel tethered DAN and NDI together with aspartic acid residues to form a dimer and three trimer molecules to study the effect of aromatic donor-acceptor connectivity.<sup>9</sup> The CT absorption, molar absorptivity, and percent hypochromism were studied for the DAN and NDI dimer and trimers (Figure 3.5). The work illustrated that simple and distinct folding patterns can be created just by changing the sequence of DAN and NDI units.

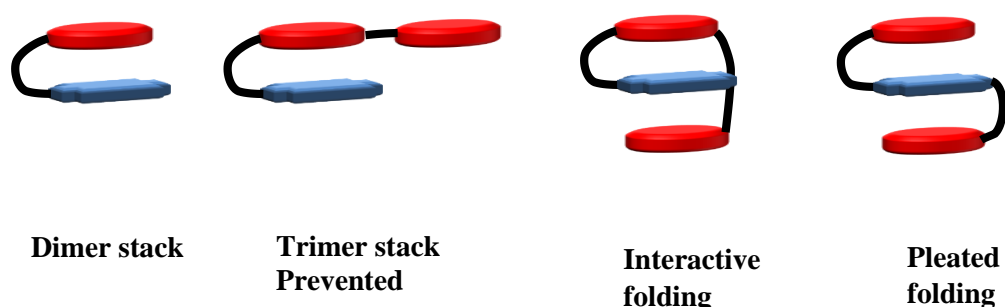


**Figure 3.5** The folding patterns targeted by DAN and NDI compounds.

Based on the successful development of other folding systems, Gabriel and Iverson designed DAN and NDI oligomers capable of self-assembling into heteroduplexes in water.<sup>37</sup> Heteroduplex formation was formed through intermolecular D-A interactions for DAN and NDI oligomers of up to four units in length (Figure 3.6). Conclusive evidence for 1:1 DAN-NDI binding was acquired using polyacrylamide gel (PAGE) titration experiments which showed that a 1:1 DAN-NDI oligomer ratio travelled farther than either the individual DAN or NDI oligomer. The PAGE gel titration also showed any excess oligomer at ratios other than 1:1 travelled less than the 1:1 complex.

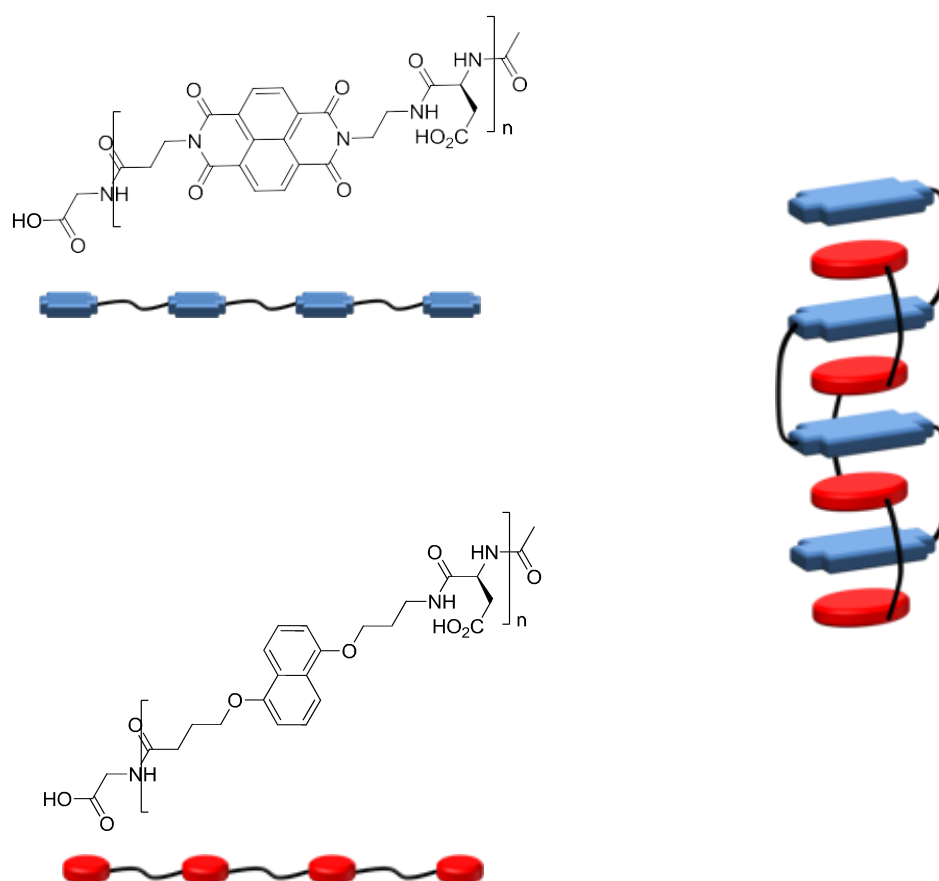


**Figure 3.6** Structures of DAN and NDI oligomers and the 1:1 DAN-NDI heteroduplex for oligomers (right).

NDI is known to be an important supramolecular building block because of its ability to adopt in to two different but entirely predictable stacking geometries. With complementary electron rich aromatic moieties such as DAN, NDI can have alternating face-centered stacking and NDI also capable of adopting into an off-set parallel self-stacking mode. Taking advantage of these two distinct states has generated several interesting systems. This Chapter describes the design, synthesis, and characterization of oligophosphodiester chains consisting of DAN or NDI repeat units, and the characterization of resulting structure from their mixture.

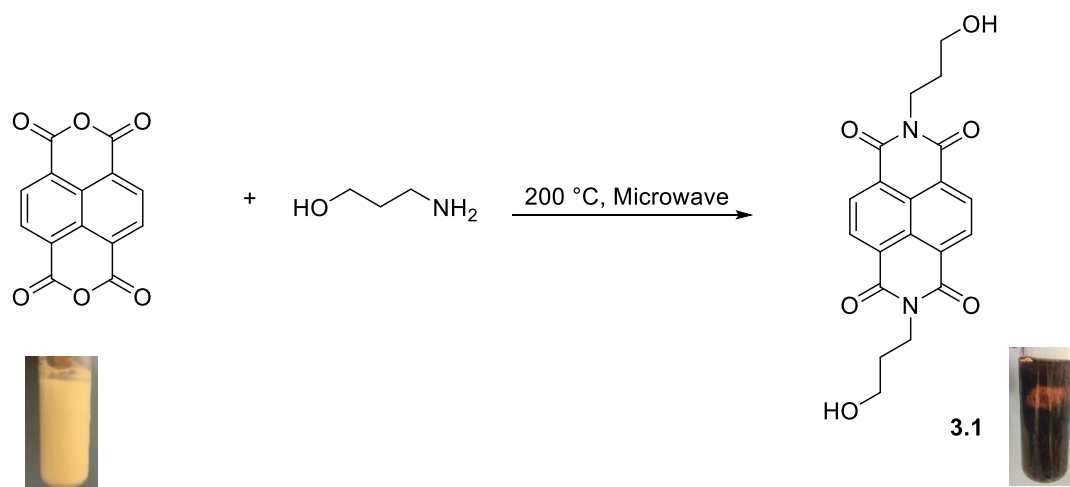
### 3.2 Aim of the Chapter.

The aim of this chapter is to lay the foundations for sequence-programmed folding of oligophosphoesters based upon CT interactions through use of DAN and NDI monomers. There are hundreds of possibilities of designed intermolecular DAN-NDI interactions in water. The chapter discuss, simple and more efficient DAN and NDI synthesis and their behaviour aqueous solutions.

### 3.3 Sequence defined DAN and NDI via solid phase synthesis.

#### 3.3.1 Synthesis of DAN and NDI monomers

The linkers/spacers attached to the main aromatic group play an important role in charge transfer complex formation. To fully utilise the hydrophobic driving force of aromatic-aromatic interactions, the polymers chains should be soluble in aqueous solution and adding prospective water-soluble spacers increase the overall polymer solubility. When a polymer is formed, these chains act as linking units for the aromatic repeat units, and the aromatic unit and spacers are incorporated as part of a linear backbone. Having specific functional groups that will carry a formal charge in solution is a likely requirement of polymer design to obtain aqueous solubility and phosphate group is ideal both from an aqueous solubility and synthetic perspectives.



**Scheme 3.1** Synthesis of NDI diol **3.1**.



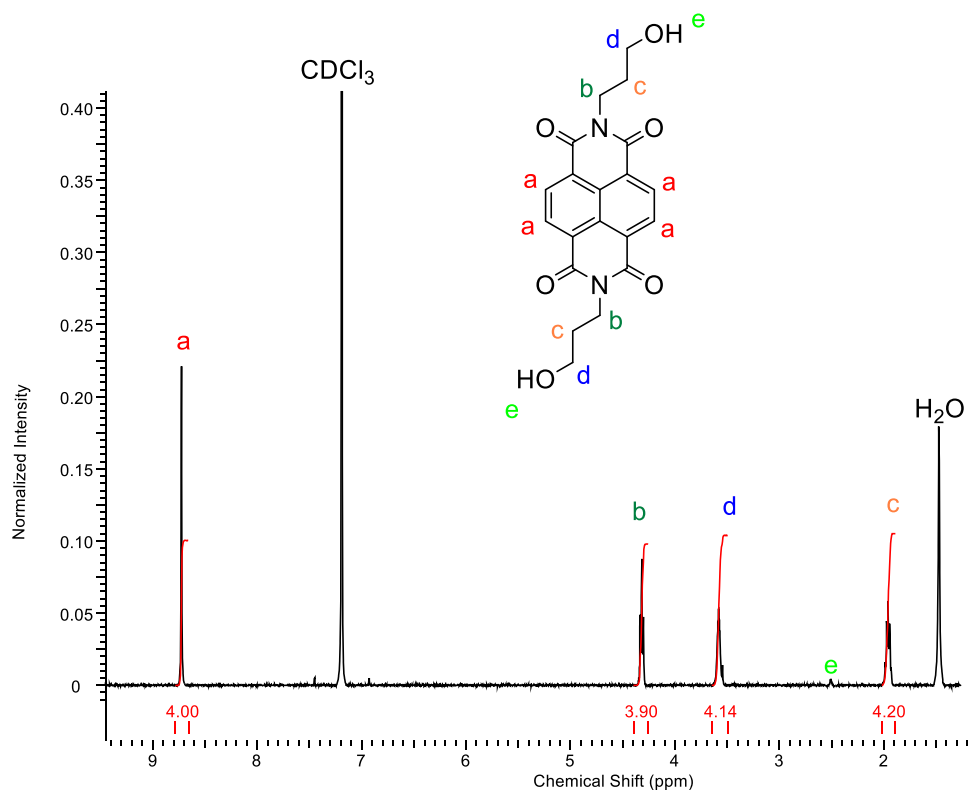


**Figure 3.7**  $^1\text{H}$  NMR spectra of the NDI diol **3.1** with  $\text{CDCl}_3$  as solvent.

Adopting a previously reported method,<sup>38</sup> an NDI diol **3.1** was synthesised reacting 1,4,5,8-naphthalenetetracarboxylic dianhydride and 3-aminopropanol in water (Scheme 3.1). The reaction was performed in a microwave, heated at 200 °C for 30 minutes. When the solution had returned to room temperature the resultant brown precipitate was filtered and washed with water and diethyl ether. The dried product gave a yield of 70%, and the identity of the product was then confirmed with proton NMR (Figure 3.7) and mas spectrum studies.

It is known that the DAN-NDI assembly is highly influenced by their spacer length and that face-to-face stacking occurs when the spacer chain length is approximately equal on both monomers.<sup>32</sup> An electron rich DAN monomer with a spacer to match

the NDI monomer was then synthesised with 1,5-dihydroxynathalene as starting material.

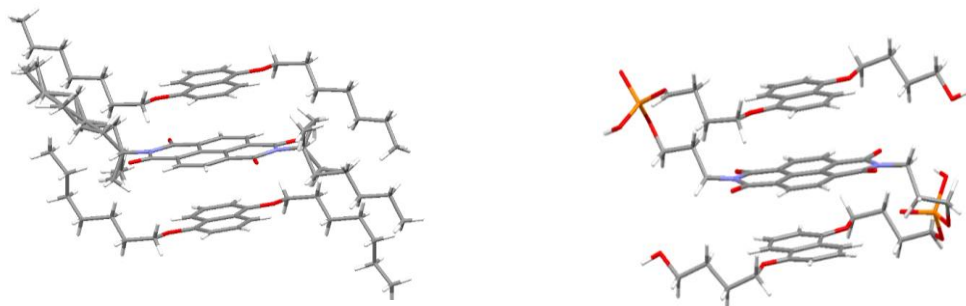
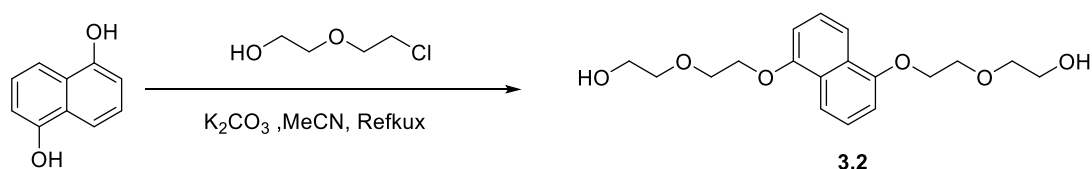


**Figure 3.8** (a) Model crystal structure from literature<sup>39</sup>(b) Hyper Chem optimised phosphate linked DAN-NDI structure.

When electron rich DAN and electron poor NDI are placed together, they form charge transfer complexes. Serpell's lab has previously synthesised DAN and NDI based and non-natural poly(phosphodiester)s in a solution-phase step-growth fashion by reacting diols with 2-cyanoethoxy-bis(N,N-diisopropylamino)phosphine and an activator, or phosphorous oxychloride (details found in Chapter 4). The pre-formation of charge-transfer complexes between the two components was confirmed with the crystal structure



**Scheme 3.2** Synthesis of DAN diol monomer **3.2**.

The DAN diol monomer **3.2** was designed with diethylene glycol spacer units. Adopting a previously reported method DAN diol monomer **3.3** was synthesised by reacting 1,5-dihydroxynaphthalene with chloroethyl ethanol (Scheme 3.2). The products were then purified and dried to obtain a second brown powder at > 50% yield.

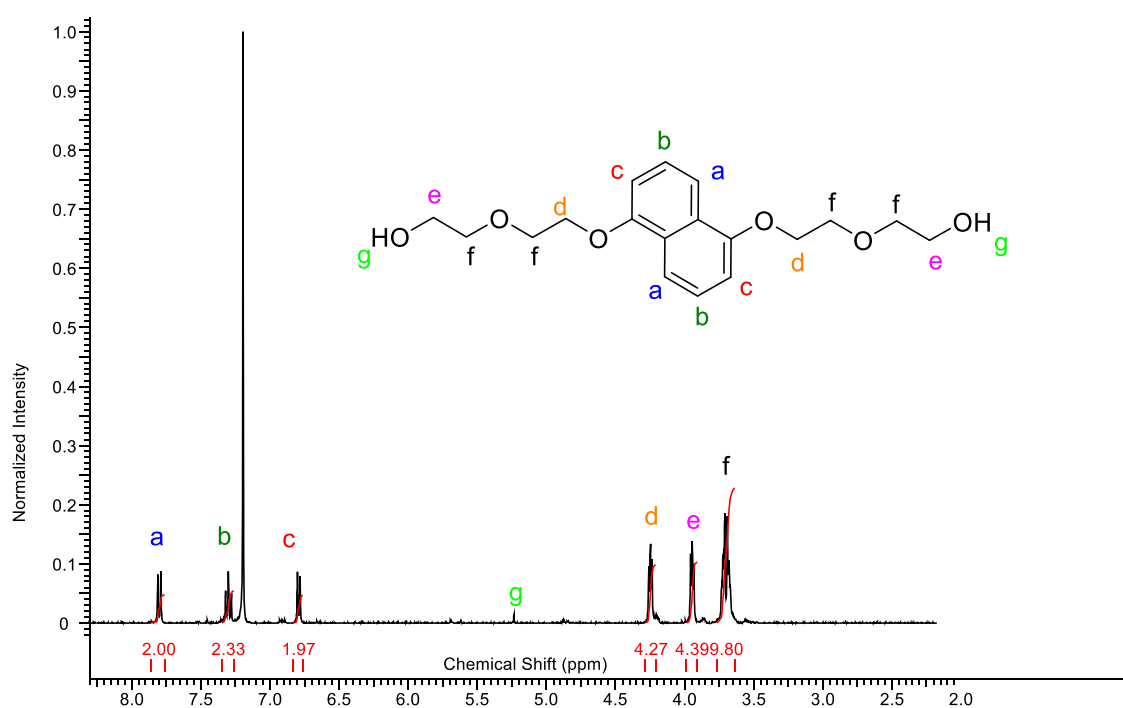


**Figure 3.9**  $^1\text{H}$  NMR spectra of the DAN diol derivative **3.2** with glycol side chains with  $\text{CDCl}_3$  as solvent.

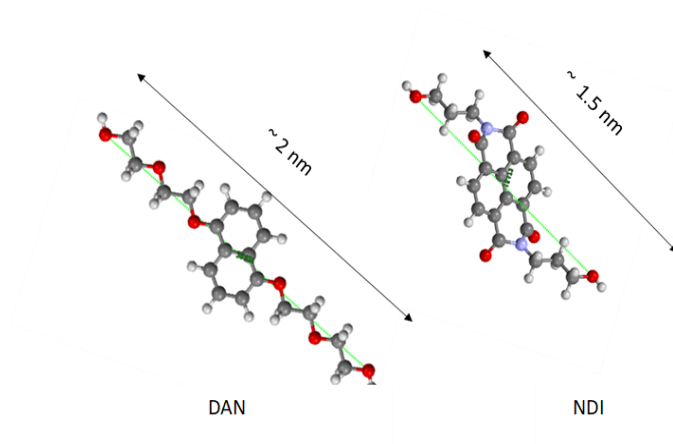


**Figure 3.10** The lengths of the side chains with the aromatic rings calculated with Mercury crystal structure visualisation software.

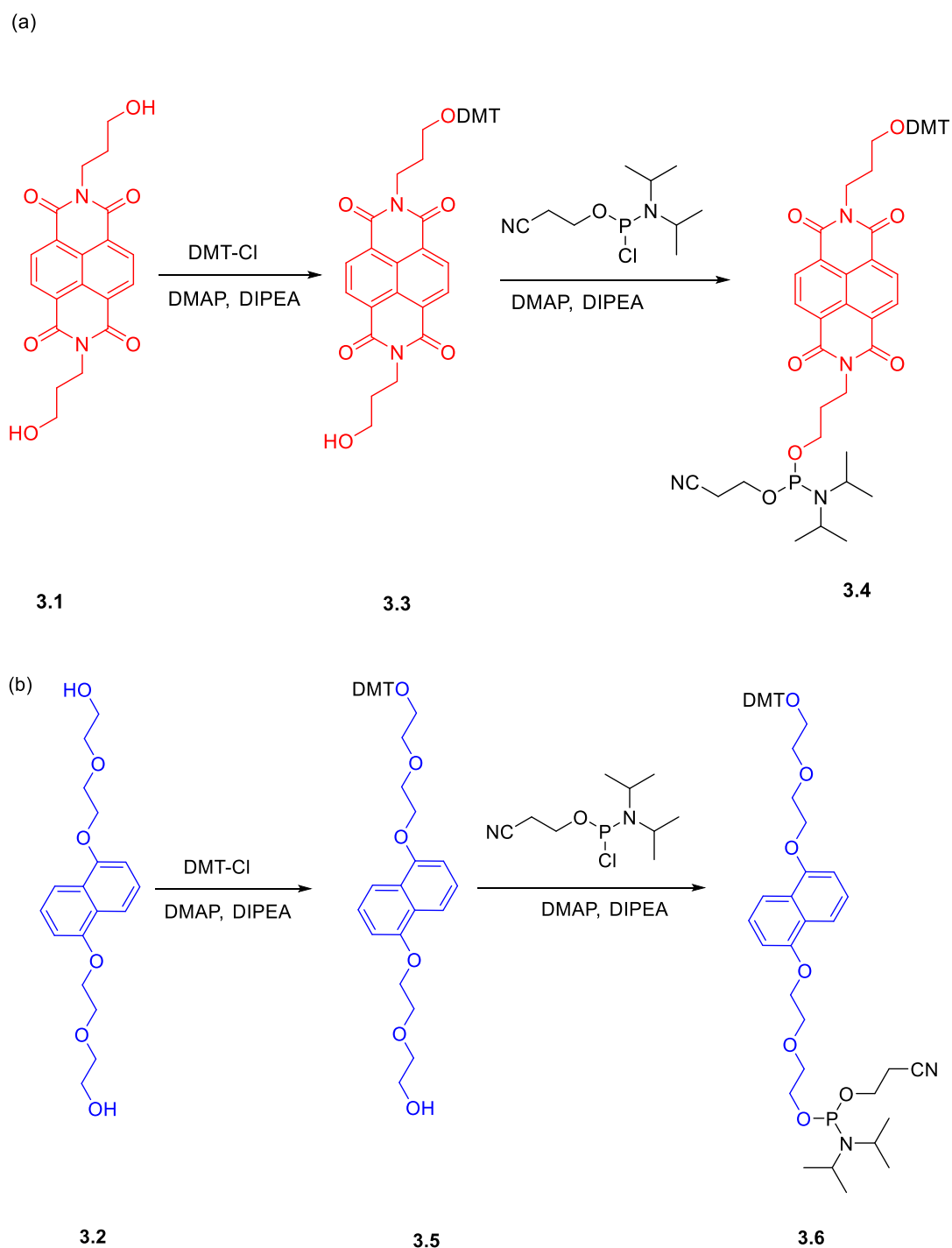
The lengths of the linkers with the aromatic rings were estimated for DAN and NDI monomers with Mercury crystal structure visualisation software using models made in Chem3D (Figure 3.10). The DAN unit was calculated as approximately 2 nm when stretched and NDI unit was found to be approximately 1.5 nm.

### 3.3.2 Synthesis of DAN and NDI polymers

We first employed the monomers in production of sequence-defined polymers using automated solid phase synthesis, discussed in Chapter 2. To make the DAN and NDI units solid phase synthesis compatible, one of the two OH groups should be protected with a dimethoxy trityl (DMT unit) and the other hydroxyl group should be activated with the phosphoramidite group.

NDI diol **3.1** and DAN diol **3.2** were separately reacted with one equivalent of dimethoxy trityl chloride (DMT-Cl) in the presence of DMAP and DIPEA. The products were then purified using column chromatography and their identities confirmed with MS spectra (Figure 3.11).

The vacuum dried mono protected derivatives were then each reacted with 2-cyanoethyl N,N-diisopropylchlorophosphoramidite to create NDI and DAN phosphoramidite reagents following the method discussed before (Chapter 2).



**Scheme 3.3** Synthesis of phosphoramidite reagent for solid phase synthesis with diols. (a) NDI phosphoramidite reagent **3.4**. (b) DAN phosphoramidite reagent **3.6**

The reaction completion was confirmed with TLC and oily DAN and NDI phosphoramidite reagents were then purified with column chromatography with basic alumina and DCM: MeOH (400:1) as the solvent.

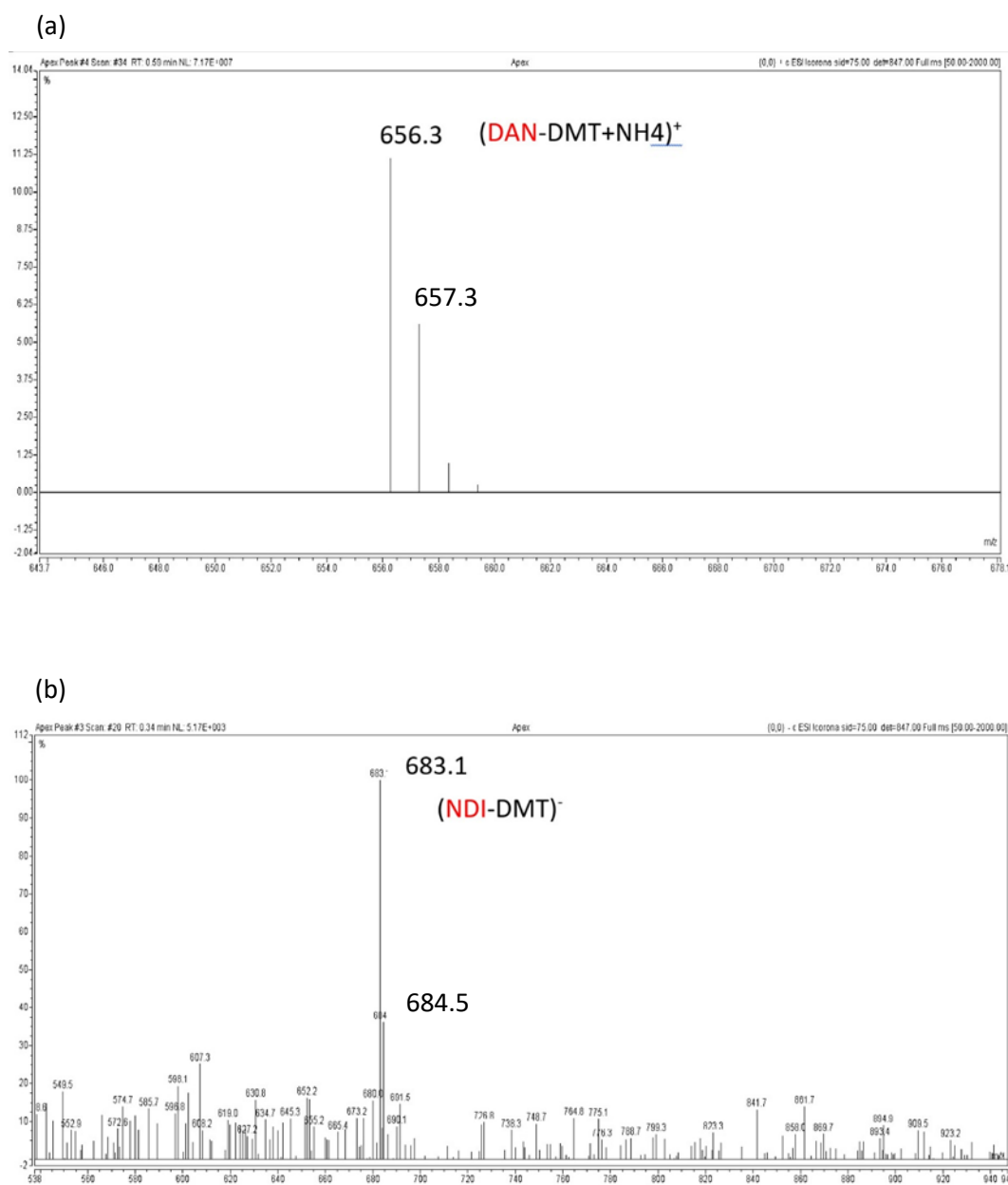


**Figure 3.11** Mass spectra of mono protected derivatives: (a) **DAN-DMT** (+ESI) (b) **NDIDMT** (-ESI).

To carry out the solid phase synthesis, the phosphoramidite derivative should be a trivalent phosphorus reagent. The trivalent phosphitylating agents are generally more

reactive than the corresponding pentavalent analogues. The DAN and NDI phosphoramidite reagents were extremely sensitive to oxygen and water, making it difficult to characterise the product.

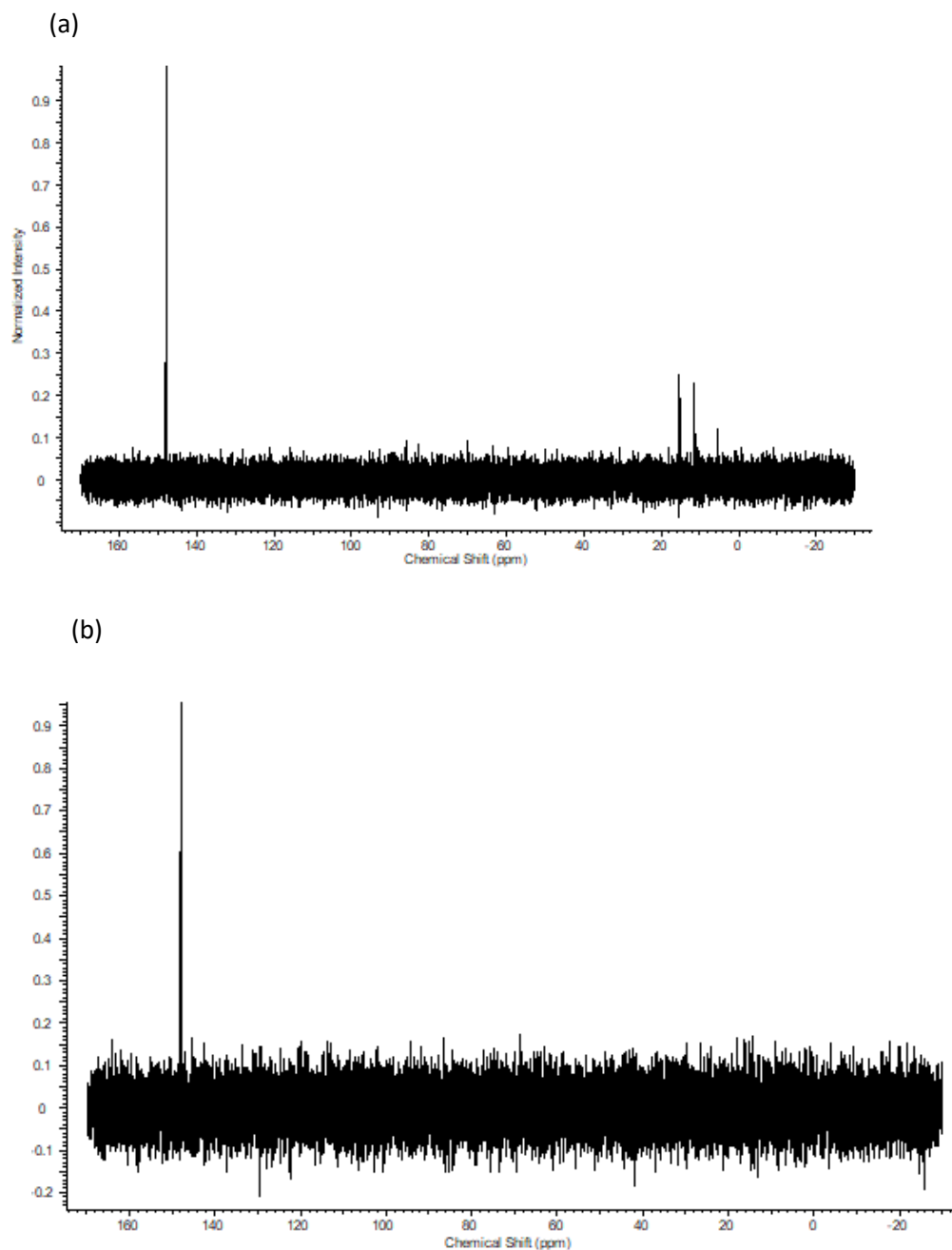


**Figure 3.12**  $^{31}\text{P}$ NMR of phosphoramidite reagents (a) DAN (b) NDI.



To avoid the oxidation of phosphoramidite, products were deployed in polymer synthesis immediately after purification, and a rapid check for P(III) by NMR. NMRs were performed in non-deuterated dichloromethane, using for DMSO- $d_6$  capillary tube for locking. The proton NMR spectrum was less visually appealing with noise, but the  $^{31}\text{P}$  NMR gave one peak around 140 ppm as expected for phosphoramidite reagents and no peak around zero for oxidized product (Figure 3.12). In DAN sample other than the expected peak at 140 ppm there are three small peaks at 0 ppm to 20 ppm. Those signals might be given by oxidized DAN phosphoramidite fractions. This confirms the obtained product is non-oxidised and suitable to apply in automated solid phase synthesis.

### 3.3.3 Synthesis and charge transfer association of DAN and NDI polymers in aqueous media

Polymer synthesis was conducted via automated solid phase synthesis using the extended coupling time protocol from Chapter 2. Controlled pore glass beads were used as the solid support. The synthesis cycle was carried out following the detritylation, coupling, capping, and oxidation steps. When the desired pattern was completed, the cycle was programmed to end with the last trityl group attached the polymer chain for the quantification purposes. As described in Chapter 2, trityl group was later removed manually and used for calculating the yield.

The initial plan was to create 20 units long polymer chains with different sequence patterns using DAN and NDI phosphoramidite reagents. **DAN<sub>20</sub>** and **NDI<sub>20</sub>** were synthesised using automated solid phase synthesis. The polymers were cleaved from the beads and deprotected with 60% ammonium hydroxide. The synthesis scale was 1  $\mu\text{mol}$  for all three polymers. The trityl histogram on the synthesizer screen showed a poor synthesis (Figure 3.13). During the automated process, the cycle was

disturbed several times but was able to complete the synthesis. After the deprotection and cleaving, all sequenced polymers were dissolved in 200  $\mu$ L of 80% acetic acid to remove the final DMT group.

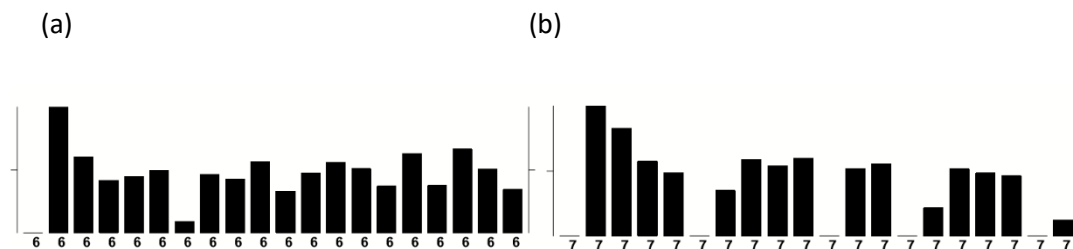


**Figure 3.13** Trityl Histogram for synthesis of (a) **DAN<sub>20</sub>** (b) **NDI<sub>20</sub>**.

The absorption for the acetic acid collected after the deprotection was calculated using Nanodrop UV absorption, and the spectrum showed a broad wavelength (190 nm to 750 nm). The typical UV absorption peak for the DMT cation appears at 499 nm but none of the polymers we designed showed a peak at that specific wavelength. This left us the question of what the exact yield of the synthesised product is. This can either be because of the last DMT was removed with the synthesis processes by default, or the DMT at the end is attached to the polymer very strongly that it cannot be removed with 80% acetic acid. We could not confirm the actual cause of the scenario. Neither of the products, **DAN<sub>20</sub>** and **NDI<sub>20</sub>** were soluble in water, TBE buffer or TAMg buffer solutions. This was a challenge, since poly-DAN and poly-NDI should be water soluble to drive the aromatic stacking, however, it is known that water solubility is a significant challenge for the polymer with a high number of naphthyl units.

DAN and NDI have well known UV absorption peak patterns as individuals.<sup>40</sup> The UV–vis absorption spectrum of NDI has two well resolved sharp absorption peaks at around 380 nm and 360 nm (Figure 3.14(a)). The CT complex formation of DAN and NDI derivatives were previously investigated by monitoring the absorption spectral change, and the absorption peak usually lies around 400 nm to 700 nm range (Figure 3.14).

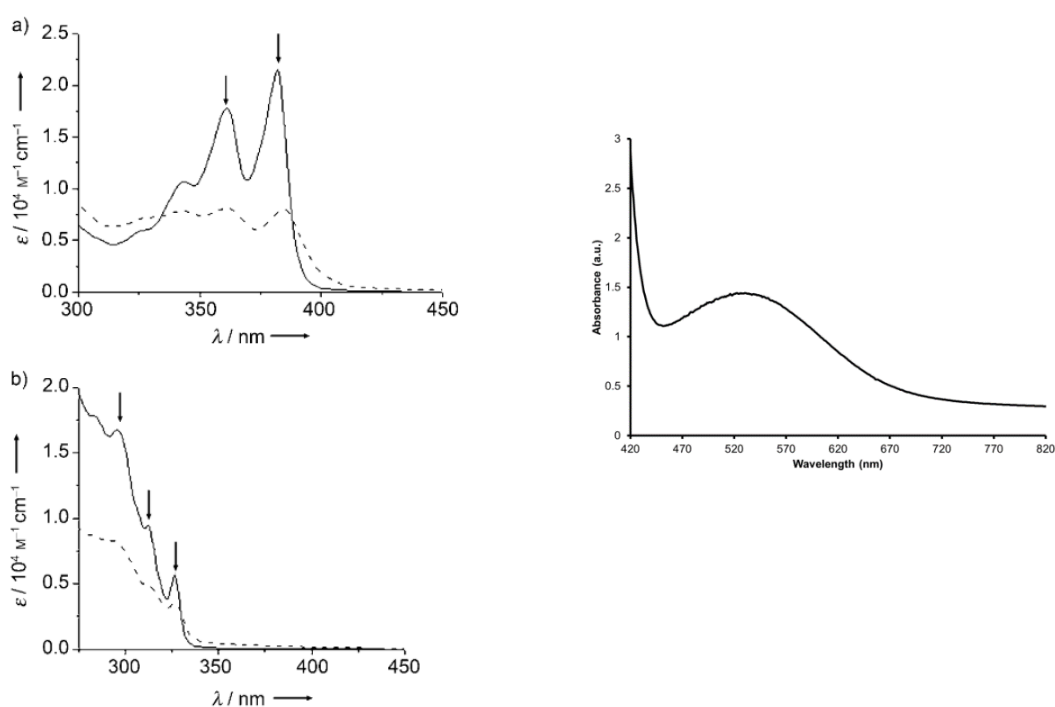


**Figure 3.14** UV/Vis spectra of a) NDI absorption is at high concentration is shown with solid line and low concentration with dashed line, b) DAN absorption is at high concentration is shown with solid line and low concentration with dashed line, and a CT region of a spectrum of donor-acceptor combination (right). Adapted with permission from reference (Chemistry - A European Journal, 2010)<sup>40</sup>

Iverson's work has previously shown that solvophobic/hydrophobic effects are the main contributor to the  $\pi$ - $\pi$  stacking of electron-rich 1,5-dialkoxynaphthalene (DAN) and electron-deficient 1,4,5,8-naphthalenetetracarboxylic diimide (NDI)<sup>15</sup>. Therefore, a **DAN<sub>20</sub>: NDI<sub>20</sub>** 1:1 mixture was expected to form a pleated structure in

water so that the DAN and NDI units were aligned in a face-centred manner to minimize the exposed aromatic surface area, and to maximize face-to-face electrostatics. We expected to see the absorption peak for the CT complex when DAN and NDI were mixed. CT absorptions bands are intense and often lie in the ultraviolet or visible portion of the spectrum, so mostly a colour change can be observed when the CT complex forms in a solution.

Unfortunately, the synthesised 20mer long DAN and NDI polymers were not soluble in water. 1 mL of water was added to each product and then heated and mixed overnight. The samples dissolved only partially in water. UV absorptions were measured for the partially dissolved **DAN<sub>20</sub>** and **NDI<sub>20</sub>** samples. From the stock solutions, 200  $\mu$ L of samples were taken and mixed to get a presumptive **DAN<sub>20</sub>:NDI<sub>20</sub>** 1:1 solution. No immediate colour change was observed after mixing. UV absorption spectra were then recorded for the mixed solution. General absorption peak pattern for DAN and NDI could not be identified for the 1:1 mixture and there was no extra band observed on the spectrum at 400 nm to 700 nm range that represents the CT formation (Figure 3.15).

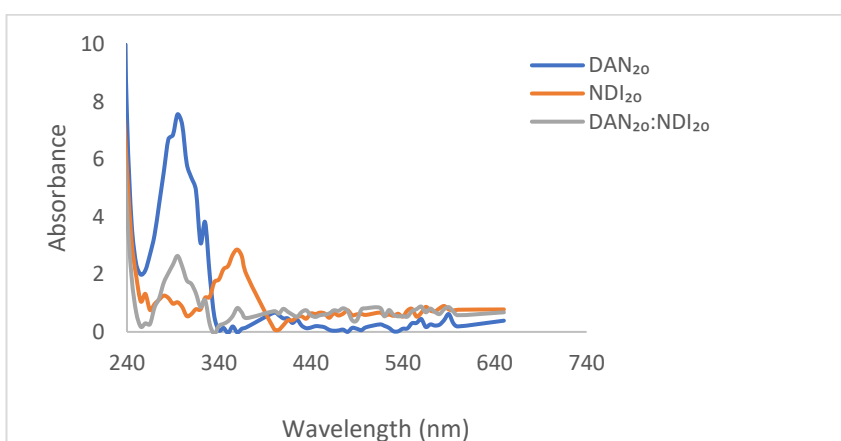


**Figure 3.15** UV absorption of DAN and NDI 20mers

Solubility plays an important role in self-assembly formation in aqueous media. Due to lack of solubility, **DAN<sub>20</sub>** and **NDI<sub>20</sub>** were not behaving as we expected. The negative formal charge on the linear polymer chain was unable to promote the aqueous solubility of DAN and NDI polymers. However, it is known that having several naphthyl units make the polymer hydrophobic. The length of the polymer may have affected the aqueous solubility as well. Taking this into account, the next set of polymers were synthesised as short oligomers consisting of DAN and NDI aromatic units with up to 12 units.

**DAN<sub>12</sub>**, **NDI<sub>12</sub>**, **DAN<sub>6</sub>NDI<sub>6</sub>** and **(DAN-NDI)<sub>6</sub>** sequences were synthesised with the solid phase phosphoramidite automated synthesis method (Figure 3.16). The last trityl group was not removed from the strands during the automated process and later it was removed manually with 80% acetic acid.

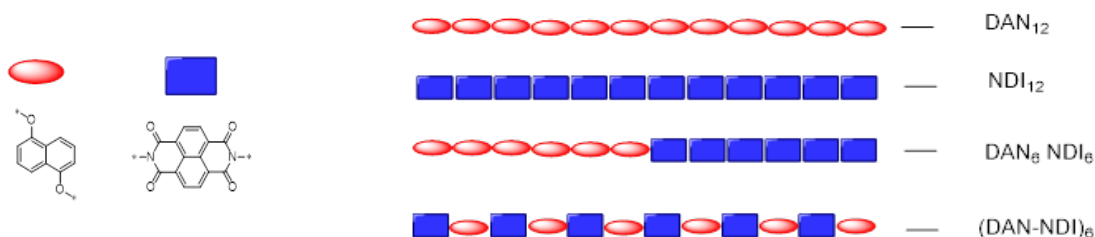


**Figure 3.16** Sequences of DAN and NDI 12mers.

**DAN<sub>12</sub>**, **NDI<sub>12</sub>** and **DAN<sub>6</sub>NDI<sub>6</sub>** completed their synthesis cycles without failing, although during the synthesis process, the **(DAN-NDI)<sub>6</sub>** sequence coupling failed before completing the cycle (Figure 3.17). The synthesised oligomers were cleaved from the beads and deprotected with 60% ammonium hydroxide solution.

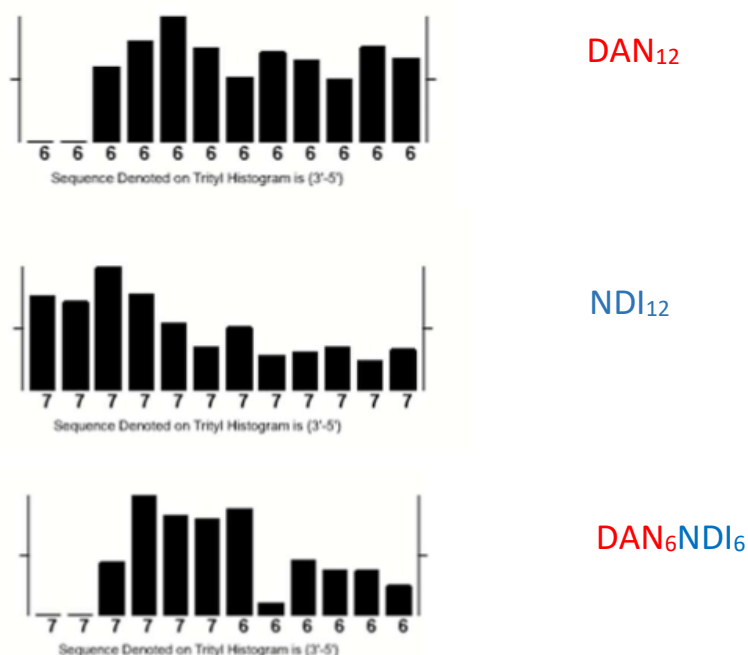


**Figure 3.17** Trityl histogram for 12mers: **DAN<sub>12</sub>**, **NDI<sub>12</sub>** and **DAN<sub>6</sub>NDI<sub>6</sub>**.

To remove the final trityl group, the four products were incubated with 80% acetic acid for an hour. After the incubation, the solution was measured by UV absorption. Similar to the previously made twenty-unit long polymers, there was no peak observed for the trityl cation, which suggests that the trityl group is still attached to the polymer, or it came off during the synthesis process. The sample was vacuum dried to remove acetic acid, then dissolved in autoclaved water and purified with small syringe column chromatography using Zetadex as the stationary phase. The yield could roughly be estimated with the trityl data shown on the DNA synthesiser screen and showed that **NDI<sub>12</sub>** and **DAN<sub>6</sub>NDI<sub>6</sub>** had a lower yield compared to **DAN<sub>12</sub>**.

Each product was dissolved in 1 mL of autoclaved water after purification, but concentration was unknown. UV absorption of the samples was measured and

recorded. **DAN**<sub>12</sub> and **NDI**<sub>12</sub> showed the specific peak pattern on UV absorption spectrum, which was previously identified by other researchers for a similar type of molecules (Figure 3.18 (a)). **DAN**<sub>6</sub>**NDI**<sub>6</sub> was expected to show both peak patterns representing DAN and NDI, but the peak shows that DAN has low intensity compared to NDI.

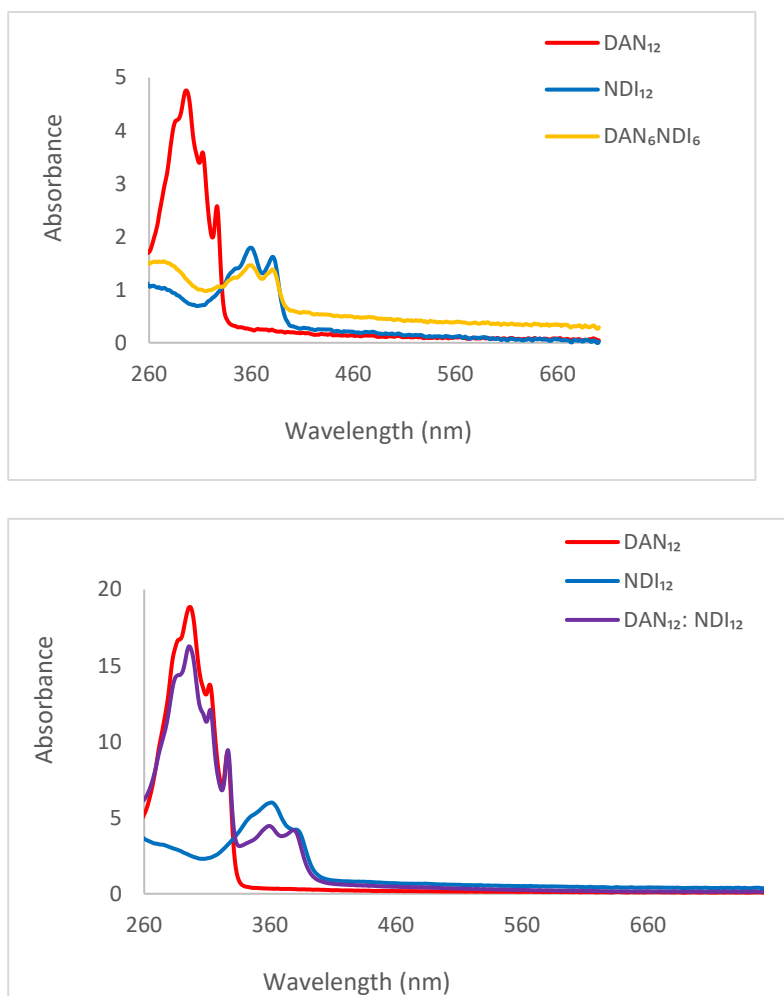


**Figure 3.18** UV absorption of DAN and NDI 12mers a) all four combinations in water b) 1:1 mixture of **DAN**<sub>12</sub> and **NDI**<sub>12</sub>.



The DAN: NDI 1:1 mixture was prepared by adding 100  $\mu\text{L}$  of both **DAN**<sub>12</sub> and **NDI**<sub>12</sub> together. Due to the characterisation difficulties we had with the samples, the DAN and NDI stock solution were assumed to have roughly similar concentrations. When mixing, the solution did not change colour significantly. DAN and NDI 1:1 solution was then observed by UV-vis to identify the DAN: NDI face-to-face association (Figure 3.18 (b)). DAN and NDI independent absorption peaks were visible on the spectrum, but there was no peak showing at around 500 nm as expected (which represents the charge transfer association). The fact that the UV-vis peaks for the aromatic-aromatic charge transfer band lack definition when the polymers are observed as 1:1 mixture, may mean that the independent chains are tightly coiled and self-stacking in solution. There was another concern regarding the NDI UV absorption peak, which is commonly expressed as two sharp peaks on the spectrum around 360 nm and 380 nm

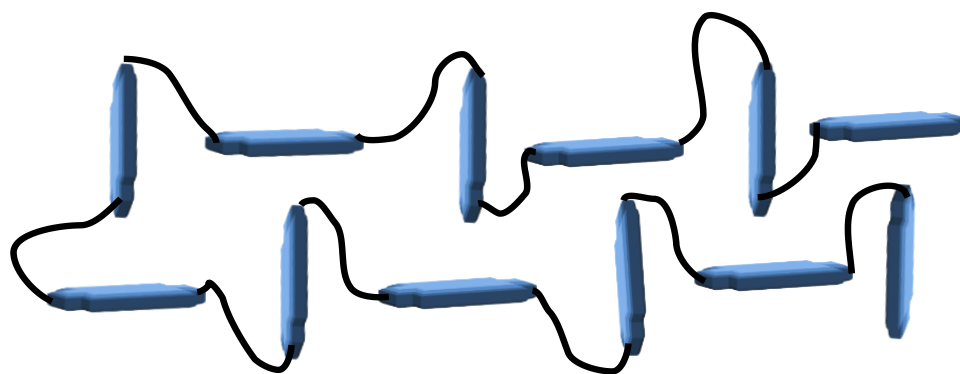


**Figure 3.19** Proposed self-stacking model for **NDI**<sub>12</sub>.

Usually, the sharp point around 380 nm is higher than the point at 360 nm. In our case, the observed absorption for **NDI**<sub>12</sub> shows switched peaks, higher 360 nm, and lower 380 nm peak point. This kind of peak shift is observed when the NDI goes on a self-stacking and the peak pattern showed up mostly in edge to face NDI self-interaction<sup>41</sup>(Figure 3.19).

To form CT interactions within DAN and NDI, the self-stacking formation of NDI should be broken down first. To distract the self-stacking and stabilize the chains in water, the DAN and NDI samples were first freeze dried (left in the freezer for overnight and then dried for about 4 hours) and then the dried samples were dissolved in MeCN (500  $\mu$ L), which was expected to interfere with the CT interaction<sup>41</sup>. However, the samples were not completely soluble in MeCN. Then 500  $\mu$ L of water was added to obtain at 1:1 MeCN: H<sub>2</sub>O composition, after which the samples were fully dissolved. The **DAN**<sub>12</sub> and, **NDI**<sub>12</sub> samples were then slowly heated to reach 90 °C to evaporate the MeCN. After the heating process, the UV absorption of the samples was taken at room temperature. However, the CT absorption band could not be observed, even after the chemical and thermal annealing process.

Gel electrophoresis was done for all the samples to confirm the size of the synthesized DAN and NDI polymers. Only **DAN**<sub>12</sub> band was visualized after staining with Stains all dye. The commercially available DNA ladders with the range of 10 bp to 300 bp was used as the reference and 10 bp, 35 bp and 50 bp were marked on the image (Figure 3.20). The molecular weight of 12mers are 4704.32 g, 5263.89 g/mol and 4984.11 g/mol for **DAN**<sub>12</sub>, **NDI**<sub>12</sub> and **DAN**<sub>6</sub>**NDI**<sub>6</sub>.

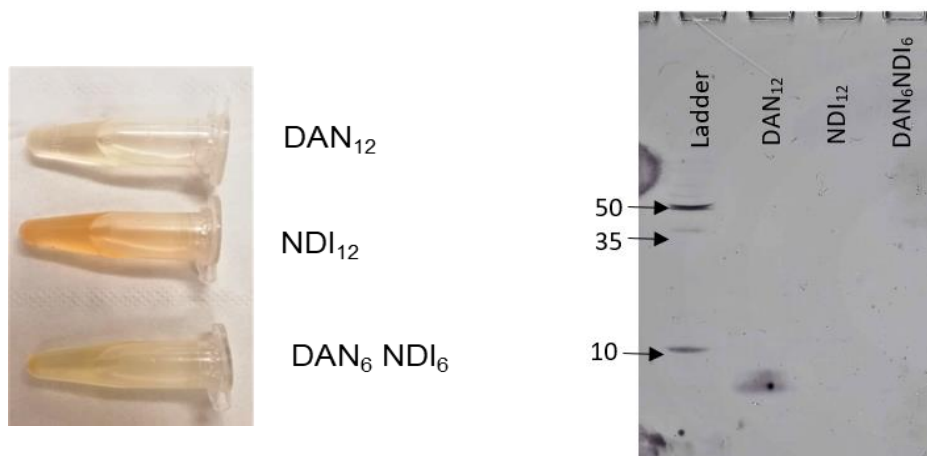


**Figure 3.20** The DAN and NDI 12mers in water (left). The DAN polymer visualized on 20% polyacrylamide gel with Stains-all (right). The ladder was marked at 10, 35, 50 base pair.

### 3.4 Sequence controlled DAN and NDI trimer complexes in aqueous media.

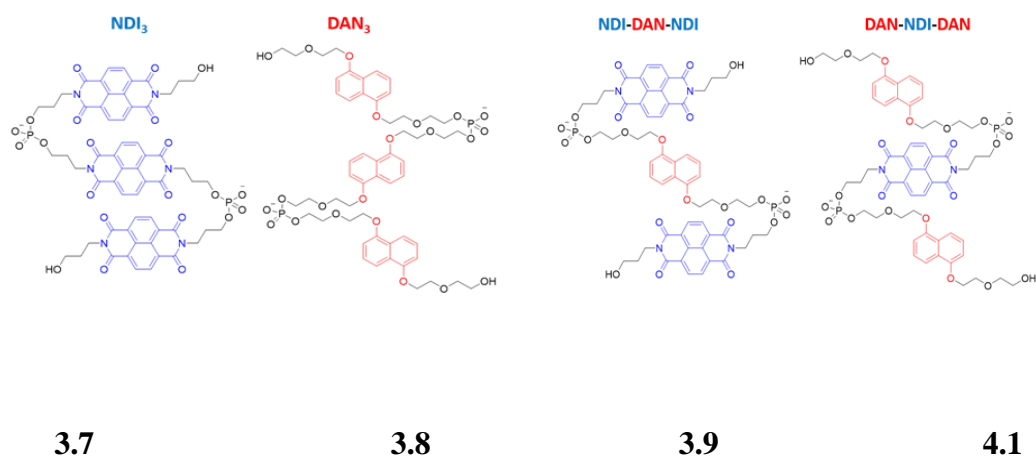
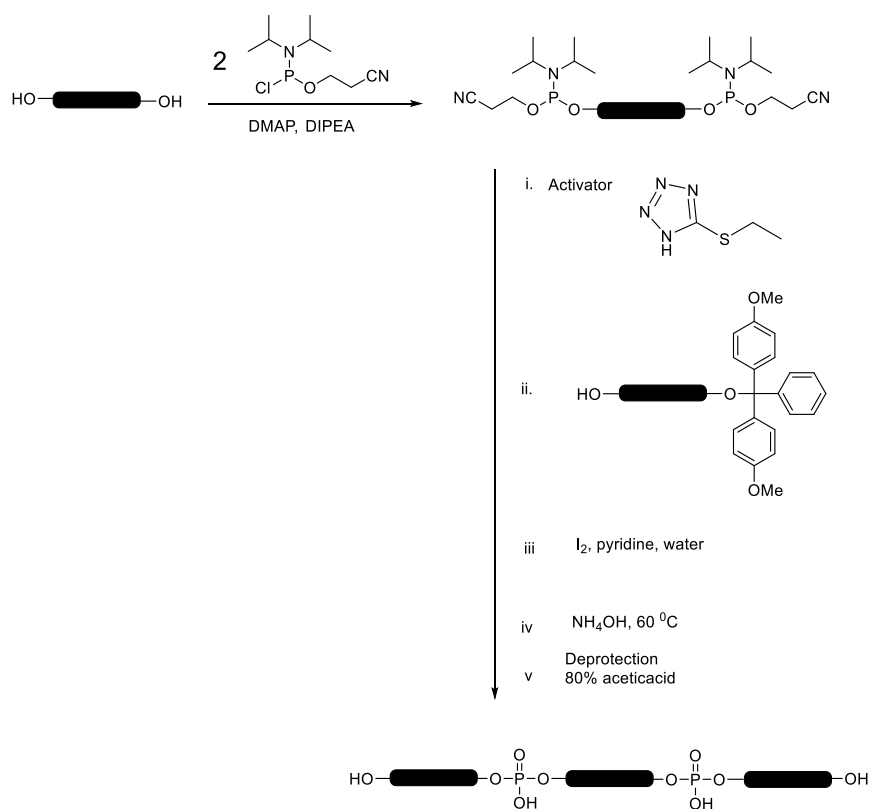
After analysing the results, the next question is whether the interaction between DAN aromatic donors and NDI aromatic acceptors could drive a folded complex formation between DAN and NDI and restrict the self fold when much shorter oligomers are created. The linkers between the aromatic units provide flexibility and the longer oligomers could easily self-stack within the chain. Oligomers with three units were chosen for synthesis and this specific number of units is the minimum number of aromatic units needed to create alternating pleated structures. The synthesis and analysis of trimers is much easier, and trimers provide enough flexibility but are also short enough to restrict the intramolecular self-assembly. The trimers were synthesised with the phosphoramidite solution phase synthesis method and studied their self-assembly in water. First, DAN and NDI homotrimers were created and then synthesised trimers that would “sandwich” the NDI face between two DAN units or *vice versa*.

### 3.4.1 Synthesis of DAN and NDI trimers

The synthesis was based on well-established phosphoramidite chemistry and reactions were carried out under N<sub>2</sub> atmosphere (Figure 3.4). DAN diol **3.2** and NDI diols **3.1** were used as the starting materials. The scheme can be divided into two stages. First, to prepare the monomers, the middle unit of the trimer was reacted with chlorophosphoramidite in 1:2 molar ratio to transform both hydroxyl parts to phosphoramidite active groups. The side units were mono protected by reacting diols with trityl chloride in a 1:1 molar ratio to give only one active hydroxyl group. The second part of the scheme was performed as a one pot reaction. The previously made phosphoramidite derivative in acetonitrile was mixed with tetrazole activator which protonate the diisopropylamino group of the nucleoside phosphoramidite and turned it in to a good leaving group. Next, the 1:2 molar equivalent of mono protected derivative was added to the mixture. The reaction was carried out for 30 minutes and then oxidation reagent (iodine, water, and pyridine) was added to convert less stable phosphate trimester to stable P(V).

The products were vacuumed dried and observed with TLC with Hexane: Ethyl acetate (1:1). Then column chromatography was carried out with alumina, but the purification method was only managed to separate fallen off DMT from rest of the fractions. Then DCM : MeOH (3:1) was used to as a solvent to purify the product with alumina column and managed to remove unreacted DAN and NDI monomers. The cyanoethyl protecting group was removed from the purified sample by adding concentrated ammonium hydroxide and heating it at 60 °C for 1 hour. NH<sub>4</sub>OH was later removed with vacuum. The sticky dark red product was then failed to dissolve in ACN, EtOH, MeOH and Acetone, but the successfully dissolved in DCM, THF and Water. Then the product dissolved in DCM was checked on TLC and three spots

appeared. The three spots identified as DMT cation, incomplete trimers, and the desired trimer. The unseparated product was then dissolved in DCM and then deprotected using 80% acetic acid.



**Scheme 3.4** Synthesis of DAN and NDI trimers and DAN and NDI trimers sequences.

The dissolved product was then filtered and filtrate and (believed DMT and incomplete trimers were dissolved in DCM) filtrant (the product) were separated. The purple colour residue was dried with heat (60 °C) and vacuum. Four different trimers were synthesised using this method. Each product, **DAN<sub>3</sub>**, **NDI<sub>3</sub>**, **DAN-NDI-DAN** and **NDI-DAN-NDI** gave 53%, 52 %, 37% and 42% yields, respectively.

### 3.4.2 Homo trimers characterisation

**DAN<sub>3</sub>** and **NDI<sub>3</sub>** homotrimers were characterised using NMR and mass spectroscopy (Figure 3.21 and Figure 3.22). Unfortunately, the NMR spectra did not provide useful results with noise. The trimers were completely soluble in water and Tris buffer. The **DAN<sub>3</sub>** was very light brown (almost colourless) and **NDI<sub>3</sub>** was light yellowish brown.

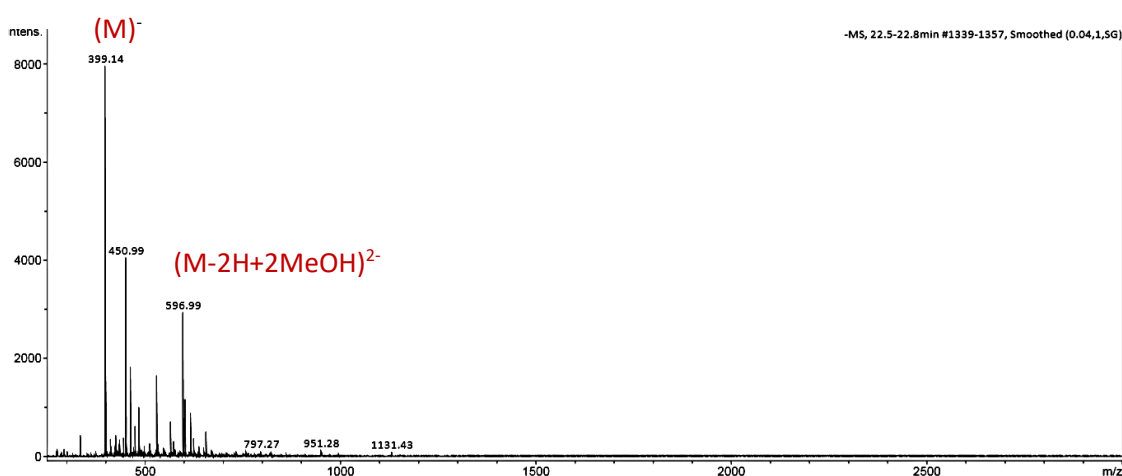


**Figure 3.21** Mass spectrum of **DAN<sub>3</sub>**, corresponding to a monoisotopic mass of 1132.38 Da.

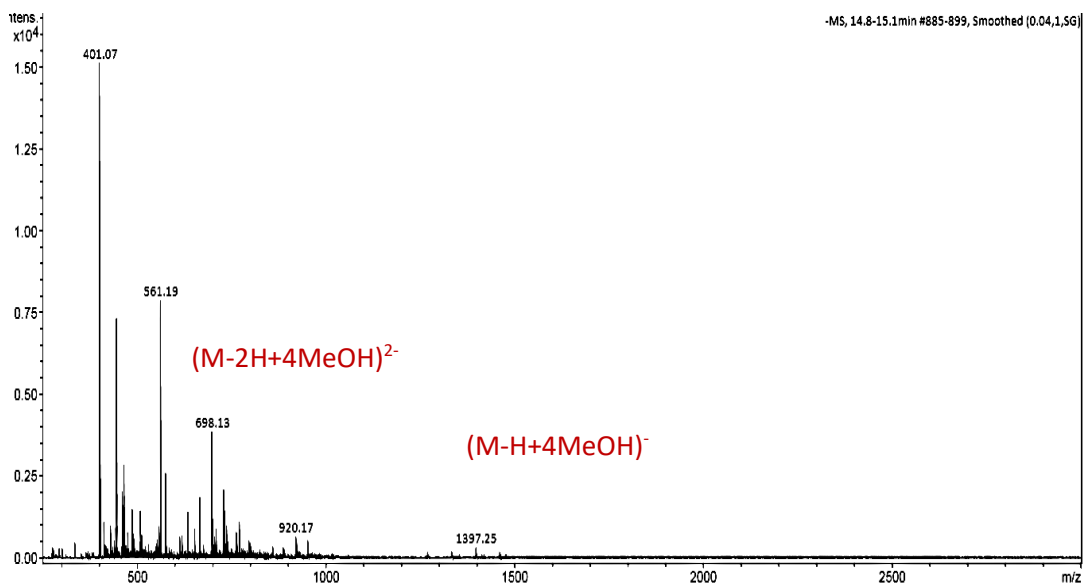


**Figure 3.22** Mass spectrum of **NDI<sub>3</sub>**, corresponding to a monoisotopic mass of 1265.25 Da.

UV absorptions were observed for **DAN<sub>3</sub>** (Figure 3.23 (a)) and **NDI<sub>3</sub>** (Figure 3.23 (b)) in water, TBE and TAMg buffer and they showed their distinct UV-vis absorption bands (around 300–400 nm) in all three solvents. Components were then mixed in 1:1 molar ratio (Figure 3.24 (a)), the mixture immediately turned in to reddish-purple solution (Figure 3.24 (b)). The mixture was then observed with UV-vis spectroscopy. The CT intensity could not be observed in low concentration but at high concentration the spectrum exhibited the expected CT absorbance at 400–700 nm (Figure 3.25). The charge transfer band observed by UV-vis are diagnostic features of DAN and NDI face-to-face association and collected UV absorption data suggest that the two components: **DAN<sub>3</sub>** **NDI<sub>3</sub>** form charge transfer complexes in solutions

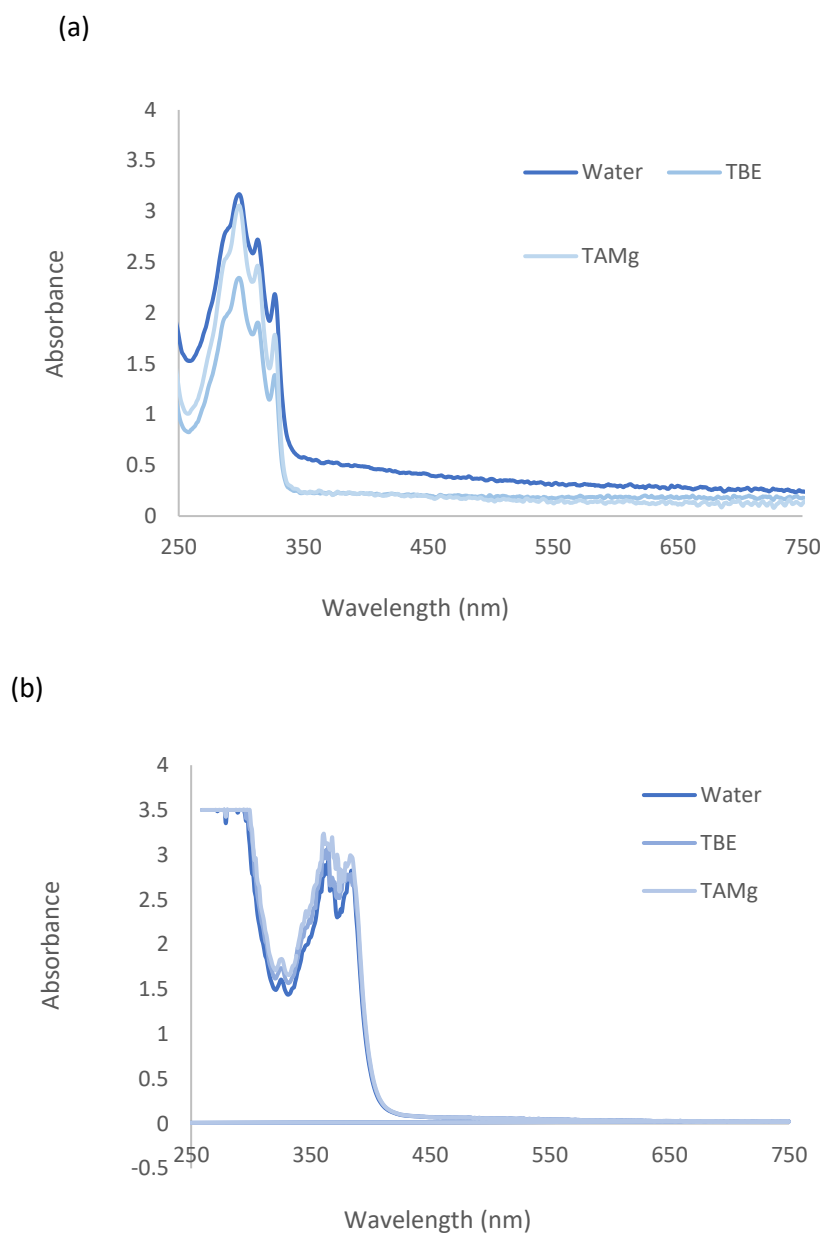


**Figure 3.23** UV absorptions of homotrimers in different solutions taken using a Nanodrop spectrometer at 1mM (a) **DAN<sub>3</sub>** (b) **NDI<sub>3</sub>**.



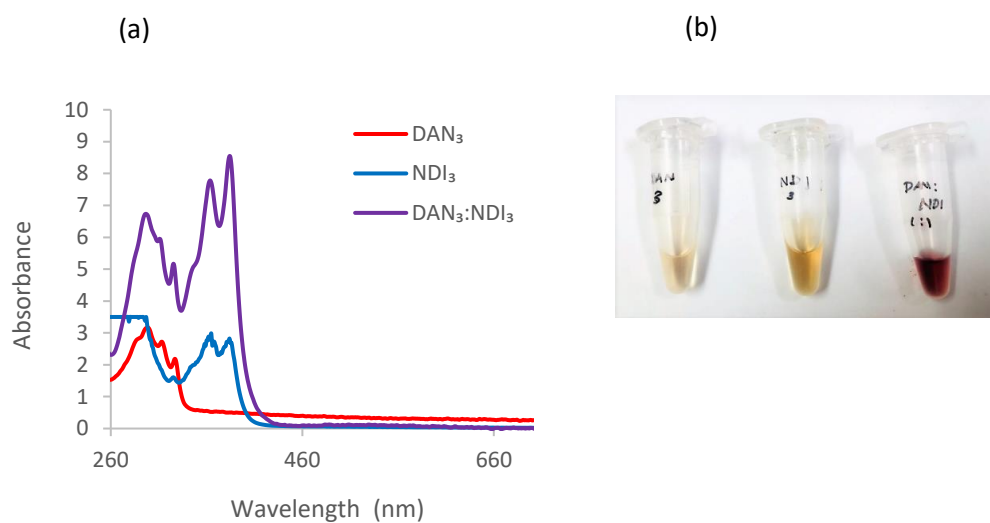


**Figure 3.24** (a) UV/Vis absorption of  $\text{DAN}_3$  (1 mM),  $\text{NDI}_3$  (1 mM) and the 1:1 mixture. (b)  $\text{DAN}_3$ ,  $\text{NDI}_3$  and 1:1 solution in water.

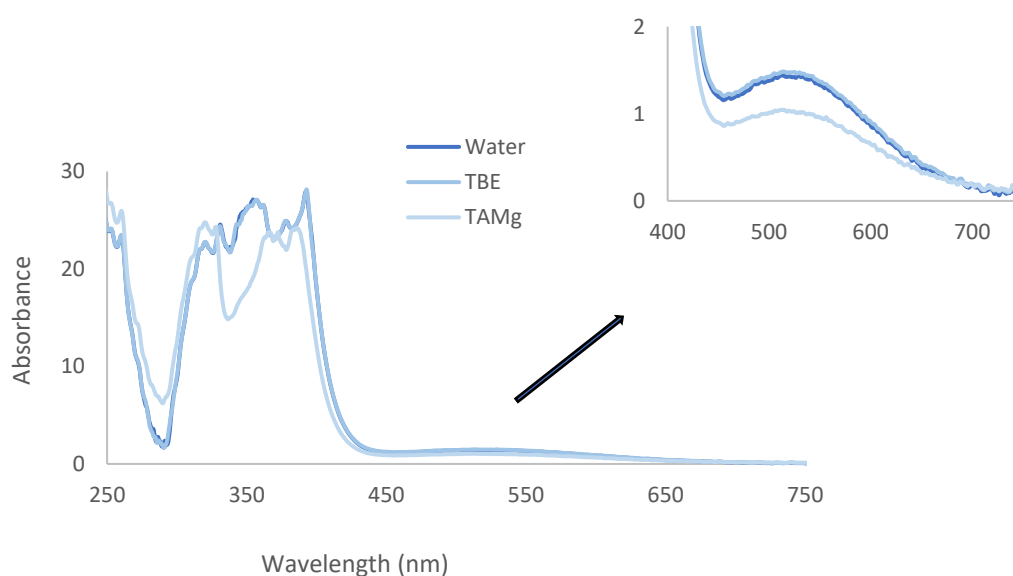


**Figure 3.25** UV absorption of  $\text{DAN}_3$   $\text{NDI}_3$  1:1 solution in different solutions at 10 mM concentration.

The UV absorbances were then measured for the  $\text{DAN}_3$  and  $\text{NDI}_3$  mixture at room temperature and, then at 45 °C to observe the sensitivity of donor-acceptor charge transfer to the temperature difference (Figure 3.26). No significant difference was

observed for the UV absorbance which suggest that **DAN<sub>3</sub>-NDI<sub>3</sub>** CT complex formed in solution is stable and temperature independent within the temperature range accessible to the spectrometer.

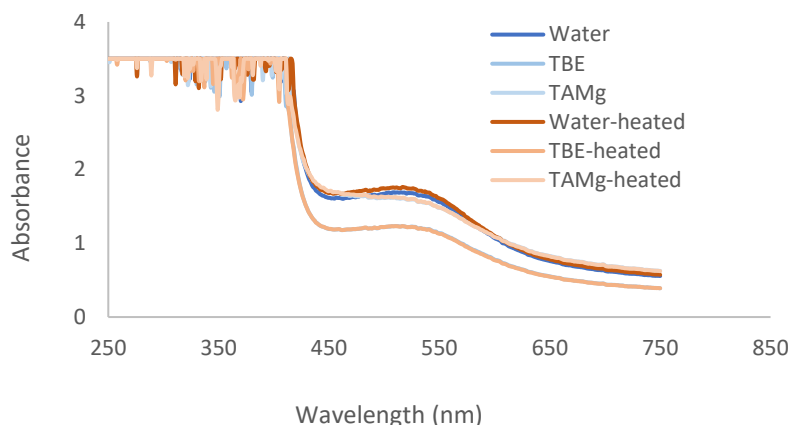


**Figure 3.26** UV/Vis absorption of **DAN<sub>3</sub>:NDI<sub>3</sub>** (1:1) at 25 °C and 45 °C in different solutions at 10 mM concentration.

UV titration was carried out for **DAN<sub>3</sub>: NDI<sub>3</sub>** mixtures to investigate the binding affinity for DAN and NDI. The data was used in BindFit software, but the experiment was not a success due to the noisy data. The structure of **DAN<sub>3</sub>** and **NDI<sub>3</sub>** homotrimeric strands were compared to the **DAN<sub>3</sub>: NDI<sub>3</sub>** mixture by AFM and TEM. For comparison, the lengths of the trimers can be estimated with the previously created computer modelled monomers (Figure 3.9). When stretched **DAN<sub>3</sub>**, strands would have about 6 nm length and **NDI<sub>3</sub>** would have about 4.5 nm length. It was found that the **DAN<sub>3</sub>** strands formed spherical shapes with the particles with ~6 nm to ~20 nm in height and ~100 nm to ~150 nm in length (Figure 3.27), while the **NDI<sub>3</sub>** strands alone formed smooth sharp structures with ~6 nm in height and varies different lengths (Figure 3.28). The mixture displayed network structures, as shown in Figure 3.29. The DAN-NDI stacking interaction drives the association of **DAN<sub>3</sub>** and **NDI<sub>3</sub>** into an oligomer network.

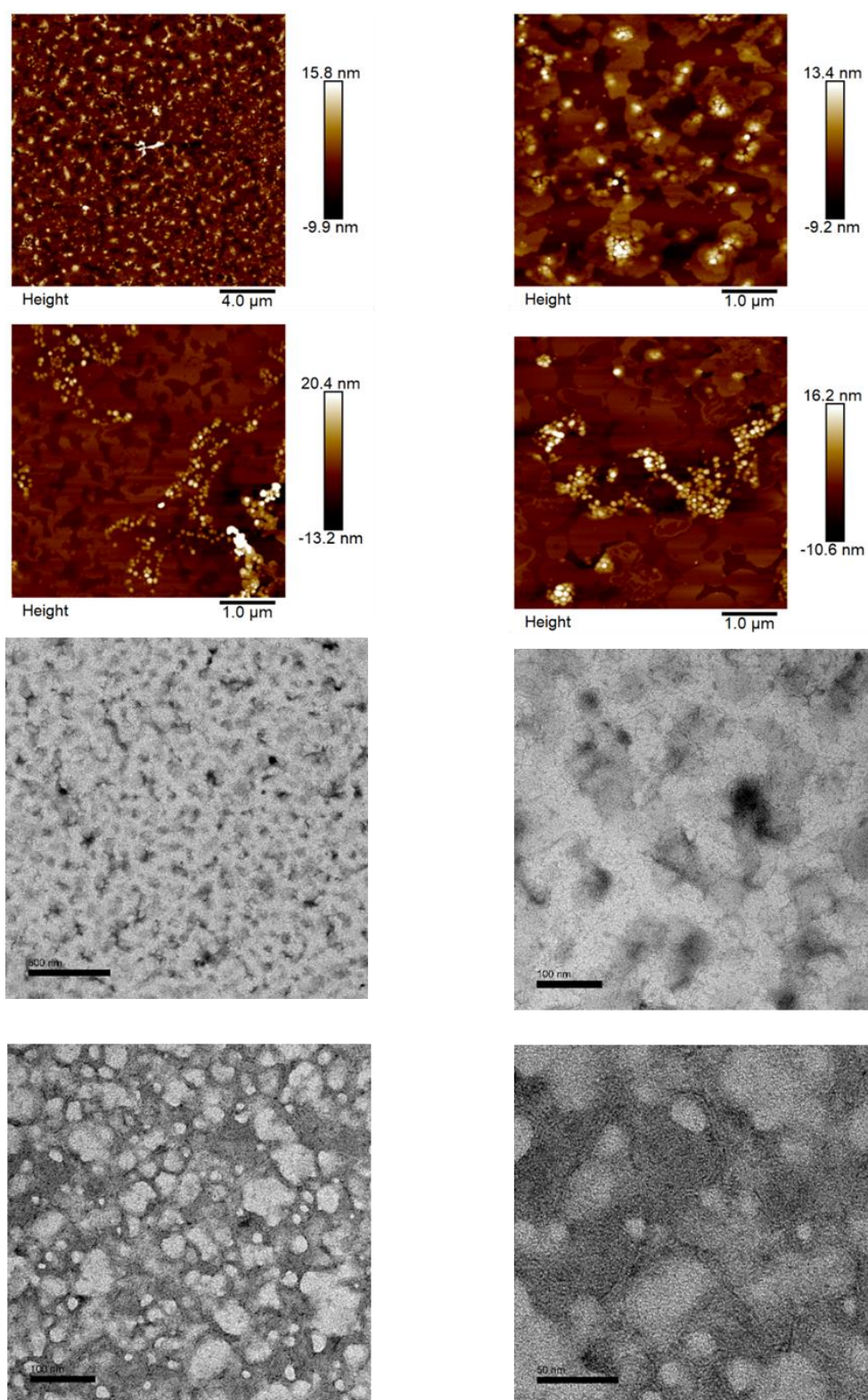


**Figure 3.27** AFM (top) and TEM (bottom) images of  $\text{DAN}_3$  deposited from water.



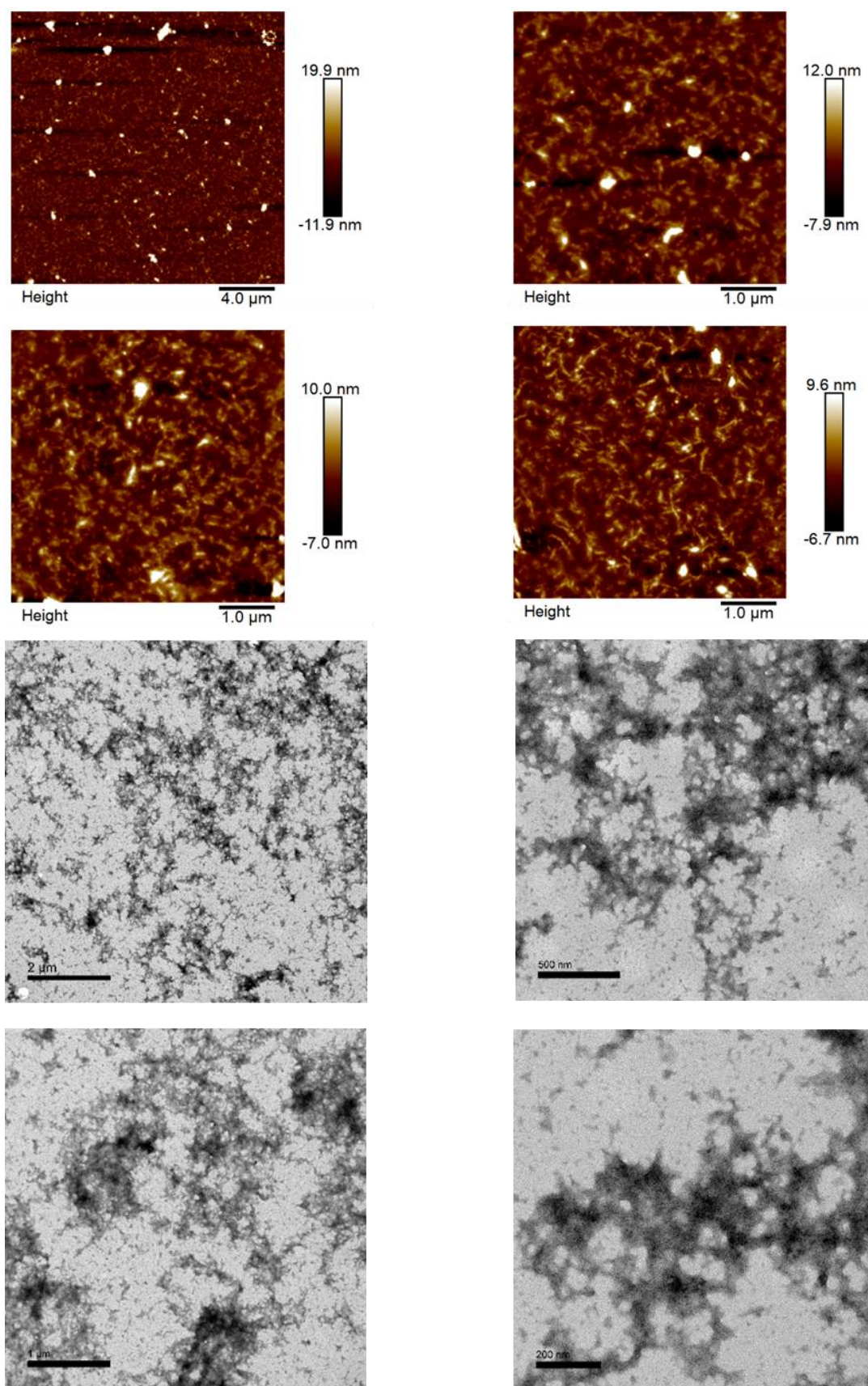


**Figure 3.28** AFM (top) and TEM (bottom) images of **NDI<sub>3</sub>** deposited from water.

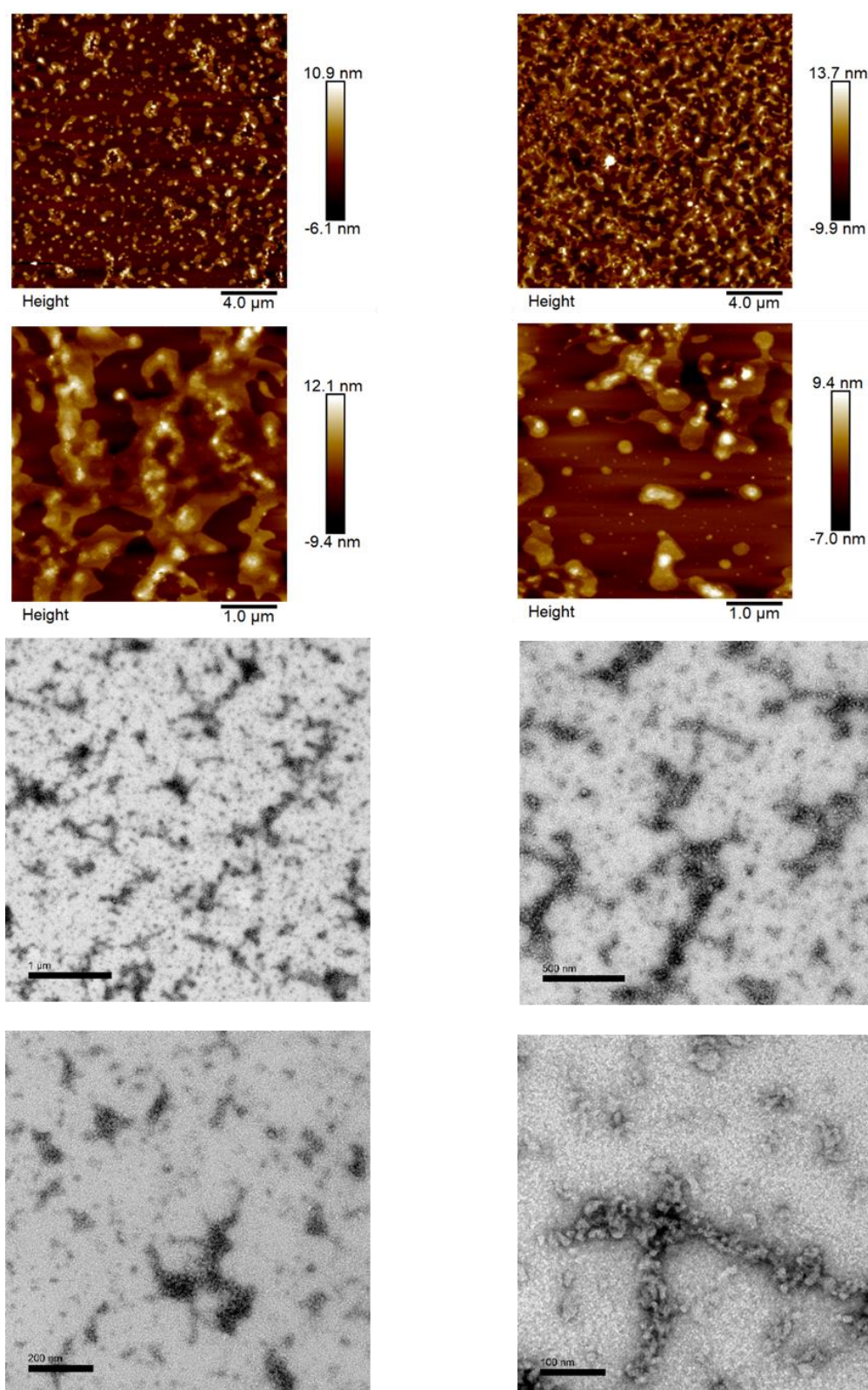
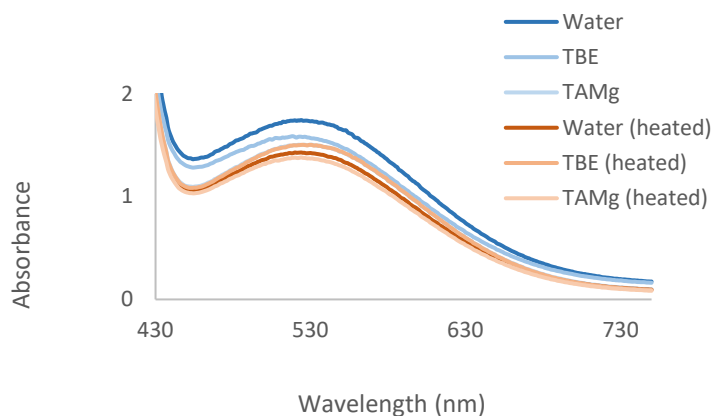


**Figure 3.29** AFM (top) and TEM (bottom) images of  $\text{DAN}_3\text{:NDI}_3$  (1:1) deposited from water.

### 3.4.3 Characterisation of heterotrimers

Both **DAN-NDI-DAN** and **NDI-DAN-NDI** gave dark purple solutions. These designed alternating trimers were dissolved in water and investigated by UV/vis, AFM and TEM. The **DAN-NDI-DAN** and **NDI-DAN-NDI** samples were prepared as 250  $\mu\text{M}$  concentration in water, TBE buffer and TAMg buffer solutions. Compared with homotrimers, heterotrimers should all exhibit absorption at CT range, regardless of self-assembly, since heterotrimers are expected to fold to form structures with intramolecular donor-acceptor association. Both compound in the solutions were purple to reddish-purple, which also suggest donor-acceptor aromatic stacking. **DAN-NDI-DAN** (Figure 3.30(a)) and **NDI-DAN-NDI** (Figure 3.30 (b)) exhibited the CT band absorbances (450-700 nm) and no significant changes were observed for the different buffers and different temperatures. The stable CT absorbance at 45  $^{\circ}\text{C}$  suggest that the CT formation is temperature independent. The TAMg buffer was used to stabilize the negatively charged phosphate group in the linkers and TBE buffer was used as the control. Samples in both buffers showed similar UV absorbance at CT range showed that the negatively charge phosphate has no effect on charge transfer formation.

(a)



(b)

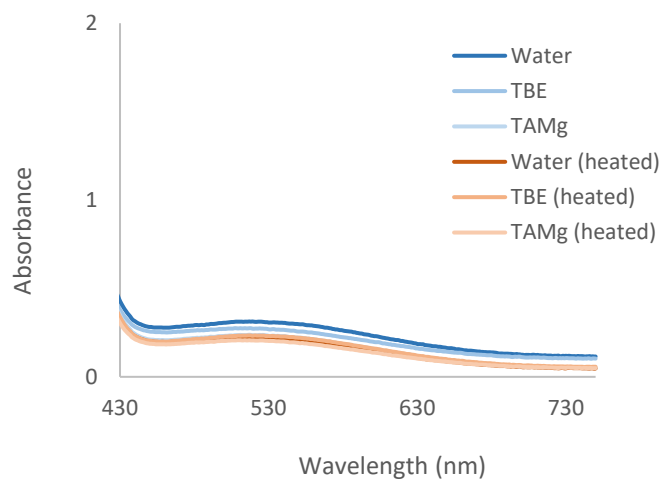


**Figure 3.30** (a) UV/vis spectra observed for **DAN-NDI-DAN** in different solutions (25 °C and heated at 45 °C). (b) UV/Vis absorption spectra for **NDI-DAN-NDI** in different solutions (25 °C and heated at 45 °C). The concentrations of both trimers were kept at 10 mM and the spectrum shows the visible region.

Heterotrimers were prepared at different concentrations (500  $\mu$ M, 1 mM, 10 mM and 20 mM) in water and UV absorptions were recorded. The absorption intensity for **DAN-NDI-DAN** (Figure 3.31 (a)) and **NDI-DAN-NDI** (Figure 3.31 (b)) increased with the concentration.



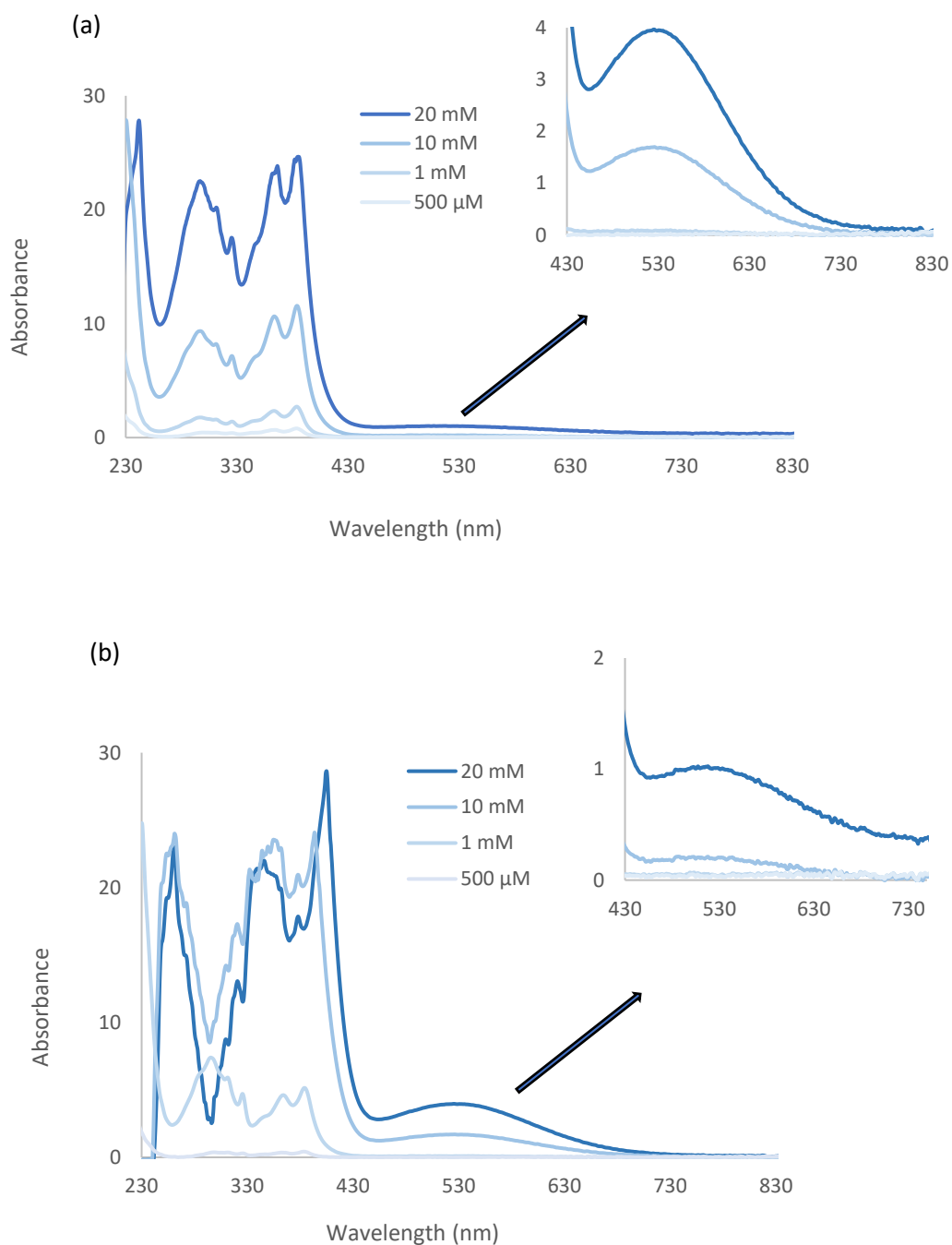


**Figure 3.31** (a) UV/vis spectra observed for **DAN-NDI-DAN** (b) UV/Vis absorption spectral observed for **NDI-DAN-NDI**. The concentrations of trimers were increased from 500  $\mu$ M to 20 mM. The side graphs show the enlarged spectra in the visible region. The spectra were measured in water at room temperature.



Compared to **DAN-NDI-DAN** trimers, **NDI-DAN-NDI** trimer shows very low intensity for CT absorption which suggest the charge transfer association was much smaller than anticipated. This absorption difference might be a result of naphthalene diimide (NDI) being a well-known versatile  $\pi$ -conjugated electron acceptor, and dialkoxynaphthalene (DAN) is being relatively an average donor. When more DAN units are present in the chain the donor ability increases but when there are more NDI units present in the chain compared to the acceptor units the association may have an effect towards the charge transfer association.

The **DAN-NDI-DAN** and **NDI-DAN-NDI** were mixed in a 1:1 ratio and the sample was investigated with UV/vis AFM and TEM. Both alternating trimers have reddish purple colour, but it was noticed that the colour had faded a little bit after mixing the two components. The obtained UV absorbance (Figure 3.32) indicated that the CT absorbance band was disturbed when the components were mixed in 1:1 ratio. The behaviour of **DAN-NDI-DAN** and **NDI-DAN-NDI** in mixture was unclear and more investigations are needed such as computer modelling or crystal structure.

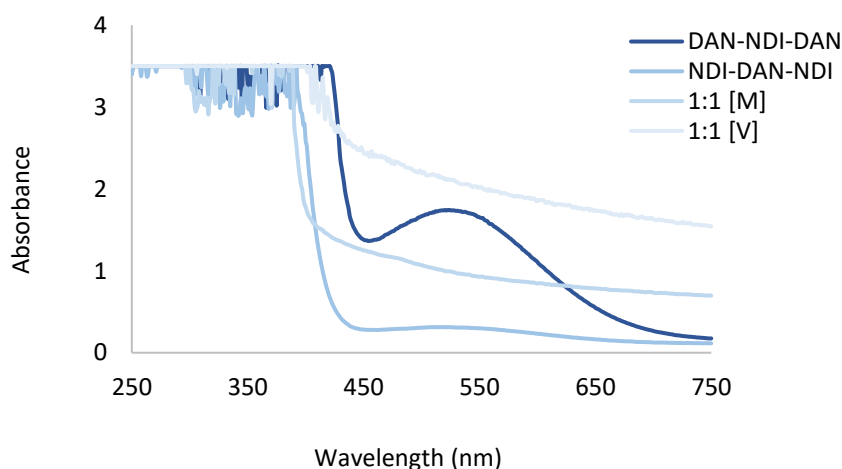


**Figure 3.32** UV absorption of 1:1 mixture of the **DAN-NDI-DAN** and **NDI-DAN-NDI** in water.

It is known that at the thermodynamic minimum, the aromatic units will tend to arrange themselves to maximize the NDI-DAN face-to-face contacts. The linker between the DAN unit and NDI unit provides flexibility to the trimer chains, which allows the molecule to fold freely and form NDI-DAN face-centered stacking. The two DAN and NDI trimer sequences, **DAN-NDI-DAN**, and **NDI-DAN-NDI** were expected to fold to give maximum face-to-face contacts as individual components in solution. The alternating sequenced trimers were expected to follow the previously shown pleated folding. A  $\pi$ - $\pi$  interaction is defined as an interaction between two aromatic rings in which has the distance between the ring centroids is less than 4.4 Å (0.44 nm) (face-to-face), or distance between the ring centroids is less than 5.5 Å (0.55 nm) (edge-to-face). The folding structures formed by alternating trimers approximately 9 nm (Figure 3.33 (a)) in height since they form two  $\pi$  interactions between three aromatic rings.

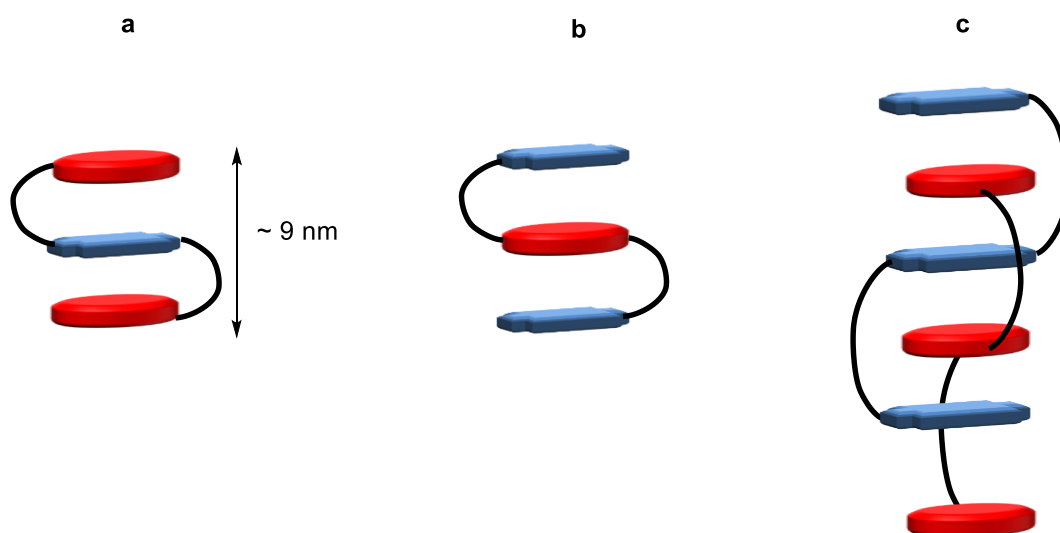


**Figure 3.33** The predicted secondary structures for DAN-NDI trimers. (a) The pleated, alternating **DAN-DAN-DAN** trimer. (b) The pleated, alternating **NDI-DAN-NDI** trimer. (c) The duplex structure (**DAN<sub>3</sub>: NDI<sub>3</sub>**).

The investigation of samples by AFM showed the **DAN-NDI-DAN** (Figure 3.34) and **NDI-DAN-NDI** (Figure 3.36) strands alone formed gathered shapes with small oval-shaped structures, but it also shows that **NDI-DAN-NDI** assembly has more random aggregation than **DAN-NDI-DAN**. The observed particles deviated from the expected structured: the small oval shapes that formed with the trimer strands are about 30 nm to 40 nm in length and 2 nm to 6 nm in height. The expected folded structure would have had particles with ~ 2 nm length and ~ 9 nm height. This information suggests that alternative sequenced trimers behave differently in aqueous solution than we had expected. Rather than folding into pleated structures, the strands are stacking with each other to form spherical shaped self-assembled particles. When the AFM images were analysed, these oval shapes gathered to form clustered environments in some areas. The structures were confirmed with TEM.

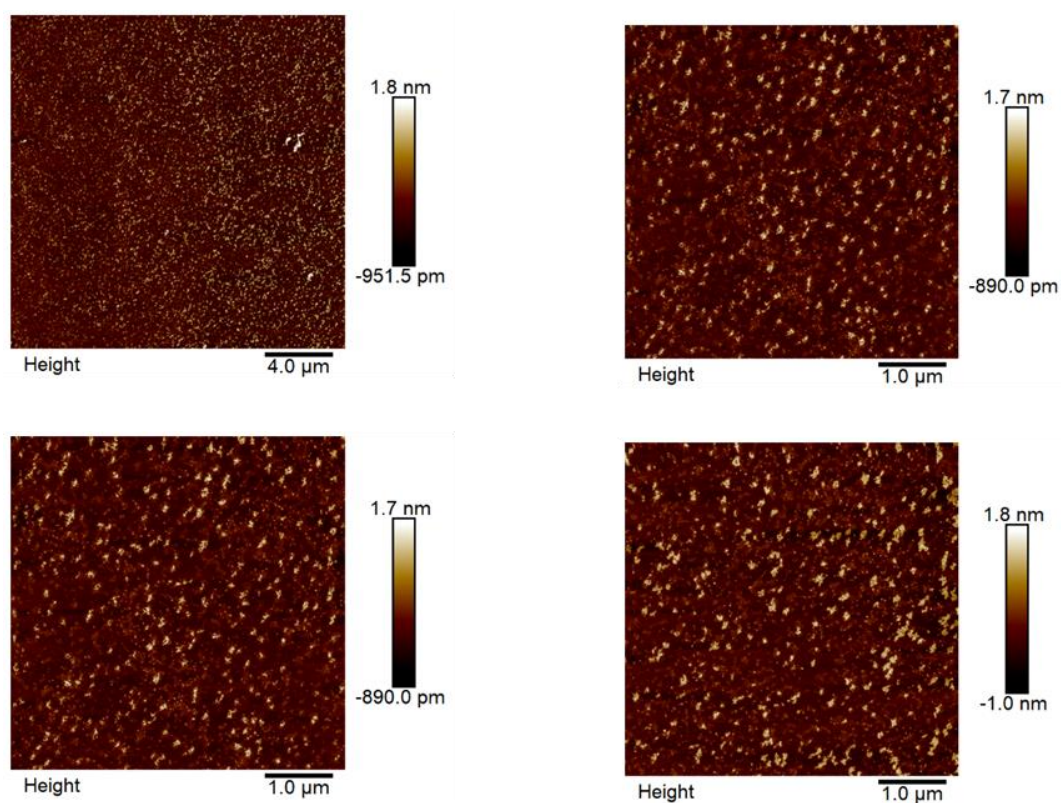


**Figure 3.34** AFM of **DAN-NDI-DAN** trimers deposited from water.

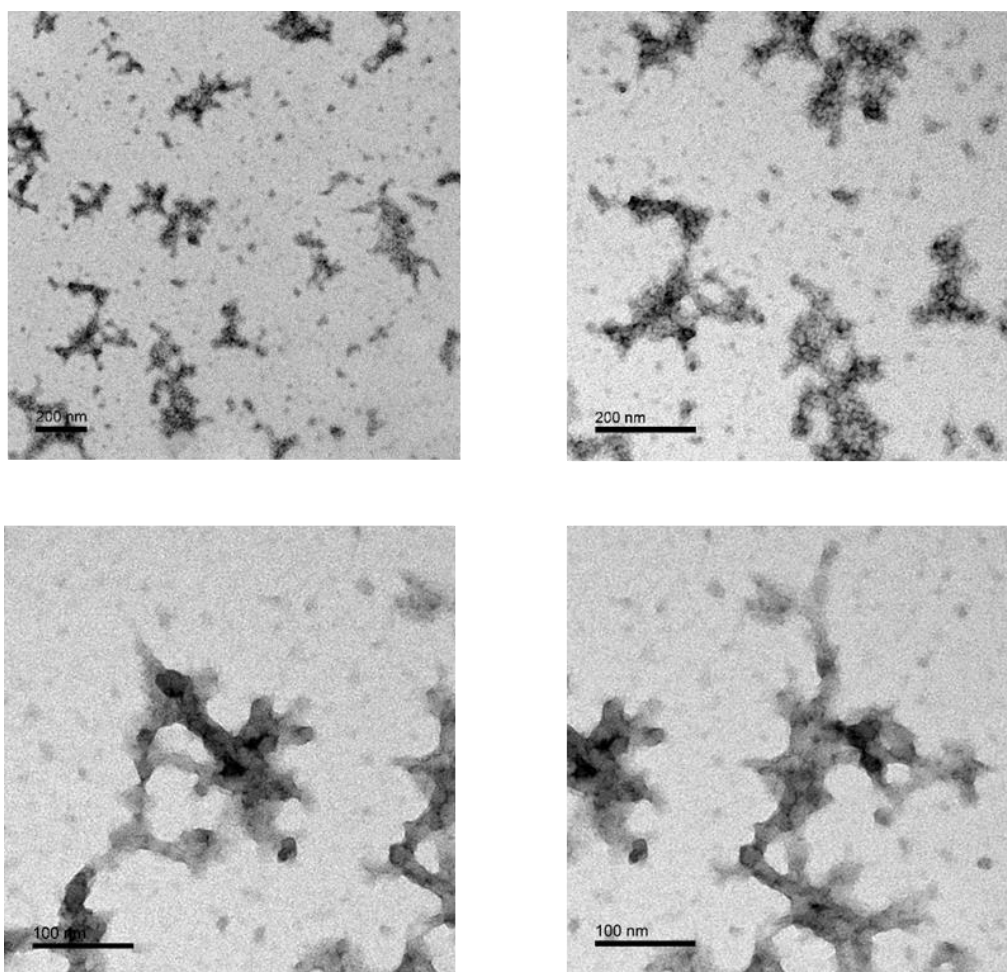


**Figure 3.35** TEM of **DAN-NDI-DAN** trimers deposited from water.



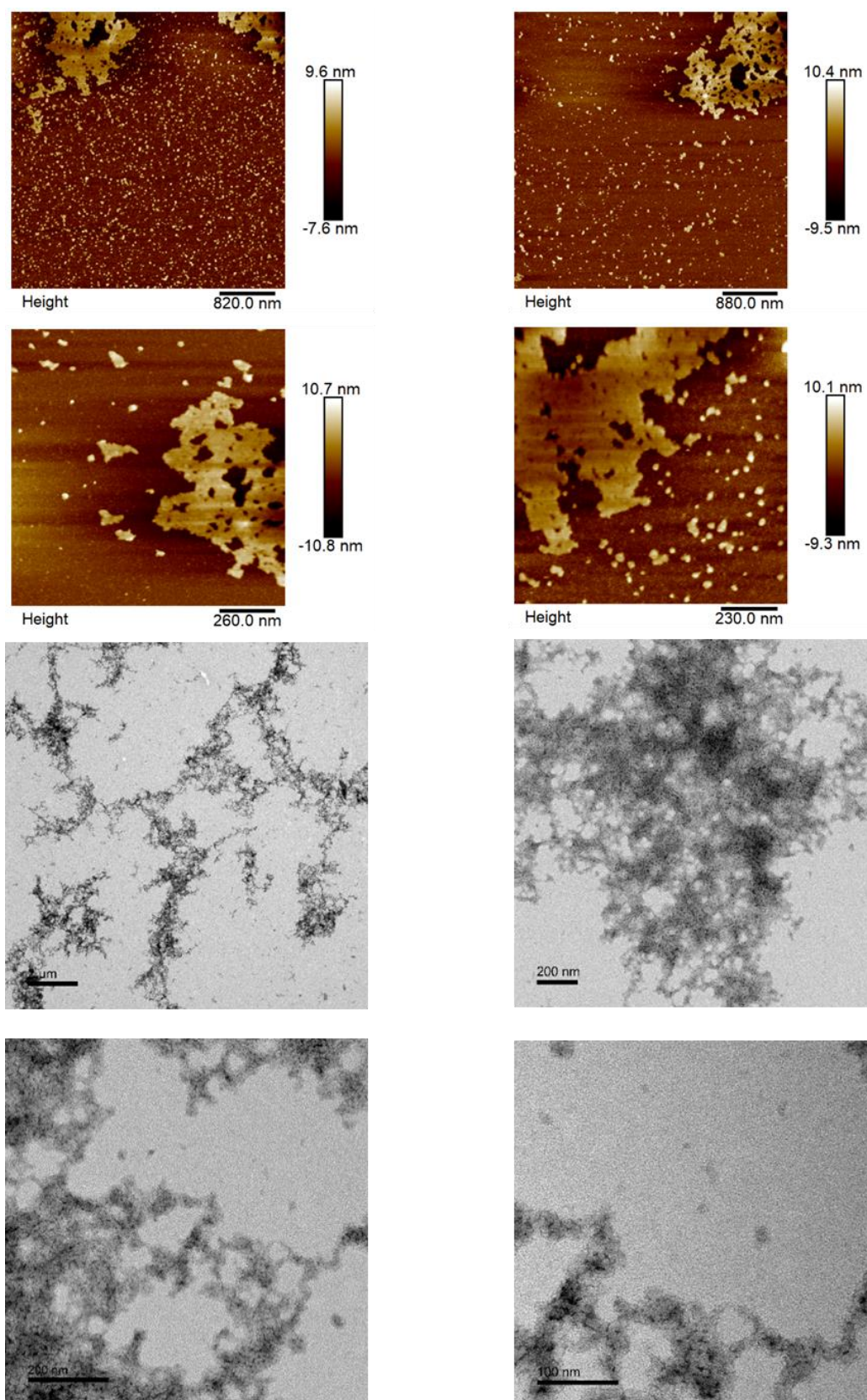


**Figure 3.36** AFM (top) and TEM (bottom) of **NDI-DAN-NDI** trimers deposited from water.

Unfortunately, the investigated alternative trimers did not form expected pleated structures and this may be due to the possible favoured intermolecular interaction over the intramolecular folding, leading to the seemingly non-specific aggregation, since donor-acceptor interactions can be satisfied within the trimer units and pack into nonspecific arrangements. Even though we designed flexible linkers between the aromatic units in trimers that allows them to fold, the donors and acceptors could also arrange on top of each other as strands and stabilize in the solution.

Even though the predicted pleated folding could not be obtained with DAN and NDI alternating trimers, they still managed to form the charge transfer formation between DAN and NDI which was confirmed with UV studies. This might be because the complementary aromatic units managed to form face-centered stacks within trimer strands rather than folding itself. The relatively temperature independent charge transfer absorbance indicates that the assembled structures have strong donor acceptor association. The proposed self-assembly for **DAN-NDI-DAN** and **NDI-DAN-NDI** are shown in Figure 3.37.

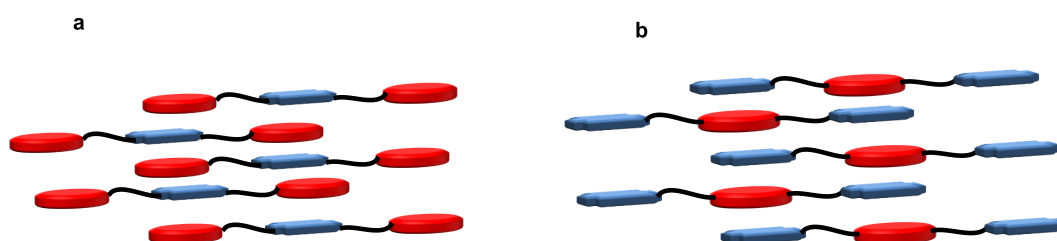


**Figure 3.37** Self-assembly of alternating trimers. (a) **DAN-NDI-DAN** (b) **NDI-DAN-NDI**.

### 3.5 Conclusion

This chapter summarizes the design and synthesis of a DAN-NDI with phosphate linkers intended for investigation of the formation of folding. Water solubility was conferred through the negatively charged phosphate linkage of the oligomers, but only in short chain. The lack of synthetic success with the solid phase synthesis shifted the focus towards solution phase phosphoramidite synthesis. The short oligomers with three units were synthesised with very simple and versatile synthetic routes. Additionally, UV-Vis data was used to evaluate the CT band of donor-acceptor stacking.

The length and the flexibility of the side chains of individual DAN and NDI units and perfect orientation of the DAN and NDI face stacking allow trimers to have different folding patterns. Even though the traditional pleated folding could not be achieved with DAN and NDI alternating trimers, they still managed to form the charge transfer formation between DAN and NDI which was confirmed with UV studies

All methods presented in this chapter provide an accessible route for future use of DAN and NDI units within oligophosphoesters, which was found to be simple and straightforward. This study put forth new possibilities for future DAN and NDI oligomers and polymers designed with greater solubility and synthetic control.

### 3.6 Reference

- (1) Yakovchuk, P.; Protozanova, E.; Frank-Kamenetskii, M. D. *Nucleic Acids Res.* **2006**, *34* (2), 564–574.
- (2) Hunter, C. A.; Sanders, J. K. M. *J. Am. Chem. Soc.* **1990**, *112* (14), 5525–5534.
- (3) Raimondi, M.; Calderoni, G.; Famulari, A.; Raimondi, L.; Cozzi, F. *J. Phys. Chem. A* **2003**, *107* (6), 772–774.
- (4) Williams, J. H.; Cockcroft, J. K.; Fitch, A. N. *Angew. Chemie Int. Ed. English* **1992**, *31* (12), 1655–1657.
- (5) Wheeler, S. E.; Houk, K. N. *J. Am. Chem. Soc.* **2008**, *130* (33), 10854–10855.
- (6) Wheeler, S. E. *J. Am. Chem. Soc.* **2011**, *133* (26), 10262–10274.
- (7) Scott Lokey, R.; Iverson, B. L. *Nature* **1995**, *375* (6529), 303–305.
- (8) Zych, A. J.; Iverson, B. L. *J. Am. Chem. Soc.* **2000**, *122* (37), 8898–8909.
- (9) Gabriel, G. J.; Sorey, S.; Iverson, B. L. *J. Am. Chem. Soc.* **2005**, *127* (8), 2637–2640.
- (10) Nguyen, J. Q.; Iverson, B. L. *J. Am. Chem. Soc.* **1999**, *121* (11), 2639–2640.
- (11) Peebles, C.; Piland, R.; Iverson, B. L. *Chem. - A Eur. J.* **2013**, *19* (35), 11598–11602.
- (12) Bradford, V. J.; Iverson, B. L. *J. Am. Chem. Soc.* **2008**, *130* (4), 1517–1524.
- (13) Kobaisi, M. Al; Bhosale, R. S.; El-Khouly, M. E.; La, D. D.; Padghan, S. D.; Bhosale, S. V.; Jones, L. A.; Antolasic, F.; Fukuzumi, S.; Bhosale, S. V. *Sci. Rep.* **2017**, (7), -11.
- (14) Ikkanda, B. A.; Iverson, B. L. *Chem. Commun.* **2016**, *52* (50), 7752–7759.
- (15) Martinez, C. R.; Iverson, B. L. *Chem. Sci.* **2012**, *3* (7), 2191–2201
- (16) Griffiths, K. E.; Stoddart, J. F. *Pure Appl. Chem.* **2008**, *80* (3), 485–506.
- (17) Forgan, R. S.; Gassensmith, J. J.; Cordes, D. B.; Boyle, M. M.; Hartlieb, K. J.; Friedman, D. C.; Slawin, A. M. Z.; Stoddart, J. F. *J. Am. Chem. Soc.* **2012**, *134* (41), 17007–17010.
- (18) Au-Yeung, H. Y.; Pantoş, G. D.; Sanders, J. K. M. *J. Org. Chem.* **2011**, *76* (5), 1257–1268.
- (19) Ashton, P. R.; Slawin, A. M. Z.; Spencer, N.; Stoddart, J. F.; Williams, D. J. *J. Chem. Soc. Chem. Commun.* **1987**, *6* (14), 1066.
- (20) Moody, G. J.; Owusu, R. K.; Slawin, A. M. Z.; Spencer, N.; Stoddart, J. F.; Thomas, J. D. R.; Williams, D. J. *Angew. Chemie Int. Ed. English* **1987**, *26* (9), 890–892.
- (21) Koshkakaryan, G.; Klivansky, L. M.; Cao, D.; Snauko, M.; Teat, S. J.; Struppe, J. O.; Liu, Y. *J. Am. Chem. Soc.* **2009**, *131* (6), 2078–2079.



- (22) Jalani, K.; Kumar, M.; George, S. J. *Chem. Commun.* **2013**, 49 (45), 5174–5176.
- (23) Ramkumar, S. G.; Ramakrishnan, S. *Macromolecules* **2010**, 43 (5), 2307–2312.
- (24) Tsiamantas, C.; de Hatten, X.; Douat, C.; Kauffmann, B.; Maurizot, V.; Ihara, H.; Takafuji, M.; Metzler-Nolte, N.; Huc, I. *Angew. Chemie Int. Ed.* **2016**, 55 (24), 6848–6852.
- (25) Basu, S.; Coskun, A.; Friedman, D. C.; Olson, M. A.; Benítez, D.; Tkatchouk, E.; Barin, G.; Yang, J.; Fahrenbach, A. C.; Goddard, W. A.; Stoddart, J. F. *Chem. - A Eur. J.* **2011**, 17 (7), 2107–2119.
- (26) Furusho, Y.; Oku, T.; Hasegawa, T.; Tsuboi, A.; Kihara, N.; Takata, T. *Chem. - A Eur. J.* **2003**, 9 (12), 2895–2903.
- (27) Iijima, T.; Vignon, S. A.; Tseng, H. R.; Jarrosson, T.; Sanders, J. K. M.; Marchioni, F.; Venturi, M.; Apostoli, E.; Balzani, V.; Stoddart, J. F. *Chem. - A Eur. J.* **2004**, 10 (24), 6375–6392.
- (28) Au-Yeung, H. Y.; Pantoş, G. D.; Sanders, J. K. M. *Angew. Chemie Int. Ed.* **2010**, 49 (31), 5331–5334.
- (29) Au-Yeung, H. Y.; Pantoş, G. D.; Sanders, J. K. M. *J. Am. Chem. Soc.* **2009**, 131 (44), 16030–16032.
- (30) Au-Yeung, H. Y.; Pantoş, G. D.; Sanders, J. K. M. *Proc. Natl. Acad. Sci.* **2009**, 106 (26), 10466–10470.
- (31) Talukdar, P.; Bollot, G.; Mareda, J.; Sakai, N.; Matile, S. *J. Am. Chem. Soc.* **2005**, 127 (18), 6528–6529.
- (32) Das, A.; Molla, M. R.; Maity, B.; Koley, D.; Ghosh, S. *Chem. - A Eur. J.* **2012**, 18 (32), 9849–9859.
- (33) Kar, H.; Molla, M. R.; Ghosh, S. *Chem. Commun.* **2013**, 49 (39), 4220–4222.
- (34) Das, A.; Ghosh, S. *Chem. Commun.* **2011**, 47 (31), 8922.
- (35) Das, A.; Ghosh, S. *Macromolecules* **2013**, 46 (10), 3939–3949.
- (36) Reczek, J. J.; Villazor, K. R.; Lynch, V.; Swager, T. M.; Iverson, B. L. *J. Am. Chem. Soc.* **2006**, 128 (24), 7995–8002.
- (37) Gabriel, G. J.; Iverson, B. L. *J. Am. Chem. Soc.* **2002**, 124 (51), 15174–15175.
- (38) Baumgartner, B.; Svirikova, A.; Bintinger, J.; Hametner, C.; Marchetti-Deschmann, M.; Unterlass, M. M. *Chem. Commun.* **2017**, 53 (7), 1229–1232.
- (39) Alvey, P. M.; Reczek, J. J.; Lynch, V.; Iverson, B. L. *J. Org. Chem.* **2010**, 75 (22), 7682–7690.
- (40) Molla, M. R.; Das, A.; Ghosh, S. *Chem. - A Eur. J.* **2010**, 16 (33), 10084–10093.
- (41) Pantoş, G. D. Privet communication

## Chapter 4

### 4 Poly phosphates via a simple synthesis method

#### 4.1 Introduction

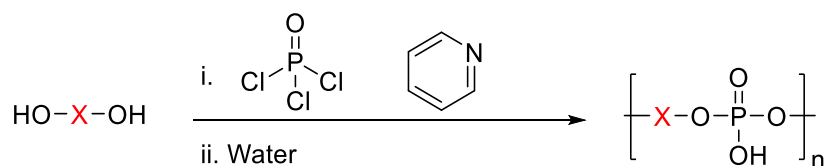
Due to its versatility, the phosphoramidite method is the most promising approach to access well-defined phosphate-based polymers. In this thesis I have discussed the successful outcome of sequence-defined polymer/oligomer synthesis via the solid-phase phosphoramidite method as well as in solution. Although the length limit of the polymerization methods was not met, both processes required chlorophosphoramidite reagents which need special care when handling. The reagents are easily oxidised, moisture-sensitive, and corrosive, and should therefore be stored in a dry environment, in a tightly closed container at  $-20\text{ }^{\circ}\text{C}$ . Due to its high reactivity, and limited supplier availability, the commercial chlorophosphoramidite reagent is expensive. It was therefore worth exploring different polymer synthesis methods, which have inexpensive access to chemicals and improved sustainability. This Chapter reports an approach to polyphosphoester synthesis, including with sequence control by reacting diols with  $\text{POCl}_3$ , and subsequent characterisation of the polymers.

General synthesis of organic phosphates involves condensation of alcohols with phosphorus substances such as  $\text{P}_2\text{O}_5$ ,  $\text{POCl}_3$ ,  $\text{PCl}_3$ ,  $\text{PCl}_5$ , and  $\text{H}_3\text{PO}_4$ .<sup>1,2</sup> This reaction produces a mixture of mono-, di-, and triesters and unreacted alcohol by-products. Phosphorus oxychloride is less reactive compared to other phosphorus chlorides and appears to be a good phosphorylating for OH-containing organic compounds. The reaction of alcohols with  $\text{POCl}_3$  in the presence of water and pyridine as a base yield phosphate monoester along with pyridine hydrochloride as a by-product. Compared

to the phosphorylating agents used in previous chapters,  $\text{POCl}_3$  is a cheap and easily available commercial chemical.

The aim of this Chapter is to investigate whether we could also make well defined and/or potentially functional polymers using simpler, less wasteful, solution-phase synthesis.

## 4.2 General polymer synthesis



**Scheme 4.1** Polymerisation reaction of diols with phosphorous oxychloride.

Polymerisation was carried out in a step growth manner, adopting a previously reported method (Scheme 4.1).<sup>3</sup> Monomers were dissolved in dry pyridine under a nitrogen atmosphere and the solution was then cooled in an ice salt bath at  $-10\text{ }^{\circ}\text{C}$ . Phosphorous oxychloride (1 equivalent) was added to the solution under nitrogen atmosphere and the mixture was stirred at  $-10\text{ }^{\circ}\text{C}$  for 30 minutes followed by hydrolysis with crushed ice. Clear solutions were obtained with these reactions, which were then evaporated under the vacuum until they became thick oils, before being dissolved in 2.5 M sodium hydroxide solution. The aqueous solutions were evaporated under reduced pressure until the smell of pyridine disappeared. Solid precipitates were then obtained under treatment with dilute hydrochloric acid and the precipitates were washed with a 1:1 ether and acetone solution.

### 4.3 Self-sequencing of donor-acceptor monomers

It has been previously found that DAN - NDI monomer mixtures create an alternating donor acceptor stack through intermolecular self-assembly. Ghosh and co-workers have carried out investigations into the molecular design of DAN and NDI self-sorting.<sup>4,5</sup> When both DAN and NDI monomers are mixed, they usually undergo charge-transfer interactions between their aromatic groups to stack alternately. We anticipate this stacking would cause a sequence alternation in the monomers prior to polymerisation due stronger interactions between closer donor acceptor units; covalent polymerisation along the pre-formed supramolecular chain would therefore be sequence-controlled, giving an alternating polymer (Figure 4.2).

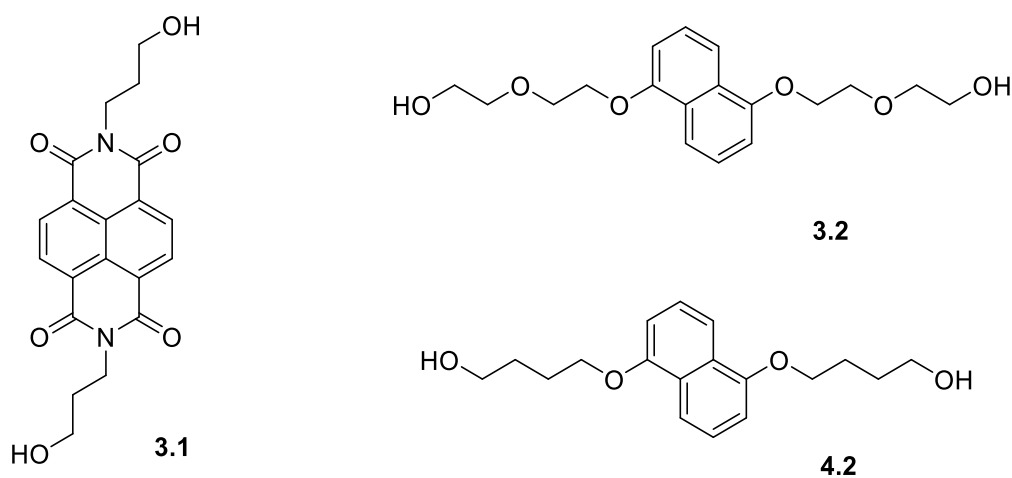


**Figure 4.1** Monomers for self-sequencing polymers.

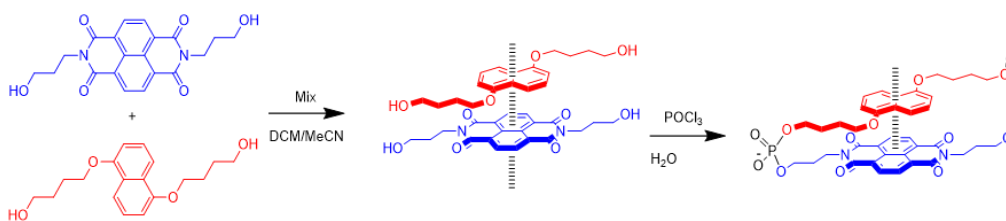
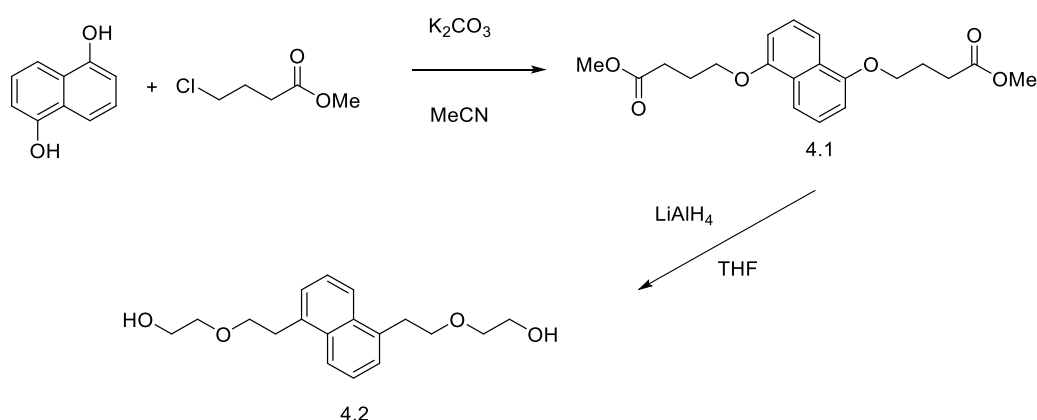


**Figure 4.2** Electron-poor (NDI) and electron-rich (DAN) aromatics form stacked charge transfer complexes in solution.

Previously discussed **DAN** (3.2) and **NDI** (3.1) monomers were synthesised as described in Chapter 3. To introduce additional, different alkyl length to side chains **DAN2** (4.2) was synthesised with two steps (Scheme 4.2).



**Scheme 4.2** Synthesis of **DAN2** (4.2) derivative as an electron rich doner monomer.

1,5-Dihydroxynaphthalene was dissolved in acetonitrile and methyl-1-4chlorobutyrate was then added to the solution. The solution was refluxed over two nights under a nitrogen atmosphere. A brown powder was obtained in 57% yield. This intermediate product was reacted directly with  $\text{LiAlH}_4$  to obtain **4.2** as a dark brown powder with yield of 53%

**Table 4.1** Sequence patterns of self-sequencing polymers with donor-acceptor monomers.

Sequence patterns	Eqv	Colour of the product
DAN + POCl <sub>3</sub>	1:1	Green
DAN2 + POCl <sub>3</sub>	1:1	Grey
NDI + POCl <sub>3</sub>	1:1	Reddish grey
DAN + DAN2 + POCl <sub>3</sub>	1:1:2	Dark grey
DAN + NDI + POCl <sub>3</sub>	1:1:2	purple
DAN + DAN2 + NDI + POCl <sub>3</sub>	1:1:1:3	Dark purple

The monomers were used in step growth reaction to deliver self-sequencing polymers according to Scheme 4.1. Different combinations of monomers (Table 4.1) were employed in the polymerisation process. Each product showed a different colour as a dried product. Homopolymers showed more grey-green colours and combined DAN-NDI polymers were purple. It is expected that the formation of alternate co-stacked donor-acceptor units will lead to the appearance of the characteristic purple colour of DAN-NDI CT complexes. This colour contrast manifests the fidelity of sequence alignments.

The synthesised trimers in Chapter 3 with **DAN** and **NDI** were not soluble in common organic solvents, but only in water and aqueous buffers. These self-sequencing polymers followed the same trend, and were not soluble in THF, DCM or acetonitrile. Most of the products dissolved in water, TBE and TAMg buffer. The products (**DAN2**)<sub>n</sub>, (**DAN-DAN2**)<sub>n</sub>, were less soluble compared with (**DAN**)<sub>n</sub>, (**NDI**)<sub>n</sub>, (**DAN-NDI**)<sub>n</sub> and (**DAN-NDI-DAN2**)<sub>n</sub>.

Agarose gel electrophoresis is generally used to separate DNA. The phosphate backbone of the DNA (and RNA) molecule is negatively charged, therefore when placed in an electric field, DNA fragments migrate to the positively charged anode. Agarose's high gel strength allows for the handling of low percentage gels for the separation of large fragments, since the lower agarose concentration gives larger pores. The step-growth synthesised polymers have a similar phosphate backbone which provides the ability to use DNA separation methods on them. After electrophoresis of all samples, only **DAN** and **DAN2** homopolymers and **DAN** + **NDI** combined polymer were visualized on the gel when stained with Stains-All dye. The cationic carbocyanine dye is able to bind to aromatic donor units better than acceptor units; we saw the same scenario with 12mers discussed in Chapter 3, with only **DAN**<sub>12</sub> was visualised with the stains. Meaningful molecular weights for the self-sequencing polymers could not be measured since the visualized bands are broad (Figure 4.3). This gives an idea about the polydispersity about the products. Self-sequencing polymers leads to products with a wide range in size.

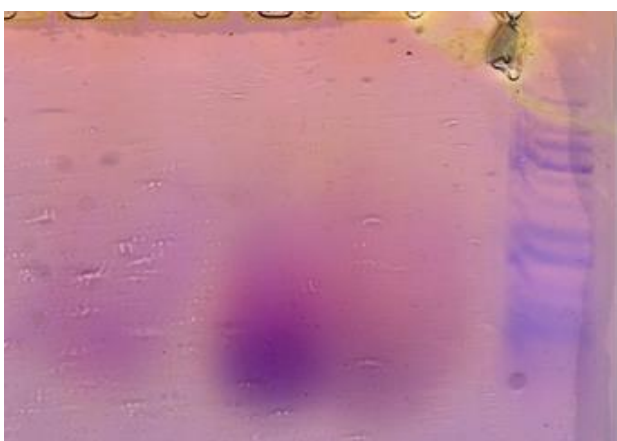


**Figure 4.3** DAN-NDI polymers. 2% agarose gel stained with stains-all.

To get an idea about the self-assembly structures of the samples, DLS experiments were carried out on all the DAN and NDI polymer sequences. Samples of 10  $\mu\text{M}$  DAN, NDI polymers were prepared in 1x TBE buffer. DLS measurements were obtained at 25  $^{\circ}\text{C}$  for each 1mL sample. Triplicate measurements were obtained for each sequence. Generally, DLS provides results for the hydrodynamic size of the particles, assuming spheres. The diameter measured in DLS called the hydrodynamic diameter and, results of DLS measurements should be compared with other techniques, which refer to different physical parameters of the sample.

Amphiphilic components have the tendency to form micelles in solution. The resulting product may contain oligomers to long polymer chains. It is important to note that dynamic light scattering produces an intensity weighted particle size distribution which means that the presence of larger particles can dominate the particle size result. The result obtained for the products showed that, the main portion of particles consisted of aggregation of 100 nm to 1000 nm diameter. DLS result (Figure 4.4) suggest that polymeric products may aggregate into large lumps with the diameter of 100 nm to 1000 nm. However, this result could not be analysed further since the DAN and NDI polymers do not form equivalent spheres. In DLS, the particle size is defined by the diameter of an equivalent sphere but the actual particles in the measured samples are not necessarily spherical.

DAN and NDI polymers were not soluble in DMSO, methanol, ethanol, or chloroform and due to this fact, it was impossible to measure an NMR spectrum. The GPC studies were also restricted because the polymer was not soluble in THF.



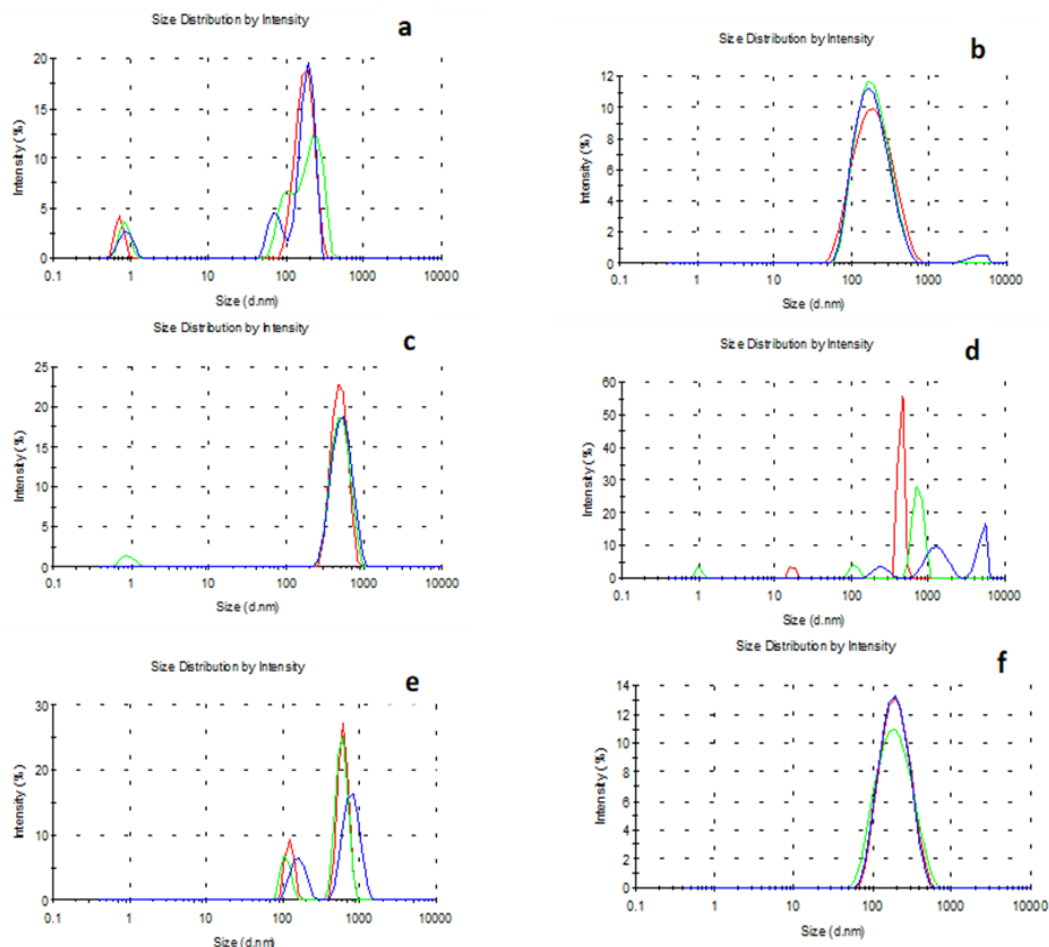


**Figure 4.4** DLS data (size - intensity distribution) for uncontrolled DAN and NDI polymers (a) **DAN** (b) **DAN2** (c) **NDI** (d) **DAN + NDI** (e) **DAN2 + NDI** (f) **DAN + DAN2 + NDI**.

#### 4.4 Phosphate based polymers with different types of monomers

The next approach was taken with estradiol monomer and bisphenol A (BPA) monomer (Figure 4.5). Both monomers are estrogenic chemicals and BPA can mimic estrogen to interact with estrogen receptors.<sup>6</sup> Bisphenol A widely used in the production of polycarbonate plastics as a commercial plasticizer and has been shown to cause negative side-effects once ingested due to its ability to act as an estrogen mimic, along with being implicated in the formation of cancers and metabolic

syndromes.<sup>6,7</sup> Estradurin (poly estradiol phosphate) is an estradiol phosphoester in the form of a polymer which mainly use in the treatment of prostate cancer in men. While these compounds are bioactive, the purpose of this section is simply to explore what other structurally interesting monomers might be compatible with the polymerisation method.

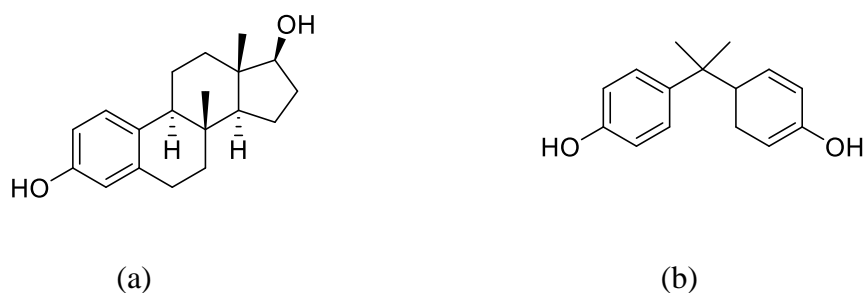


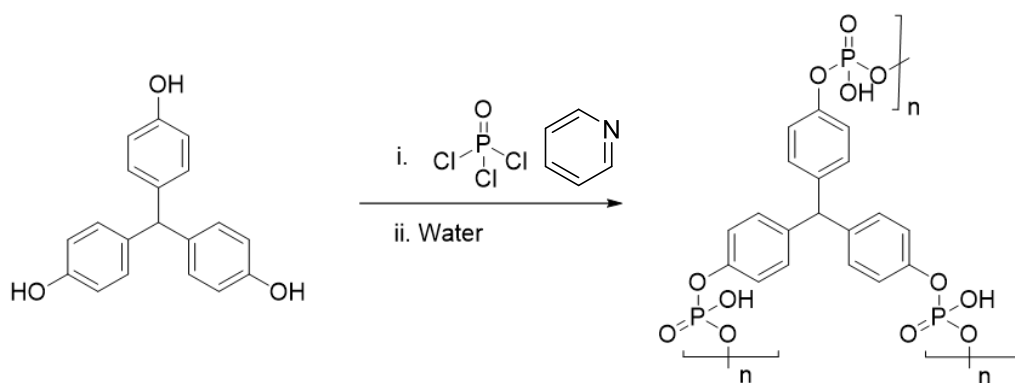
**Figure 4.5** Estradiol (a) and BPA (b) monomers.

Estradurin and poly (BPA-phosphate) can be prepared with reaction phosphorous oxychloride with their monomer units. The phenolic hydroxyl groups and the aliphatic hydroxy group reacts with  $\text{POCl}_3$  and the molecular weight can controlled with the reaction time. The first approach taken was synthesis of homopolymers and then it was planned to attach both estradiol and BPA structural units to the polymer chain to have more versatility.

Poly estradiol phosphate was synthesized via polycondensation according to the Scheme 4.1 reacting 1.1 mmol (300 mg) estradiol with 1 eqv  $\text{POCl}_3$ . The reaction yielded a white precipitate. The obtained product was not soluble in DMSO, methanol or ethanol. The poly BPA phosphate was synthesized following the same scheme reacting monomer 2.7 with 1 eqv  $\text{POCl}_3$ . The produced polymer yielded a yellowish white precipitate. Obtained precipitates were then washed with 1:1 ether

acetone mixture five times. Both polymer products were completely insoluble, and characterisation was unsuccessful due to its solubility issues.

#### 4.5 Crosslinked polymer



**Scheme 4.3** Synthesis of crosslinked polymer with 4,4',4''-methanetriyltriphenol

Branched polymers without formation of the cross-links where the chains start from one point and develop are also known to be a very interesting structure formation and these non-cross-linked regularly branched polymers are known as dendrimers. There are also branched polymers that form cross-links and join the molecules into a network to create more compact structures.<sup>8</sup> The cross-linked polymer materials can be synthesised with a wide range of molecules, and they are usually used in applications such as drug delivery and use as adsorbents. As an example, crosslinked polystyrene has been one of the most used polymeric adsorbents.<sup>9,10</sup> Crosslinked polyacrylamide has already featured in this thesis, as a gel electrophoresis matrix. Crosslinked polyphosphoesters could be branched with aliphatic or aromatic units and even hybridised by attaching biomolecule such as DNA or create more branches by further substituting phosphate groups. The potential presence of nitrogen,

phosphorus, and sulfur within the dendritic skeleton (core, branching units, and peripheries) makes it very suitable for interaction with biological systems.<sup>11–13</sup>

The highly cross-linked frameworks with rigid structures can create porous organic polymers (POPs). Porous structures are generated by interconnecting networks that are not densely packed, but form voids and they have properties such as high specific surface area, porosity and high physiochemical stability.<sup>14</sup> Organic chemistry offers an extensive library of molecules as building blocks for polymeric materials. Reticulation of those building blocks by stitching them together in a designed way into an extended framework gives endless opportunities to create interesting molecule networks.

Crystalline POPs are structurally more ordered, and the pore size is more uniform, and they have highly symmetric building blocks. Covalent organic frameworks (COFs) are examples of crystalline porous organic polymers and were first reported in 2005 by Yaghi based on the dehydration reaction of 1,4-benzenediboronic acid (BDBA) (Figure 4.6).<sup>15</sup>

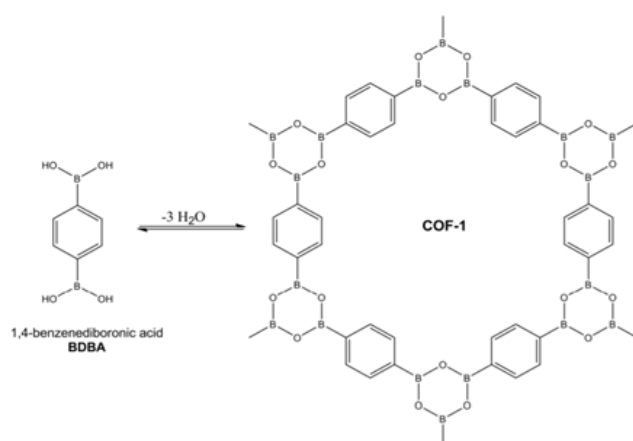


**Figure 4.6** Reaction scheme for the self-condensation reaction of COF-1. Adapted with permission from reference (Synfacts, 2006)<sup>15</sup>

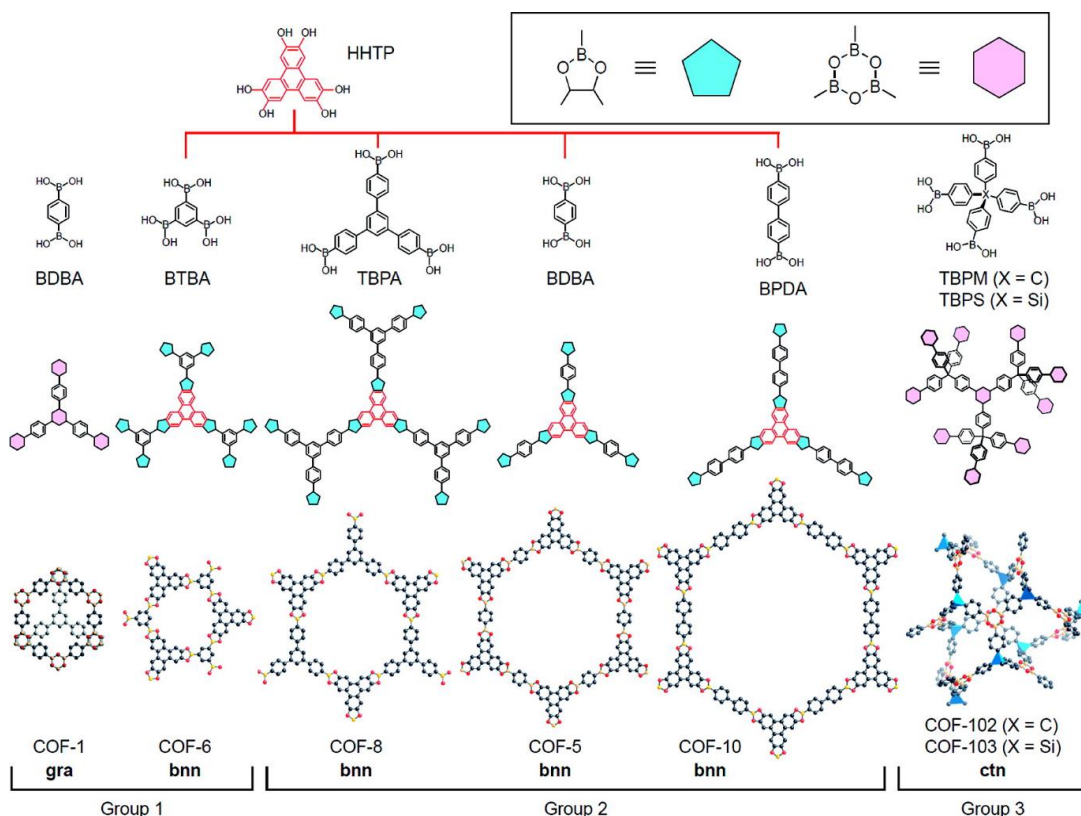


**Figure 4.7** Summary of classical COFs and their structure. Adapted with permission from reference ( American Chemical Society, 2009).<sup>16</sup>

COFs can be controlled in two dimensions or three dimensions. With appropriate choice of rigid monomers, well-defined structures can be designed since the location of atoms and bonds in the porous framework could be predicted before synthesis of the material. When designing such a structure, star-shaped monomers acting as nodes and those monomers are linked by linear monomers for formation of a porous framework (Figure 4.7).

A previous study has suggested that incorporating phosphate sites within absorbent material effective for pharmaceutical pollutant removal.<sup>17</sup> Porous organic polymers with phosphate base were previously reported by Choe's group.<sup>18</sup> They have synthesised porous organic polymers using diphenyl phosphate base with 1,1,2,2-

tetraphenylethylene and 1,3,5-triphenylbenzene as linkers (**Error! Reference source not found.**)

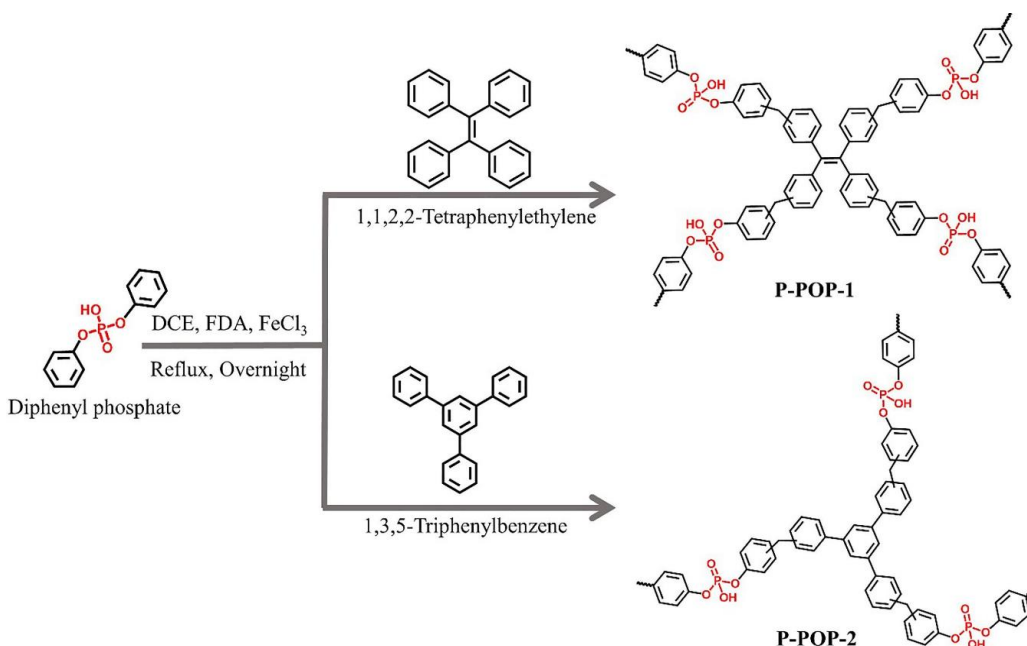


**Figure 4.8** Synthesis of phosphate-based porous organic polymers P-POP-1 and P-POP-2. Adapted with permission from reference (Chemical Engineering Journal, 2020)<sup>18</sup>

Here we created phosphate linked, porous network architecture with 4,4',4''-methanetriyltriphenol using simpler, less wasteful synthesis (**Error! Reference source not found.**).

#### 4.5.1 Result and discussion

The polymer network was synthesised using Scheme 4.1. Monomer, 4,4',4''-methanetriyltriphenol was reacted with POCl<sub>3</sub> (1:3) to obtain a bright orange colour precipitate after treatment with HCl. The three hydroxyl groups in the monomer allow the polymerisation to process through three directions and it leads to form a complex crosslinked-network structure.

The orange precipitate gave an apparent yield of 135% after drying using a high vacuum with heat for two days. Percentage yields must naturally be less than 100% , so it can appear greater than 100% only if the measured product of the reaction contains impurities that cause its mass to be greater than it would be if the product were pure. Soxhlet extraction was therefore used to remove remaining impurities. This method is used when the desired compound has limited solubility in solvents, but the impurity is at least slightly soluble in the solvent used. Here the method was used in reverse manner. Acetone was used as the solvent and in the solvent the impurity was expected to dissolve but not the polymeric compound. The solvent was heated and refluxed at 60 °C for 3 hours using a Soxhlet extraction apparatus. After the extraction, the precipitate was vacuum dried for a week. However, the product yield was calculated to be 105%. A chemically cross-linked polymer can increase its volume several folds by absorbing larger amounts of solvent. But swelling characteristics of the polymer depend on the type and amount of crosslinker, monomer composition, process of polymerisation, temperature, and particle size of the product. The synthesised monomer would have the ability to absorb pyridine which was used as the solvent for the polymerising reaction. Because of the complicated network formation, the solvent might be trapped inside the bulky structure. Since taking out the trapped solvent was challenging with the available facilities, further investigation was not processed on the crosslinked polymer material. It was hard to confirm the swelling property of the crosslinked-network polymer obtained with polycondensation method with reasonable supporting information from our study.

The product was not soluble in any solvent or pure water. The insolubility of covalently linked conjugated skeleton of polymer makes their structural

characterization relatively complicated in comparison with crystalline organic porous frameworks.

To characterise the crosslinked polymer product, solid phase  $^{31}\text{P}$  NMR was obtained (Figure 4.9) and spectrum shows a single peak at 0 ppm. In  $^{31}\text{P}$ -NMR experiments, the reference standard used to determine the 0 ppm point is usually phosphoric acid peak. This shows that phosphate groups are present in the crosslinked polymer product.

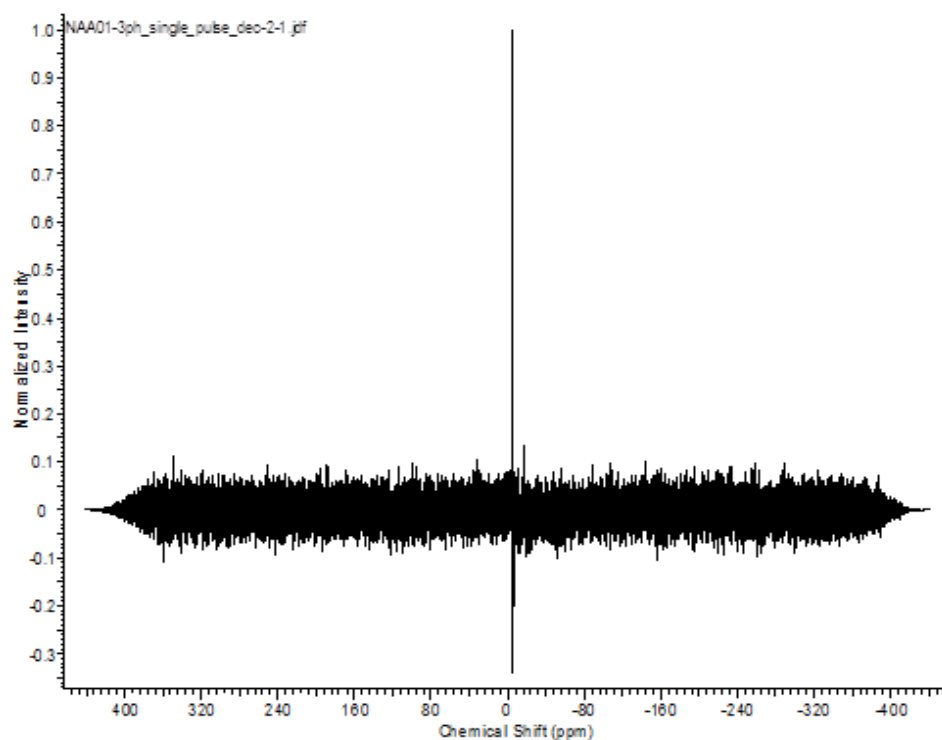


**Figure 4.9** Solid phase  $^{31}\text{P}$  NMR spectrum for cross linked-network polymer.

The 4,4',4''-methanetriyltriphenol crosslinked- network polymer was also analysed using 2% agarose gel electrophoresis (Figure 4.10). A broad band was visualised



with stains-all dye. The agarose gel image shows that the particle size in the sample is relatively very large.

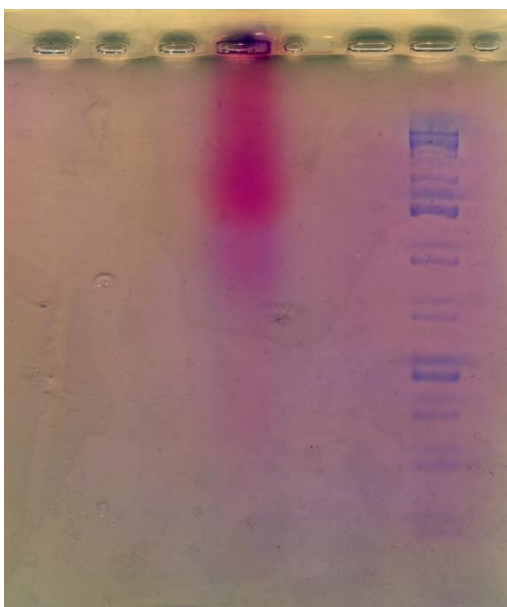


**Figure 4.10** Triphenyl crosslinked polymer against 1 Kb DNA ladder in 2% agarose gel stained with Stains-All.

In conclusion, the approach to synthesis 4,4',4''-methanetriyltriphenol crosslinked-network polymer through the polycondensation at relatively low cost is still need improve to reach to the succuss. Although the networks prepared through the method was amorphous and was not well characterized at this stage, these results open a strategy to prepare phosphate based, well ordered organic porous polymer materials in the future. Introduction of new functional groups, linkages, and structures using novel building blocks would be the next approach and development of structure characterization techniques would also be needed for the development of porous organic polymers in the future.

## 4.6 Conclusion

While fully sequence-defined polymers have been a trending topic in science for more than a decade, the chemicals required for the synthesis can be toxic and expensive. Early chapters in this thesis we have discussed the solid phase and solution phase phosphoramidite methods for sequence defined polyphosphoesters synthesis and used in easily oxidised, moisture-sensitive and corrosive and therefore much expensive reagents. In this chapter we proposed less wasteful, sustainable, and inexpensive method for polyphosphoester synthesis.

The method was applied to synthesis polymers with DAN-NDI, estradiol, BPA and 4,4',4''-methanetriyltriphenol monomers. At first it was thought that having several negative charges incorporated into a polymer chain would allow it to be sufficiently solvated. However, polymers were not soluble in most organic solvents, including THF which restricted from gel permeation chromatography analysis (GPC). In future experiments next generation polymers can be designed with greater solubility and introducing more electronegative atoms such as oxygen and nitrogen on to the linear polymer architecture could improve the solubility. Polymer purification needs to be done properly to remove unreacted monomers from the product and polymer weight should be analysed with GPC.

## 4.7 Reference

- (1) Kuiper, J. M.; Hulst, R.; Engberts, J. B. F. N. *Synthesis (Stuttg)*. **2003**, No. 5, 695–698.
- (2) Dueymes, C.; Pirat, C.; Pascal, R. *Tetrahedron Lett*. **2008**, 49 (36), 5300–5301.
- (3) Diczfalussy, E.; Fernö, O.; Fex, H.; Högberg, B.; Linderot, T.; Rosenberg, T. *Acta Chem. Scand*. **1953**, 7, 913–920.
- (4) Molla, M. R.; Das, A.; Ghosh, S. *Chem. Commun*. **2011**, 47 (31), 8922–8934.
- (5) Molla, M. R.; Das, A.; Ghosh, S. *Chem. - A Eur. J*. **2010**, 16 (33), 10084–10093.
- (6) Gao, H.; Yang, B.-J.; Li, N.; Feng, L.-M.; Shi, X.-Y.; Zhao, W.-H.; Liu, S.-J. *Medicine (Baltimore)*. **2015**, 94 (1), e211.
- (7) Chen, D.; Kannan, K.; Tan, H.; Zheng, Z.; Feng, Y.-L.; Wu, Y.; Widelka, M. *Environ. Sci. Technol*. **2016**, 50 (11), 5438–5453.
- (8) Abbasi, E.; Aval, S. F.; Akbarzadeh, A.; Milani, M.; Nasrabadi, H. T. **2014**, 1–10.
- (9) Castaldo, R.; Gentile, G.; Avella, M.; Carfagna, C.; Ambrogio, V. *Polymers (Basel)*. **2017**, 9 (12), 1–22.
- (10) Jeřábek, K.; Hanková, L.; Prokop, Z. *React. Polym*. **1994**, 23 (2–3), 107–112.
- (11) Albrecht, K.; Higashimura, H.; Yamamoto, K. *Synth. Commun*. **2014**, 44 (15), 2239–2247.
- (12) Caminade, A. M. *Chem. Commun*. **2017**, 53 (71), 9830–9838.
- (13) Caminade, A. M.; Maraval, V.; Laurent, R.; Turrin, C. O.; Sutra, P.; Leclaire, J.; Griffe, L.; Marchand, P.; Baudoin-Dehoux, C.; Rebout, C.; Majoral, J. P. *Comptes Rendus Chim*. **2003**, 6 (8–10), 791–801.
- (14) Sarkar, C.; Shit, S. C.; Das, N.; Mondal, J. *Chem. Commun*. **2021**, 57 (69), 8550–8567.
- (15) Ockwig, N. W.; Co, A. P.; Keeffe, M. O.; Matzger, A. J.; Yaghi, O. M. **2005**, 310 (November), 1166–1171.
- (16) Furukawa, H.; Yaghi, O. M. *J. Am. Chem. Soc*. **2009**, 131 (25), 8875–8883.
- (17) Álvarez-Torrellas, S.; Peres, J. A.; Gil-Álvarez, V.; Ovejero, G.; García, J. *Chem. Eng. J*. **2017**, 320, 319–329.
- (18) Ravi, S.; Choi, Y.; Choe, J. K. *Chem. Eng. J*. **2020**, 379 (April 2019), 122290,

## Chapter 5

### 5. Experiment

#### 5.1 Solvents and reagents

All commercial reagents and solvents used were purchased from Acros, Fisher Scientific or Sigma Aldrich and used without further purification, unless otherwise specified. All dry solvents were commercially obtained in sealed bottles. THF and dry DCM were obtained from an Innovative Technology PS-Micro Solvent Purification System.

All synthesiser reagents including spacer-CE Phosphoramidite C12 (C12) and, spacer-CE Phosphoramidite 18 (HEG) were purchased from LinkTech. Universal 1000 Å CPG solid support was purchased from GeneCust. Buffers were prepared with Milli-Q water. TAMg buffer is composed of 45 mM Tris and 12.5 mM  $\text{Mg}(\text{OAc})_2 \cdot 6\text{H}_2\text{O}$  with pH adjusted to 8.0 using glacial acetic acid. TBE buffer is 90 mM Tris, 90 mM boric acid and 1.1 mM EDTA with a pH of 8.0.

#### 5.2 Instrumentation

**Solid-phase Synthesis:** The automated solid-phase synthesis was performed on an ABI Expedite<sup>TM</sup> 8909 synthesiser on a 1 µmol scale on a universal 1000 Å CPG solid support. Detritylation was done for 50 s with the 3% trichloroacetic acid in dichloromethane. Coupling time was extended to 600 s. Acetic anhydride/pyridine/THF 1/1/8 and *N*-methyl imidazole in acetonitrile solution was

used for capping and oxidizing was carried out with iodine in water/pyridine/THF for 45 s. Between each step the column was washed with Acetonitrile (30 s) and flushed argon for 10 s.

**NMR:** The spectra were obtained on a Bruker AV2 400 MHz spectrometer and the data was processed using ACD labs software. The NMR chemical shifts values are reported in parts per million (ppm) and calibrated to the centre of the residual solvent peak.

**Mass Spectrometry:** The equipment was used to determine the mass of compounds. Electrospray mass spectra were recorded on a Bruker micrOTOF-Q II mass spectrometer. Samples were separated on-line by reverse-phase HPLC on a Phenomenex Nucleosil C18 column (3 $\mu$ m, 150 x 2.0 mm) running on an Agilent 1100 HPLC system at a flow rate of 0.2 mL/min using a water, 15 mM triethylamine, 400 mM hexafluoroisopropanol (HFIP) , methanol gradient: mobile phase (A), 15 mM TEA, 400 mM HFIP in water; mobile phase (B), methanol; 10% (B) for 5 minutes, then a linear gradient 10 – 100% (B) in 25 minutes, then 100% (B) for 5 minutes, before returning to the initial conditions. The eluant was monitored at 260 nm and then directed into the electrospray source at -3.5 kV and mass spectra recorded from 250-3000 m/z. Data was analysed with Bruker's Compass Data Analysis software

**PAGE:** For gel electrophoresis, the polymers were loaded (100  $\mu$ M, 10  $\mu$ L, to which 10  $\mu$ L of 8 M urea was added) on to 20 % polyacrylamide gel (TBE buffer plus 2.4 M urea) and electrophoresis carried out at room temperature for 1 hour at constant

current of 15 mA. The gels were stained to visualize the individual bands created by electrophoresis with methylene blue stain.

**Dynamic light scattering:** The self-assembled structures of sequenced polymers in liquid environments were investigated using DLS with the ZetaSizer Nano-ZS by Malvern Instruments Limited. Samples were prepared in TBE and TAMg buffer (100  $\mu$ L of 100  $\mu$ M). For the dilution studies, 100  $\mu$ L of 10  $\mu$ M was prepared by diluting 100  $\mu$ M sample 10x with 1x TBE and 1x TAMg buffer, and 500  $\mu$ L of 1  $\mu$ M was prepared by diluting the 10  $\mu$ M samples with buffer. All the measurements were carried out at 25 °C and measurements were repeated three times to check their reproducibility.

**Fluorescence:** : The sequence-defined polymer samples at 100  $\mu$ M, 10  $\mu$ M and 1  $\mu$ M (100  $\mu$ L, 100  $\mu$ L and 500  $\mu$ L respectively) were prepared, from stocks in pure water, in TBE buffer and in TAMg buffer, and 4.5  $\mu$ L of Nile Red working solution (0.001M, acetone) was added for 100  $\mu$ L samples, and 22.5  $\mu$ L for 500  $\mu$ L samples. The samples were vortexed briefly and fluorescence spectra were recorded using an Agilent Cary Eclipse fluorescence spectrophotometer at room temperature in low volume quartz cuvettes. All the spectra were taken using an excitation wavelength of 535 nm, and monitoring emission between 560 and 750 nm. The samples were sealed and incubated overnight at room temperature in the absence of light before recording the 24 hour timepoint.

**TEM:** Samples for TEM were prepared in TBE and TAMg buffer and left overnight for self-assembly to stabilise, and then dropped onto a carbon coated copper 200 mesh TEM grids and negatively stained using 2% uranyl acetate (5  $\mu$ L, 30 seconds). The stain was wicked off. Samples were imaged on a Jeol 1230 TEM, operating at

an accelerating voltage of 80 kV and images were recorded with a Gatan Multiscan 790 digital camera.

**AFM:** Samples for AFM were prepared in TBE and TAMg buffer (100  $\mu$ M, 5  $\mu$ L). Samples were deposited on freshly cleaved mica sheets for one minute, followed by 5 water washes with 5  $\mu$ L of water. Excess liquid was wicked off with the edge of a filter paper. Prepared mica plates were dried under vacuum for one hour. Measurements were conducted on a Bruker Multi-Mode microscope with a Quadrexed Nanoscope III controller using Bruker ScanAsyst-Air silicon tip on nitride lever, with frequency of 70 Hz. Data were analyzed using Nanoscope Analysis 1.5 software (Bruker, CA, US).

**Scattering experiments:** Scattering experiments were conducted for only C12<sub>10</sub>-HEG<sub>10</sub> samples. C12<sub>10</sub>-HEG<sub>10</sub> polymer appeared to produce particles and assemblies of far greater mass than (C12-HEG)<sub>10</sub> so would be expected to effect far greater scattering per sample concentration. Samples were investigated in TBE and TAMg buffer.

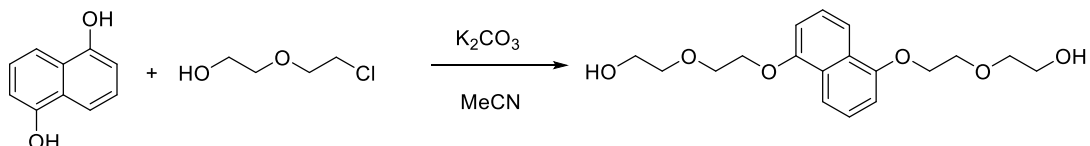
**Small angle X-ray scattering (SAXS):** Small-angle X-ray scattering (SAXS) measurements were made using a Xenocs Xeuss 2.0 equipped with a micro-focus Cu K $\alpha$  source collimated with Scatterless slits. The scattering was measured using a Pilatus 300k detector with a pixel size of 0.172 mm x 0.172 mm. A radial integration as a function of scattering length, q, was performed on the 2-dimensional scattering profile and the resulting data corrected for absorption and background from sample holder.

Microwave reactions were carried out using a Discover SP Microwave System with Explorer 12 Hybrid Autosampler.

## 5.3 Chemical synthesis

### 5.3.1 Synthesis of monomers

#### DAN Diol



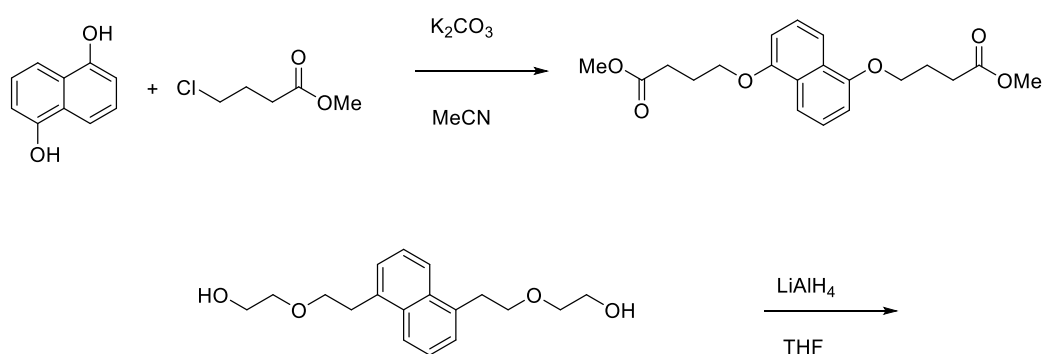
Potassium carbonate (187.3 mmol, 25.86 g) was suspended in acetonitrile and the solution degassed under nitrogen. 18.73 mmol (3.00 g) of 1,5-dihydroxynaphthalene was added to the solution. 41.2 mmol (4.35 mL) of chloroethoxyethanol was added next, and the solution was refluxed over three nights under a nitrogen atmosphere. The solvent was evaporated, and the residue was dissolved in dichloromethane and washed with H<sub>2</sub>O (x1), NaOH (x2) and brine water (x1) then dried over anhydrous MgSO<sub>4</sub>. The filtered product was dried under vacuum and the light brown powder was obtained in 52 % yield.

<sup>1</sup>H-NMR (400 MHz, CDCl<sub>3</sub>, 25 °C): δ (ppm) 7.80 (d, 2H Ar), 7.33 (t, 2H Ar), 6.81 (d, 2H Ar), 4.16 (t, 2H), 2.01 (t, 2H)

<sup>13</sup>C-NMR (1400 MHz, CDCl<sub>3</sub>, 25 °C): δ (ppm) 153.96, 125.14, 122.15, 114.54, 195.03, 70.51, 66.97, 30.93, 24.79

HR ESI-MS: Found 337.1663 m/z. Calculated for [M+H]<sup>+</sup> 337.1646 m/z



**DAN2 Diol**

Potassium carbonate (187.3 mmol, 25.86g) was dissolved in acetonitrile and the solution degassed under nitrogen. 18.73 mmol (3.00 g) of 1,5-dihydroxynaphthalene was added to the solution followed by 41.2 mmol (5.01 mL) of methyl-1-4-chlorobutyrate. The solution was refluxed over two nights under nitrogen atmosphere. Solvent was evaporated after two night of refluxing and the solute remaining was dissolved in dichloromethane and washed with water (x1), NaOH (x2) and brine water (x1) then dried over MgSO<sub>4</sub>. The filtered product was dried under vacuum. The obtained brown powder gave a 37% yield of intermediate.

<sup>1</sup>H-NMR (400M Hz CDCl<sub>3</sub>, 25 °C): δ 7.80 (d, 1H) 7.33 (t, 1H), 6.81 (d, 1H), 4.16 (t, 2H), 3.68 (s, 3H)

$^{13}\text{C}$ -NMR ( $\text{CDCl}_3$ , 1400 MHz):  $\delta$  173.70, 154.14, 126.27, 125.29, 114.20, 105.63, 67.30, 52.03, 31.39, 24.96 ppm

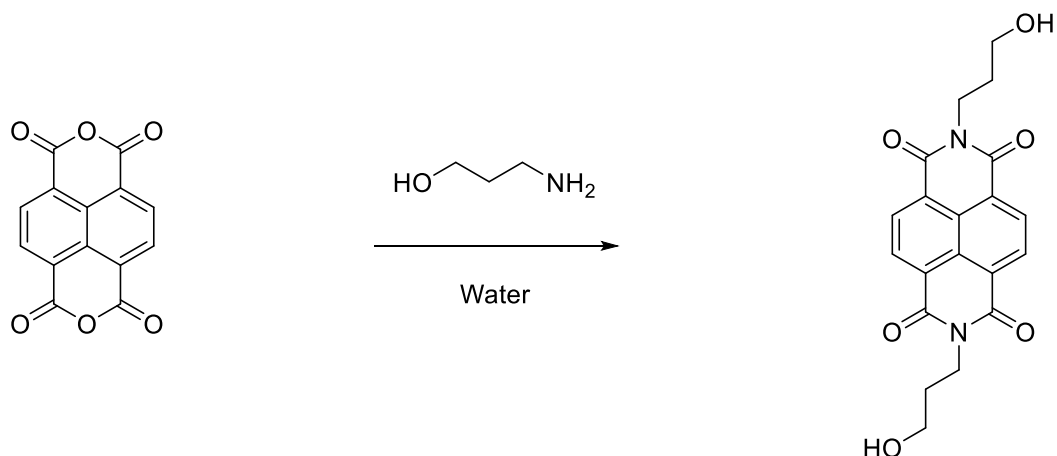
The intermediate product (6.937 mmol, 2.5 g) was dissolved in 200 mL of dry THF. The solution was then added drop wise using pressure equalising dropping funnel to 27.7 mmol (1.05 g) of  $\text{LiAlH}_4$  suspended in dry THF in an ice bath under nitrogen atmosphere. When mixture reached the room temperature it was refluxed for one hour. Then diethyl ether was added and cooled down to 0 °C. 1 mL of  $\text{H}_2\text{O}$  was added to the solution and then 1.5 mL of 10% NaOH followed by 3 mL of  $\text{H}_2\text{O}$ . The mixture was brought back to room temperature and stirred for 15 minutes and dried over  $\text{MgSO}_4$  and the dark brown powder was obtained under vacuum with yield of 43%

$^1\text{H}$ -NMR (400 MHz,  $\text{CDCl}_3$ , 25°C):  $\delta$  7.82 (d, 1H), 7.34 (t, 1H), 6.83 (d, 1H), 4.17 (t, 2H), 3.77 (t, 2H) 2.01 (m, 2H), 1.86 (m, 2H)

$^{13}\text{C}$ -NMR (400 MHz,  $\text{CDCl}_3$ , 25 °C):  $\delta$  158.70, 128.27, 125.29, 115.20, 107.63, 70.30, 62.30 ppm

HR ESI-MS: Found 304.1759 m/z. Calculated for  $[\text{M}+\text{H}]^+$  304.1675m/z

## **NDI Diol**



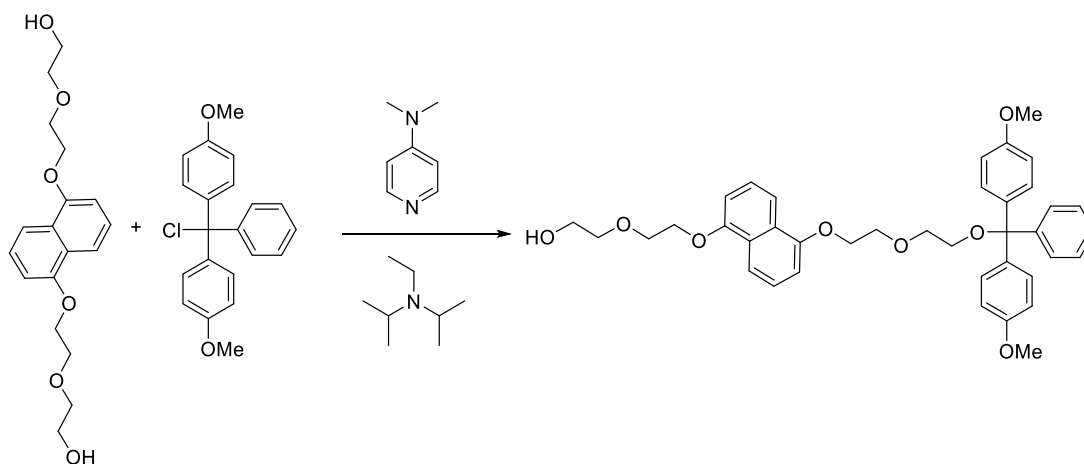
1,4,5,8-Naphthalenetetracarboxylic dianhydride (1.86 mmol, 0.5 g), water (20 mL) 3-aminopropanol (3.7 mmol, 282 uL) were added to a microwave tube, heated at 200 °C for 30 minutes in the microwave. When the solution has reached the room temperature the precipitated solid was filtered and washed with water and diethyl ether, giving the pure product as white crystals in 97% yield.

$^1\text{H-NMR}$  (400 MHz,  $\text{CDCl}_3$ , 25 °C):  $\delta$  (ppm) 8.78 (s, 2H Ar), 4.37 (t, 2H), 3.63 (d, 2H), 2.62 (t, 2H), 2.01 (t, 2H)

$^{13}\text{C-NMR}$  (400 MHz,  $\text{CDCl}_3$ , 25 °C):  $\delta$  (ppm) 131.41, 58.70, 37.85, 31.44, 2.02

HR ESI-MS: Found 383.1246 m/z. Calculated for  $[\text{M}+\text{H}]^+$  383.1238 m/z

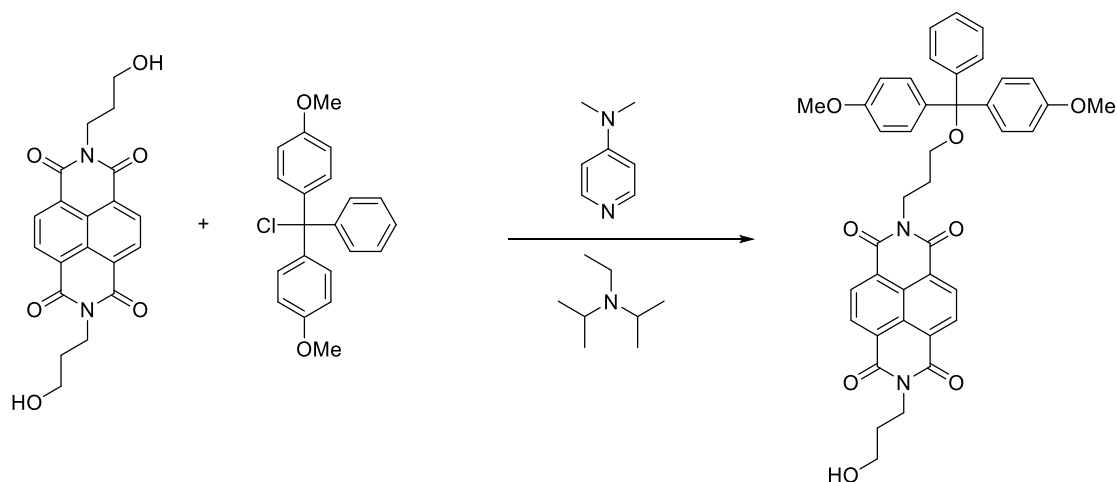
### Monoprotected DAN



DAN diol (2.29 mmol, 770 mg) and dimethylaminopyridine (0.46 mmol, 56.1 mg) were dissolved in 200 mL of dry dichloromethane. Dimethoxytrityl chloride (2.29 mmol, 775 mg) was then added, followed by the dropwise addition of diisopropylamine (2.98 mmol, 0.519 mL) over a period of 30 minutes. The mixture was left stirring under an atmosphere of nitrogen for an additional 24 hours. After the dichloromethane was removed under vacuum, the crude product, a beige powder, was purified by column chromatography with a basic alumina stationary phase, eluted with dichloromethane:methanol (400:1). The dried product was obtained at 520 mg with 35% yield

$^1\text{H-NMR}$  (400 MHz, DMSO- $d_6$ , 25 °C):  $\delta$  (ppm) 7.75 (t, 2H Ar), 7.40 (t, 3H Ar), 6.81 (d, 2H Ar), 4.16 (t, 2H), 2.01 (t, 2H)

$^{13}\text{C-NMR}$  (400 MHz, DMSO- $d_6$ , 25 °C):  $\delta$  (ppm) 158.42, 154.41, 145.48, 136.23, 130.12, 128.23, 128.18, 127.04, 126.48, 125.85, 113.55, 106.38, 85.74, 70.44, 69.61, 68.29, 63.42 ESI-MS: Found 656.3 m/z. Calculated for  $[\text{M}+\text{NH}_4]^+$  656.3 m/z

**Monoprotected NDI**

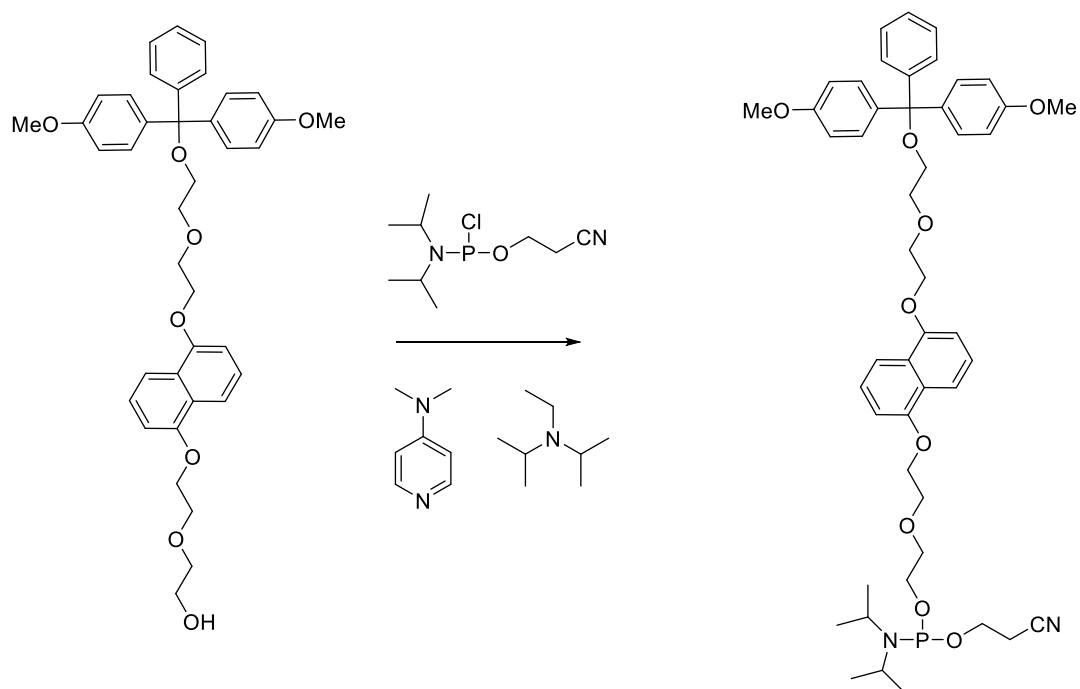
NDI diol (2.29 mmol, 874 mg) and dimethylaminopyridine (0.46 mmol, 56.1 mg) were dissolved in 200 mL of dry dichloromethane. Dimethoxytrityl chloride (2.29 mmol, 775 mg) was then added, followed by the dropwise addition of diisopropylethylamine (2.98 mmol, 0.519 mL) over a period of 30 minutes. The mixture was left stirring under an atmosphere of nitrogen for an additional 24 hours. After the dichloromethane was removed under vacuum, and the crude product, a brown powder, was purified by column chromatography using a basic alumina stationary phase, eluted with dichloromethane:methanol (400:1). The dried product 3b was obtained at 485 mg with 30% yield.

<sup>1</sup>H-NMR (400 MHz, DMSO-d<sub>6</sub>, 25 °C): δ (ppm) 8.67 (s, 4H Ar), 7.24 (d, 2H Ar), 7.19 (t, 2H Ar), 7.13 (t, 1H Ar), 7.07 (d, 4H Ar), 6.69 (d, 4H Ar), 4.58 (t, 2H), 4.16 (p, 4H), 3.66 (s, 6H), 3.53 (q, 2H), 3.07 (t, 2H)

<sup>13</sup>C-NMR (400 MHz, DMSO-d<sub>6</sub>, 25 °C): δ (ppm) 163.39, 159.03, 155.42, 148.30, 148.17, 140.22, 130.66, 129.55, 129.47, 128.17, 127.57, 126.96, 126.83, 112.84, 112.57, 106.85, 81.40, 59.95, 54.67, 53.84, 38.17, 31.04

ESI-MS: Found 683.1 m/z. Calculated for [M-H]<sup>-</sup> 683.2 m/z

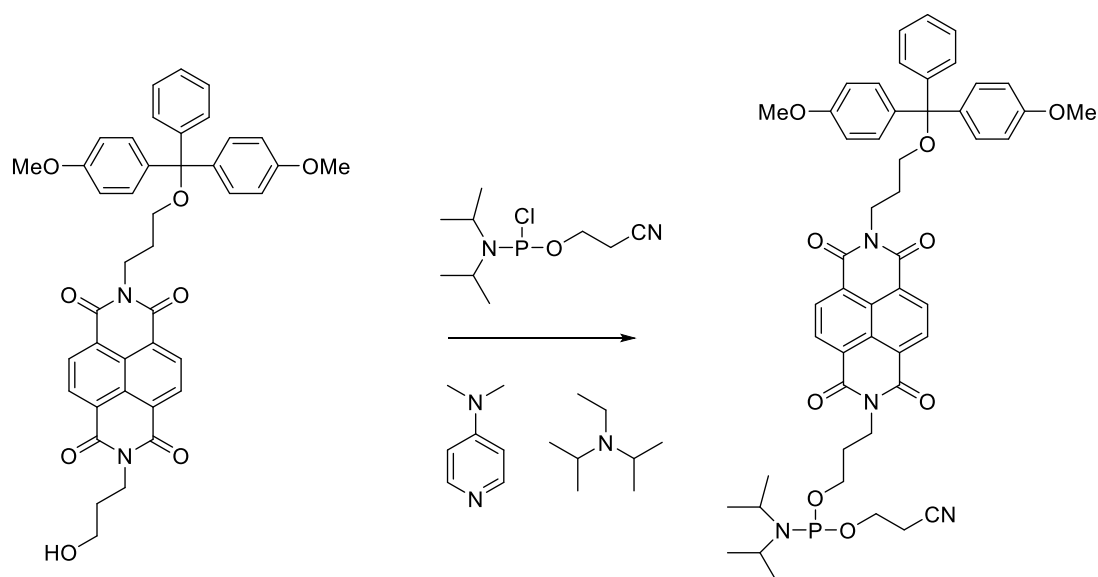
### DAN phosphoramidite reagent



Monoprotected DAN product (0.96 mmol, 617 mg), and dimethylaminopyridine (0.46 mmol, 56.1 mg) was dissolved in 50.0 mL of dry DCM, diisopropylethylamine (4.4 mmol, 0.836 mL) and, 2.89 mmol of 2-cyanoethyl diisopropyl chlorophosphoramidite (0.646 mL) were added. Under an atmosphere of nitrogen, the mixture was then stirred at room temperature for 2 hours. After the DCM was removed to obtained thick brown oil.

<sup>31</sup>P NMR: (400 MHz, DMSO-d<sub>6</sub>, 25 °C) 147.85 ppm

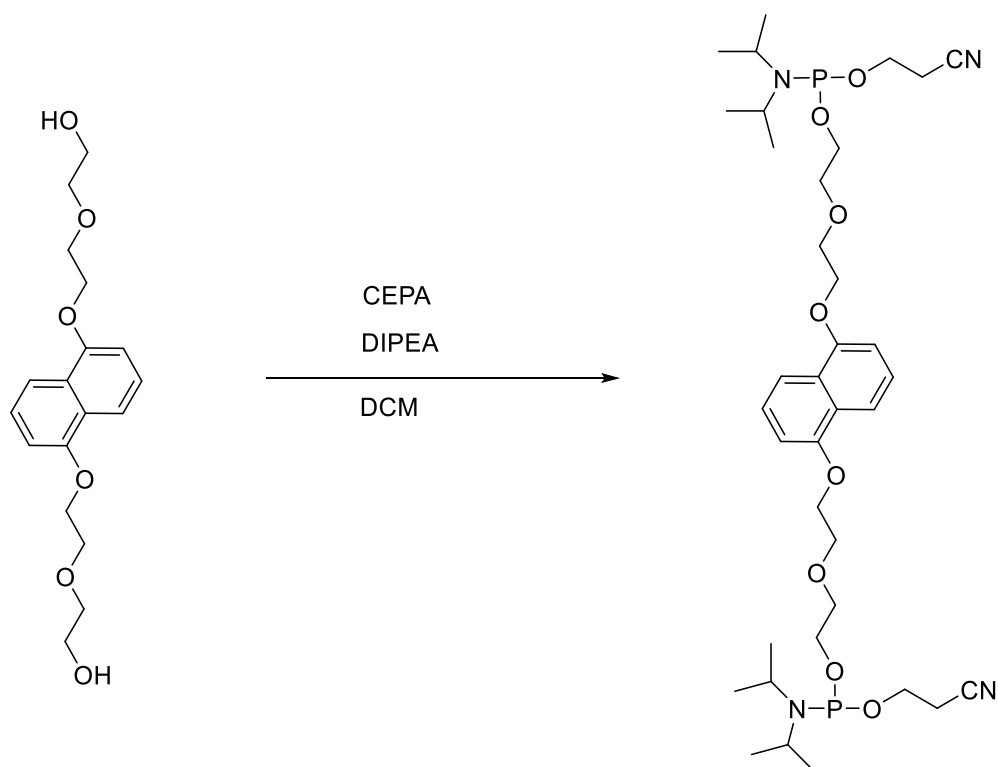
### NDI phosphoramidite reagent



Monoprotected NDI product (0.96 mmol, 664 mg), and dimethylaminopyridine (0.46 mmol, 56.1 mg) was dissolved in 50.0 mL of dry DCM, diisopropylethylamine (4.4 mmol, 0.836 mL) and, 2.89 mmol of 2-cyanoethyl diisopropyl chlorophosphoramidite (0.646 mL) were added. Under an atmosphere of nitrogen, the mixture was then stirred at room temperature for 2 hours. After the DCM was removed to obtained thick brown oil.

$^{31}\text{P}$  NMR: (400 MHz, DMSO- $d_6$ , 25 °C) 147.90 ppm

### Double phosphoramidite activated DAN

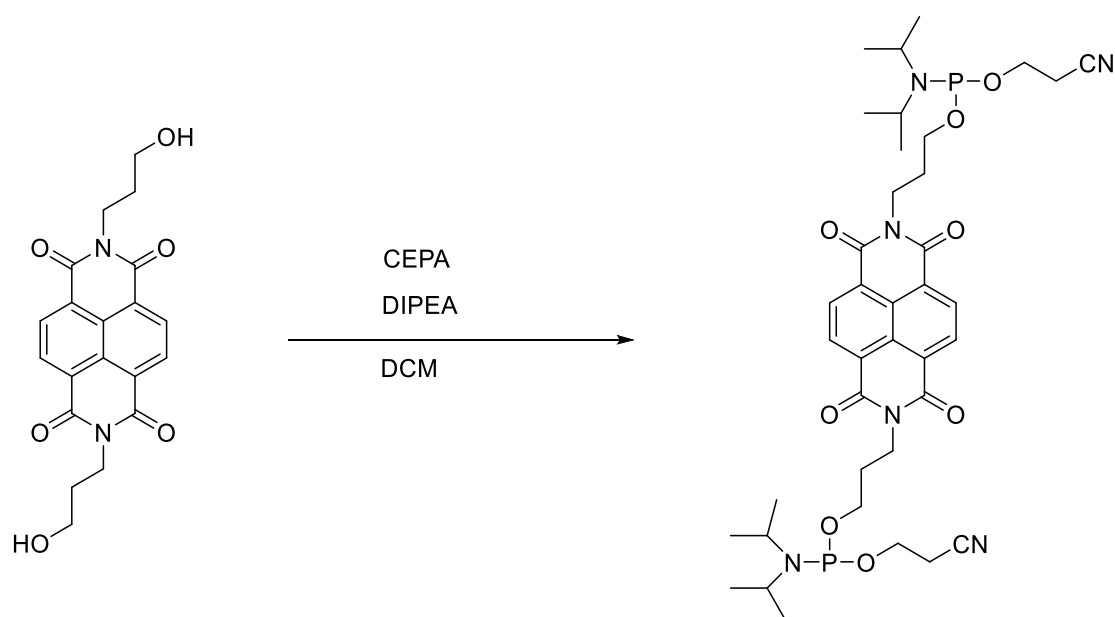


DAN diol (2 mmol, 672 mg), and dimethylaminopyridine (75 mg) were dissolved in 100 mL of dry DCM, to which diisopropylethylamine (10 mmol, 1.742 mL) and 2-cyanoethyl diisopropylchlorophosphoramidite (6 mmol, 1.33 mL) were then added. The mixture was then stirred at room temperature under an atmosphere of nitrogen, for 2 hours. After the DCM was removed under vacuum, and a thick brown oil was obtained, which was used immediately after obtaining  $^{31}\text{P}$  spectrum.

$^{31}\text{P}$  NMR: (400 MHz, DMSO- $d_6$ , 25 °C) 148.03 ppm

#### Double phosphoramidite activated NDI





NDI diol 1b (2 mmol, 764 mg), and dimethylaminopyridine (75 mg) was dissolved in 100 mL of dry DCM, to which diisopropylethylamine (10 mmol, 1.742 mL) and 2-cyanoethyl diisopropylchlorophosphoramidite (6 mmol, 1.33 mL) were added. The mixture was then stirred at room temperature under an atmosphere of nitrogen, for 2 hours. After the DCM was removed under vacuum, and a thick brown oil was obtained, which was used immediately after obtaining  $^{31}\text{P}$  spectrum.

$^{31}\text{P}$  NMR: (400 MHz, DMSO- $d_6$ , 25 °C) 147.14 ppm

### 5.3.2 Synthesis of Trimers

Synthesis was carried out as a one-pot reaction. Double phosphoramidite derivatives (either 2a or 2b) were dissolved in 50 mL of acetonitrile. 5 mL of 0.25M 5-ethylthio-1H-tetrazole activator was added to the mixture. Three molar equivalents of mono protected derivative (either 3a or 3b) was added, and reaction was stirred for 30 minutes. 5 mL of oxidation mix (0.015 M iodine in water/pyridine/THF 2/20/78) was added to the mixture and reaction was stirred for another 10 minutes. The

products were vacuumed dried and column chromatography was carried out using a basic alumina stationary phase, eluted with hexane:ethyl acetate (1:1), and then again using basic alumina eluted with DCM: MeOH (3:1). The cyanoethyl protecting group was removed from the purified sample by adding 5 mL of concentrated ammonium hydroxide and heating it at 60 °C for 1 hour, with NH<sub>4</sub>OH subsequently removed under vacuum. A 4:1 acetic acid:water mixture was then added to remove DMT protecting groups. After removal of solvent under vacuum, 20 mL of DCM was added to the solid sonicated for 2-5 minutes to remove soluble impurities (protecting groups). This process was repeated three times and the remaining residue was dried with heat (60 °C) and vacuum. Each product, DAN<sub>3</sub>, NDI<sub>3</sub>, DAN-NDI-DAN and NDI-DAN-NDI gave 53%, 52 %, 37% and 42% yields, respectively.

### 5.3.3 Reactions with phosphorous oxychloride

#### **DAN + POCl<sub>3</sub>**

DAN monomer 0.00149 mole (0.5 g) was dissolved in 20 mL of dry pyridine in a N<sub>2</sub>(g) atmosphere. POCl<sub>3</sub> (0.00149 mole, 140 µL) was added to the solution and mixture was stirred at -10°C for 30 minutes. Then the mixture was quenched with some crushed ice. The clear solution was then dried and obtained a thick oil. The oil was then dissolved in 40 mL of 10% NaOH. The solution was evaporated, and green precipitate was obtained under 0.1M HCl. The precipitate was washed with small quantities of water and then washed with 1:1 mixture of ether and acetone.

#### **DAN<sub>2</sub> + POCl<sub>3</sub>**

DAN2 monomer 0.00164 mole (0.5 g) was dissolved in 20 mL of dry pyridine in a  $N_2(g)$  atmosphere.  $POCl_3$  (0.00164 mols, 150  $\mu L$ ) was added to the solution and mixture was stirred at  $-10^\circ C$  for 30 minutes. Then the mixture was quenched with some crushed ice. The clear solution was then dried and obtained a thick oil. The oil was then dissolved in 40 mL of 10% NaOH. The solution was evaporated, and grey precipitate was obtained under 0.1M HCl. The precipitate was washed with small quantities of water and then washed with 1:1 mixture of ether and acetone.

#### **NDI + $POCl_3$**

NDI monomer 1.30 mmol (0.5 g) was dissolved in 20 mL of dry pyridine in  $N_2(g)$  atmosphere.  $POCl_3$  (1.30 mmol, 120  $\mu L$ ) was added to the solution and mixture was stirred in  $-10^\circ C$  for 30 minutes. Then the mixture was quenched with some crushed ice. The clear solution was then dried and obtained a thick oil. The oil was then dissolved in 40 mL of 10% NaOH. The solution was evaporated, and reddish grey precipitate was obtained under 0.1M HCl. The precipitate was washed with small quantities of water and then washed with 1:1 mixture of ether and acetone.

#### **DAN + DAN<sub>2</sub> + $POCl_3$**

DAN monomer 0.82 mmol (0.25 g) and DAN2 monomer 0.82 mmol (0.25 g) were dissolved in 20 mL of dry pyridine in  $N_2(g)$  atmosphere.  $POCl_3$  (1.64 mmol, 150  $\mu L$ ) was added to the solution and mixture was stirred at  $-10^\circ C$  for 30 minutes. Then the mixture was quenched with some crushed ice. The clear solution was then dried and obtained a thick oil. The oil was then dissolved in 40 mL of 10% NaOH. The solution was evaporated, and dark grey precipitate was obtained under 0.1M HCl. The precipitate was washed with small quantities of water and then washed with 1:1 mixture of ether and acetone.

**DAN + NDI + POCl<sub>3</sub>**

DAN monomer 0.82 mmol (0.25 g) and NDI monomer 0.82 mmol (0.31 g) were dissolved in 20 mL of dry pyridine in N<sub>2</sub>(g) atmosphere. POCl<sub>3</sub> (0.00164 mols, 150  $\mu$ L) was added to the solution and mixture was stirred at -10°C for 30 minutes. Then the mixture was quenched with some crushed ice. The clear solution was then dried and obtained a thick oil. The oil was then dissolved in 40 mL of 10% NaOH. The solution was evaporated, and purple precipitate was obtained under 0.1M HCl. The precipitate was washed with small quantities of water and then washed with 1:1 mixture of ether and acetone.

**DAN + DAN2 + NDI + POCl<sub>3</sub>**

DAN monomer 0.82 mmol (0.25 g), DAN2 monomer 0.82 mmol (0.25 g) and NDI monomer 0.82 mmol (0.31 g) were dissolved in 20 mL of dry pyridine in N<sub>2</sub>(g) atmosphere. POCl<sub>3</sub> (2.46 mmol, 225  $\mu$ L) was added to the solution and mixture was stirred at -10°C for 30 minutes. Then the mixture was quenched with some crushed ice. The clear solution was then dried and obtained a thick oil. The oil was then dissolved in 40 mL of 10% NaOH. The solution was evaporated, and dark purple precipitate was obtained under 0.1M HCl. The precipitate was washed with small quantities of water and then washed with 1:1 mixture of ether and acetone.

**BPA + POCl<sub>3</sub>**

BPA monomer 1.30 mmol (0.3 g) was dissolved in 20 mL of dry pyridine in N<sub>2</sub>(g) atmosphere. POCl<sub>3</sub> (1.30 mmol, 122  $\mu$ L) was added to the solution and mixture was stirred at -10°C for 30 minutes. Then the mixture was quenched with some crushed ice. The clear solution was then dried and obtained a thick oil. The oil was then dissolved in 40 mL of 10% NaOH. The solution was evaporated, and white

precipitate was obtained under 0.1M HCl. The precipitate was washed with small quantities of water and then washed with 1:1 mixture of ether and acetone.

#### **Estradiol +POCl<sub>3</sub>**

Estradiol monomer 1.10 mmol (0.30 g) was dissolved in 20 mL of dry pyridine in N<sub>2</sub>(g) atmosphere. POCl<sub>3</sub> (1.10 mmol, 100 µL) was added to the solution and mixture was stirred at -10°C for 30 minutes. Then the mixture was quenched with some crushed ice. The clear solution was then dried and obtained a thick oil. The oil was then dissolved in 40 mL of 10% NaOH. The solution was evaporated, and white precipitate was obtained under 0.1M HCl. The precipitate was washed with small quantities of water and then washed with 1:1 mixture of ether and acetone.

#### **Triphenyl + POCl<sub>3</sub>**

Triphenyl monomer 0.0102 mol (3 g) was dissolved in 20 mL of dry pyridine in N<sub>2</sub>(g) atmosphere. POCl<sub>3</sub> (0.0306 mol, 2.9 mL) was added to the solution and mixture was stirred in -10°C for 30 minutes. Then the mixture was quenched with some crushed ice. The clear solution was then dried and obtained a thick oil. The oil was then dissolved in 40 mL of 10% NaOH. The solution was evaporated, and orange colour precipitate was obtained under 0.1M HCl. The precipitate was washed with small quantities of water and then washed with 1:1 mixture of ether and acetone and then soxhlet extraction was conducted with acetone in reverse manner.